



**University of  
Nottingham**  
UK | CHINA | MALAYSIA

# **Molecular Characterization of Endocannabinoid Signalling**

Submitted July 2020, in fulfilment of the conditions for the award of  
Doctor of Philosophy degree

Yousra Adel Abdulwahab Abdulmaqsood  
BSc (Highest Honour), MSc (Distinction)

Supervised by:

Dr Stephen Alexander

Faculty of Medicine and Health Sciences

University of Nottingham

I hereby declare that this thesis is all my own work, except as indicated in the text as a  
PhD student at the University of Nottingham

## Abstract

The endocannabinoid system has gained an increased focus in exploiting its therapeutic potential for the management of multiple diseases. This research aimed to investigate two components of the EC system, the EC-hydrolysing enzyme ABHD6 and signalling through CB<sub>2</sub> receptor. Selective inhibition of ABHD6 was reported to possess anti-inflammatory and neuroprotective effects and was implicated in diverse pathological processes. Likewise, selective modulation of CB<sub>2</sub> receptors could have a therapeutic potential in the management of inflammatory, neuropathic pain and degenerative diseases without inducing the psychoactive effects of CB<sub>1</sub> receptor activation. This research initially aimed to develop a rapid, cost-effective, reproducible and sensitive HTS assay for screening human recombinant ABHD6. The investigated substrate 4-MUH was a promising tool for screening novel ABHD6 inhibitors. The assay also identified the potential for ABHD6 to recognise multiple endogenous lipids, which may be natural substrates of the enzyme. Nonetheless, the assay in its current configuration employed to ‘real’ tissues, of rat intestine and hippocampus, generated data that were complex and difficult to interpret. It is possible that further adapting this assay may resolve these issues.

Subsequent sections of the thesis provide comprehensive investigation of CB<sub>2</sub> receptor signalling, the effects of ligands derived from multiple pharmacophores and the dominant amino acids involved in the receptor’s signalling and function. The signalling pathways investigated in this study focused on rapid (typically <15 min) timepoints including Ca<sup>2+</sup> mobilization, ERK phosphorylation, and cAMP accumulation, in addition to exploring changes in [<sup>35</sup>S]-GTPγS, [<sup>3</sup>H]-CP55940 and fluorescent ligand binding assays. A series of compounds synthesised at the University of Nottingham based on fenofibrate namely FD24, FD43, FD44 and FD46 were initially investigated along with two commercially available alternatives reported to have agonist and inverse agonist/antagonist properties namely SER601 and COR170. This led to the identification of a promising novel CB<sub>2</sub> receptor agonist, FD24 with a ‘balanced’ agonist profile across the investigated signalling pathways. Further investigations pertaining to the selectivity of FD24 at CB<sub>2</sub> receptors compared to CB<sub>1</sub> receptors could identify beneficial therapeutic effects devoid of psychotropic effects. Furthermore, SER601 was identified as an ERK-phosphorylation biased agonist, without agonist activity in the other signalling pathways. Subsequent to further investigations, this compound could be a beneficial starting point for managing inflammatory or neuropathic pain through selective targeting of CB<sub>2</sub>

receptors (and possibly PPAR $\alpha$ ). Additional range of commercially available, structurally diverse agents reported to be CB<sub>2</sub> receptor-selective agonists, CB65, GP2a, GW405833, HU308, L759656 and MDA19, were investigated to assess their potential for bias within the same rapid responding assays. HU308 and MDA19 were efficacious CB<sub>2</sub> receptor agonists ‘balanced’ at the investigated pathways. HU308 is suggested to be useful as a ‘balanced’/unbiased agonist for characterization of CB<sub>2</sub> receptors and the current study confirms this profile. GW405833 acted as a low efficacy agonist/antagonist, dependent on the signalling pathway. GP2a displayed an inverse agonist profile in the cAMP pathway and was ineffective in all of the investigated pathways, while L759656 evoked inhibition of cAMP accumulation with no effects on the other pathways. The profile of CB65 was consistent with a low efficacy agonist/antagonist and not consistent with the literature. For investigation of *in vivo* profiles of synthetic CB<sub>2</sub> receptor-selective agents, it would be interesting to compare the profiles of L759656, SER601 and GW405833 or HU308 to investigate whether signalling bias through the pathways investigated here align with potentially beneficial therapeutic properties.

Following investigations of CB<sub>2</sub> receptor signalling, the concluding part of the project aimed to investigate the role of specific residues contributing towards CB<sub>2</sub> receptor signalling. The hydrophobic amino acids F117, F200 and W258 were mutated to their alanine counterparts and assessed in the rapid signalling pathways ERK phosphorylation and [<sup>3</sup>H]-cAMP accumulation. Mutations of F117A, F200A and W258A led to complete loss of functional activity via both signalling pathways. It was not possible to confirm expression of the mutant receptors through immuno- and/or molecular tagging techniques. Thus, the lack of coupling of the mutated receptors could be attributed to either the vital nature of these amino acids or that the receptor was not expressed subsequent to mutation. In order to gain solid conclusions regarding the prominence of these amino acids, future investigations could aim to utilise alternative approaches of transfection of the mutated receptor to gain more confidence that the receptor was expressed. Moreover, mutating an amino acid that was not involved in the receptor signalling or ligand binding could be used as a comparison that the receptor was functional subsequent to site-directed mutagenesis. Overall these investigations enhanced our understanding of the EC system.

## Acknowledgement

I would like to express endless gratitude to my supervisor Dr Stephen Alexander for his continued guidance throughout my PhD journey. Dr Steve was always a continued support both on the scientific and the personal level, a true mentor, scientist and role model. Dr Steve's passion towards research, comprehensive knowledge and commitment as a real scientist that was evident during my MSc degree motivated me to pursue my PhD degree under his supervision and I am sincerely fortunate for having him as my supervisor.

Deepest gratitude to my father, a girl's first love and the first person applauding my achievements since kindergarten to high school years, my BSc and MSc degrees and will definitely be the first person in line after achieving my PhD degree. The person who believed in me more than myself. To my beautiful mother, all her comforting talks, her continued support and her heart-warming laugh. To my loving husband for his unconditional love, encouragement and for always being there for me. To my dearest sister and brother for being the best of my world and for always drawing a smile on my face. To my lovely son, who joined us at the end of my PhD journey. To my beautiful family, you are all my backbone.

Special word of thanks to Dr Dmitry Veprintsev and David Sykes of COMPARE for their collaboration in the FRET assay. Special thanks to Dr Razan Al Momani for cloning and mutating the CB<sub>2</sub> receptors and Dr Nada Mahmoud for transfecting the HEKS cell line with ABHD6 and to Dr Andrew Bennett for providing me with the HeLa cell line.

Sincere appreciation to my dearest friends Razan Al Momani and Wafa Hourani and for all the special memories we created together. I would also like to thank all my lab colleagues and technicians around specially Michael Garle, Maxine Fowler, Julie Ellerby, Maria Isabel, Samar Salem, Paul Fodor and Nneoma Akaniro-Ejim.

## **Publications and Poster Presentations**

Adel Y and Alexander SPH (2021) Neuromolecular Mechanisms of Cannabis Action, in Cannabis and Neuropsychiatric Disorders (Murillo-Rodriguez E, Pandi-Perumal SR and Monti JM eds) pp 15-28, Springer International Publishing, Adv Exp Med Biol.

Yousra Adel and Steve PH Alexander. A comparison of ligand-evoked signalling through multiple pathways (cAMP, CA<sup>2+</sup>, ERK) in CB<sub>2</sub> receptor recombinant expression. The 29<sup>th</sup> Annual Symposium of the International Cannabinoid Research Society, Washington, United States of America, June 29 - July 4, 2019.

Nada Mahmoud, Yousra Abdulmaqsood, Sadia Shabnam, Andy J Bennett & Steve PH Alexander. *In vitro* esterase assays for human recombinant monoacylglycerol hydrolases (MAGL, ABHD6, ABHD12). The 28th Annual Symposium of the International Cannabinoid Research Society, Montreal, Canada, June 22 - June 27, 2017.

Nada Mahmoud, Yousra Abdulmaqsood, Sadia Shabnam, Andy J Bennett & Steve PH Alexander. The application of a fluorogenic substrate for recombinant  $\alpha\beta$  hydrolase 6 (ABHD6) activity. The 8th European Workshop on Cannabinoid Research, University of Roehampton, UK, August 31 – September 2, 2017.

## Table of Contents

Abstract.....	II
Acknowledgement.....	IV
Publications and Poster Presentations .....	V
Table of Contents .....	VI
Table of Figures .....	XI
Table of Tables.....	XV
Abbreviations.....	XVII
Chapter 1 : Introduction .....	1
1.1 G Protein-Coupled Receptors .....	1
1.1.1 Structure and Function.....	1
1.1.2 Signalling Mechanisms.....	4
1.2 The Endocannabinoid System.....	7
1.2.1 Endogenous Cannabinoids.....	7
1.2.2 Biosynthesis of Endocannabinoids.....	10
1.2.3 Hydrolysis and Degradation of ECS.....	12
1.2.4 Therapeutic Potential of Targeting EC Hydrolyzing Enzymes .....	14
1.2.5 Pathophysiological Implications of ABHD6.....	15
1.3 Discovery and Classification of the Cannabinoid Receptors.....	18
1.4 The Cannabinoid CB <sub>1</sub> Receptor.....	19
1.5 The Cannabinoid CB <sub>2</sub> Receptor.....	21
1.5.1 The Cannabinoid CB <sub>2</sub> Receptor Crystal Structure .....	22
1.5.2 The Cannabinoid CB <sub>2</sub> Receptor Signalling .....	23
1.5.3 The Cannabinoid CB <sub>2</sub> Receptor Expression Profile in Humans .....	26
1.5.4 Therapeutic Potential of Targeting CB <sub>2</sub> Receptors.....	26

1.5.5 Fenofibrate as a CB <sub>2</sub> Receptor Ligand.....	32
1.5.6 Biased agonism of CB <sub>2</sub> Receptors.....	33
1.6 Aims of the project.....	36
Chapter 2 : Materials and Methods.....	37
2.1 Materials and Reagents.....	37
2.2 ABHD6 Enzyme Assay .....	41
2.2.1 Statistical Data Analysis .....	42
2.3 Cell Culture.....	43
2.3.1 Cell Passaging .....	43
2.3.2 Cryopreservation and Thawing of cell lines.....	44
2.3.3 Cell counting and cell seeding.....	45
2.3.4 Generation and maintenance of transfected cell lines using XtremeGENE Reagent.....	46
2.4 Western Blotting.....	49
2.4.1 Gel Preparation: 10% SDS-Polyacrylamide Gel .....	49
2.4.2 RIPA Buffer .....	51
2.4.3 Immunoblotting.....	51
2.5 Preparation of Cellular Homogenates .....	53
2.6 Determination of Protein Concentration.....	54
2.7 Calcium Mobilization Assay .....	55
2.7.1 Preparation of HEPES Buffer.....	55
2.7.2 Assay Procedure .....	55
2.7.3 Statistical Data Analysis .....	57
2.8 In-cell Western: MAP Kinase ERK1/2 Activation .....	58
2.8.1 Preparation of 4% Paraformaldehyde.....	58
2.8.2 Assay Procedure .....	58
2.8.3 Statistical Data Analysis .....	60

2.9	[ <sup>3</sup> H]-CP55,940 Competition Binding Assay.....	61
2.9.1	[ <sup>3</sup> H]-CP55,940 Competition Binding Buffers .....	61
2.9.2	Assay Procedure .....	61
2.9.3	Statistical Data Analysis .....	62
2.10	[ <sup>35</sup> S]-GTPγS Assay.....	64
2.10.1	[ <sup>35</sup> S]-GTPγS Binding Buffers.....	64
2.10.2	Assay Procedure .....	64
2.10.3	Statistical Data Analysis .....	65
2.11	Fluorescent Binding Assay .....	67
2.11.1	Statistical Data Analysis .....	69
2.12	[ <sup>3</sup> H]-cAMP Accumulation .....	71
2.12.1	Column Preparation.....	71
2.12.2	[ <sup>3</sup> H]-cAMP Accumulation Assay Procedure .....	72
2.12.3	[ <sup>3</sup> H]-cAMP and [ <sup>14</sup> H]-cAMP Recovery .....	73
2.12.4	[ <sup>3</sup> H]-cAMP Generation Data Analysis .....	74
2.13	CB <sub>2</sub> Receptor Cloning and Site-Directed Mutagenesis.....	75
2.14	Statistical Data Analysis.....	76
Chapter 3 : Development of a high-throughput screening fluorescent assay for the ABHD6 enzyme .....		78
3.1	Results .....	80
3.1.1	4-NPA as a potential HTS substrate .....	80
3.1.2	4-MUO as a potential HTS substrate .....	83
3.1.3	4-MUH as a potential HTS substrate.....	85
3.2	Discussion .....	101
3.2.1	4-MUH as an ABHD6 Substrate.....	101
3.2.2	Definition of a high-throughput screening assay .....	103
3.2.3	The use of 4-MUH in native tissues .....	104



Chapter 6 : Mutation of Phe117 Phe200 and W258 amino acids of CB <sub>2</sub> receptors .....	171
6.1 Results .....	179
6.2 Discussion .....	192
6.3 Conclusion.....	194
Chapter 7 : General Discussion and Future Implications.....	195
7.1 Conclusion.....	201
7.2 Future Implications .....	202
Chapter 8 : References.....	204

## Table of Figures

Figure 1.1 Schematic diagram of the general GPCR structure. ....	2
Figure 1.2 Schematic representation of the G-protein cycle.....	6
Figure 1.3 Structures of common representative endocannabinoids, phytocannabinoids and synthetic cannabinoids. ....	9
Figure 1.4 Simplistic representation of the endocannabinoid synthesis, hydrolysis and transformation (Fowler et al., 2017).....	14
Figure 1.5 Stimulation of CB <sub>2</sub> receptor accommodates multiple receptor conformational changes leading to an array of different signalling mechanisms .....	25
Figure 2.1 Cleavage of the 4-MUH ester bond produces the fluorescent compound 4-methylumbelliferone detected via the Fluoroskan <sup>TM</sup> at $\lambda_{ex}$ 355nm; $\lambda_{em}$ 460nm and the by-product, heptanoic acid.....	42
Figure 2.2 The transfection procedure followed using X-tremeGENE.....	47
Figure 2.3 The three main steps involved in immunoblotting.....	51
Figure 3.1 (A) 4-Nitrophenyl acetate hydrolysis to acetic acid and 4-nitrophenol, which can be detected by monitoring absorbance at 405 nm. ....	79
Figure 3.2 Hydrolysis of 2 mM 4-NPA by (A) particulate and (B) soluble fractions of HEKS293 cells. ....	80
Figure 3.3 Hydrolysis of various 4-NPA concentrations by MAGL1 or pcDNA-transfected HEK293 cell by (A) particulate and (B) soluble preparations.....	81
Figure 3.4 Hydrolysis of 2 mM 4-NPA by five protein dilutions. ....	82
Figure 3.5 Hydrolysis of various concentrations of 4-MUO by the soluble fraction of rat liver. ....	83
Figure 3.6 Hydrolysis of 12.5 $\mu$ M 4-MUO by (A) particulate and (B) soluble fractions of HEK293 cells expressing the recombinant enzyme transfects.....	84
Figure 3.7 Time course of 250 $\mu$ M 4-MUH hydrolysis by (A) particulate and (B) soluble preparations from transiently transfected HEK293 cells. ....	85
Figure 3.8 Hydrolysis of a range of 4-MUH concentrations by human recombinant ABHD6 particulate preparations. ....	86
Figure 3.9 Hydrolysis of 50 $\mu$ M 4-MUH by human recombinant ABHD6 in the presence of eleven enzyme inhibitors (1 $\mu$ M) of different selectivities. ....	87

Figure 3.10 The potency of four different inhibitors on the hydrolysis of 50 $\mu$ M 4-MUH by human recombinant ABHD6.....	89
Figure 3.11 Hydrolysis of 50 $\mu$ M 4-MUH by human recombinant ABHD6 in the presence of 36 potential inhibitors at 10 $\mu$ M; WWL70 as the positive control was assessed at 1 $\mu$ M. ....	91
Figure 3.12 The effect of increasing orlistat concentration on the hydrolysis of 50 $\mu$ M 4-MUH by human recombinant ABHD6. ....	92
Figure 3.13 Hydrolysis of 50 $\mu$ M 4-MUH by human recombinant ABHD6 in the presence of potential alternative substrates (100 $\mu$ M).....	93
Figure 3.14 Hydrolysis of 50 $\mu$ M 4-MUH by Wistar rat small intestine preparations diluted 125-fold (~50 $\mu$ g/mL protein). ....	94
Figure 3.15 Hydrolysis of a range of 4-MUH concentrations by Wistar rat small intestine preparations diluted 125-fold in the presence and absence of 1 $\mu$ M WWL70. ....	95
Figure 3.16 Hydrolysis of a range of 4-MUH concentrations by Wistar rat hippocampal preparations in the presence and absence of 1 $\mu$ M WWL70. ....	96
Figure 3.17 Hydrolysis of 50 $\mu$ M 4-MUH by the rat hippocampus in the presence of eleven inhibitors screened at 1 $\mu$ M.....	97
Figure 3.18 The effect of increasing WWL70 concentration on the hydrolysis of 50 $\mu$ M 4-MUH in rat hippocampus. ....	98
Figure 3.19 The hydrolysis of 50 $\mu$ M 4-MUH by rat hippocampus preparations, where eleven inhibitors (1 $\mu$ M) were screened in the presence and absence of 1 $\mu$ M WWL70. ....	99
Figure 4.1 (A) Displacement binding of $^3$ H-CP55,940 to membrane suspensions of CHO-CB <sub>2</sub> cells reported as dpm. ....	111
Figure 4.2 Specific binding of [ $^3$ H]-CP55,940 from membrane suspensions of CHO-CB <sub>2</sub> cells. ....	113
Figure 4.3 Specific binding of [ $^3$ H]-CP55940 to membrane suspensions of CHO-CB <sub>2</sub> cells displaced by AM630 and SER601.....	114
Figure 4.4 Determination of saturation binding of the fluorescent compound R07297590 to human CB <sub>2</sub> receptor membranes.....	116
Figure 4.5 Kinetic competition analysis for binding of R07297590 in the presence of the indicated concentrations of FD24, FD43, FD44, FD46, SER601 and COR170. ....	117

Figure 4.6 Determination of pK <sub>i</sub> values of the six investigated compounds at 1 h and 2 h following the kinetic reading of the plates expressed Log ligand concentration versus the HTRF emission ratio at 665 and 620 nm wavelengths. ....	118
Figure 4.7 The time-course of Ca <sup>2+</sup> ion elevation induced by the compounds indicated, expressed as RFU from a single experiment. ....	120
Figure 4.8 Calcium responses evoked by cannabinoid ligands (1 μM) expressed as a percentage of responses to 10 μM ATP (positive control). ....	121
Figure 4.9 Concentration dependence of fenofibrate analogues evoked Ca <sup>2+</sup> responses. ....	122
Figure 4.10 Calcium responses to fenofibrate analogues in the absence and presence of putative antagonists. ....	124
Figure 4.11 (A) Time course of ERK phosphorylation in CHO-CB <sub>2</sub> cells in the presence of the CB <sub>2</sub> receptor agonists CP55940 and fenofibrate at 1 μM. ....	126
Figure 4.12 Activation of the ERK signalling pathway by CB <sub>2</sub> receptor ligands (1 μM) measured at 5 min of ERK activation. ....	127
Figure 4.13 Concentration response curves for CB <sub>2</sub> receptor ligand evoked ERK phosphorylation measured at 5 min of ERK activation. ....	128
Figure 4.14 An investigation of the antagonist potential of FD44 and FD46. ....	129
Figure 4.15 Investigating CB <sub>2</sub> receptor-mediated effects of quinolone-3-carboxamide analogues. ....	131
Figure 4.16 2AG-evoked ERK phosphorylation in CHO-CB <sub>2</sub> cells. ....	132
Figure 4.17 The [ <sup>35</sup> S]-GTPγS binding in membrane suspension of CHO-CB <sub>2</sub> cells in the presence of cannabinoid ligands. ....	133
Figure 4.18 Modulation of forskolin-induced cAMP accumulation in CHO-CB <sub>2</sub> cells by cannabinoid ligands. ....	134
Figure 4.19 Modulation of forskolin stimulated cAMP accumulation in CHO-CB <sub>2</sub> cells. ....	135
Figure 4.20 Antagonism of CB <sub>2</sub> receptor agonist inhibition of cAMP accumulation in CHO-CB <sub>2</sub> cells. ....	137
Figure 5.1 Specific binding of [ <sup>3</sup> H]-CP55940 to membrane suspensions of CHO-CB <sub>2</sub> cells. ....	157
Figure 5.2 Effects of CB <sub>2</sub> receptor ligands on calcium levels in CHO-CB <sub>2</sub> cells. ....	158
Figure 5.3 Effects of CB <sub>2</sub> receptor ligands on calcium levels in CHO-CB <sub>2</sub> cells. ....	159

Figure 5.4 Activation of the ERK signalling pathway by CB <sub>2</sub> receptor ligands (1 μM). .....	160
Figure 5.5 The concentration dependence of ERK phosphorylation induced by HU308, L759,656 and MDA19.....	161
Figure 5.6 Effects of combining CB <sub>2</sub> receptor ligands with the endogenous agonist 2-AG on activation of the ERK pathway in CHO-CB <sub>2</sub> cells. ....	162
Figure 5.7 Effects of the CB <sub>2</sub> receptor ligands on forskolin-induced cAMP accumulation in CHO-CB <sub>2</sub> cells. ....	163
Figure 5.8 Effects of CB <sub>2</sub> receptor ligands on forskolin-induced cAMP accumulation in CHO-CB <sub>2</sub> cells by (A) GW405833, HU308, L759,656, MDA19 and (B) GP2a. ....	164
Figure 6.1 Two-dimensional snake plot diagram of the cannabinoid CB <sub>2</sub> receptor demonstrating the mutated amino acids Phe117, Phe200 and W258 respectively highlighted in red which were mutated to the corresponding alanine residues. ....	178
Figure 6.2 The transfection ratios and latency of GFP expression in CHO-K1. ....	180
Figure 6.3 On-cell western performed using the CB <sub>2</sub> receptor polyclonal antibody CNR2 to detect cell surface expression of CB <sub>2</sub> receptors. ....	181
Figure 6.4 CHO-K1 cells were transfected using the transfection reagent X-tremeGENE at 1:1, 1:2, 1:3 and 1:4 ratios. ....	182
Figure 6.5 HeLa cells were transfected at 1:2 transfection ratio using WT-CB <sub>2</sub> receptor with the DNA vector as the negative control. The primary antibody used in the blot was the polyclonal antibody CNR2.....	183
Figure 6.6 HeLa cells were transfected at 1:2 transfection ratio using WT-CB <sub>2</sub> receptor with the DNA vector as the negative control. The primary antibody used in the blot was the CB <sub>2</sub> receptor monoclonal antibody (C37).....	184
Figure 6.7 Forskolin induced cAMP accumulation in transiently transfected CHO-K1 cells. ....	185
Figure 6.8 Activation of the ERK signalling pathway in transiently transfected CHO-K1 cells. ....	187
Figure 6.9 Activation of the ERK signalling pathway by CP55940 in transiently transfected HeLa cells, normalised to the response to 1% FBS. ....	189
Figure 6.10 FLAG tagged CB <sub>2</sub> receptors were transfected in the HeLa cells at 1:2 ratio with X-tremeGENE. ....	191

## Table of Tables

Table 1.1 Classification of the G <sub>α</sub> subtypes and their effects (Milligan and Kostenis, 2006)	5
Table 2.1 Structures of the investigated compounds	38
Table 2.2 Seeding densities for the cell lines employed	45
Table 2.3 Seeding and transfection conditions used	46
Table 2.4 Composition of 10% SDS-Polyacrylamide Gel Electrophoresis (Harlow and Lane, 1988)	49
Table 2.5 Buffers used in immunoblotting	50
Table 2.6 Antibodies used in immunoblotting	50
Table 2.7 Settings applied in SoftMax Pro for calcium FlexStation 3	57
Table 2.8 ERK Antibodies used in the assay	60
Table 3.1 The properties and potencies of the inhibitors used in the screening assay	88
Table 3.2 Potencies of the four inhibitors at human recombinant ABHD6 investigated at n=5 for WWL70 and WWL123 and n=4 for JJKK048 and MAFP	89
Table 3.3 Calculated K <sub>m</sub> values for 4-MUH hydrolysis by rat hippocampal preparations investigated at n=5	96
Table 4.1 The pK <sub>i</sub> values of the investigated compounds at 1 and 2 h from three independent experiments	118
Table 4.2 Binding parameters of the compounds interacting with CB <sub>2</sub> receptors	119
Table 4.3 Concentration-response parameters for fenofibrate analogue-evoked calcium elevations in CHO-CB <sub>2</sub> cells performed at n=3 for CP55,940 and fenofibrate and n=4 for FD24 and FD43	122
Table 4.4 Parameters for concentration-dependent stimulation of ERK phosphorylation in CHO-CB <sub>2</sub> cells performed at n=5	128
Table 4.5 Quantitative assessment of SER601 and COR170 influences on the binding of [ <sup>35</sup> S]-GTPγS to CHO-CB <sub>2</sub> membranes performed at n=3	133
Table 4.6 Concentration-dependence for modulation of cAMP accumulation by cannabinoid ligands in CHO-CB <sub>2</sub> cells performed at n=3 for CP55,940, fenofibrate, FD24, AM630 and n=4 for FD43	136
Table 4.7 Effects induced by the ligands at the different signalling pathways	138

Table 5.1 Chemical structures and physicochemical properties of the CB <sub>2</sub> receptor ligands investigated in this chapter .....	154
Table 5.2 Pharmacological properties of the CB <sub>2</sub> receptor ligands investigated in this chapter .....	155
Table 5.3 The quantitative parameters for HU308, L759,656 and MDA19 activation of ERK phosphorylation in CHO-CB <sub>2</sub> cells performed at n = 5 for HU308, MDA19 and n = 3 for L759,656 .....	161
Table 5.4 Quantitative parameters for HU308, L759,656 and MDA19 regulation of cAMP accumulation in CHO-CB <sub>2</sub> cells performed at n=3. ....	165
Table 5.5 Summary of the effects induced by the compounds at the different CB <sub>2</sub> receptor signalling pathways.....	166
Table 6.1 Mutagenesis studies of the human cannabinoid CB <sub>2</sub> receptor .....	174

## Abbreviations

Abbreviations used throughout the thesis are listed below. The abbreviations that are used only once are presented within the text itself and are not listed below.

$\Delta^9$ -THC	$\Delta^9$ -Tetrahydrocannabinol
2AG	2-arachidonoylglycerol
4-MUH	4- Methylumbelliferylheptanoate
5-HT	5-hydroxytryptamine
AA	Arachidonic acid
ABHD4	$\alpha\beta$ hydrolase 4
ABHD6	$\alpha\beta$ hydrolase 6
ABHD12	$\alpha\beta$ hydrolase 12
AEA	N-arachidonylethanolamide (anandamide)
ATP	Adenosine 5'-triphosphate
CB <sub>1</sub>	Cannabinoid receptor 1
CB <sub>2</sub>	Cannabinoid receptor 2
CHO	Chinese hamster ovary
COX	Cyclo-oxygenase
CYP450	Cytochrome P450
DAG	Diacylglycerol
DAGL	Diacylglycerol lipase
DMSO	Dimethyl sulfoxide
EC	Endocannabinoid
ERK	Extracellular signal-regulated kinase
FAAH	Fatty acid amide hydrolase

FBS	Fetal Bovine Serum
GDP	Guanosine diphosphate
GFP	Green fluorescent protein
GPCR	G protein-coupled receptor
GTP	Guanosine triphosphate
HEK293	Human Embryonic Kidney cells
IP3	Inositol-1,4,5-trisphosphate
JNK	c-Jun N-terminal kinase
MAG	Monoacylglycerol
MAGL	Monoacylglycerol lipase
MAPK	Mitogen-activated protein kinase
PBS	Phosphate buffered saline
PCR	Polymerase chain reaction
PLC	Phospholipase C
PPAR	Peroxisome proliferator-activated receptor
PTX	Pertussis toxin
PUFA	Polyunsaturated fatty acid
RIPA	Radioimmunoprecipitation assay buffer
TEMED	<i>N, N, N', N'</i> -Tetramethylethylenediamine
TM	Transmembrane
TRPV1	Transient receptor potential vanilloid receptor 1

## Chapter 1 : Introduction

### 1.1 G Protein-Coupled Receptors

#### 1.1.1 Structure and Function

The G protein-coupled receptor (GPCR) superfamily is the largest group of transmembrane (TM) proteins involved in vital roles of cell signalling (Vass et al., 2018). GPCRs comprise a diversified family of membrane proteins which control significant physiological functions including neurotransmission, sensory perception, cell communication, chemotaxis and senses of taste, sight and smell. These processes are modulated by multiple extracellular ligands that incorporate ions, biogenic amines, nucleotides, peptides and others (Tuteja, 2009). The first GPCR to be identified and purified was the  $\beta$ -adrenergic receptor ( $\beta$ -adrenoceptor) by Shorr et al. in 1981 and it was recognized as a hormone binding subunit (Shorr et al., 1981). GPCRs are characterized by their ability to detect multiple chemical signals in a profoundly selective manner (for many examples) and further transmit the signal from the ligand-receptor interactions into intracellular responses (Hauser et al., 2017). Given this high selectivity and their tissue-specificity, GPCRs represent the targets of 20-30% of existing FDA approved medications and are used in the management of a wide array of diseases including hypertension, schizophrenia, pain and asthma as of 2017 (Wacker et al., 2017; Zhou et al., 2019). The Human Genome Project had formerly recognized more than 800 GPCR genes and most of the GPCR-targeting medications in current therapeutic use exert their function on around 30 of them only (Wise et al., 2004). Thus, this affords possibilities for further investigation and drug discovery in the field of GPCR where the medical requirements are yet unmet.

All GPCRs share some structural commonalities. First, they are composed of seven TM  $\alpha$ -helices composed of multiple aliphatic amino acids, an intracellular carboxyl terminus, an extracellular amino terminus and three interhelical loops on both sides of the cell membrane. Thus, GPCRs are often referred to as “7-transmembrane receptors” or “heptahelical receptors”. The considerable homology among the TM segments allows some confidence in the identification of the finite numbers of GPCRs in particular genomes. The major structural differences within the GPCR family are observed in the intracellular loop spanning TM5 and TM6. The greatest diversities in length are observed at the carboxyl terminus and the amino terminus with sizes ranging between 371 and 879 amino acid residues, respectively (Kobilka, 2007). Investigations of around 200 GPCR sequences concluded that the total length of GPCRs ranges between 311 and 1,490 amino acid residues. GPCRs can recognize an array of diverse extracellular chemical and physical signals including peptides,  $\text{Ca}^{2+}$ , nucleotides and photons. Upon identification of the external signals, GPCR function as endpoints in signalling pathways that impact an array of metabolic and differentiated functions (Hill, 2006).

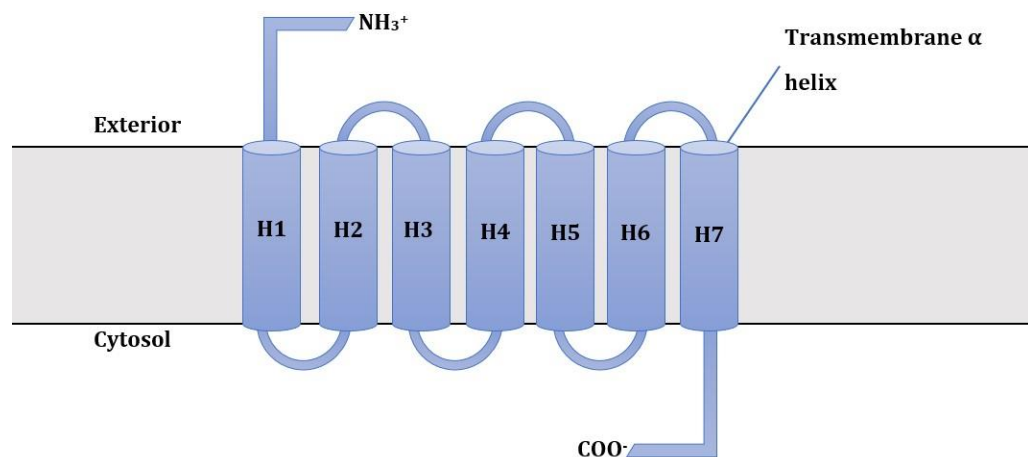


Figure 1.1 Schematic diagram of the general GPCR structure. H1-H7= transmembrane domains. The third intracellular loop between TM5 and TM6, and in certain conditions the second intracellular loop between helices 3 and 4, facing the cytosolic compartment are dominant for interactions with the coupled G proteins (Kobilka, 2007).

The superfamily of GPCRs is divided into six major families that display minor sequence homology between one another and little functional similarity. The site of the ligand binding domain has been identified for multiple families of GPCRs. Small organic agonists typically bind within the TM segments while proteins and peptide hormones, on the other hand, tend to bind at the amino-terminus and loops connecting the TM domains extracellularly. The size of the ligand is not a completely reliable predictor for anticipating the location of the binding site, for instance calcium and glutamate bind to the quite large amino-terminus to stimulate their cognate receptors (Kobilka, 2007).

The major family of GPCRs is **Family A**, often described as the rhodopsin-like family, which includes receptors for small ligands and odorants. Family A may be further subdivided into three groups: Group 1, Group 2 and Group 3. Group 1 is composed of receptors for small ligands, mainly the  $\beta$ -adrenoceptors and rhodopsin and their binding region is placed within the seven transmembrane domains. Group 2 is formed of peptide receptors and their binding site is located in the extracellular loops, the amino-terminus and the superior portions of the transmembrane regions. Finally, Group 3 consists of glycoprotein hormone receptors with a binding site located in the extracellular domains.

The second family, **Family B** is also referred to as the secretin receptor family and is composed of around 60 members. This family is characterised by the availability of a large amino terminus extending within the extracellular space. Moreover, family B exhibits comparable morphology to group A3, but they do not have any sequence homology. The compounds associated with this group are comprised of hormones incorporating calcitonin, corticotropin releasing factor, glucagon, growth hormone releasing hormone and secretin.

The third family, **Family C**, also referred to as the metabotropic glutamate receptor family, consists of around 24 GPCRs including the calcium sensing receptors, the metabotropic glutamate receptors, GABA<sub>B</sub> receptors and taste receptors. This family also have a large amino terminus extending extracellularly where ligand binding occurs.

**Family F** also referred to as the frizzled/smoothened receptor family includes the “smoothened” and “frizzled” receptors implicated in embryonic growth.

The two remaining families are not found in mammals and are not exploited therapeutically and are subsequently often grouped together. **Family D** is the fungus pheromone receptor family, while **Family E** is the cAMP receptor family, only found in the slime mould *D. discoideum*.

### 1.1.2 Signalling Mechanisms

Heterotrimeric G-proteins act as molecular switches that initiate intracellular signalling cascades in response to stimulation of GPCRs by extracellular stimuli. Thus G-proteins play a substantial function in determining the attributes of the cellular responses. Heterotrimeric G-proteins are comprised of three subunits:  $\alpha$ ,  $\beta$ , and  $\gamma$ . Their function is usually focussed on the capability of the  $\alpha$ -subunit  $G\alpha$  to cycle between the guanosine diphosphate (GDP) inactive conformation and the guanosine triphosphate (GTP) active conformation, which in turn mediates the effects of downstream proteins (Oldham and Hamm, 2008). Even though the GPCR superfamily is so diverse, these proteins tend to interact with a relatively limited number of G-proteins to initiate intracellular signalling cascades.  $G\alpha$  subunits are coded by 16 genes,  $G\beta$  subunits are coded by 5 genes and 12  $G\gamma$  subunits have been identified in humans. Hetero-trimers are classified into four major classes depending on the primary sequence similarity of the  $G\alpha$  subunit and functional similarities into  $G\alpha_s$ ,  $G\alpha_{i/o}$ ,  $G\alpha_q$  and  $G\alpha_{12}$  (Simon et al., 1991). The distinct subtypes in turn couple to different signalling pathways through interaction with effector proteins (Table 1.1) (Cabrera-Vera et al., 2003). Up till now, it is not completely elucidated as to how the subtype selectivity of the G protein is regulated (Hurowitz et al., 2000; Michael et al., 2009). The  $G\beta\gamma$  subunits also mediate downstream signalling cascades, where they are implicated in the stimulation of the c-Jun N-terminal kinase (JNK) (Coso et al., 1996), the extracellular signal-regulated kinase (ERK) and mitogen-activated protein kinase (MAPK) pathways (Belcheva and Coscia, 2002). The  $G\beta\gamma$  subunit is also involved in the regulation of phospholipase C- $\beta$ , and particular adenylyl cyclase isoforms (Chen et al., 1995).

Table 1.1 Classification of the  $G\alpha$  subtypes and their effects (Milligan and Kostenis, 2006)

Family	Subtypes	Effectors
<b>Gs</b>	<ul style="list-style-type: none"> <li>• <math>G\alpha_{s(s)}</math>, <math>G\alpha_{s(L)}</math>, <math>G\alpha_{s(XL)}</math>, <math>G\alpha_{olf}</math></li> </ul>	<ul style="list-style-type: none"> <li>• <math>\uparrow</math> Adenylyl cyclase</li> <li>• <math>\uparrow</math> GTPase of tubulin</li> </ul>
<b>Gi</b>	<ul style="list-style-type: none"> <li>• <math>G\alpha_{i1}</math>, <math>G\alpha_{i2}</math>, <math>G\alpha_{i3}</math></li> <li>• <math>G\alpha_{oA}</math>, <math>G\alpha_{oB}</math>, <math>G\alpha_z</math>, <math>G\alpha_{t1}</math>, <math>G\alpha_{t2}</math>, <math>G\alpha_g</math></li> </ul>	<ul style="list-style-type: none"> <li>• <math>\downarrow</math> Adenylyl cyclase</li> <li>• <math>\uparrow</math> ERK/MAP Kinase</li> <li>• <math>\uparrow</math> GTPase of tubulin</li> <li>• <math>\downarrow</math> <math>Ca^{2+}</math> channels</li> <li>• <math>\uparrow</math> <math>K^+</math> channels</li> </ul>
<b>Gq</b>	<ul style="list-style-type: none"> <li>• <math>G\alpha_q</math>, <math>G\alpha_{11}</math>, <math>G\alpha_{14}</math>, <math>G\alpha_{15}</math> or <math>16</math></li> </ul>	<ul style="list-style-type: none"> <li>• <math>\uparrow</math> Phospholipase <math>C\beta</math></li> <li>• <math>\uparrow</math> <math>G\alpha_q</math> <math>K^+</math> channels</li> </ul>
<b>G12/13</b>	<ul style="list-style-type: none"> <li>• <math>G\alpha_{12}</math> and <math>G\alpha_{13}</math></li> </ul>	<ul style="list-style-type: none"> <li>• <math>\uparrow</math> Phospholipase D</li> </ul>
<b>G<math>\beta\gamma</math></b>	<ul style="list-style-type: none"> <li>• <math>G\beta_{1-5}</math>, <math>G\gamma_{1-12}</math></li> </ul>	<ul style="list-style-type: none"> <li>• <math>\downarrow</math> Adenylyl cyclase</li> <li>• <math>\uparrow</math> Phospholipase <math>C\beta</math></li> <li>• <math>\downarrow</math> <math>Ca^{2+}</math> (N-, P/Q-, R-) channels</li> </ul>

The regulatory cycle of G-proteins is demonstrated in Figure 1.2, in its resting state, the receptor remains unbound. In this inactive state, the  $G\alpha$  subunit incorporates a GDP molecule bound to it and a  $G\beta\gamma$  dimer. Following ligand interaction with the receptor, a conformational shift is prompted in the GPCR. GPCR prompts the G-protein alpha subunit to catalyse the exchange of GDP to GTP. The G-protein bound complex of the receptor is temporary and displays high-agonist affinity. Consequently, the G-protein receptor complex dissociates into  $\alpha$ -GTP and  $\beta\gamma$  subunits respectively. Both of these elements are individually capable of modifying intracellular second messenger cascades or ion channel activity and effectors continue to amplify the signal to other second messengers. The GPCR then catalyses the exchange of guanine nucleotides of GTP back to GDP allowing the formation of the  $G\alpha\beta\gamma$  complex once more, hence inactivating the G-protein signalling cascade (Michael et al., 2009; Oldham and Hamm, 2008).

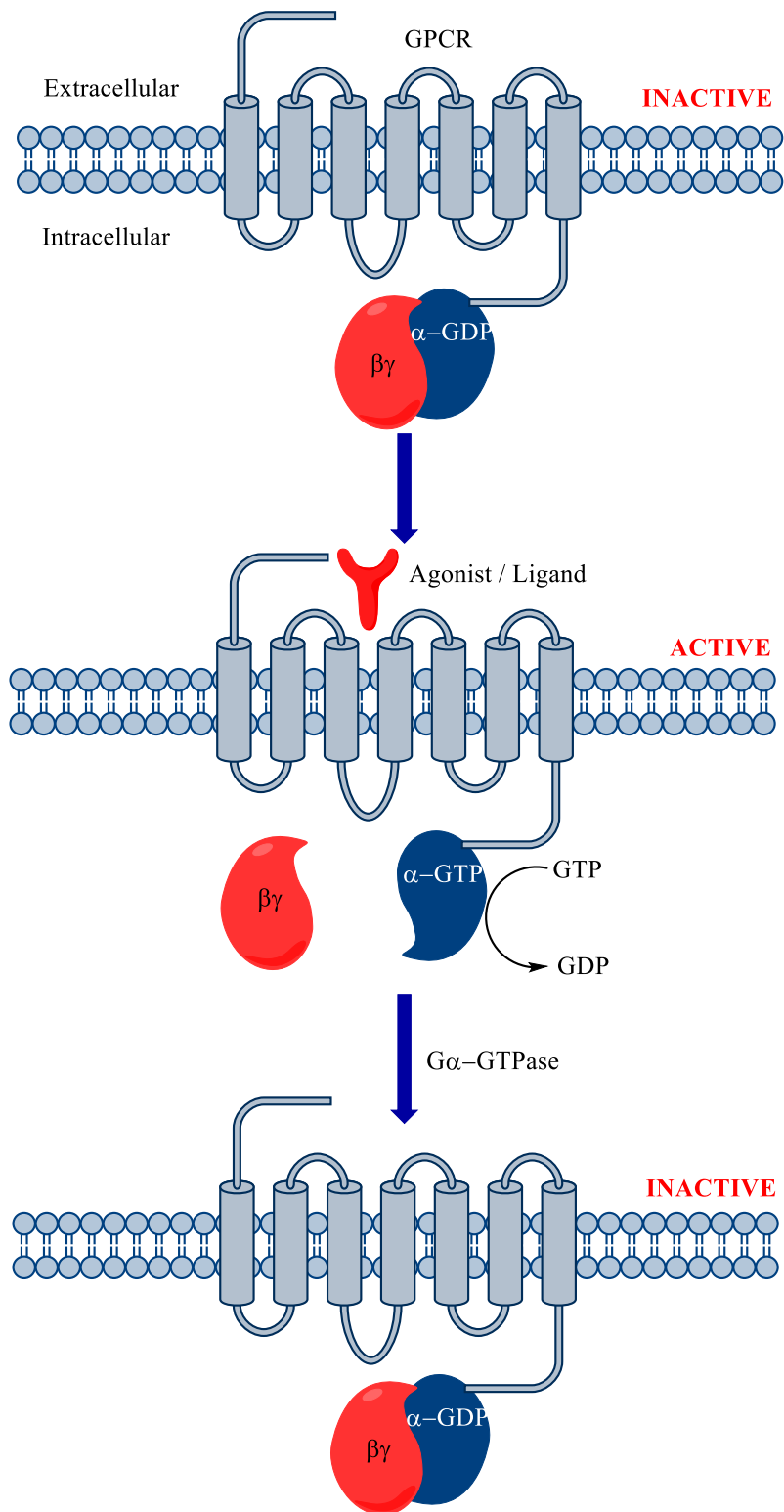


Figure 1.2 Schematic representation of the G-protein cycle.

Agonist stimulation of the G-protein receptor occurs subsequent to the binding of an agonist to the extracellular domain of the receptor. Agonist binding initiates conformational change of the receptor promoting nucleotide exchange of GDP to GTP. This is followed by dissociation of the GPCR into  $G\alpha$  and  $\beta\gamma$  subunits which each in turn independently mediate cellular response. The GTPase activity of the  $G\alpha$  subunit subsequently catalyses the exchange of GTP back to GDP restoring the  $G\alpha\beta\gamma$  complex.

## 1.2 The Endocannabinoid System

### 1.2.1 Endogenous Cannabinoids

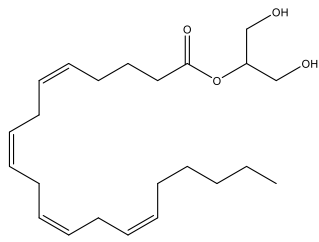
*Cannabis* preparations, often referred to as hashish, marijuana or weed, are obtained from the plant *Cannabis sativa*. In many countries, it is an illicit drug used for recreational purposes because of its euphoric effects. More than 400 distinct compounds have been identified in herbal cannabis (Ashton, 2001) with the principle psychoactive ingredient being  $\Delta^9$ -tetrahydrocannabinol ( $\Delta^9$ -THC) which was described by Raphael Mechoulam in Israel, derived from hashish (Gaoni and Mechoulam, 1964). The pharmacology of the cannabinoid receptors commenced in the late 1960s following the first isolation and synthesis of  $\Delta^9$ -THC. Endocannabinoids (ECs) are described as amide and ester derivatives of long chain polyunsaturated fatty acids (PUFA), typified by arachidonic acid (AA), that bind to and stimulate the cannabinoid receptors endogenously (Cascio and Marini, 2015). The EC system is composed of the two GPCRs the cannabinoid receptor 1 (CB<sub>1</sub>) and the cannabinoid receptor 2 (CB<sub>2</sub>), the endogenous ligands that activate these receptors, a putative membrane transport system and the enzymes that generate and metabolise the EC ligands (Pertwee et al., 2010). Currently, cannabinoids is a broad term that encompasses the ECs produced by most mammalian cells, the phytocannabinoids present in the *Cannabis* plant in addition to the synthetic cannabinoids (Pertwee et al., 2010).

N-arachidonylethanolamide (anandamide, AEA) (Devane et al., 1992) and the polyunsaturated monoacylglycerol (MAG) 2-arachidonylglycerol (2AG) (Sugiura et al., 1995) are the earliest identified and most intensively studied endogenous cannabinoids (Mechoulam et al., 1995). They are both synthesized upon demand subsequent to increased intracellular calcium levels (Pertwee et al., 2010). Anandamide (AEA) functions as a partial agonist at both CB<sub>1</sub> and CB<sub>2</sub> receptors with a slightly higher binding affinity at the CB<sub>1</sub> receptors;  $K_i$ = 89 nM and 321 nM respectively, while 2AG functions as a 'full' agonist at both receptors with moderate to low affinity. The  $K_i$  of 2AG at CB<sub>1</sub> and CB<sub>2</sub> receptors was reported to be 472 nM and 1400 nM respectively (Kendall

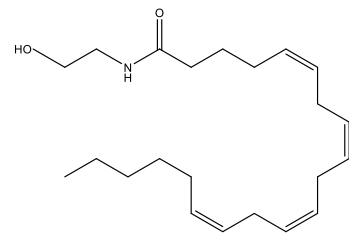
and Yudowski, 2016; Pertwee et al., 2010). Both 2AG and AEA were also reported to act at non-cannabinoid receptors (Zou and Kumar, 2018), such that 2AG was described to bind and regulate a precise site at the GABA<sub>A</sub> receptor subtype (Sigel et al., 2011). 2AG was reported to stimulate peroxisome proliferator-activated receptor  $\gamma$  (PPAR $\gamma$ ) leading to anti-inflammatory and neuroprotective effects (Garcia et al., 2011). Moreover, AEA was reported to activate the transient receptor potential vanilloid receptor 1 (TRPV1) (Zygmunt et al., 1999) which is predominantly involved in pain transmission. AEA is also capable of interacting with PPARs, regulating multiple physiological outcomes of ECs including anti-inflammatory effects and analgesia (Stone et al., 2018). 2-AG was reported at higher concentrations in the brain and reproductive tissues than AEA (Fonseca et al., 2013) where it functions in multiple routes of lipid metabolism. Other compounds that have been identified and recognised to act as ECs include N-palmitoylethanolamine (PEA), N-oleoylethanolamine (OEA), N-linoleoylethanolamide (LEA), 9,10-Z-octadecanoamide (oleamide or ODA), N-dihomo- $\gamma$ -linolenylethanolamine, N-docosahexaenylethanolamine (DHEA), N-eicosapentaenylethanolamine (EPEA) and N-docosatetraenylethanolamine (Alharthi et al., 2018).

The EC system has become a target for the potential management of multiple disorders considering its dominant roles in an array of physiological conditions including appetite-stimulation, emesis, immune modulation, inflammatory responses, metabolism, memory, learning and analgesia (Andre et al., 2016; Fraguas-Sanchez and Torres-Suarez, 2018). Variations in EC levels have been associated with neurological diseases including Parkinson's disease (PD), multiple sclerosis (MS), Alzheimer's disease (AD), Huntington's Disease (HD), and ischemia (Fernandez-Ruiz et al., 2015) as well as certain types of cancers where it influences the growth, migration and metastasis of certain tumours (Thapa et al., 2011).

## Endocannabinoids

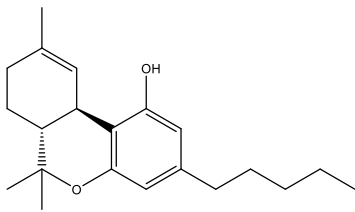


2AG

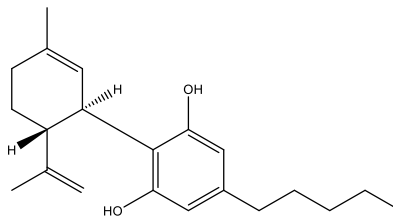


Anandamide

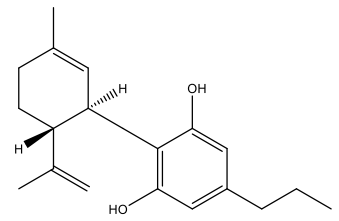
## Phytocannabinoids



$\Delta^9$ -THC

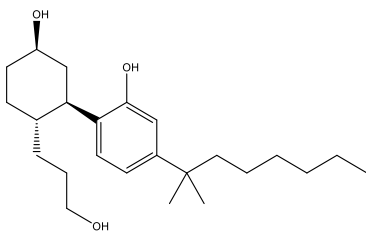


Cannabidiol

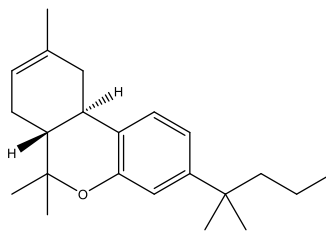


Cannabidivarin

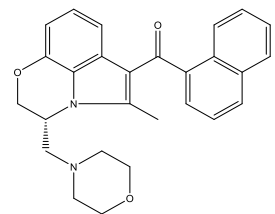
## Synthetic Cannabinoids



CP55,940



JWH-133



WIN55,212-2

Figure 1.3 Structures of common representative endocannabinoids, phytocannabinoids and synthetic cannabinoids.

## 1.2.2 Biosynthesis of Endocannabinoids

The ECs are broadly classified into two main types: the long chain PUFA amides, which encompass N-acylethanolamines (NAEs), and ester derivatives, MAGs. Their synthesis, metabolism and pharmacology have been extensively investigated. ECs and their active lipid ligands are mainly produced by hydrolases and/or acyltransferases from membrane phospholipids in response to cellular stimuli. After performing their function, ECs are rapidly metabolized by hydrolase enzymes. The EC synthesizing enzymes are present at much lower quantities than the hydrolysing enzymes to permit on-demand production and rapid hydrolysis of ECs and their respective bioactive lipid ligands (Ueda et al., 2013).

### 1.2.2.1 AEA and other NAEs

AEA is reported to have multiple physiological roles within the central and autonomic nervous systems as well as within the immune, gastrointestinal tract, endocrine and reproductive systems (Battista et al., 2012a; Taylor et al., 2010). AEA was found to produce antiproliferative effects, induce analgesia, stimulate appetite, decrease emesis as well as modulate motor activity (Fonseca et al., 2013). The synthesis of AEA and other NAEs including stearic (C18:0; stearoylethanolamide, SEA), palmitic (C16:0; palmitoylethanolamine, PEA) and oleic (C18:1; oleoylethanolamine, OEA) are generated upon demand following an increase in intracellular calcium levels as well as neuronal depolarization from the membrane bound lipid N-acyl phosphatidylethanolamine (NAPE) (Fonseca et al., 2013). NAPE is subsequently hydrolysed to AEA via the calcium-dependent phosphodiesterase phospholipase D selective for NAPE (NAPE-PLD) (Schmid et al., 1983). This two-stage process initiates with the relocation of an acyl chain from the *sn*-1 position of the glycerophospholipid phosphatidylcholine activated via the calcium dependent enzyme N-acyltransferase (NAT) to the amino group of the hydroxyethyl component of phosphatidylethanolamine (PE) (Di Marzo et al., 2005). Nevertheless, NAPE-PLD knockout in mice brain revealed unaltered concentrations of multiple polyunsaturated NAEs including AEA (Leung et al.,

2006) and thus, alternative synthetic pathways have been proposed. It has been suggested that AEA is also synthesized from N-acyl-lysophosphatidylethanolamine via a lysophospholipase-D (lyso-PLD) activity (Sun et al., 2004). AEA could also be synthesized through a phospholipase C (PLC) dependent pathway where PLC has been proposed to hydrolyse NAPE to phosphoanandamide which is subsequently dephosphorylated by a phosphatase to produce AEA (Fonseca et al., 2013; Liu et al., 2006). AEA is also synthesized by the  $\alpha\beta$  hydrolase 4 (ABHD4) enzyme which interacts with either NAPE, lyso-NAPE or N-arachidonoyl phosphatidylethanolamine (NArPE) to produce glycerophospho-arachidonoyl ethanolamine (GpAEA), which is consequently transformed to AEA by a specific phosphodiesterase (Simon and Cravatt, 2006).

### **1.2.2.2 2AG and other MAGs**

The elevation in intracellular calcium is an important trigger for the synthesis of 2AG from the membrane phospholipids encompassing phosphoinositides (PI) by PI selective PLC to diacylglycerol (DAG). This is in turn transformed by membrane associated diacylglycerol lipase  $\alpha$  or  $\beta$  isoenzymes (DAGL $\alpha$  or DAGL $\beta$ ) to 2AG and other MAGs (Di Marzo et al., 2005; Sugiura et al., 2006). The production of 2AG may also be mediated through phospholipase A1 (PLA1) which produces 2-arachidonoyl-lysophospholipid, which is in turn hydrolysed by lyso-phospholipase C (lyso-PLC) to 2AG (Sugiura et al., 2006; Sugiura et al., 1995). Both  $\alpha$  and  $\beta$  DAGL isoenzymes function at neutral pH, they are both activated by calcium and glutathione (GSH) and both are inactivated by Ser/Cys hydrolase inhibitors including HgCl<sub>2</sub> and *p*-hydroxy-benzoate-mercuric inhibitors (Bisogno et al., 2003). Other biosynthetic pathways for 2-AG have also been suggested (Sugiura et al., 2002), but their physiological importance is yet to be fully elucidated.

### 1.2.3 Hydrolysis and Degradation of ECS

After their synthesis and release, ECs exert their effect on the cannabinoid receptors. Uptake ensues by either membrane diffusion or by a putative EC membrane transporter (EMT) which accumulates both AEA and 2AG (Battista et al., 2012a). Termination of cannabinoid signalling takes place via a two-step process of intracellular transport of the ECs followed by degradation through hydrolysis or oxidation pathways. Intracellular transport of ECs also occurs through diffusion given their lipophilic nature and is driven by the hydrolysis of the fatty acid amide hydrolase (FAAH) (Day et al., 2001) or by compartmentalization of AEA following diffusion (Hillard and Jarrahian, 2003) as well as by endocytosis (McFarland et al., 2004).

AEA and other NAEs including PEA, OEA and SEA are primarily hydrolysed by the amidase FAAH or a species-limited paralogue FAAH2 (Wei et al., 2006) to the respective fatty acid and ethanolamine. FAAH is an intracellular membrane bound enzyme that belongs to the amidase signature family of serine-hydrolase enzymes (Ahn et al., 2009) which attains maximal activity at pH 8-10 (Cascio and Marini, 2015) and is rich in serine, glycine and alanine residues (Ahn et al., 2009). Metabolism products of FAAH are inactive at the cannabinoid receptors, hence this is considered the predominant mechanism of EC signal termination (Di Marzo et al., 2005). AEA also functions as a substrate at cyclooxygenase-2 (COX-2) (Ross et al., 2002) but not cyclooxygenase-1 (COX-1) (Yu et al., 1997), the lipoxygenases 12 and 15 (LOXs) (Yu et al., 1997) and cytochrome P450 (CYP450) (Piscitelli and Di Marzo, 2012). COX-2 hydrolysis of AEA produces prostaglandin-ethanolamides also referred to as prostamides (Ross et al., 2002). Prostamides were found to be modestly effective at CB<sub>1</sub> and CB<sub>2</sub> receptors but were found to activate TRPV1 receptors. Nevertheless, their physiological relevance has not been completely elucidated (Matias et al., 2004; Ross et al., 2002). 12 and 15 LOX activities transform AEA to 12- and 15-hydroperoxyeicosatetraenoylethanolamide (12-HETE-EA, 15-HETE-EA) via the addition of oxygen molecules (Ueda et al., 1995; Ueda et al., 1999). CYP450 enzymes oxidise AEA to 5,6-epoxyeicosatrienoic acid ethanolamide (5,6-EET-

AEA) which was found to be a potent agonist at CB<sub>2</sub> receptors (Snider et al., 2009). AEA and NAEs are also hydrolysed by an acid ceramidase-like lysosomal cysteine hydrolase called N-acylethanolamine hydrolysing acid amidase (NAAA) to fatty acids and ethanolamine. NAAA has higher affinity towards PEA than the AEA (Tsuboi et al., 2004) and is only active at an acidic pH (Brown et al., 2013).

The predominant hydrolysis of 2-AG in the brain ~85% is enacted by the serine hydrolase monoacylglycerol lipase (MAGL) (Blankman et al., 2007). MAGL is present in both cytosolic and membrane fractions (Di Marzo et al., 2005; Lambert and Fowler, 2005) composed of 303 amino acids and its catalytic triad is comprised of Ser122, His269 and Asp239 (Karlsson et al., 1997). Immunodepletion experiments demonstrated that enzymes other than MAGL contribute to 2AG hydrolysis (Dinh et al., 2004). Two integral membrane serine hydrolases the  $\alpha\beta$  hydrolase 6 (ABHD6) and  $\alpha\beta$  hydrolase 12 (ABHD12) possessing the catalytic triad serine-aspartic acid-histidine were implicated in the degradation of 2AG (Savinainen et al., 2012). Moreover, 2AG is a substrate for COX-2 leading to the oxidized novel lipid prostaglandin H<sub>2</sub> glycerol ester (PGH<sub>2</sub>-G) which is a substrate for PGD synthase leading to the production of prostaglandins derived from 2AG (Kozak et al., 2000). 15-LOX-1 and 15-LOX-2 oxygenate 2-AG to the corresponding 15(S)-hydroperoxyeicosatetraenoic acid glyceryl ester (15-HETE-G) which in turn functions as an agonist at the PPAR $\alpha$  receptors (Kozak et al., 2002). CYP450 mediated metabolism of 2-AG was reported to produce 2-11,12-epoxyeicosatrienoylglycerol (2-11,12-EET-EG) and 2-14,15-epoxyeicosatrienoylglycerol (2-14,15-EET-EG) and both exhibit enhanced binding at CB<sub>1</sub> receptors compared to 2AG (Zelasko et al., 2015).

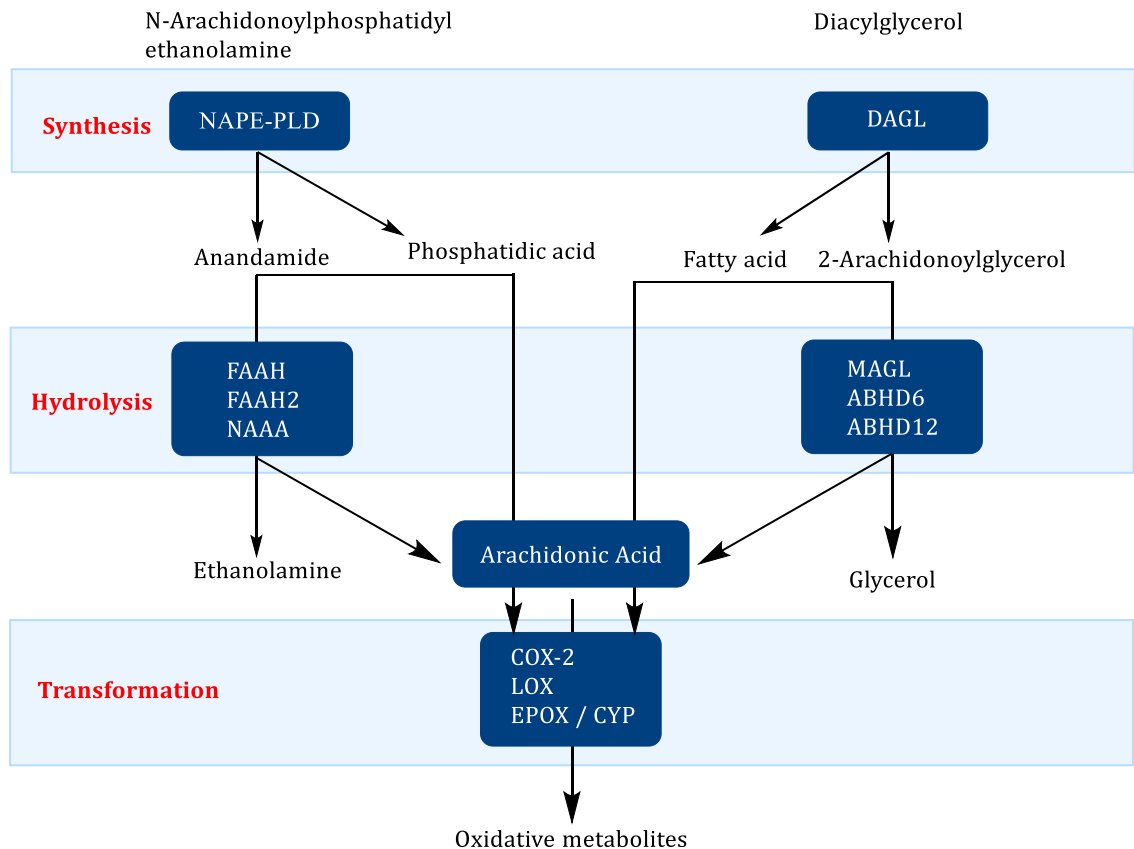


Figure 1.4 Simplistic representation of the endocannabinoid synthesis, hydrolysis and transformation (Fowler et al., 2017)

### 1.2.4 Therapeutic Potential of Targeting EC Hydrolyzing Enzymes

The relatively selective, irreversible MAGL inhibitor JZL184 (Fowler et al., 2017) mimicked the effects of  $\Delta^9$ -THC or other CB<sub>1</sub> receptor agonists *in vivo*, thus these psychoactive effects may restrict the therapeutic exploitation of MAGL inhibitors (Long et al., 2009). Nevertheless, ongoing research suggests that MAGL inhibitors can be therapeutically beneficial as anxiolytics, for pain alleviation, controlling nausea and vomiting and in neuroprotection models of Parkinson's disease (Fowler et al., 2017). The selective ABHD6 inhibitor, WWL70 (Fowler et al., 2017) demonstrated neuroprotective effect in traumatic brain damage of an experimental mouse model *in vivo* where it enhanced movement and memory post-insult. Additionally, it was found that manipulation of ABHD6 activity may produce

neuroprotective as well as anti-inflammatory properties in traumatic brain injury (Tchantchou and Zhang, 2013).

Similarly, FAAH inhibitors were found to increase AEA levels in the nervous tissues by prolonging its effect at activating CB<sub>1</sub> receptors and producing analgesic effects in rodents (Di Marzo et al., 2004). The FAAH inhibitor PF-04457845, was developed for the management of osteoarthritic pain by Pfizer (New York, NY, USA). It reached phase II clinical trials but following two-randomized, double-blinded placebo and active drug controlled clinical trials, it was concluded that PF-04457845 demonstrated no clinical efficacy (Mallet et al., 2016).

### **1.2.5 Pathophysiological Implications of ABHD6**

The serine hydrolase enzyme ABHD6 is an integral membrane protein with a mass of 30 kDa, with a nucleophilic catalytic triad of Ser-Asp-His (S148-D278-H306) (Navia-Paldanius et al., 2012). ABHD6 was found to be widely expressed and high mRNA levels reported in murine brain, small intestine, testis, brown adipose tissue, heart, liver, muscle and kidneys (Poursharifi et al., 2017). ABHD6 is proposed to subserve a substantial role in distinct physiological processes in multiple peripheral tissues, including signal transduction via its vital substrate MAG. Hydropathy and biochemical investigations, demonstrated that ABHD6 was a membrane bound protein with its active site facing towards the interior cytosol of the postsynaptic neurons; therefore, suggesting that it regulates the intracellular levels of 2AG (Navia-Paldanius et al., 2012) where the majority of 2AG biosynthesis occurs. Despite contributing towards 4% only of the overall 2AG metabolism in brain homogenates, the selective blockade of ABHD6 was found to modify and fine-tune the cannabinoid signalling profile consequent to localised elevated levels of 2AG (Blankman et al., 2007). Selective blockade of ABHD6 was found to possess anti-inflammatory and neuroprotective effects in diseased animal models of traumatic brain injury, MS in addition to inducing antiepileptic effects (Baggelaar et al., 2018). Therefore, since alterations in ABHD6 expression levels and functionality were reportedly implicated in diverse pathological

processes, ABHD6 could potentially become a candidate therapeutic potential for the management of diverse pathological diseases.

#### **1.2.5.1 Cardiometabolic Diseases**

The serine hydrolase ABHD6 and its MAG substrate have been reported to be implicated in the maintenance of multiple physiological and pathological processes comprising autoimmune conditions, adipose browning (Zhao et al., 2016), neurotransmission, insulin secretion, food intake, neurological, metabolic ailments and cancers (Poursharifi et al., 2017). Recent investigations revealed that selective peripheral knockdown of the ABHD6 enzyme in mice metabolic tissues guarded the mice from obesity consequent to high fat diet. Moreover, ABHD6 was found to be substantially involved in hepatic de novo lipogenesis (Thomas et al., 2013). ABHD6 was also reportedly involved in the metabolism of multiple lipid substrates, thus, confirming the prominence of ABHD6 in glycerophospholipid hydrolysis and lipid signal transduction (Kind and Kursula, 2019). Therefore, ABHD6 could potentially serve as a novel therapeutic target for the management of type II diabetes, obesity, non-alcoholic fatty liver disease and metabolic syndrome.

#### **1.2.5.2 Cancer**

ABHD6 was described to possess elevated expression levels in several types of tumours including bone, prostate, leukemia, liver and ovarian tumours (Cao et al., 2019; Li et al., 2009). Moreover, ABHD6 pertained elevated expression levels in mice and human pancreatic ductal adenocarcinoma tumour cell lines and subsequent to ABHD6 block, there was a notable decrease in tumour metastasis both *in vivo* and tumour cell proliferation *in vitro* (Gruner et al., 2016). The ABHD6 substrate 2AG was reported to produce anti-invasive effects in prostate carcinoma, hence, modulators of 2AG could potentially be evolved in therapeutic targets for the management of prostate cancers (Endsley et al., 2007). However, further research remains to be performed to gain an enhanced understanding of the ABHD6 role in the development, growth and

apoptosis of the different malignancies, and its application as a therapeutic target.

### **1.2.5.3 Anti-inflammatory Properties**

The ABHD6 induced metabolism of 2AG leads to the generation of AA, which is an eminent precursor required in the synthesis of prostaglandins, thus suggesting the potential involvement of ABHD6 in mediating certain inflammatory processes (Ricciotti and FitzGerald, 2011). Selective inhibition of ABHD6 in microglia and macrophages resulted in elevated levels of 2AG, which in turn demonstrated 2AG induced activation of CB<sub>2</sub> receptors leading to anti-inflammatory properties (Wen et al., 2015). Thus, ABHD6 inhibition could become a potential therapeutic candidate in the regulation of inflammatory diseases.

These investigations imply that ABHD6 could be a promising therapeutic target possessing an array of health benefits. Nevertheless, further cellular, animal and clinical studies persist to be performed to gain a profound understanding of the physiological and pathophysiological effects of ABHD6.

### 1.3 Discovery and Classification of the Cannabinoid Receptors

In 1990, the orphan GPCR SKR6 was reported to influence the pharmacological impacts of  $\Delta^9$ -THC in rat cerebral cortex and this receptor is currently known as CB<sub>1</sub> receptor (Matsuda et al., 1990). Three years later, the GPCR CX5 present in the HL60, human promyelocytic leukemic cell line, was discovered as the second cannabinoid receptor, CB<sub>2</sub> receptor (Munro et al., 1993). These receptors share 44% amino acid sequence homology and belong to the rhodopsin GPCR family A that signal through the pertussis toxin (PTX)-sensitive G<sub>i/o</sub> proteins and function by activating MAPK and inhibiting adenylyl cyclase (Howlett et al., 2002; Pertwee et al., 2010).

Differences between these two receptor subtypes includes distinct tissue distribution and pharmacology (Howlett et al., 2002). Other than CB<sub>1</sub> and CB<sub>2</sub> receptors, other GPCRs, ion channel and nuclear receptors have been described to be stimulated by ECs and exogenous cannabinoid ligands (Kano et al., 2009). These receptors include GPR119 (Chu et al., 2010), GPR55 and GPR18 (McHugh et al., 2012), which possess low sequence homology to CB<sub>1</sub> and CB<sub>2</sub> receptors (Pertwee et al., 2010). The pharmacology of GPR18 suggests it could be considered as the third cannabinoid receptor (Alexander, 2012). Moreover, cannabinoid ligands both natural and synthetic were found to stimulate TRP channels (Di Marzo and De Petrocellis, 2010) as well as glycine receptors (Hejazi et al., 2006).

## 1.4 The Cannabinoid CB<sub>1</sub> Receptor

The CB<sub>1</sub> receptor is coded by the *CNR1* gene (Pertwee et al., 2010) present on chromosome 6 (Kano et al., 2009) and is composed of 472 amino acids in humans (Zou and Kumar, 2018). Investigations utilizing immunocytochemistry, quantitative autoradiography and in situ hybridization (Howlett et al., 2002) revealed that CB<sub>1</sub> receptor is abundantly expressed in the CNS at the terminals of central and peripheral neurons where they modulate the inhibition of the release of multiple neurotransmitters (Pertwee, 2015). There is intense expression specifically in the cerebellum, olfactory bulb, neocortex, basal ganglia, brain stem and hippocampus (Kendall and Yudowski, 2016), such that activation of the CB<sub>1</sub> receptor affects cognition, memory and motor function as well as induces analgesia. Peripherally, CB<sub>1</sub> receptor is expressed on nerve terminals of the testes (Howlett et al., 2002), vascular endothelium, spleen, in the enteric nervous system of the gastrointestinal (GI) tract (Izzo and Sharkey, 2010), adipocytes and the retina. The CB<sub>1</sub> receptor is precisely expressed at presynaptic and axonal locations limiting its effects presynaptically (Zou and Kumar, 2018). In addition to the cloned CB<sub>1</sub> receptor, two NH<sub>2</sub> terminal splice variants have been described, that differ in being shorter in length, possess different compound binding properties or affinities (Ryberg et al., 2005) and are expressed at significantly lower levels in various tissues (Ryberg et al., 2005; Shire et al., 1995) when compared to the full-length receptor. Nevertheless, the physiological and the pharmacological effects of these genetic polymorphisms are yet to be fully elucidated (Zou and Kumar, 2018).

$\Delta^9$ -THC binds to and activates the CB<sub>1</sub> receptor which mediates its psychotropic effects in the CNS. The CB<sub>1</sub> receptor is also activated by AEA and 2-AG in addition to synthetic cannabinoid compounds including CP55,940 (Munro et al., 1993) (Figure 1.3), WIN55,212-2 (Bridges et al., 2001), JWH018 (Reggio, 2010) and HU210 (Reggio, 2010). In addition to coupling to Gi/o, CB<sub>1</sub> receptors couple to Gs and Gq proteins and stimulate adenylate cyclase (Bosier et al., 2010). CB<sub>1</sub> receptors positively couple to A-type, inwardly rectifying potassium channels and negatively couple to the L, N and P/Q-type voltage gated Ca<sup>2+</sup> channels (Bosier et al., 2010; Dalton et al., 2009; Howlett et al., 2002). The

CB<sub>1</sub> receptor also enhances intracellular Ca<sup>2+</sup> release via the G protein-dependent stimulation of phospholipase C-β (PLC-β) by the G<sub>i/o</sub> βγ subunits which catalyse inositol-1,4,5-trisphosphate (IP<sub>3</sub>) release (Bosier et al., 2010).

The CB<sub>1</sub> receptor antagonist rimonabant (SR141716A) (Baur et al., 2012) was structurally modified to the respective CB<sub>1</sub> receptor antagonist AM6538 which was recently crystalized with the CB<sub>1</sub> receptor. This is a useful step towards adequately comprehending structure-function activity of this receptor and hence would aid in novel drug design and synthesis (Hua et al., 2016). An enhanced interpretation of the mechanism of G<sub>i</sub> activation by CB<sub>1</sub> receptor was obtained with the structure of a CB<sub>1</sub>-G<sub>i</sub> signalling complex bound to MDMB-Fubinaca (FUB) (Krishna Kumar et al., 2019). FUB is a highly potent agonist at both CB<sub>1</sub> and CB<sub>2</sub> receptors that is frequently used as an illicit synthetic cannabinoid (Gamage et al., 2018).

## 1.5 The Cannabinoid CB<sub>2</sub> Receptor

The CB<sub>2</sub> receptor is coded by the *CNR2* gene (Pertwee et al., 2010) located on chromosome 1p36 (Sugiura et al., 2006) and is composed of 360 amino acids in humans (Zou and Kumar, 2018). Investigations using in situ hybridization, northern blot and receptor autoradiography (Howlett et al., 2002; Pertwee, 1997) revealed that CB<sub>2</sub> receptor was predominantly expressed in macrophages, spleen (Munro et al., 1993), tonsils (Carayon et al., 1998) and immune cells. The precise immune cells found to abundantly express CB<sub>2</sub> receptor included monocytes, B cells, polymorphonuclear neutrophils, natural killer cells, CD4<sup>+</sup> and CD8<sup>+</sup> T cells (Galiègue et al., 1995; Schatz et al., 1997) and when stimulated, they regulate immune cell migration and cytokine release (Pertwee, 2015). Using quantitative PCR-based techniques, CB<sub>2</sub> receptor was also detected in monocytes and macrophages of the spleen and certain leukocyte populations, precisely the eosinophils (Galiègue et al., 1995). The CB<sub>2</sub> receptor's expression was also evaluated in other human organs and it was determined that the receptor was absent from the majority of non-immune organs with the exception of the uterus, pancreas and the lungs which incorporated low levels of CB<sub>2</sub> receptor mRNA (Turcotte et al., 2016). The CB<sub>2</sub> receptor was also found to perform a predominant role in affecting the fertility of male and female and was detected in the reproductive tissues of both sexes (Battista et al., 2012b; Grimaldi et al., 2009). Therefore, CB<sub>2</sub> receptor is often referred to as the *peripheral* cannabinoid receptor given its abundant peripheral presence (Howlett et al., 2002), compared to its limited CNS expression (Gong et al., 2006). Nevertheless, recent investigations detected the expression of CB<sub>2</sub> receptor in the CNS by microglia (Atwood and Mackie, 2010) following neuroinflammation, degeneration (Ashton et al., 2007), in neuropathic pain (Zhang et al., 2003) and in multiple sclerosis and amyotrophic lateral sclerosis (Yiangou et al., 2006). The expression level of CB<sub>2</sub> receptor was variable and determined by the state of the cell, i.e. microglia do not express CB<sub>2</sub> receptor in healthy human brain (Stella, 2004). The degree of CB<sub>2</sub> receptor expression in the neurons and their physiological role persists to be fully elucidated.

Selective modulation of CB<sub>2</sub> receptors could possess therapeutic potential in the management of fibrotic, inflammatory, neuropathic pain and neurodegenerative diseases (Contino et al., 2017) without inducing the psychoactive effects of CB<sub>1</sub> receptor stimulation. Recent investigations described the human CB<sub>2</sub> receptor crystal structure bound to the antagonist AM10257 (Li et al., 2019) and to the agonist WIN55,212-2 (Xing et al., 2020).

### **1.5.1 The Cannabinoid CB<sub>2</sub> Receptor Crystal Structure**

Until recently, the 3D structure of CB<sub>2</sub> receptor was not reported or identified which represented a hindrance in the rational drug design of compounds that selectively target the CB<sub>2</sub> receptor. This was imperative in order to identify vital residues that participate in the drug interaction and recognition to selectively act at CB<sub>2</sub> receptors over the CB<sub>1</sub> receptors and circumvent the undesired psychotropic side-effects secondary to CB<sub>1</sub> receptor activation.

The CB<sub>2</sub> receptor crystal structure bound to the potent antagonist AM10257 elucidated that the antagonist binding pocket was rather discrete and incorporated a smaller binding pocket than the CB<sub>1</sub> receptor antagonist binding pocket while it possessed a similar size and ligand interaction residues comparable to the CB<sub>1</sub> receptor agonist binding pocket (Li et al., 2019). This could provide an elucidation for the high degree of CB<sub>1</sub> and CB<sub>2</sub> receptor selectivity induced by the currently available cannabinoid receptor antagonists and could similarly provide an explanation for the currently observed findings that structurally discrete CB<sub>2</sub> receptor antagonists induce a partial CB<sub>1</sub> receptor agonist effect (Janero and Makriyannis, 2009). These structural observations could also account for the low selectivity between CB<sub>1</sub> and CB<sub>2</sub> receptors and the psychotropic side-effects implicated subsequent to CB<sub>1</sub> receptor activation (Li et al., 2019). The CB<sub>2</sub> receptor crystal structure bound to the potent agonist WIN55,212-2 elucidated that the agonist incorporated the same orthosteric binding pocket as the antagonist AM10257. WIN55,212-2 stabilized the CB<sub>2</sub> receptor in its active conformation via interaction with the Phe258 amino acid residue in TM6 which was reported to be important for differentiating agonists from antagonists (Xing et al., 2020). With regards to the CB<sub>2</sub> receptor ligand recognition and selectivity, the extracellular loop 2, residues from TM2, TM3

and TM6 were imperative (Xing et al., 2020), thus facilitating future rational drug design of CB<sub>2</sub> receptor selective compounds. Even though numerous synthetic CB<sub>2</sub> receptor selective agonists have been described with the potential of becoming promising therapeutic targets at CB<sub>2</sub> receptors, few have achieved clinical trials, and none have been licensed. The recent reporting of CB<sub>2</sub> receptor bound to both the agonist and the antagonist could support the development of potent, selective CB<sub>2</sub> receptor compounds with potential therapeutic targets.

### 1.5.2 The Cannabinoid CB<sub>2</sub> Receptor Signalling

The cannabinoid CB<sub>2</sub> receptors belong to class A GPCR receptors that couple to G<sub>i/o</sub> proteins and mediate multiple signalling pathways including the MAPK, the nuclear factor of activated T cells, adenylyl cyclase, cAMP response element binding protein and enhancing transcription factors, Akt kinase/protein kinase B in addition to a number of calcium and potassium ion channels. Although CB<sub>2</sub> receptors stimulate multiple signalling pathways, extensive investigations are predominantly concentrated on the adenylyl cyclase and ERK 1/2 pathways, whilst the others including arrestin, ion channel modulation and Akt and their modulated physiological processes are much less examined (Dhopeshwarkar and Mackie, 2014). Moreover, CB<sub>2</sub> receptor is well-known to couple to G<sub>α<sub>i/o</sub></sub>, there is additionally limited research on the coupling to G<sub>α<sub>q</sub></sub> and till date, there is no indication for G<sub>α<sub>s</sub></sub> mediated coupling to CB<sub>2</sub> receptors (Saroz et al., 2019).

MAP kinases participate in multiple biological roles by phosphorylating target molecules like transcription factors and thus modulating cellular responses including cellular proliferation, differentiation and apoptosis. There are comparatively fewer studies concerning CB<sub>2</sub> receptor mediated activation of MAPK as compared to CB<sub>1</sub> receptor. Time and concentration-dependent stimulation of ERK1/2 in CHO cells stably transfected with CB<sub>2</sub> receptors was reported. This stimulation was found to be pertussis toxin sensitive confirming the involvement of G<sub>i/o</sub> proteins (Bouaboula et al., 1996; Ibsen et al., 2017). The activation of CB<sub>2</sub> receptor leads to the inhibition of adenylyl cyclase and reduced levels of cAMP (Felder et al., 1995). Activation of CB<sub>2</sub> receptors in human lymphocytes evoked reduced inhibition of forskolin-stimulated adenylyl

cyclase compared to CB<sub>2</sub> receptors transfected in CHO or human embryonic kidney cells (Pertwee, 1997). CB<sub>2</sub> receptors also activate the inwardly rectifying potassium channels mediated via the Gβγ subunit and inhibit voltage-gated Ca<sup>2+</sup> channels (Ibsen et al., 2017).

To summarise, stimulation of CB<sub>2</sub> receptors either by natural or synthetic ligands affects multiple signalling cascades including

- ☞ Inhibition of adenylyl cyclase and reduced cAMP generation, which leads to lower stimulation of cAMP dependent protein kinase (PKA)
- ☞ Stimulation of the MAPK pathway and hence enhancing cell survival
- ☞ Stimulating Akt/protein kinase B and in turn enhancing cell survival, differentiation and growth
- ☞ Inhibition of particular voltage-gated calcium channels and opening other G-protein-gated inwardly rectifying potassium channels (GIRK)

All of these pathways have been linked to alterations in gene expression.

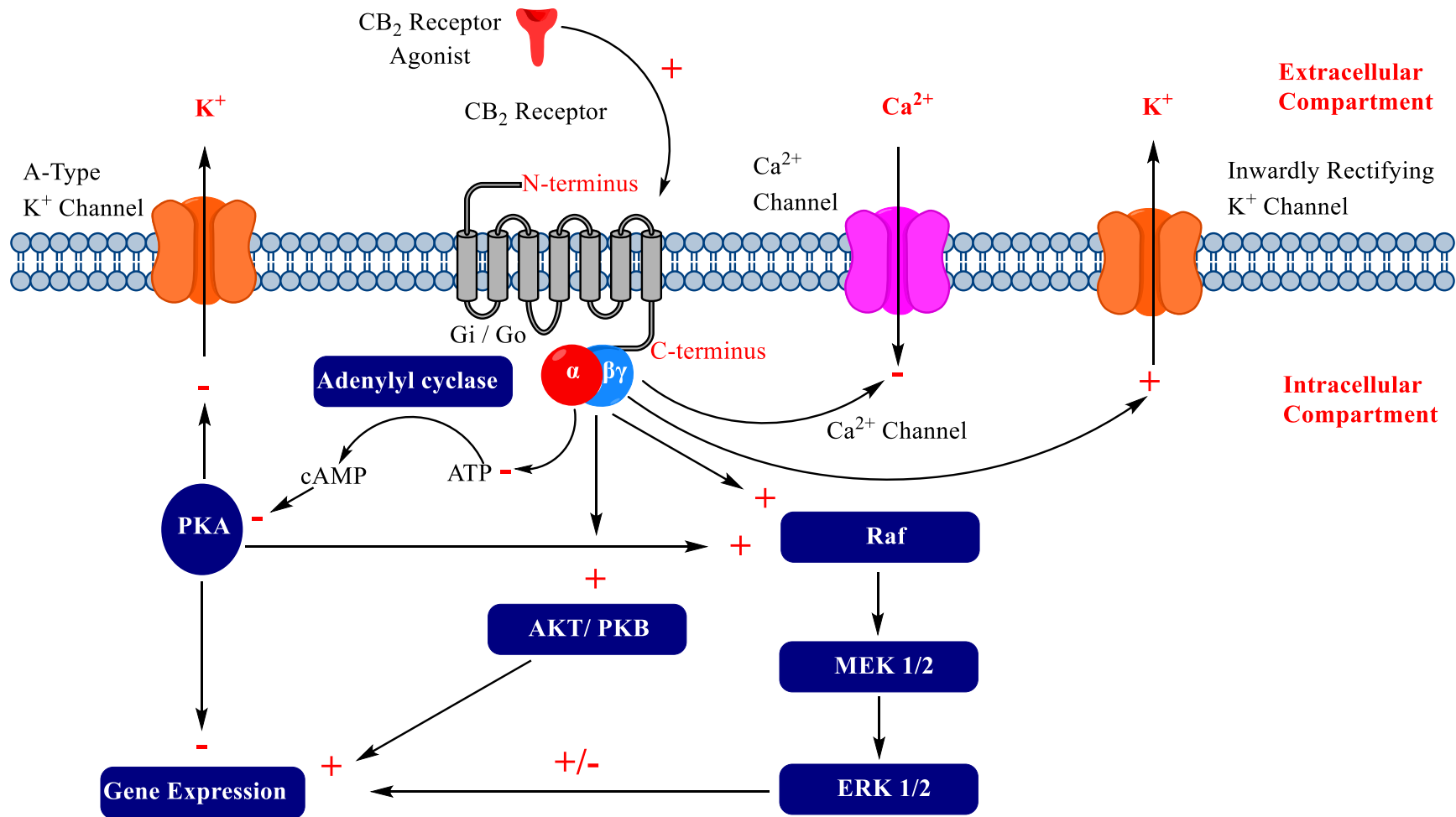


Figure 1.5 Stimulation of CB<sub>2</sub> receptor accommodates multiple receptor conformational changes leading to an array of different signalling mechanisms

### **1.5.3 The Cannabinoid CB<sub>2</sub> Receptor Expression Profile in Humans**

The CB<sub>2</sub> receptor was first cloned in 1993 by Munro et al. from promyelocytic leukaemic cell line HL-60. Following this cloning, they segregated a fragment of a rat homologue by PCR (Munro et al., 1993). This homologue was used to investigate different rat tissues, which allowed the detection of high CB<sub>2</sub> receptor mRNA levels in the spleen. Moreover, cell sorting identified CB<sub>2</sub> receptor expression in the monocyte and macrophages of the spleen and certain leukocyte populations, specifically eosinophils that reflect higher amount of CB<sub>2</sub> receptor mRNA as opposed to neutrophils (Galiègue et al., 1995). Further investigations found abundant CB<sub>2</sub> receptor mRNA in the tonsils, thymus, peripheral blood mononuclear cells and the spleen. CB<sub>2</sub> receptor was identified in the tonsils by immunohistochemistry using an anti-CB<sub>2</sub> receptor polyclonal antibody (Grimaldi et al., 2009). The expression of CB<sub>2</sub> receptor mRNA was also assessed in multiple human organs and it was concluded that CB<sub>2</sub> receptor mRNA was absent in most non-immune tissues apart from the uterus, pancreas and the lungs which expressed moderately low quantities of mRNA. In addition to various reports that demonstrated the presence of CB<sub>2</sub> receptors in both male and female reproductive tissues, it was therefore concluded that CB<sub>2</sub> receptors play a prominent role in influencing the fertility of both genders (Battista et al., 2012b). As a result of the abundant peripheral expression of CB<sub>2</sub> in the immune system and the reproductive system, CB<sub>2</sub> was formerly referred to as ‘peripheral cannabinoid receptor’. However, recent studies demonstrated the expression of CB<sub>2</sub> in the brain microglia during neuro-inflammation (Tanaka et al., 2020).

### **1.5.4 Therapeutic Potential of Targeting CB<sub>2</sub> Receptors**

The primary constraints that delayed research in the development of CB<sub>1</sub> receptor-agonists are the undesirable psychotropic effects that occur upon activation of these receptors. CB<sub>2</sub> receptor agonists on the contrary, do not appear to produce these psychotropic effects and thus provided a promising pathway for treating certain medical disorders (Deng et al., 2015).

#### **1.5.4.1 Analgesia**

CB<sub>2</sub> receptor activation was reported to produce antinociceptive effects as a result of acute thermal stimulus (Malan et al., 2001), which was devoid of any psychoactive side-effects of cannabinoid agonists following CB<sub>1</sub> receptor or opioid receptor activation including abuse potential, anxiety and sedation (Malan et al., 2003). Nociceptive pain is commonly associated with inflammation, as inflammatory mediators produced subsequent to injury aggravate pain (Scott et al., 2019). Former investigations revealed that CB<sub>2</sub> receptors evoked positive effects in coordinating the immune response, inflammation and the correlated pain where CB<sub>2</sub> receptor agonists diminished inflammatory and neuropathic pain (Malan et al., 2003; Yamamoto et al., 2008). Thus, rendering the CB<sub>2</sub> receptor an appealing drug target for the management of acute, inflammatory and neuropathic pain. The development of efficacious and safe medicines targeting pain and the correlated inflammation acting at CB<sub>2</sub> receptors required certain criteria; including being able to selectively bind to CB<sub>2</sub> receptors over CB<sub>1</sub> receptors to circumvent any psychoactive side-effects, stimulate the CB<sub>2</sub> receptor via the Gi pathway to inhibit cAMP generation as well as block immune cell proliferation. Nevertheless, further research is still required in order to determine the ability of these compounds to advance into preclinical and clinical studies.

#### **1.5.4.2 Anti-inflammatory Properties**

Selective stimulation of CB<sub>2</sub> receptors induced anti-inflammatory and tissue protecting properties devoid of CNS-mediated side-effects (Malan et al., 2001). Orally bioavailable CB<sub>2</sub> receptor agonists were found to possess therapeutic potential in inflammation and/or oxidative stress-related issues, including inflammatory kidney diseases (Mukhopadhyay et al., 2016). CB<sub>2</sub> receptor stimulation also induced a protective effect by evoking substantial decrease of renal fibrosis (Nettekoven et al., 2016). Selective potent agonists at CB<sub>2</sub> receptors were found to be promising candidates for the treatment of skin inflammatory disorders such as allergic contact dermatitis (Mugnaini et al., 2019) or for colon inflammatory processes (Leleu-Chavain et al., 2019). In

murine models of the inflammatory disease, rheumatoid arthritis, there was an observed enhancement in arthritis symptoms, decrease in bone destruction and leukocyte infiltration in the joints of the murine in response to a CB<sub>2</sub> receptor agonist (Fukuda et al., 2014). Moreover, administration of the selective CB<sub>2</sub> receptor agonist HU308 to murine models of rheumatoid arthritis was reported to alleviate swelling, joint destruction and synovial inflammation (Gui et al., 2015). However, none of these compounds have obtained FDA approval or proved effective in pre-clinical or clinical studies.

#### **1.5.4.3 Anti-obesity Treatment**

The previously promising effect of the CB<sub>1</sub> receptor inverse agonist rimonabant in the management of obesity (Despres et al., 2005) drew attention towards cannabinoid receptors in the treatment of metabolic disorders. This positive effect was nevertheless short-lived and the drug was withdrawn from the market in 2006 due its adverse psychiatric impact and increased incidence of depression and suicidal thoughts (Alexander, 2016). Consequently, attention was drawn towards the CB<sub>2</sub> receptor and its role in regulating energy homeostasis (Verty et al., 2015). The CB<sub>2</sub> receptor is predominantly located peripherally (Section 1.5.3) nevertheless, it was subsequently localised in the brain regions mediating appetite (Verty et al., 2015) and adipose tissue (Starowicz et al., 2008) thus, suggesting the potential role of CB<sub>2</sub> receptors in energy haemostasis and obesity disorders. Investigations involving blockade of CB<sub>2</sub> receptor using AM630 reported that it evoked a substantial enhancement of food intake in non-obese rodents (Onaivi et al., 2008). Chronic activation of CB<sub>2</sub> receptor, by contrast, diminished body weight gain (Rossi et al., 2018). Likewise, CB<sub>2</sub> receptor knockdown decreased the susceptibility of mice suffering from age-related and diet-induced insulin resistance (Agudo et al., 2010). CB<sub>2</sub> receptor activation was reported to enhance glucose tolerance in non-obese rats administered glucose overload implying a therapeutic role for CB<sub>2</sub> receptors in the management of obesity induced diabetes (Verty et al., 2015). Therefore, these findings confirm the promising therapeutic potential of targeting CB<sub>2</sub> receptor for the management of obesity and insulin resistance devoid of undesired influences on mood.

#### 1.5.4.4 Neurodegenerative Diseases

Cannabinoid CB<sub>2</sub> receptor agonists were found to impact microglial function associated with multiple neurodegenerative conditions comprising Alzheimer's disease (AD), Parkinson's disease (PD) and Huntington's disease (HD), and is expected to be a promising therapy in managing these conditions (Ehrhart et al., 2005; Fagan and Campbell, 2014) with minimal psychotropic effects. AD is an age-related neurodegenerative disease characterised by gradual progressive loss of cognitive dysfunction. Several studies on AD animal models revealed that CB<sub>2</sub> receptor agonists were capable of decreasing AD pathology as a result of decreasing inflammation associated with the disorder. Stimulation of CB<sub>2</sub> receptor was also reported to enhance cognitive function in AD animal models by regulating microglial migration and penetration into the brain regions with active neuroinflammation and deterioration (Aso and Ferrer, 2016). Nonetheless, localization of CB<sub>2</sub> receptors modulating these events and its comprehensive clinical evaluation has not yet been fully elucidated.

PD is the second most frequent neurodegenerative disorder implicated by gradual loss of dopaminergic neurons with no current treatments available to reverse its pathological processes (Cassano et al., 2017). CB<sub>2</sub> receptor knockdown in mice demonstrated aggravated PD pathology associated with elevated microglial stimulation, neural modifications and functional deficits (Gomez-Galvez et al., 2016). Activation of CB<sub>2</sub> receptors was found to induce neuroprotective effects in the pathophysiology of PD diseased models (Cassano et al., 2017).

HD is a congenital neural disorder characterised by motor, intellectual and psychiatric symptoms. CB<sub>2</sub> receptor expression in the striatum of HD was reported to be elevated in response to neurodegeneration and stimulation of these CB<sub>2</sub> receptors induced significant neuroprotective properties through a mechanism implicated via glial cells in reactive microglial cells. Activation of CB<sub>2</sub> receptors also decreased the production of proinflammatory molecules like TNF $\alpha$  (Sagredo et al., 2009). Accordingly, all these data indicate that CB<sub>2</sub> receptors depict a novel therapeutic target that could delay the

progression of degeneration of AD, PD, HD in addition to other neurodegenerative disorders.

#### **1.5.4.5 Cancers**

The antiproliferative properties of cannabinoid ligands were initially reported by Munson et al. where they observed that  $\Delta^9$ -THC diminished lung adenocarcinoma growth *in vitro* and in mice (Munson et al., 1975). CB<sub>2</sub> receptor agonists demonstrated promising effects in preclinical cancer models in multiple forms of cancer including prostate cancer, melanoma, lymphoma, pancreatic cancer, lung cancer, bone cancer, thyroid carcinoma and breast cancer. CB<sub>2</sub> receptor agonists are anticipated to prompt apoptosis, inhibit tumour growth as well as inhibit neo-angiogenesis (Chakravarti et al., 2014). The investigation of the cannabinoid agonists  $\Delta^9$ -THC and JWH015 revealed their ability in inhibiting tumour growth in xenograft models of hepatocellular carcinoma (Vara et al., 2011). CB<sub>2</sub> receptor agonists decreased cell migration, proliferation, vascularization and augmented apoptosis both *in vitro* and in mice models *in vivo* in non-small cell lung cancer growth and metastasis (Preet et al., 2011). A selective CB<sub>2</sub> receptor agonist was reported to decrease migration and the invasiveness of cancer growth in breast cancer (Nasser et al., 2011). The precise mechanism through which cannabinoids exert their anticancer effects are not yet completely understood.

#### **1.5.4.6 Cardiovascular Disorders**

The CB<sub>2</sub> receptor was also reported to evoke promising effects in the management of myocardial disorders. The administration of a CB<sub>2</sub> receptor agonist to mice at the end of an ischemic attack, was found to substantially diminish infarct size compared to mice injected with placebo. The agonist also evoked a reduction in the generation of reactive oxygen species and neutrophil infiltration into the infarcted myocardium as well as stimulating the signal transduction pathways responsible for inducing cardio-protection. Additionally, the CB<sub>2</sub> receptor agonist substantially diminished serum levels of the cardiac troponin I; a clinical marker produced from necrotic cardiomyocytes

(Montecucco et al., 2009). Based on preclinical data, the pharmacological mediation of CB<sub>2</sub> receptors was found to possess a therapeutic potential in the management of myocardial infarction. Nonetheless, the efficacious advancement of the promising preclinical data to clinical research still necessitates an enhanced understanding of CB<sub>2</sub> receptor signalling, pharmacology, its therapeutic window in cardiac disorders and the safety of the CB<sub>2</sub> receptor ligands subsequent to chronic administration (Steffens and Pacher, 2012).

#### **1.5.4.7 Multiple Sclerosis**

MS is a multifactorial chronic disease of the CNS comprising multiple components of inflammatory, neurodegeneration and demyelination and is classified as the primary cause of neurological disability in young adults (Docagne et al., 2008). Nabiximols (Sativex®) is composed of an equal ratio of  $\Delta^9$ -tetrahydrocannabinol : cannabidiol in an oromucosal formulation (Rog et al., 2005), and is approved and used in the UK to relieve spasticity and neuropathic pain in MS patients with resistant spasticity. CB<sub>2</sub> receptor agonists ameliorated neurological deficits of MS disease models in mice probably through decreasing microglial activation inducing anti-inflammatory properties, reducing the CD4+ infiltrating T cells into the spinal cord thus, enhancing motor recovery (Arevalo-Martin et al., 2003), tremor and spasticity in diseased mice (Yiangou et al., 2006). Nonetheless, the precise role of CB<sub>2</sub> receptor remains to be fully elucidated to establish the precise pathways and mechanisms triggered by CB<sub>2</sub> receptor in MS to allow the development of novel compounds that target the disease (Mecha et al., 2020).

### 1.5.5 Fenofibrate as a CB<sub>2</sub> Receptor Ligand

Fibrates were first approved and therapeutically used in the USA in 1967 with the introduction of clofibrate, followed by gemfibrozil in the early 1980s and fenofibrate in 1998. Formerly, they were considered the first-line treatment for hypercholesterolemia, where they decreased triglycerides and raised high-density lipoprotein levels, but have taken a back seat with the introduction of statins (3-hydroxy-3-methylglutaryl coenzyme A reductase inhibitors). The fibrate mechanism of action is complex and includes multiple steps in the hydrolysis of lipids; however, they mainly activate PPAR alpha (PPAR $\alpha$ ). PPAR are nuclear receptors that mainly participate in glucose homeostasis, insulin resistance, lipid metabolism, and hypertension and are expressed in greater levels in the kidney, liver, muscle tissue and heart (Backes et al., 2007). Recently, fenofibrate has been recognized as a potent agonist at CB<sub>2</sub> receptors, with a complex action at CB<sub>1</sub> receptors. Fenofibrate possessed relatively high binding affinities - pK<sub>i</sub> values of 6.3 and 7.7 in CB<sub>1</sub> and CB<sub>2</sub> receptors, respectively. Given these findings, and the interactions of fenofibrate with the cannabinoid receptors, this could afford pathways for the advancement of compounds that function as cannabinoid receptor agonists as well as PPAR $\alpha$  ligands (Priestley et al., 2015).

### 1.5.6 Biased agonism of CB<sub>2</sub> Receptors

The theory of “biased agonism” (also known as “functional selectivity” or “ligand-directed trafficking”) is the pharmacological concept that agonists for a certain receptor might selectively and differentially stimulate precise downstream signalling pathways over the others (Urban et al., 2007). Compounds acting as agonists at GPCRs do not consistently stimulate all cellular signal transduction pathways associated with the receptor. Therapeutically, this could possess therapeutic significance in selectively activating pathways that treat certain disorders (Kenakin and Christopoulos, 2013). As an illustration, opioids are effective analgesics that are reported to induce respiratory depression. This respiratory depression side-effect was associated with the stimulation of  $\beta$ -arrestin. Consequently, designing an opioid receptor agonist capable of activating the opioid analgesic pathways while circumventing the activation of the  $\beta$ -arrestin pathway could be anticipated to decrease side effects and respiratory depression (Groer et al., 2007). Oliceridine (TRV130) is a novel  $\mu$ -opioid GPCR biased agonist developed by Trevena Inc. for the management of moderate to severe pain. This analgesic compound is suggested to surpass the traditional morphine as it is anticipated to decrease the respiratory adverse effects by inducing low  $\beta$ -arrestin recruitment to the  $\mu$ -receptor (Singla et al., 2017). Oliceridine acts as a potent analgesic while simultaneously prompting lower incidence of respiratory symptoms and GI events including nausea and vomiting as opposed to morphine (Gan and Wase, 2020). Thus, the compound acquired the FDA approval in August 2020 for short-term IV use in hospital settings for the management of moderate to severe acute pain in adults. Another example of a promising biased ligand effect at GPCRs is the  $\beta$ -adrenergic receptor antagonist carvedilol. Carvedilol is therapeutically used as an antihypertensive in addition to the management of chronic systolic heart failure. Recent investigations revealed that carvedilol acted as a  $\beta$ -arrestin biased ligand at the  $\beta_2$ -adrenergic receptor, activating  $\beta$ -arrestin dependent signalling but not G protein-dependent signalling (Andresen, 2011). Activation of this pathway specifically could introduce a novel approach for the management of frailty, sarcopenia, and muscle wasting secondary to aging or other muscle-wasting disorders. When investigated in murine models, chronic

administration of carvedilol improved the contractile strength of skeletal muscles that is mediated via  $\beta$ -arrestin 1 (Kim et al., 2020). These outcomes indicate a potential unique clinical role of carvedilol in enhancing skeletal muscle contractility while circumventing the adverse effects of  $\beta$ -adrenergic receptor agonists, if proved effective in subsequent clinical trials.

Since the CB<sub>2</sub> receptor has an interesting therapeutic potential, interpreting signalling bias in response to diverse agonists' activation is highly desirable for a comprehensive understanding of its pharmacology and biology. Nonetheless, few studies have reported or investigated the functional selectivity or biased agonism of CB<sub>2</sub> receptor (Atwood et al., 2012). The CB<sub>2</sub> receptor agonists CP55,940 and 2AG were investigated in the different signalling pathways incorporating MAPK stimulation pathway, activation of calcium transients and inhibition of adenylyl cyclase. The authors concluded that CB<sub>2</sub> receptor agonists demonstrated a distinct rank order of potencies and receptor occupancies for controlling intracellular effectors. Thus, providing an indication of the functional selectivity in responses of the cannabinoid receptor agonists acting at CB<sub>2</sub> receptor (Shoemaker et al., 2005) and increasing the capacity and diversity of CB<sub>2</sub> receptor signalling. Moreover, investigation of the CB<sub>2</sub> receptor agonists CP55,940, HU308 and WIN55212-2 in the [<sup>35</sup>S]-GTP $\gamma$ S binding assay, concluded that CP55,940 and HU308 acted as full potent agonists, while WIN55212-2 produced a partial agonist profile (Soethoudt et al., 2017). Additionally, operational analysis of the effects of  $\Delta^9$ -THC at the human CB<sub>2</sub> receptors demonstrated statistically significant bias of the compound towards the ERK signalling pathway as opposed to the  $\beta$ -arrestin and [<sup>35</sup>S]-GTP $\gamma$ S pathways. The signalling bias of the endocannabinoids AEA and 2AG at the CB<sub>2</sub> receptor was also explored, whereby, AEA demonstrated signalling bias towards the ERK pathway over the cAMP. 2AG on the other hand demonstrated substantial bias towards GIRK (Soethoudt et al., 2017).

The theory of functional selectivity could also account for the lack of CB<sub>2</sub> receptor ligands advancing from the preclinical models to clinical trials (Dhopeswarkar and Mackie, 2016) and investigating this ligand bias phenomena could clarify the reason behind CB<sub>2</sub> receptor agonists failing in clinical trials. Furthermore, the CB<sub>2</sub> receptor agonists HU308 and HU910

demonstrated differences in their signalling profiles between human and mouse CB<sub>2</sub> receptor, such that both compounds behaved as well-balanced agonists devoid of any substantial bias towards any signalling pathway in the human CB<sub>2</sub> receptor. Nevertheless, both HU308 and HU910 produced profound bias towards the  $\beta$ -arrestin and cAMP pathways in mouse CB<sub>2</sub> receptor. Thus, these outcomes of interspecies differences in signalling preference for the translation of preclinical to clinical models should predominantly be considered during the investigations of novel CB<sub>2</sub> receptor ligands (Soethoudt et al., 2017). There is still a broad field to be investigated in identifying and establishing the functional selectivity of CB<sub>2</sub> receptors that remains to be investigated and accounted for. While this remains an attractive hypothesis and despite the identification of multiple biased agonists possessing promising *in vitro* profiles, their therapeutic benefit *in vivo* is not yet confirmed (Kenakin and Christopoulos, 2013).

## 1.6 Aims of the project

- To establish a high-throughput screening assay for human recombinant ABHD6 activity
- To characterise the signalling of fenofibrate and its amide analogues as ligands at human CB<sub>2</sub> cannabinoid receptors
- To investigate agonist bias at the cannabinoid CB<sub>2</sub> receptor by commercially available CB<sub>2</sub>-selective agonists
- To investigate the contribution of the hydrophobic amino acids Phe117, Phe200, Trp258 towards function and signalling of the cannabinoid CB<sub>2</sub> receptor

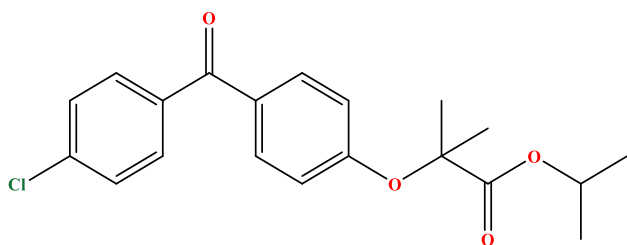
## Chapter 2 : Materials and Methods

### 2.1 Materials and Reagents

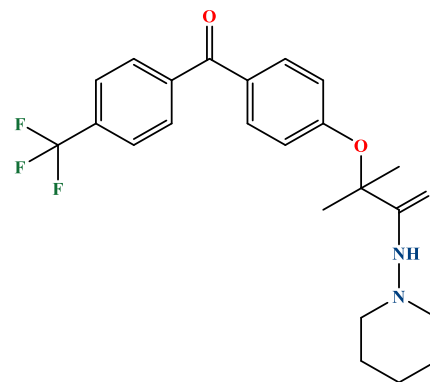
The Chinese Hamster Ovary (CHO) cell line stably expressing human CB<sub>2</sub> receptors and the CHO-K1 cells were obtained from Pfizer Neusentis Ltd (Cambridge, UK) and the HeLa cell line was a kind donation of the FRAME laboratory. The investigated compounds were as follows; fenofibrate and AM630 were obtained from Sigma-Aldrich Chemical Company, UK and the investigated ligands FD24, FD43, FD44 and FD46 were prepared at the Centre of Biomolecular Sciences, University of Nottingham. The compounds SER601, COR170, CB65, GP2a, GW405833, HU308, L759656 and MDA19 were obtained from Tocris Bioscience.

All cannabinoid ligands were dissolved in absolute ethanol at a concentration of 10 mM, except for the FD series which were dispersed in dimethyl sulfoxide (DMSO), aliquotted and stored at -20°C to avoid excessive freeze and thaw cycles. The final concentration of ethanol and DMSO in all of the investigated assays were confirmed to not exceed 0.1% (v/v). The structures of the investigated ligands are identified in table 2.1. and any other materials used in the performed experiments are mentioned through the text along with their sources.

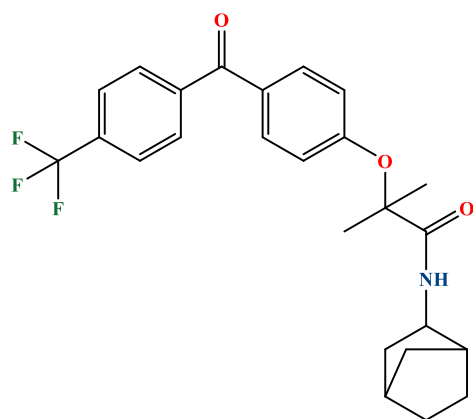
Table 2.1 Structures of the investigated compounds



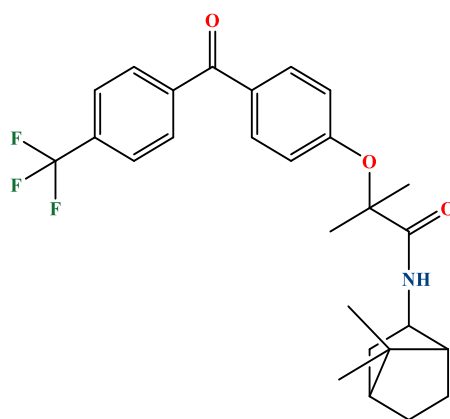
**Fenofibrate**



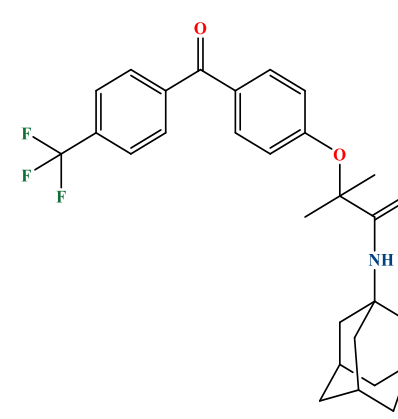
**FD24**



**FD43**

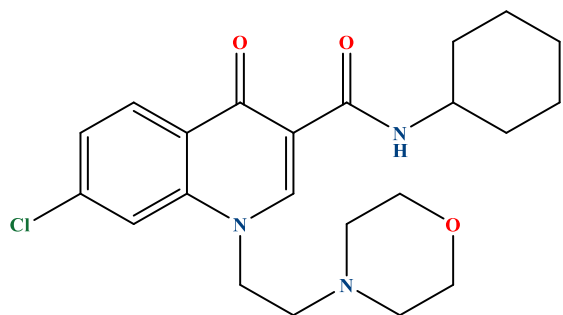


**FD44**

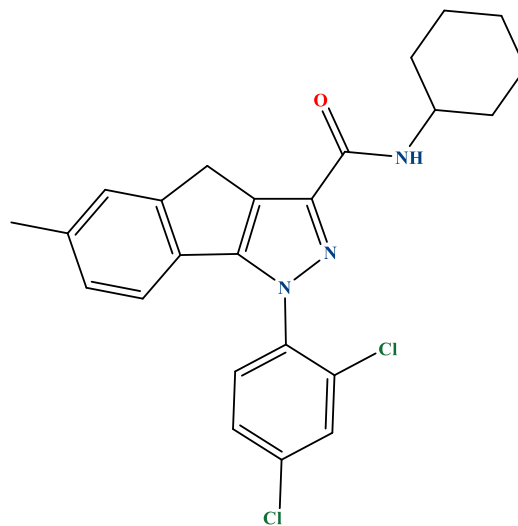


**FD46**

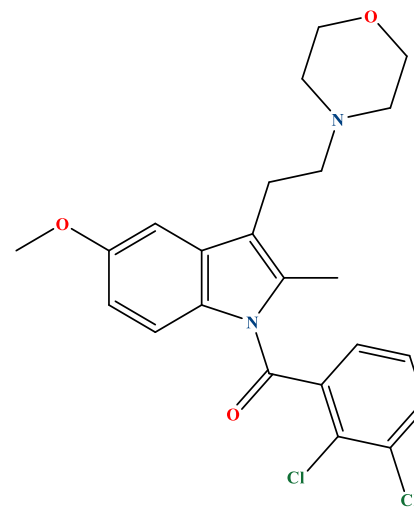
Table 2.1 Structures of the investigated compounds



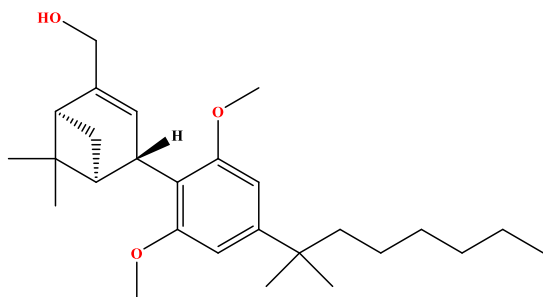
**CB65**



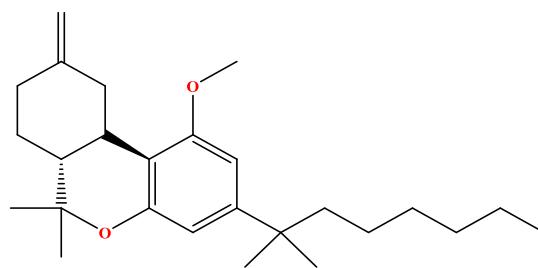
**GP2a**



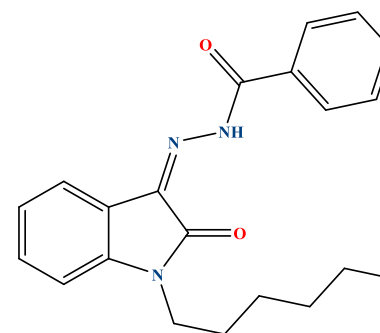
**GW405833**



**HU308**

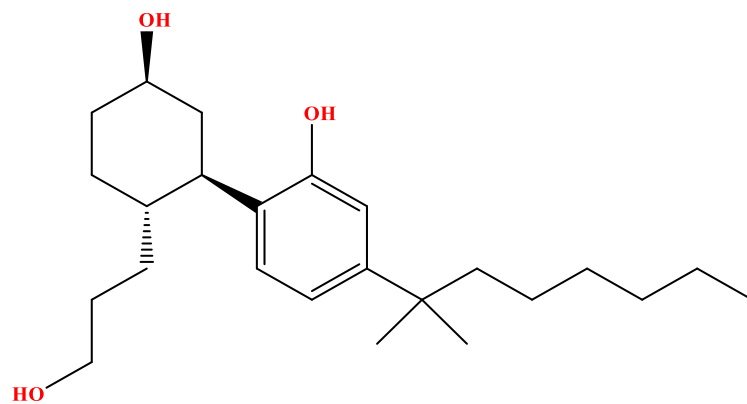


**L759656**

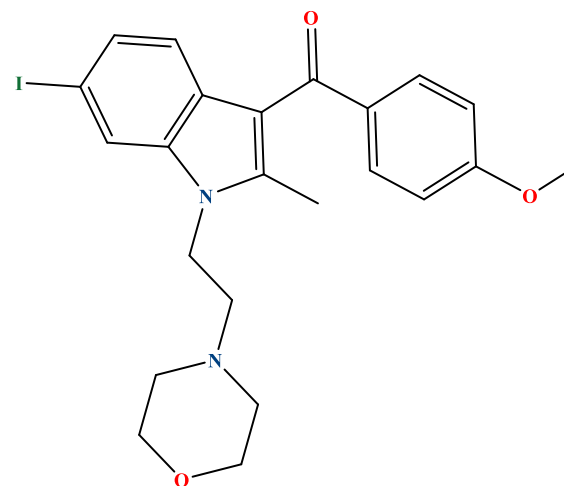


**MDA19**

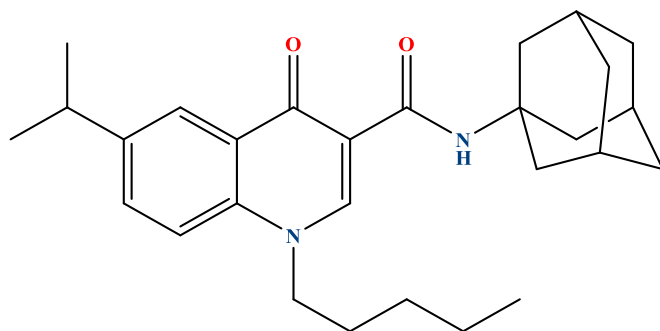
Table 2.1 Structures of the investigated compounds



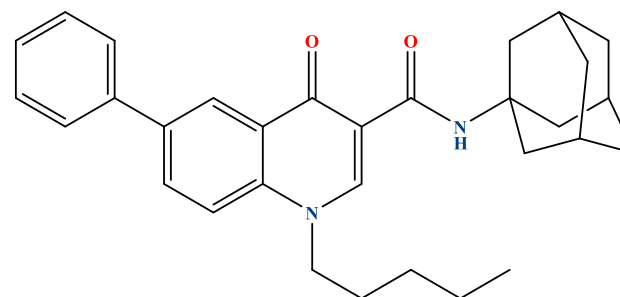
**CP55,940**



**AM630**



**SER601**



**COR170**

## 2.2 ABHD6 Enzyme Assay

Unless otherwise indicated, all of the chemicals utilized in the optimization of a high throughput ABHD6 screening assay were obtained from (Sigma-Aldrich) while the substrates 1-OG, 2AG, 2-OG and 2-PG were obtained from Tocris Bioscience. Human embryonic kidney cells (HEK293) cell line transiently expressing the human recombinant ABHD6 (prepared by Nada Mahmoud) were utilized in all of the conducted experiments. Particulate and soluble fractions were prepared fresh and then stored at  $-80^{\circ}\text{C}$  in the form of aliquots thawed only on the assay day. Tissues including small and large intestine, as well as the hippocampus, were obtained from male and female Wistar rats and stored in Tris/EDTA (50 : 1mM) buffer at  $\text{pH} = 7.4$  as aliquots at  $-80^{\circ}\text{C}$  and only defrosted upon use.

This esterase assay was based upon the quantification of the fluorescence product 4-methylumbelliferone upon hydrolysis of the fluorogenic substrate 4-methylumbelliferylheptanoate (Gilham and Lehner, 2005) . A total reaction volume of 100  $\mu\text{L}$  and 50  $\mu\text{M}$  final concentration of MUH (based on pilot experiments) was used in all experiments. With respect to experiments aimed at determining substrate affinity and maximal rates of hydrolysis, a range of 4-MUH concentrations was used with the top concentration at 500  $\mu\text{M}$ . The generated fluorescence was measured at excitation/ emission wavelengths of 355nm/ 460nm continuously for up to 90 min via the Fluoroskan<sup>TM</sup> Microplate Fluorometer (ThermoFisher Scientific) at  $37^{\circ}\text{C}$ . Compound screening was conducted with potential inhibitors pre-incubated at 1  $\mu\text{M}$  final concentration with the enzyme preparations for 15 min, where indicated, at  $37^{\circ}\text{C}$  followed by the addition of 50  $\mu\text{M}$  4-MUH. This was followed by 60 min incubation on a temperature-controlled shaker at  $37^{\circ}\text{C}$  and the fluorescence was measured as a single endpoint.

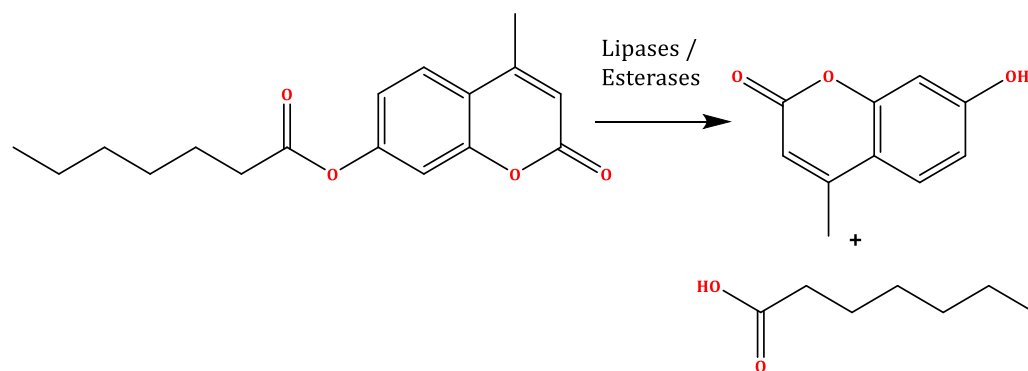


Figure 2.1 Cleavage of the 4-MUH ester bond produces the fluorescent compound 4-methylumbelliferone detected via the Fluoroskan™ at  $\lambda_{ex}$  355nm;  $\lambda_{em}$  460nm and the by-product, heptanoic acid.

### 2.2.1 Statistical Data Analysis

Data obtained from the Fluoroskan™ plate reader in the form of Relative Fluorescence Units (RFU) were analysed using Graph-Pad Prism 8.0. A single-blind study was conducted for experiments involving the use of multiple inhibitors/alternative substrates which were analysed by one-way ANOVA followed by Dunnett's multiple comparison test. Thereafter, the compound coding was deciphered by Dr Steve Alexander.

## 2.3 Cell Culture

### 2.3.1 Cell Passaging

CHO-CB<sub>2</sub> cells stably expressing human CB<sub>2</sub> receptors were utilized with the passage range 28-45; all of the cell culture investigations were performed in a completely aseptic environment within class II sterile laminar flow hoods (Thermo-Scientific, UK) and all cell culture reagents were warmed up to 37°C before use. Splitting was performed every 48 h with cells incubated at 37°C, 5% CO<sub>2</sub> and high humidity until they approached ≈95% confluency. Cell culture was performed in canted 75 cm<sup>2</sup> Costar Corning® (Flintshire, UK) sterile culture flasks using Dulbecco's Modified Eagle's Medium/Nutrient Mixture F-12 Ham (DME/F-12, Sigma-Aldrich) fortified with 2 mM L-glutamine solution (Sigma-Aldrich), 10% sterile fetal bovine serum (FBS, Sigma-Aldrich) and 400 µg/mL G418 sulfate; Geneticin® (Calbiochem) selection antibiotic. Monolayers were initially washed using Dulbecco's phosphate buffered saline (PBS, Sigma-Aldrich) and incubated with 2 mL 1X Trypsin-EDTA (Sigma-Aldrich), for two min at 37°C to allow cell detachment from the flasks. It was ensured that trypsinization of the cells did not surpass 2-3 min to prevent harming the cell line by stripping the cell surface CB<sub>2</sub> receptors and killing off the cells. Following incubation, cells were displaced from their monolayer by mild tapping of the flask and the addition of 8 mL DME/F-12 to deactivate trypsin. The wall of the 75 cm<sup>2</sup> flask was triturated with a pipette several times and the cell mixture was transferred to an aseptic 30 mL universal tube (Starlab) and the cell suspension was centrifuged at 1000 rpm for five min in a Centaur 2 benchtop centrifuge (MSE, DJB Labcare Ltd). The supernatant was aspirated and the retrieved cell pellet was resuspended in 5 mL fresh DME/F-12 and 500 µL of the freshly resuspended cell suspension were added to a fresh 75 cm<sup>2</sup> flask containing 15 mL fresh culture medium; for a subculture ratio of 1:10 and 400 µg/mL G418 sulfate antibiotic and the flasks were incubated as previously mentioned.

The sub culturing of CHO-K1 was performed as stated above without the use of the G418 sulfate selection antibiotic at a subculture ratio of

1:10 every 48 h. The HeLa cells were also cultured in a similar manner, but the medium used was Minimum Essential Medium Eagle (MEM, Sigma-Aldrich) at a subculture ratio of 1:5 every 48-72 h in 175 cm<sup>2</sup> Costar Corning® (Flintshire, UK) sterile culture flasks containing 30 mL of fresh MEM and similarly, no selection antibiotic was used.

### **2.3.2 Cryopreservation and Thawing of cell lines**

With respect to the freezing of the cells for subsequent usage, the aforementioned protocol was performed, until the step of resuspension of the cell pellet. After confirming that the cells possessed a viability that was greater than 90%, and that the concentration of the live cells was between 1-2 x 10<sup>6</sup> cells per mL, the final cell pellet was suspended in the previously prepared, pre-warmed freezing solution composed of 10% (v/v) DMSO and 90% FBS. Consequently, 1 mL aliquots were moved to 1.2 mL Nalgene® sterile cryogenic vials (Sigma-Aldrich). The cryogenic vials were then arranged in Corning CoolCell Freezing® polystyrene freezing container (Cole-Parmer® scientific experts, UK) which regulates the freezing rate to be -1°C per minute. This is predominant to prevent cell damage since the rate of freezing imposes considerable influence on cell viability. The freezing container was retained at -80°C for at least 24 h before being transferred to polypropylene cryobox (Fisherband™, Fisher Scientific, UK) and stored in a liquid nitrogen tank for future use. This gradual cell freezing was predominant in producing reproducible and consistent cell cryopreservation. When the cells were required, the cryovials were removed from the liquid nitrogen tank and recovered by rapid thawing of the cryovial in a 37°C maintained water-bath with gentle swirling of the vial while ensuring that the cap was outside the water bath for 2-5 min. The contents of the vial were then added to an aseptic 30 mL falcon tube containing 5 mL fresh medium which was centrifuged at 1000 rpm for 5 min. The supernatant layer was discarded, and the obtained cell pellet was suspended in 5 mL fresh medium and added to a 75 cm<sup>2</sup> flask comprising 10 mL fresh DME/F-12 and incubated as aforementioned. This step was essential to eliminate the 10% DMSO in which the cells were frozen. Cells were sub-cultured for three passages before being used in the performed assays.

### 2.3.3 Cell counting and cell seeding

In order to check cell viability or the concentration of live cells, 10  $\mu\text{L}$  of the cell suspension was thoroughly mixed with 10  $\mu\text{L}$  of Trypan Blue Dye 0.4% sterile-filtered solution (Bio-Rad) in an autoclaved 1.5 mL Eppendorf (Eppendorf® UK Ltd) (1:1) ratio. 10  $\mu\text{L}$  of the well-mixed mixture was dispensed to one chamber of the cell counting slides TC10™ dual chamber slides (Bio-Rad). The slide was then loaded into the TC20™ automated cell counter (Bio-Rad) and the total cell concentration, live cell concentration per mL and viability are displayed on the screen. The dilution calculator was subsequently used in order to obtain the desired cell density for seeding into the relevant plates and wells. After appropriate mixing of the prepared dilution of sample suspension, the prepared suspension was poured into 50 mL sterile reagent reservoir (Corning Incorporated Costar®, UK) in order to seed the respective plates.

Table 2.2 Seeding densities for the cell lines employed

Culture Vessel	Growth Surface Area	Seeding Density	Total Medium Volume
<b>CHO-CB<sub>2</sub></b>			
75 cm <sup>2</sup> flask	75 cm <sup>2</sup>	2-3 * 10 <sup>6</sup>	15 mL
175 cm <sup>2</sup> flask	175 cm <sup>2</sup>	4-5 * 10 <sup>6</sup>	30 mL
24-well plate	1.90 cm <sup>2</sup>	2.5 * 10 <sup>5</sup>	2 mL
96-well plate	0.32 cm <sup>2</sup>	2-3 * 10 <sup>5</sup>	200 $\mu\text{L}$
<b>CHO-K1</b>			
75 cm <sup>2</sup> flask	75 cm <sup>2</sup>	2-3 * 10 <sup>6</sup>	15 mL
6-well plate	9.40 cm <sup>2</sup>	1.0 * 10 <sup>6</sup>	2 mL
24-well plate	1.90 cm <sup>2</sup>	2.5 * 10 <sup>5</sup>	2 mL
96-well plate	0.32 cm <sup>2</sup>	3.0 * 10 <sup>5</sup>	200 $\mu\text{L}$
<b>HeLa</b>			
175 cm <sup>2</sup> flask	175 cm <sup>2</sup>	5-6 * 10 <sup>6</sup>	30 mL
6-well plate	9.40 cm <sup>2</sup>	2.5 * 10 <sup>6</sup>	2 mL
96-well plate	0.32 cm <sup>2</sup>	3.5 * 10 <sup>5</sup>	200 $\mu\text{L}$

### 2.3.4 Generation and maintenance of transfected cell lines using XtremeGENE Reagent

CHO-K1 and HeLa cells were seeded into the appropriate culture vessel that was going to be subsequently used at the seeding density displayed in Table 2.2 for 24 hours. Following incubation and at 70-80% confluency of the respective cell lines, the cells were transfected using the relevant DNA plasmids and the transfection reagent X-tremeGENE (Roche, Germany).

Table 2.3 Seeding and transfection conditions used

<b>Culture Vessel</b>	<b>Seeding Density</b>	<b>DNA added per well (1:1) Ratio</b>	<b>Transfection complex per well</b>
6-well plate	$1.0-2.5 * 10^6$	2 $\mu\text{g}$	200 $\mu\text{L}$
24-well plate	$2.5 * 10^5$	0.5 $\mu\text{g}$	50 $\mu\text{L}$
96-well plate	$2.0-3.5 * 10^5$	0.1 $\mu\text{g}$	10 $\mu\text{L}$

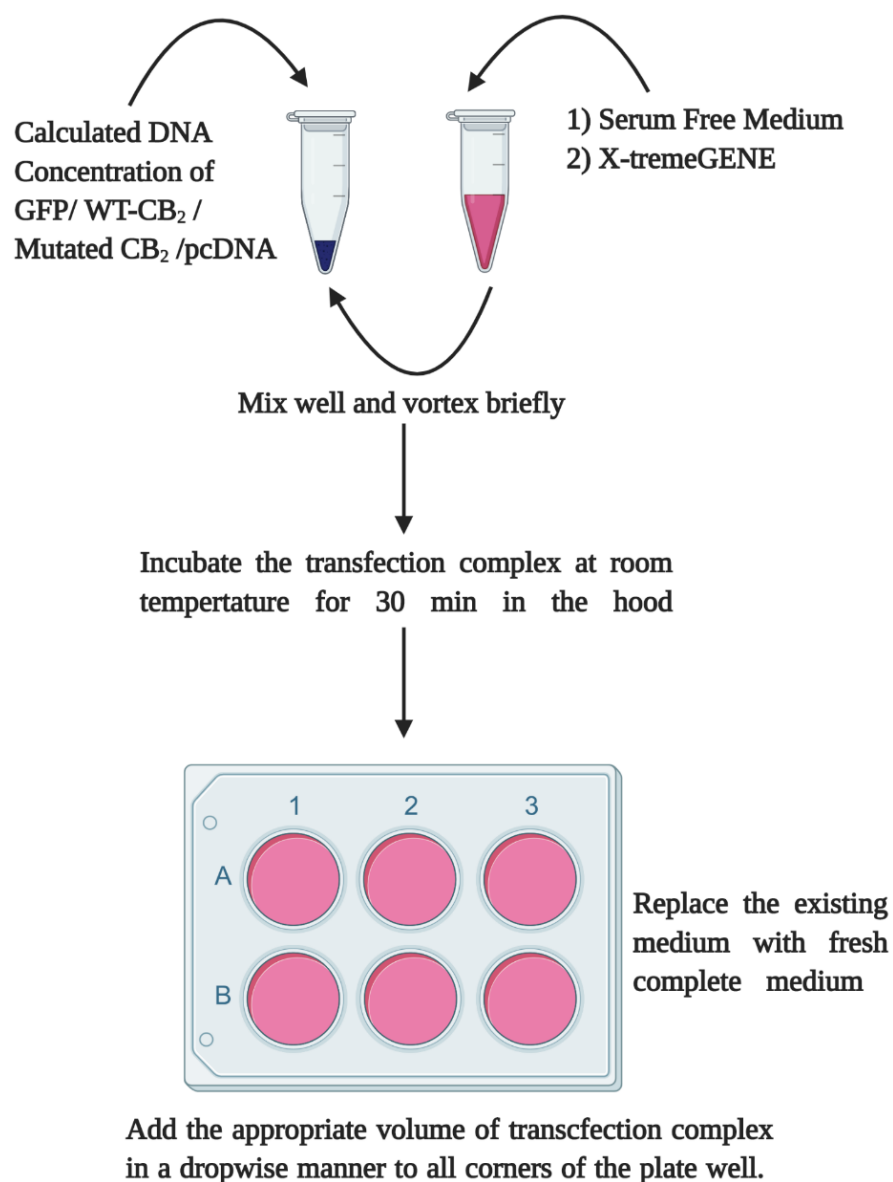


Figure 2.2 The transfection procedure followed using X-tremeGENE

As a control, CHO-K1 cells were transfected with green fluorescence protein (GFP, donated from the FRAME Lab) in order to determine the appropriate transfection ratio and to select the appropriate transfection time point (24 vs 48 h). Fluorescent cells were viewed under the Zeiss Axiovert S100 fluorescent microscope. Following transfection of CHO-K1 and HeLa cells with the mutated CB<sub>2</sub> receptor DNA plasmids F117A, F200A, W258A, cells were harvested after 24-48 h with fresh medium changed in between or functional assays were performed on the transiently transfected cell line after 48 h of transfection.

Harvesting of the 6-well plate involved initial aspiration of the medium, and then plate wells were washed once with ice-cold PBS. The plate wells were harvested in PBS using cell scraper (Corning™ Cell Scraper, Fisher scientific) and washed three times in ice cold PBS. The cell suspension was collected in 1.5 mL Eppendorf tubes and preserved on ice. The tubes were then centrifuged for 5 min at 1000 rpm and 4°C in a refrigerated benchtop centrifuge (Eppendorf®, Fisher Scientific) and washed with fresh PBS three times. After the last wash, the PBS supernatant layer was discarded, and the residual pellet was suspended in 100 – 300 µL radioimmunoprecipitation assay buffer (RIPA) lysis buffer ([2.4.2](#)) depending on the pellet size for membrane homogenates used in immunoblotting only. The cell suspension was subsequently homogenised via the benchtop ultrasonic disintegrator Soniprep 150® (MSE, UK). The disintegrator probe was initially cleaned using 70% alcohol followed by distilled water. Samples were placed in the probe and disintegrated at the lowest amplitude for 10 s followed by placing the samples on ice for 10 s. This was performed in three cycles and the samples were subsequently placed on an Eppendorf roller drum (Stuart™ Rotator Disk, Fisher Scientific) in the cold room for 45 min to ensure gentle yet effective mixing of the samples. The samples were then centrifuged at 30,000 g at 4°C for 15 min to get rid of any debris. The supernatant layer was moved to fresh 1.5 mL Eppendorf tubes and the protein concentration was determined using a [Lowry Assay](#) and the protein homogenates were retained at -80°C until use.

## 2.4 Western Blotting

### 2.4.1 Gel Preparation: 10% SDS-Polyacrylamide Gel

10% SDS-PAGE gels composed of resolving and stacking gels was used in immunoblotting. The components of the resolving gel and stacking gel were thoroughly mixed in the same order stated in Table 2.4. This was pertinent since the addition of TEMED and ammonium persulphate induced gel polymerization. Instantly following the appropriate mixing of the resolving gel components, the solution was briefly vortexed and poured instantly into the 1.0 mm glass cast (Bio-Rad) fitted into the casting stand (Bio-Rad) and situated into sandwich clamp assemblies (Bio-Rad). It was essential to confirm that the resolving gel was added 0.5 - 2 cm beneath the base of the comb teeth (1.0 mm comb, Bio-Rad). Isopropanol (Fisher Scientific) was placed above the resolving gel in order to ensure that the resolving gel polymerized uniformly and to eliminate any bubbles. After 30-45 min, isopropanol was discarded, and any traces of isopropanol were aptly washed with water and excess water was carefully dried out using Whatman™ filter paper (Fisher Scientific). The components of the stacking gel were mixed well, vortexed and added above the resolving gel with the 1.0 mm comb inserted instantaneously into the stacking gel. The gel polymerised within 30 min and was used on the same day of preparation or stored in 1X running buffer at 4°C for up to one week.

Table 2.4 Composition of 10% SDS-Polyacrylamide Gel Electrophoresis (Harlow and Lane, 1988)

Chemical	Volume (mL)	Manufacturer
<b>Resolving Gel: 10 mL</b>		
Distilled Water	4.0	
30% Acrylamide / Bis-acrylamide (29:1)	3.3	Bio-Rad
1.5 M Tris (pH 8.8)	2.5	Sigma-Aldrich
10% Sodium Dodecyl Sulphate (SDS)	0.1	Acros Organics
10% Ammonium persulphate	0.1	Sigma-Aldrich
<i>N, N, N', N'</i> -Tetramethyl ethylenediamine (TEMED)	0.004	Sigma-Aldrich

<b>Stacking Gel: 3 mL</b>		
Distilled Water	2.1	
30% Acrylamide/Bis-acrylamide	0.5	Bio-Rad
1.0 M Tris (pH 6.8)	0.38	Sigma-Aldrich
10% SDS	0.03	Acros Organics
10% Ammonium persulphate	0.03	Sigma-Aldrich
TEMED	0.003	Sigma-Aldrich

Table 2.5 Buffers used in immunoblotting

<b>Buffers Used</b>	<b>Recipe</b>
Running Buffer	25 mM Trizma® base (Sigma-Aldrich), 0.1% SDS and 190 mM glycine (Fisher Scientific)
Transfer Buffer	25 mM Trizma® base, 190 mM glycine and 20% methanol (Fisher Scientific)
TBST	20 mM Trizma® base, 150 mM NaCl (Fisher Scientific) and 0.1% Tween® 20 (Bio-Rad)

Table 2.6 Antibodies used in immunoblotting

<b>Antibody</b>	<b>Band size</b>	<b>Host</b>	<b>Dilution</b>	<b>Source</b>	<b>Code</b>
$\alpha$ -Tubulin	50 kDa	Mouse	1:5000	Sigma-Aldrich	T9026
$\beta$ -Actin	42 kDa	Mouse	1:5000	Sigma-Aldrich	A5441
<b>Primary Antibody</b>					
CNR2 Polyclonal Antibody	~60 kDa	Rabbit	1:500	ThermoFisher Scientific	PA1-744
CB <sub>2</sub> Monoclonal Antibody (C37)	62 kDa	Mouse	1:500	Santa Cruz Biotechnology	Sc-293188
FLAG Tag		Mouse	1:20,000	Sigma-Aldrich	F3165
<b>Secondary Antibody</b>					
IRDye® 680RD Goat anti-mouse IgG		Mouse	1:3000	Licor® Biosciences	925-68070
IRDye® 800CW Goat anti-Rabbit IgG		Rabbit	1:3000	Licor® Biosciences	926-32219

## 2.4.2 RIPA Buffer

The RIPA buffer comprised 150 mM NaCl, 25 mM Tris-HCl (Sigma-Aldrich), 1% Triton X-100 (Sigma-Aldrich), 1% sodium deoxycholate (Sigma-Aldrich), 0.1% SDS and 1x EDTA-free protease inhibitor cocktail (Roche). The protease inhibitor cocktail was prepared as 25x stock in advance, aliquotted as 100  $\mu$ L, stored at  $-20^{\circ}\text{C}$  and was mixed with RIPA buffer prior use only. It was ensured that both RIPA and the protease inhibitor cocktail were used within three months of preparation.

## 2.4.3 Immunoblotting

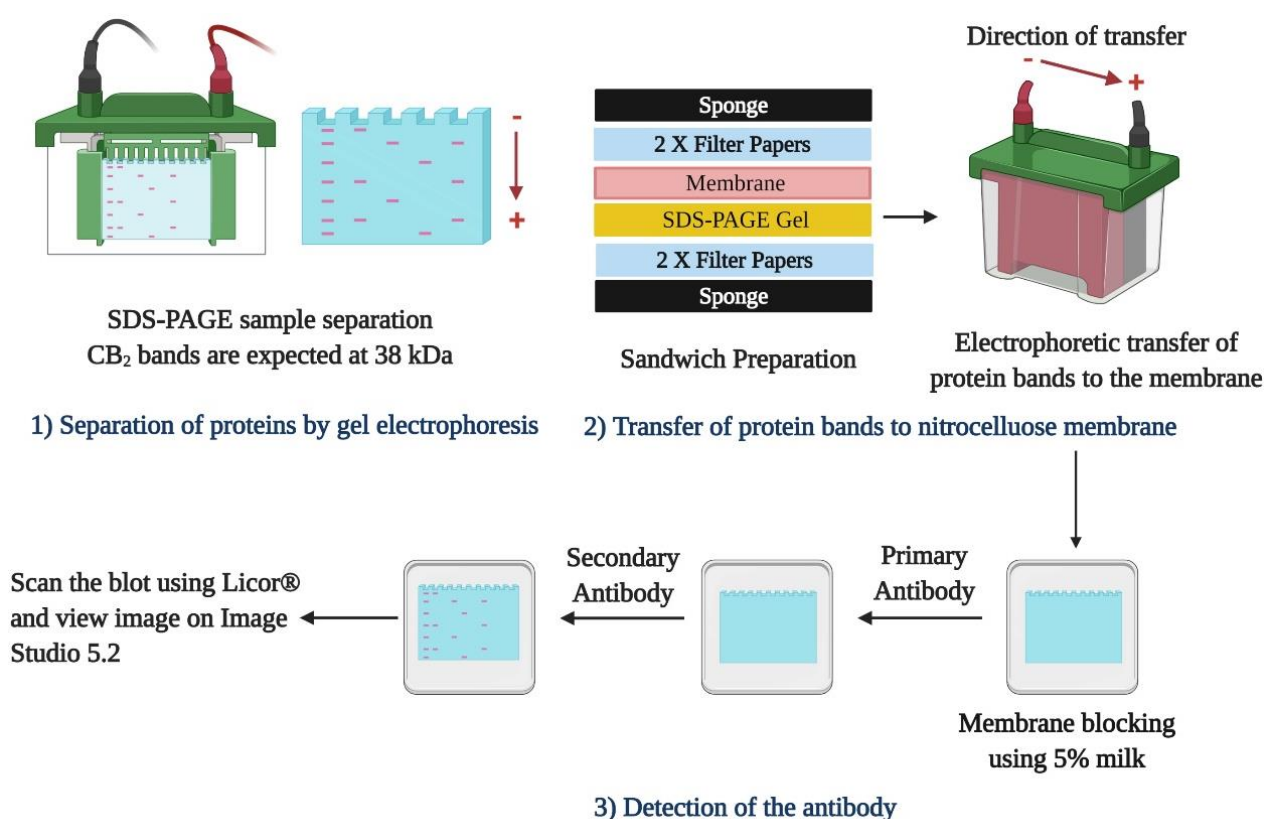


Figure 2.3 The three main steps involved in immunoblotting

Immunoblotting was performed to confirm expression of the wildtype and mutated CB<sub>2</sub> receptor and to determine the appropriate transfection ratio and time point. The samples prepared following transfection and harvesting (2.3.4) were initially mixed with 6X Laemmli SDS buffer (Fisher Scientific) and heated at  $95^{\circ}\text{C}$  for 5 min in order to disrupt and linearise the proteins for SDS-

PAGE electrophoresis. Equal amounts of protein lysates and protein ladder (PageRuler™ Plus Prestained Protein Ladder, Thermo Scientific) were added to separate wells in the previously prepared 10% SDS-PAGE gel assembled in an electrophoresis unit (Mini-Protean® II electrophoresis cell, Bio-Rad) and loaded with running buffer. The assembled electrophoresis unit was covered with the lid, ensuring the accurate orientation of the plugs with the electric jacks. The samples were run at 100 V for 15 min in order to allow the samples to run through the stacking gel followed by another run at 200V for 45 min to further induce the running of the samples through the resolving gel.

The existing running buffer was discarded and replaced with transfer buffer along with a cooling unit of ice block placed in the tank. The proteins were then electrophoretically transferred onto the nitrocellulose membrane (0.45 µm pore size, Amersham™ Protran) to immobilise them. All of the equipment used in the transfer were initially equilibrated with transfer buffer for 10 min before use, including the sponge, filter paper, nitrocellulose membrane and the roller. The gel was positioned in immediate proximity with nitrocellulose membrane and sandwiched between filter paper in a specific order (sponge, filter paper, gel with the separated protein bands, nitrocellulose membrane, filter paper, sponge) while simultaneously confirming that any bubbles were rolled out following each layer addition. Transfer was performed at 300 A for 90 min which transferred the membrane homogenates from the SDS-PAGE gel onto the membrane and rapid reversible staining using 1:10 Ponceau S (Sigma-Aldrich) was done to validate transfer efficiency. Subsequent to the confirmation the presence of the protein bands, the membrane was washed with deionized water until clear. The membrane was subsequently incubated with blocking buffer composed of 5% milk (dried skimmed milk, Marvel®, UK) in TBST in an adequate volume to completely envelope the membrane with gentle agitation (Stuart Scientific STR6 platform shaker, UK) at room temperature for 1 h. Subsequent to blocking any non-specific antibody binding, the membrane was incubated in a 50 mL universal centrifuge tube (Camlab Ltd, UK) incorporating 5% milk and the primary antibody (Table 2.6) on a roller (Stuart™ Analogue tube roller, Fisher Scientific, UK) at 4°C overnight.

The following day, the primary antibody was discarded, and the membrane was rinsed three times in TBST for 10 min with gentle agitation at room temperature to eliminate residual non-specific background signal. Subsequent to the appropriate washing steps, the blot was incubated with the IRDye® secondary antibodies (Table 2.6) in 5% milk covered with foil for 1 h at ambient temperature on the orbital shaker. After 1-h incubation, the secondary antibodies were removed, and the blot was rinsed again as performed formerly. The blots were scanned using an Odyssey Infrared Imaging System 3.0 (Licor, Inc) via the Image studio software version 5.2. The blots were rolled appropriately on the scanner to ensure that there were no bubbles introduced in the system. The Image studio settings were adjusted to resolution 169, 0.5 mm focus offset, medium quality, intensity 5 and confirmed that both 700 and 800 channels were switched on.

## 2.5 Preparation of Cellular Homogenates

CHO-CB<sub>2</sub> cells were cultured as in [Section 2.3.1](#), but in 175 cm<sup>2</sup> flasks rather than the conventional 75-cm<sup>2</sup> flasks. Once they approached 95-100% confluency, the flasks were washed once with ice-cold PBS supplemented with 2 mM ethylenediamine tetraacetic acid (EDTA, VWR Chemicals BDH®, US) and the cells were scraped off utilizing the cell scraper and transferred to 50 mL universal tube. The cell pellet was subsequently collected by centrifugation at 200 g for 5 min discarding the supernatant. All of the subsequent steps were performed at 0 - 4°C to avoid protein degradation. The collected homogenates were suspended again in ice-cold homogenisation buffer composed of 50 mM Tris, 2 mM EDTA, pH 7.4 and homogenized in a 2 mL Polytron homogenizer (Cole-Parmer PTFE Tissue Grinder, Glass vessel) in an overhead stirrer (Heidolph RZR 2021 overhead stirrer, Heidolph Instruments GmbH, Germany) for 10 s over three cycles with intermittently placing the protein lysates on ice for 10 s. The suspension was centrifuged at 30,000 x g for 10 min in a pre-cooled centrifuge at 4°C (Harrier 18/80 MSE, refrigerated centrifuge, UK) and the supernatant was removed. The obtained pellet was re-suspended in fresh homogenization buffer followed by centrifugation twice. The final membrane pellet was dispersed in fresh homogenization buffer and the protein

concentration was quantified via the [Lowry protein assay](#). The protein lysates were re-adjusted to 1 mg/mL and aliquoted, stored at -80°C and used within three months of preparation.

## **2.6 Determination of Protein Concentration**

Both protein lysates prepared in RIPA buffer and using the conventional TRIS-EDTA buffer were quantified using the same protocol. Serial dilutions of Bovine Serum Albumin (BSA, Sigma-Aldrich) were prepared from a stock concentration of 1 mg/mL, where dilutions of BSA were prepared commencing from 0.45 mg/mL decreasing to 0.05 mg/mL alongside membrane dilutions of 1:20 in Lowry reagent. The Lowry reagent was composed of 200 mM Na<sub>2</sub>CO<sub>3</sub> (VWR BDH chemicals, UK), 100 mM NaOH (Fisher Scientific), 7 mM SDS (Acros Organics, UK), 0.005% NaK Tartrate (VWR BDH chemicals) and 0.0025% CuSO<sub>4</sub> (Fisher Scientific) was added to all serial dilutions of BSA and membranes followed by 10 min incubation at ambient temperature. In the meantime, a solution of 1:1 Folin phenol reagent (Folin & Ciocalteu's phenol, Sigma-Aldrich) to distilled water was prepared and added to all samples and incubated for 45-90 min at ambient temperature and the protein homogenates were covered with foil. The samples were vortexed appropriately and added to a clear Costar® 96-well plate at a volume of 200 µL in triplicates. The plate was read at an absorbance at 750 nm using a spectrophotometric plate reader (SpectraMax M2/M2e microplate reader, Molecular Devices, USA) and the protein concentrations were converted to mg/mL using SoftMaxPro 7.0 calculated on the standard curve of BSA.

## 2.7 Calcium Mobilization Assay

### 2.7.1 Preparation of HEPES Buffer

HEPES buffer was prepared and used within one month of preparation composed of 2 mM sodium pyruvate (Fluka analytical®, Germany), 137 mM NaCl, 10 mM D-glucose (Fisher Scientific), 5.4 mM KCl (VWR BDH chemicals), 1 mM MgSO<sub>4</sub>·7H<sub>2</sub>O (Fisher Scientific), 1.3 mM CaCl<sub>2</sub> (Fisher Scientific), 1.5 mM NaHCO<sub>3</sub> (VWR BDH chemicals), 10 mM HEPES (Fisher Scientific) and 2.5 mM probenecid (Sigma-Aldrich) and the pH was adjusted to 7.45 via 1M NaOH. D-glucose and probenecid were added to the required volume of buffer to be used fresh on the assay itself.

### 2.7.2 Assay Procedure

Costar black-walled, clear bottom 96-well plates (Corning®, Flintshire, UK) were seeded for 24 h at 37°C, 5% CO<sub>2</sub> and high humidity at a seeding density of 40,000 cells/well and 200 µL/well. After seeding the plates, they were placed in the hood for 30-45 min at room temperature to minimize the edge-effect, before being placed in the incubator. On the assay day, a stock solution of 1 mM Fluo-4 dye (Fluo-4 AM cell permeant, ThermoFisher Scientific) was prepared using equivalent volumes of sterile DMSO (Sigma-Aldrich) and pluronic F-127 (Pluronic™ F-127 20% solution in DMSO, ThermoFisher Scientific) to enhance the solubility of the dye and used within one week. A stock solution of 250 mM probenecid was also made up using equivalent volumes of 1 M NaOH and HEPES buffer (2.7.1) to counteract cellular extrusion of the fluo-4 dye and was prepared on the assay day itself. Following the 24-h incubation, the existing medium was aspirated and substituted with fresh medium composed of 2.5 mM probenecid (an inorganic anion transporter inhibitor) and 2.26 µM fluo-4 dye which allows the detection of changes in intracellular calcium levels. 100 µL of this freshly prepared solution was added per well, and the plate was covered with aluminum foil to shield the light sensitive dye and incubated for 50 min at 37°C, 5% CO<sub>2</sub> and high humidity.

During the incubation period, ligand dilutions were prepared using HEPES buffer at 6-fold the desired final concentration and plated in the compound plate; 96-well plate U-Bottom (Corning®, Flintshire, UK). 10  $\mu$ M adenosine 5'-triphosphate disodium salt hydrate (ATP, Sigma-Aldrich) was used as the positive control to ensure that the cells responded appropriately and was used for normalizing data between experiments. After the 50 min incubation period, the dye was aspirated and the wells were washed once using 100  $\mu$ L HEPES and consequently, 100  $\mu$ L HEPES were added per well and incubated for 20 min at 37°C and 0% CO<sub>2</sub>. Both the assay and the compound plates were placed in the FlexStation 3 Multi-Mode Microplate Reader (Molecular Devices, USA) for 10 and 5 min, respectively, prior to commencing with the measurement of the intracellular calcium influx. The intracellular calcium release was recorded on the SOFTmax® PRO software following the transfer of 20  $\mu$ L ligand from the compound plate and their addition to the assay plate at 15 s intervals at 37°C by FlexStation 3. Baseline readings were initially recorded for 15-20 s before commencing with the actual calcium influx readings.

Table 2.7 Settings applied in SoftMax Pro for calcium FlexStation 3

<b>Reading Mode: Fluorescence (Flex Mode)</b>	
Wavelengths	Excitation: 485
	Emission: 520
	Cut off: Auto (515)
Time Settings	Time: 120 s
	Interval: 1.52 s
	Reads: 79
	Minimum Interval: 1.52s
	Minimum Run Time: 37s
Sensitivity	High
Assay Plate	96-well Costar blk/clr btm
Compound Plate	96-well Costar Ubt clear 3 mL
<b>Compound Transfer</b>	
Initial Volume	100 $\mu$ L
Pipette Height	50 $\mu$ L
Pipette Volume	20 $\mu$ L
Rate	2
Time point	17 s
Transfers	1
Auto-calibrate	Once
Auto-read	Off

### 2.7.3 Statistical Data Analysis

The calcium traces output on SoftMax Pro were in the form of Relative Fluorescence Units (RFU). Data were exported to Excel and area under the curve (AUC) was calculated to compute the elevated levels of intracellular calcium release and analysed using GraphPad Prism 8.02. The baseline indicating the levels of calcium ions prior to the addition of the agonist was calculated for the first 17 s of the readings while the AUC was calculated commencing from 18 s till 120 s. 10  $\mu$ M ATP was utilised as the positive control and for data normalisation to account for individual experimental variations.

## **2.8 In-cell Western: MAP Kinase ERK1/2 Activation**

### **2.8.1 Preparation of 4% Paraformaldehyde**

PFA was prepared in a well-ventilated fume hood and aliquotted in 15 mL aliquots stored at -20°C wrapped in foil which were thawed only before use. The following protocol was used to prepare 1L of 4% PFA. 600 mL of distilled water was initially warmed up to 60°C and 4 g of PFA (Sigma-Aldrich) were mixed with the water while being placed on a hotplate stirrer (Camlab Ltd, UK) for 10-15 min. This was followed by subsequent addition of 2 M NaOH in a dropwise manner to facilitate dissolution and until the solution becomes adequately clear. The solution was brought down to room temperature and in the meantime, PBS was prepared. 3X PBS was prepared by dissolving PBS tablets (Dulbecco A tablets, Oxoid Ltd) in 300 mL deionised water and the pH was adjusted to 7.2 in HCl (Fisher Scientific). The final volume was made up to 1 L using PBS and the full volume was filtered using Whatman® filter paper (Whatman® 1PS phase separator filter papers, Sigma-Aldrich) and the full volume was aliquoted as mentioned in advance.

### **2.8.2 Assay Procedure**

Costar® clear 96 well-plates were seeded for 24 h at 37°C, 5% CO<sub>2</sub> and high humidity at a seeding density of 40,000 cells/well and 200 µL/well for the CHO-K1 and CHO-CB<sub>2</sub>, while HeLa cells were seeded at 70,000 cells/well. After seeding the plates, they were placed in the hood for 30-45 min at room temperature to minimize the edge-effect, before being transferred to the incubator. Following 24 h incubation, the plates were serum-starved for a further 24 h in order to sustain the cells in the non-proliferative cycle which leads to a reduction of cellular basal activity and an enhancement of signal-to-noise ratio subsequent to agonist stimulated signalling. The compounds were prepared at 10-fold the desired final concentration and plated in a 96-well compound plate. 1% FBS was used as the positive control and for normalizing the data between experiments. On the third day, the existing medium was discarded and replaced with 180 µL/well of fresh prewarmed serum starved medium and incubated for

10 min. 20  $\mu$ L of the prepared ligands were then added to the assay plate in a staggered timing step and columns were stimulated by agonist addition every 30 s and incubated for five min. The staggering step was performed at 37°C on a temperature controlled dry block heater. The medium was then aspirated using an 8-channel manifold (BRAND® BT aspirator, Sigma-Aldrich), every 30 s and the wells were instantly washed with ice-cold PBS to stop the reaction which was then aspirated and this was followed by the addition of 110  $\mu$ L of the fixing 4% PFA added per well.

The plate was then wrapped with aluminum foil, since PFA is light sensitive and incubated for 30 min at ambient temperature on the bench. Subsequently, PFA was aspirated, and 110  $\mu$ L of the 0.1% Triton X-100 was added to permeabilize the cells and incubated for another 30 min. Following incubation, Triton X-100 was discarded and 100  $\mu$ L of 5% dried skimmed milk in a PBS solution was added per well and incubated for 30 min. Subsequent to blocking the cells, the milk was aspirated and 70  $\mu$ L of the primary antibodies added (anti-phospho-ERK 42/44 and anti-total ERK 42/44 prepared in 5% milk at 1:500 dilution) to all wells except the blank background wells. The plate was wrapped with aluminum foil and incubated on an orbital plate shaker at 4°C overnight in the cold room. On the fourth day, the primary antibody was aspirated from the respective wells followed by three washes with ice-cold PBS with 5 min intervals while placing the plate on the orbital shaker at 350 rpm (Confido Micromixer FinePCR, Daigger® Scientific Inc, USA). Subsequent to the washes, 100  $\mu$ L of 5% milk containing the secondary antibodies (goat anti-rabbit red (GR) and goat anti-mouse green (GM) at a dilution of 1:3000) were added to all wells including the blank wells. The plate containing the secondary antibodies was incubated on an orbital shaker at ambient temperature for 1 h. The secondary antibody was then aspirated and followed by three washes with cold PBS with 5 min interval and the plate was scanned on the Licor Odyssey Infrared Imaging System 3.0 (Licor, Inc) via the Image studio software version 5.2. The software settings used were those recommended by Image Studio 5.2 for scanning microplates including medium quality, 169  $\mu$ m resolution, 3 mm offset, and 5 intensity. When performing the on cell western, the same assay

procedure was followed with the exception of the permeabilization step induced by Triton X-100 addition.

Table 2.8 ERK Antibodies used in the assay

<b>Antibody</b>	<b>Host</b>	<b>Dilution</b>	<b>Source</b>	<b>Code</b>
<b>Primary Antibody</b>				
Polyclonal total p44/42 MAPK (ERK1/2)	Rabbit	1:500	Cell Signaling Technology, UK	9102
Monoclonal Phospho-p44/42 MAPK (ERK1/2) (Thr202/Tyr204)	Mouse	1:500	Cell Signaling Technology, UK	9106
<b>Secondary Antibody</b>				
IRDye® 680RD Goat anti-rabbit IgG	Rabbit	1:3000	Licor® Biosciences	925-68071
IRDye® 800CW Goat anti-mouse IgG	Mouse	1:3000	Licor® Biosciences	925-32210

### 2.8.3 Statistical Data Analysis

The image obtained from the Image Studio 5.2 software was analysed on Image Studio. The blank wells not treated with the primary antibody were used to quantify background intensity while basal levels were the detected intensity in the absence of ligand stimulation. The background signals from the blank wells were subtracted from all signals to quantify the corrected intensities. The obtained values were exported to Excel and the 680 channel signal readings were divided by the 800 channel signal readings to attain the normalised intensity of the ratio of phosphorylated ERK/total ERK ratios to account for variations. The positive control used was 1% FBS and it was used for normalizing data between experiments.

## 2.9 [<sup>3</sup>H]-CP55,940 Competition Binding Assay

### 2.9.1 [<sup>3</sup>H]-CP55,940 Competition Binding Buffers

This assay required the preparation of drug buffer, assay buffer and wash buffer which were all prepared and utilised within one month of preparation. The wash buffer was initially prepared composed of 50 mM Tris, 2 mM EDTA, 5 mM MgCl<sub>2</sub> (Fisher Scientific). The difference between room temperature and the buffers was calculated and accounted for while adjusting the pH of the wash, drug and assay buffers. The wash buffer was adjusted to be at 4°C while the drug and assay buffers were adjusted at 30°C. After pH adjustment, BSA was added to all buffers as 0.5 mg/mL wash buffer, 5 mg/mL and 0.2 mg/mL for drug and assay buffer respectively, stirred for 15-30 min and stored at 4°C until use.

### 2.9.2 Assay Procedure

This assay was performed in 24 round-bottom polystyrene tubes (Falcon™, Fisher Scientific) to an ultimate reaction volume of 1000 µL. The investigated ligands were prepared at 10-fold the desired final concentration diluted in drug buffer (2.9.1) prepared in advance. The homogenate concentration of CHO-CB<sub>2</sub> to be used was optimised to be 100 µg and was only thawed from -80°C upon use. Initially, 100 µL of drug buffer or the respective prepared ligand concentrations were added to the 24 test tubes. Unlabelled (cold) CP55,940 at 1 µM was used to measure the nonspecific binding (NSB), drug buffer alone without competing ligand was a measure of the total binding and the control binding was measured in the absence of unlabelled ligands. 750 µL assay buffer were subsequently added to all test tubes; and the addition of 100 µL of the membrane homogenate prepared in assay buffer at 100 µg per test tube. Ultimately, 50 µL of the radio labelled CP55,940 (CP55,940 [side-chain-2,3,4(N)-<sup>3</sup>H], 4.877 TBq/mmol in ethanol, PerkinElmer, USA] at a final concentration of 0.25 nM prepared in assay buffer was added using a repeater pipette (Eppendorf® UK Ltd) to commence the reaction. All test tubes were adequately vortexed, covered with parafilm (Parafilm® roll, Sigma-Aldrich) and

placed in a 30°C maintained shaking water bath (Thermo Electron Precision 2872 reciprocal shaking bath, LabX, USA) for 2 h to reach steady state.

Following the 2 h incubation period, binding was stopped by filtration using a 24 place Brandel cell harvester (Biomedical research and development laboratories inc, USA). Initially, GF/B filter paper (Whatman GF/B filter paper FP-100, Brandel, USA) was washed once using the formerly prepared ice-cold wash buffer. The assay tubes were removed from the water bath and the reaction was stopped by filtering the tubes via the 24 place Brandel cell harvester and washing the tubes three times using the ice-cold wash buffer as well. The filter papers were cut appropriately and collected in 20 mL scintillation vials (Sarstedt Inc Scintillation vial, Fisher Scientific). 3 mL scintillation fluid was subsequently added to all scintillation vials (Scintillation fluid, Ultima Gold XR, PerkinElmer, Waltham, USA) and the scintillation vials were vortexed adequately and allowed to set for 6 h in order to confirm thorough absorption of the scintillation fluid by the filter papers. Radioactivity was measured using the radioactivity beta counter (Packard Tri-Carb Liquid Scintillation Counter, 2100TR, GMI Trusted Laboratory Solutions, USA) for a counting period of 5 min and the data were recorded in the form of disintegrations per minute (dpm). The equilibrium dissociation constant ( $K_d$ ) and the total density of receptors in the sample ( $B_{max}$ ) was formerly identified by preliminary studies and were used in the performed investigations in this thesis.

### **2.9.3 Statistical Data Analysis**

In the analysis of radioligand occupancy assays, there were several hypotheses assumed. It was presumed that binding was reversible and complied with the law of mass action, receptors were homogenous, and binding was reversible. It was also presumed that when the compound was bound to the receptor in a complex, the system was at steady state and there was no positive or negative cooperativity, receptors were homogenous.

NSB was determined in the presence of 1  $\mu$ M unlabelled CP55,940 (100%) and total binding (basal) was determined using drug buffer alone (0%). The specific binding was determined by subtracting the NSB from

the total binding (TB) and data were normalised against the total binding. Data were analysed on GraphPad Prism using non-linear regression analysis. The  $K_i$  for each investigated compound was then computed via the Cheng-Prusoff equation (Cheng and Prusoff, 1973).

$$K_i = \frac{IC_{50}}{1 + [L]/K_d}$$

- $K_i$ : equilibrium dissociation constant for the competitor ligand
- $IC_{50}$ : concentration of unlabelled ligand that inhibits specific binding by 50%
- $L$ : concentration of radioligand (nM)
- $K_d$ : equilibrium dissociation constant of the radioligand in the binding assay

The  $IC_{50}$  values of the compounds were obtained from the four-parameter logistic nonlinear regression analysis. Concentration-response curves of unlabelled CP55,940 were used in preliminary studies to calculate the  $K_d$  and the  $B_{max}$  based upon homologous competition analysis using nonlinear regression analysis. For heterologous competition, the  $K_i$  was calculated by nonlinear regression analysis according to the Cheng-Prusoff equation.

$$K_i = \frac{IC_{50}}{1 + L/K_d}$$

- $L$ : the concentration of free CP55,940 radioligand (nM)
- $B_{max}$ : total receptor density present within the sample representing the maximum specific binding
- $K_d$ : equilibrium dissociation constant and represents the total concentration of the unlabelled compound required to attain half-maximum binding at equilibrium (nM)
- $K_i$ : inhibitor dissociation constant

## 2.10 [<sup>35</sup>S]-GTP $\gamma$ S Assay

### 2.10.1 [<sup>35</sup>S]-GTP $\gamma$ S Binding Buffers

Drug and assay buffers were prepared and utilised within one month of preparation. Both buffers comprised 50 mM Tris pH 6.4, 100 mM NaCl, 10 mM MgCl<sub>2</sub>·6H<sub>2</sub>O at pH 7.4 and 30°C. They differed in the final concentration of BSA used which was 5 mg/mL for the drug buffer and 0.2 mg/mL for the assay buffer.

### 2.10.2 Assay Procedure

This assay was also performed in round-bottom polystyrene tubes in a final volume of 1000  $\mu$ L. The stock [<sup>35</sup>S]-GTP $\gamma$ S (guanosine 5'-( $\gamma$ -thio) triphosphate [<sup>35</sup>S]-, 46.25 TBq/mmol, PerkinElmer, USA) was prepared by diluting the 20  $\mu$ L stock via the addition of 2 mL aliquoting buffer composed of 10 mM tricine (Sigma-Aldrich), 10 mM DTT (Sigma-Aldrich), pH 7.6 and stored as 6  $\mu$ L aliquots at -20°C. Similar to the competition binding assay, the membrane homogenates of CHO-CB<sub>2</sub> cells were thawed from -80°C upon use. The membrane homogenates were diluted to 25  $\mu$ g/mL protein in assay buffer. Guanosine 5'-diphosphate sodium salt (GDP, Sigma-Aldrich) was added to the homogenate at a final concentration of 500  $\mu$ M prepared in assay buffer and the combination was incubated for 20 min at 30°C to maximise levels of the GDP bound G $\alpha$  protein. During the pre-incubation of the membrane homogenates, the compounds were prepared at 10 times the desired final concentration in drug buffer. Unlabelled Guanosine 5'-[ $\gamma$ -thio] triphosphate tetralithium salt (GTP $\gamma$ S) prepared in drug buffer at 10  $\mu$ M final concentration was used to define nonspecific binding and the presence of drug buffer alone was used to define total binding. Following the 20 min pre-incubation, 100  $\mu$ L of the membrane GDP mixture was added using a repeater pipette to commence the reaction in all 24 assay tubes containing 100  $\mu$ L of the ligands prepared in drug buffer, 700  $\mu$ L assay buffer and 100  $\mu$ L of the radioligand [<sup>35</sup>S]-GTP $\gamma$ S at 0.02 nM final concentration added in this order. The assay tubes were then vortexed, covered with parafilm and incubated in a shaking water bath for 90 min at 30°C to attain

steady state. Before terminating the reaction, GF/B filter paper was soaked in ice-cold deionised distilled water (ddH<sub>2</sub>O). The reaction was terminated through swift filtration and harvesting the homogenates as formerly stated using the 24-well Brandel cell harvester. This was followed by three washes in ice-cold ddH<sub>2</sub>O. The filter papers were cut and collected in 20 mL scintillation vials. 3 mL scintillation fluid was added to the filters before vortexing and the radioactivity was quantified via a radioactivity beta counter for a counting period of 5 min as counts per min (CPM).

### 2.10.3 Statistical Data Analysis

The statistical analyses followed here were the same as that followed for the occupancy study in [section 2.9.3](#). For [<sup>35</sup>S]-GTPγS binding, data were represented as a percentage of the activation of [<sup>35</sup>S]-GTPγS binding. NSB was determined in the presence of 10 μM unlabelled [<sup>35</sup>S]-GTPγS (100%) and total binding (basal) was determined using drug buffer alone (0%). The specific binding was determined by subtracting the NSB from the TB. Data were represented as a percentage of specific binding by normalizing the data against that of the total binding. Data were analysed on GraphPad Prism using non-linear regression analysis via the four-parameter logistic equation computed on GraphPad Prism for the determination of E<sub>max</sub> and EC<sub>50</sub>. Results were represented as a percentage of maximum response.

$$E = \frac{E_{\max} [A]^{nH}}{EC_{50}^{nH} + [A]^{nH}}$$

- E: the observed agonist effect
- A: the agonist concentration
- E<sub>max</sub>: indicates the maximal response
- nH: Hill slope - defines the steepness of the curves
- EC<sub>50</sub>: the concentration of agonist necessary to induce a response halfway between the baseline and the maximal response.
- pEC<sub>50</sub>: the negative logarithm of the EC<sub>50</sub> (pEC<sub>50</sub> = -Log EC<sub>50</sub>)

The four-parameter model derives the best-fit values for the top plateau, bottom plateau, the  $EC_{50}$  and the Hill slope of the sigmoidal dose-response curve without constraining the slope and thus, no previous assumptions are made regarding the nature of interaction between the ligand and the receptor. This is opposed to the three-parameter logistic equation where the slope is constrained to 1. When the response of the ligand is closely coupled to receptor occupancy, the slope factor is equal to 1. Hence assumptions about the nature of interaction between the receptor and ligand are deduced in advance, assuming that the ligand is closely coupled to receptor occupancy.

## 2.11 Fluorescent Binding Assay

HEKS293T cells were maintained in DME supplemented with 10% FBS, Zeocin (20 µg/mL, Invitrogen™, ThermoFisher) and blasticidin (5 µg/mL; Invitrogen™, ThermoFisher) were SNAP-tagged with human CB<sub>2</sub> receptors cDNA. The tagged receptors were transfected to the HEKS293T cells using the PEI Transfection Kit (Invitrogen™, ThermoFisher). This was followed by the generation of a stably expressing cell line by selecting the resistant colonies to blasticidin and zeocin. With the intention of inducing the expression of the tagged receptors, the cells were seeded into 175 cm<sup>2</sup> flasks supplemented with fresh medium and 1 µg/mL tetracycline until they approached confluency. On the following day, the cells were labelled with SNAP-Lumi4-Tb labelling reagent (CisBio, PerkinElmer) and membrane preparations were isolated. The medium was discarded, and cells were initially washed once with pre-warmed PBS, followed by 1X Tag-lite labelling medium (LABMED, CisBio, PerkinElmer) to ensure the thorough removal of any existing medium. This was followed by the addition of 10 mL LABMED Tag-Lite buffer supplemented with 100 nM SNAP-Lumi4-Tb and incubated at 37°C for 1 h. The cells were rinsed once again with PBS to remove any residual SNAP-Lumi4-Tb and the adherent cells were detached using 5 mL GIBCO enzyme-free Hank's based cell dissociation buffer (GIBCO, Carlsbad, USA) and collected in a universal tube loaded with 5 mL fresh medium. The cell suspension was centrifuged at 1500 rpm for 5 min, the supernatant layer was aspirated, and the pellets were frozen down to -80°C and membrane homogenates were performed as aforementioned. These previous steps were performed by David Sykes, COMPARE lab, and the membrane homogenates were kindly provided in order to perform the fluorescent binding assay.

The fluorescent binding assay was performed in white 384-well plate (OptiPlate-384, White Opaque 384-well microplate, CisBio, PerkinElmer, USA) in an assay binding buffer. The assay binding buffer was composed of 0.02% pluronic acid (F127, Sigma-Aldrich), 0.5% BSA (Sigma-Aldrich), 5 mM HEPES (1M STEMCELL Technologies Inc, UK) at pH 7.4 and 1X LABMED, Tag-lite labelling medium (LABMED 5X, CisBio, PerkinElmer), and was used

within one week of preparation. The final reaction volume used was 40  $\mu\text{L}$ /well with 1  $\mu\text{M}$  SR144,528 (Tocris Bioscience, UK) to establish the NSB while total binding was based on including assay binding buffer alone. The NSB was subtracted from the TB to calculate the specific binding for the concentration response curves. The investigated compounds were prepared in the assay binding buffer at 10-fold the desired final concentration. In order to assess the binding affinity of the investigated ligands, this assay was based upon simple competition binding between 100 nM of the fluorescent ligand R07297590 (Patent compound by Roche) and increasing concentrations of the competing investigated ligands added simultaneously to the CB<sub>2</sub> HEK293-TR homogenates. Six concentrations of R07297590 from 200 nM to 6.25 nM were prepared for every plate in order to assess the association rate ( $k_{\text{on}}$ ), dissociation rate ( $k_{\text{off}}$ ) and the observed rate of associations ( $k_{\text{ob}}$ ).

The prepared compounds and appropriate blanks were all added to the 384-well plate, and the CB<sub>2</sub> HEK293-TR membrane homogenates at 0.75  $\mu\text{g}$ /well final concentration were prepared. The homogenates prepared in the assay binding buffer were mixed with 100  $\mu\text{M}$  final concentration of GppNHp (Abcam plc, USA) which was vortexed-well and incubated at ambient temperature for 15 min to allow the receptor to achieve ground state. GppNHp was mixed with the membrane homogenates in order to eliminate the high agonist affinity population of the GPCR that could induce two different populations of binding sites in the membrane homogenates. This was necessary because the Motulsky-Mahan model is solely applicable for compounds competing at one site. Following a 15 min incubation, the membrane lysates were added to the full plate to commence the reaction and the plate was immediately placed in the PHERAstar FSX microplate reader (PHERAstar®, BMG LABTECH, Germany) and the plate was read kinetically for 2 h at ambient temperature with orbital shaking. The terbium donor was excited through eight laser flashes at 337 nm wavelength. The signals emitted by TR-FRET were identified at 665 nm for the acceptor and 620 nm for the donor of the fluorescent compound R07297590. The ratios attained by these were respectively divided and multiplied by 10,000.

### 2.11.1 Statistical Data Analysis

The extent of R07297590 fluorescent ligand binding to the receptor was evaluated at several time points which allowed the generation of association kinetic curves. The analysis of data obtained following the 2 h kinetic measurement was initially through fitting the data into a global fitting model and the calculation of  $k_{on}$  and  $k_{off}$ , as follows, using GraphPad Prism to calculate the single best-fit estimate of  $k_{on}$  and  $k_{off}$ :

$$k_{ob} = ([L] * k_{on}) + k_{off}$$

$$Y = Y_{max} * (1 - e^{(-1*k_{obs}*X)})$$

- $k_{on}$  and  $k_{off}$ : the association and dissociation rate constants of the fluorescent compound R07297590
- $k_{obs}$ : the rate at which equilibrium is attained
- $Y_{max}$ : the maximum level of binding
- X: time (min)
- L: the concentration of fluorescent ligand (nM)

The level of saturation binding was determined via non-linear regression of the one-site binding equation derived by fitting both NSB and total binding. The individual measurement of the  $k_d$  (fluorescent ligand dissociation constant) was calculated as follows:

Total binding = Specific binding + NSB

$$= B_{max} * [L]/k_d + [L] + slope * [L] + Background$$

$$NSB = Slope * [L] + Background$$

The approach of fitting both the total and NSB concurrently and sharing the same slope value, stipulates one best-fit value for both  $B_{max}$  and  $k_d$ . Sigmoidal curves were fitted to competition displacement binding values using the four-parameter logistic equation which allowed calculation of the fluorescent ligand binding affinity:

$$Y = \text{Bottom} + \frac{\text{Top} - \text{Bottom}}{1 + 10^{(\log \text{IC}_{50} - X) * nH}}$$

The  $\text{IC}_{50}$  values obtained from the inhibition curves were subsequently used to calculate the corresponding  $K_i$  values via the Cheng and Prusoff equation.

$$K_i = \frac{\text{IC}_{50}}{1 + L/K_d}$$

## 2.12 [<sup>3</sup>H]-cAMP Accumulation

One of the extremely precise methods of measuring cAMP production from ATP secondary to adenylyl cyclase stimulation in living cells is to trace this transformation via radiolabeled precursors (Hill et al., 2010). The principle of this methodology involves pre-labelling of intact cells with <sup>3</sup>H-adenine followed by sequential dowex/alumina column chromatography (Minneman et al., 1979) which segregates <sup>3</sup>H-cAMP from the respective tritium labelled adenine derivatives. Despite being time-consuming this method is extremely sensitive, produces a direct read-out over a significant range over which cAMP responses could be quantified (Hill et al., 2010).

### 2.12.1 Column Preparation

Alumina columns were prepared by adding 600 mg of activated, neutral alumina oxide (Brockmann Activity, Sigma-Aldrich) to individual Poly-Prep® chromatography columns (Bio-Rad). Before every use, alumina columns were regenerated with two washes using 10 mL 0.1 M imidazole (Sigma-Aldrich).

The Dowex ion exchange column was prepared by mixing resin (Dowex® 50WX4 hydrogen form 200-400 mesh, Sigma-Aldrich) with ddH<sub>2</sub>O to produce a slurry at 1:1 ratio in a glass beaker and stirred gently for 15-30 min until a uniform mixture was attained. 2 mL of the prepared resin was transferred directly from the stirred suspension to the Poly-Prep® chromatography columns via a 5 mL serological pipette (Corning™ Stripette™ Polystyrene Serological Pipettes, Fisher Scientific). Before each experiment, Dowex columns were prepared with one wash using 10 mL 1 M HCl and two washes with ddH<sub>2</sub>O each at 10 mL.

### 2.12.2 [<sup>3</sup>H]-cAMP Accumulation Assay Procedure

CHO-K1 and CHO-CB<sub>2</sub> cells were seeded in a 24-well plate Corning® (Flintshire, UK) for 24 h at 37°C, 5% CO<sub>2</sub> and high humidity at a seeding density of 250,000 cells/well in a total volume of 1 mL/well. After seeding the plates, they were placed in the hood for 30-45 min at room temperature before being placed in the incubator to minimize the edge-effect. After 24 h, the complete medium was substituted with serum starved medium supplemented with 37 kBq (~2\*10<sup>6</sup> dpm) <sup>3</sup>H-adenine, (adenine [2,8-<sup>3</sup>H], 37MBq/mL, PerkinElmer, USA) in 500 µL/well, which was further incubated for 14-18 h at 37°C in 5% CO<sub>2</sub> and high humidity. On the third day, the medium was discarded, and the plate wells were washed once using fresh SFM to remove any existing [<sup>3</sup>H]-adenine. 10 µM of the phosphodiesterase inhibitor rolipram (Sigma-Aldrich) prepared in fresh SFM were added to the full plate: 500 µL to the basal wells containing rolipram only (baseline levels), 450 µL to the positive control (forskolin) and 400 µL to all of the remaining wells. The 24-well plates were organized such that every experiment was performed in duplicate or triplicate. The plate was incubated for 15 min at 37°C in the incubator and in the meantime the investigated ligands were prepared. The ligands were prepared in fresh pre-warmed SFM at 10-fold the desired final concentration. Following the 15 min incubation, 50 µL of the prepared ligands were added to the respective wells and the plate was incubated for 10 min at 37°C. This was followed by the addition of 50 µL of the freshly prepared 10 µM forskolin (from *Coleus forskohlii*, ≥98% HPLC powder, Sigma-Aldrich) to the full plate except the blank wells. After 15 min at 37°C, the reaction was terminated, and the cells were lysed by moving the plate onto ice and adding 50 µL of 12 M HCl to each well. The total adenine integrated into the cells (mainly in the form of [<sup>3</sup>H]-ATP and [<sup>3</sup>H]-ADP) was determined by removing 50 µL per well for quantitation. Subsequently, 3 mL scintillation fluid was added to all vials which were vortexed, and the radioactivity was assessed via a scintillation counter. The plates were frozen at -20°C for at least three hours before running the columns in order to improve permeabilization and extraction of the labelled nucleotides.

### 2.12.3 [<sup>3</sup>H]-cAMP and [<sup>14</sup>C]-cAMP Recovery

The plates were thawed and 100 µL (~2000 dpm) of adenosine 3',5'-cyclic phosphate, ammonium salt, [8-<sup>14</sup>C] (57.6 mCi/mmol, Hartmann Analytical, Germany) prepared in ddH<sub>2</sub>O was added per well. 100 µL of [<sup>14</sup>C]-cAMP was also added to two scintillation vials and were used as 100% recovery standards. The complete content of each well was loaded to the regenerated Dowex column and left to drip through. The polyphosphate nucleotides pass through the columns while mononucleotides are retained on the resin (Jo K Smith, PhD thesis, 1999). The Dowex columns were then rinsed once with 3 mL ddH<sub>2</sub>O water in order to remove the more negatively charged molecules while leaving behind the less negatively charged [<sup>14</sup>C] cAMP adsorbed on the resin. The Dowex columns were then placed over the regenerated alumina columns and then washed with 6 mL ddH<sub>2</sub>O, which was allowed to run to waste. This induced the transfer of the [<sup>14</sup>C]-cAMP from the Dowex columns to the alumina columns. After the ddH<sub>2</sub>O had drained completely, the Dowex columns were set aside, the alumina columns were placed on top of 20 mL scintillation vials and 5 mL 0.1 M imidazole was added to all alumina columns in order to induce the elution of [<sup>14</sup>C]-cAMP into the scintillation vials. 5 mL 0.1 M imidazole was also added to the standard [<sup>14</sup>C] cAMP 100% recovery vials. This was followed by the addition of 8 mL scintillation fluid to all vials before being vortexed well and counting in the scintillation counter. Dual channel counting allowed quantification of [<sup>3</sup>H]-cAMP derived from [<sup>3</sup>H]-adenine while the <sup>14</sup>C measured the chromatographic cAMP recovery. The radioactivity beta counter was set for a counting period of 5 min and the values were quantified as dpm.

#### 2.12.4 [<sup>3</sup>H]-cAMP Generation Data Analysis

cAMP levels from blank wells and those containing 10 μM forskolin (positive control) were represented as 0 and 100% responses, respectively. The total [<sup>3</sup>H]-adenine transformed to [<sup>3</sup>H]-cAMP was determined as follows:

$$[{}^3\text{H}] - \text{cAMP} = ([{}^3\text{H}] - \text{cAMP eluted}) * \frac{\text{total } [{}^{14}\text{C}] \text{ added to sample}}{\text{counted } [{}^{14}\text{C}] \text{ standard}}$$

In order to account for the differences in the extent of [<sup>3</sup>H]-adenine uptake or the differences in cell numbers among the plate wells and the integration of [<sup>3</sup>H]-ATP in each well, cAMP levels were presented as a percentage of the total adenine nucleotides (mostly [<sup>3</sup>H]-ATP and [<sup>3</sup>H]-ADP) converted to [<sup>3</sup>H]-cyclic AMP, calculated as:

$$([{}^3\text{H}] - \text{adenine nucleotides}) * \frac{\text{total } [{}^{14}\text{C}] \text{ added to sample}}{\text{counted } [{}^{14}\text{C}]}$$

The adjusted dpm counts were used to construct agonist concentration response curves. On GraphPad Prism, the data were normalised such that the basal and forskolin responses were set as 0 and 100% responses, respectively.

## 2.13 CB<sub>2</sub> Receptor Cloning and Site-Directed Mutagenesis

Cloning was conducted to sequence the CB<sub>2</sub> receptor expressed in the CHO cell line. CHO-CB<sub>2</sub> cells were seeded in 24-well plate at 2.5\*10<sup>5</sup> cells/well seeding density and the RNA was isolated employing the TRIzol reagent (ThermoFisher Scientific) following the manufacturer's guidelines. Subsequently, 500 ng RNA was reverse transcribed into cDNA by applying the Affinityscript (Affinityscript cDNA Synthesis Kit-TaqMan, ThermoFisher Scientific) as reported by the manufacturer. The primers used for cloning were as follows:

Forward primers 5'-3': GATCGCGGCCGCATGGAGGAATGCTGGGTGAC

Reverse primers 5'-3':

GATCCTCGAGTCAGCAATCAGAGAGGTCTAGATCT

Amplification of the cDNA by polymerase chain reaction (PCR) was completed using Phusion High-Fidelity DNA Polymerase (New England BioLabs®) as stated by the manufacturer and the PCR product was purified via the PCR purification kit as per the producer's guidelines (Sigma-Aldrich). The DNA acquired following PCR cloning and purification, along with the utilised plasmid expression vector, were ligated via the NotI and XhoI restriction enzymes (New England BioLabs®) as per the company's guidelines. The DNA inserts were in turn ligated to pcDNA following the guidelines of T4 ligase (New England BioLabs®). The pcDNA was transformed into *E. coli* and the ligated bacterial colonies were detected and isolated via the BioTaq™ DNA polymerase (Bioline Bioscience®). The colonies were assessed by gel electrophoresis and the appropriate colony was selected. The identified and selected DNA was purified from the bacterial culture via Mini-prep protocol and 100 ng was sent for sequencing through Source Bioscience®.

The obtained sequence was a 100% match compared to the Q63 and H316 human CB<sub>2</sub> receptor sequence described on NCBI ([https://www.ncbi.nlm.nih.gov/protein/NP\\_001832.1](https://www.ncbi.nlm.nih.gov/protein/NP_001832.1)). In order to mutate the selected CB<sub>2</sub> receptor phenylalanine and tryptophan to the respective alanine residues, F117A, F200A and W258A the QuickChange™ XL Site-Directed

Mutagenesis Kit (Stratagene, USA) was utilised as per the manufacturer's recommendation. The cloning of CB<sub>2</sub> receptors and their site-directed mutagenesis was performed by Razan Al Momani (FRAMELAB).

## 2.14 Statistical Data Analysis

All data were analysed using GraphPad Prism 8.0 Software (GraphPad Software, San Diego, USA) as previously indicated. Data described in the upcoming results chapters were obtained from an *n* number of performed experiments mentioned respectively for each experiment and represented as mean ± SEM. A total of at least three independent biological repeats were performed in duplicate or triplicate. The statistical significance of datasets compared to one control dataset was assessed via one-way ANOVA with Dunnett's multiple comparison test. The two-way ANOVA test was applied to compare datasets including two or more variables. Statistical significance indicated by the *p* values are specified along with the figures in the upcoming chapters; *p* ≤ 0.05 was determined to be significant and \* *p* < 0.05, \*\* *p* < 0.01, \*\*\* *p* < 0.001 and \*\*\*\* *p* < 0.0001.

For concentration response curves, the agonists were fitted using four-parameter logistic nonlinear regression equation as follows:

$$E = \frac{E_{\max} [A]^{nH}}{EC_{50}^{nH}} + [A]^{nH}$$

- E: the observed agonist effect
- A: the agonist concentration
- E<sub>max</sub>: indicates the maximal response
- nH: Hill slope – defines the steepness of the curves
- EC<sub>50</sub>: the concentration of agonist necessary to induce a response halfway between the baseline and the maximal response.
- pEC<sub>50</sub>: the negative logarithm of the EC<sub>50</sub> (pEC<sub>50</sub> = -Log EC<sub>50</sub>)

The four-parameter model derives the best-fit values for the top plateau, bottom plateau, the EC<sub>50</sub> and the Hill slope of the sigmoidal dose-response curve without constraining the slope and thus, no previous assumptions

are made regarding the nature of interaction between the ligand and the receptor. This is opposed to the three-parameter logistic equation where the slope is constrained to 1. When the response of the ligand is closely coupled to receptor occupancy, the slope factor is equal to 1. Hence assumptions about the nature of interaction between the receptor and ligand are deduced in advance, assuming that the ligand is closely coupled to receptor occupancy.

### **Chapter 3 : Development of a high-throughput screening fluorescent assay for the ABHD6 enzyme**

The identification and characterization of the enzymes that metabolise endocannabinoids is essential to gain a complete recognition of the endocannabinoid signalling mechanisms which would allow the most appropriate therapeutic exploitation ([Chapter 1.2.5](#)) for various pathological conditions. Preceding research in the laboratory assessed the hydrolysis of the chromogenic substrate 4-nitrophenyl acetate (4-NPA), the fluorogenic substrates 4-methylumbelliferyl heptanoate (4-MUH) in addition to its analogue 4-methylumbelliferyl oleate (4-MUO) (figure 3.1) as potential substrates for the human recombinant enzymes MAGL (the primary variant is described as MAGL1), a second splice variant of MAGL referred to as MAGL2, ABHD6 and ABHD12 *in vitro*. Of these, there was no single substrate suitable for the screening of all the recombinant enzymes. 4-NPA and 4-MUO were of limited value in the investigation of MAGL *in vitro*. By contrast, 4-MUH appeared to be a promising substrate for the screening of recombinant ABHD6 given it was rapidly and readily metabolised by the ABHD6 transfects. The generation of the fluorescent product 4-methylumbelliferone has provided a sensitive, feasible and economical detection method for an array of biochemical assays. 4-MUH was revealed to be a stable ABHD6 substrate, with a low background activity over time accompanied with a differential effect over the other recombinant enzymes.

This chapter, therefore, aimed to establish a high-throughput screening assay that would be rapid, cost-effective, reproducible, feasible and sensitive for the human recombinant ABHD6 enzyme. These aims could be achieved by optimizing the 4-MUH assay, which might allow application of this screening assay into ‘real tissue’ systems.

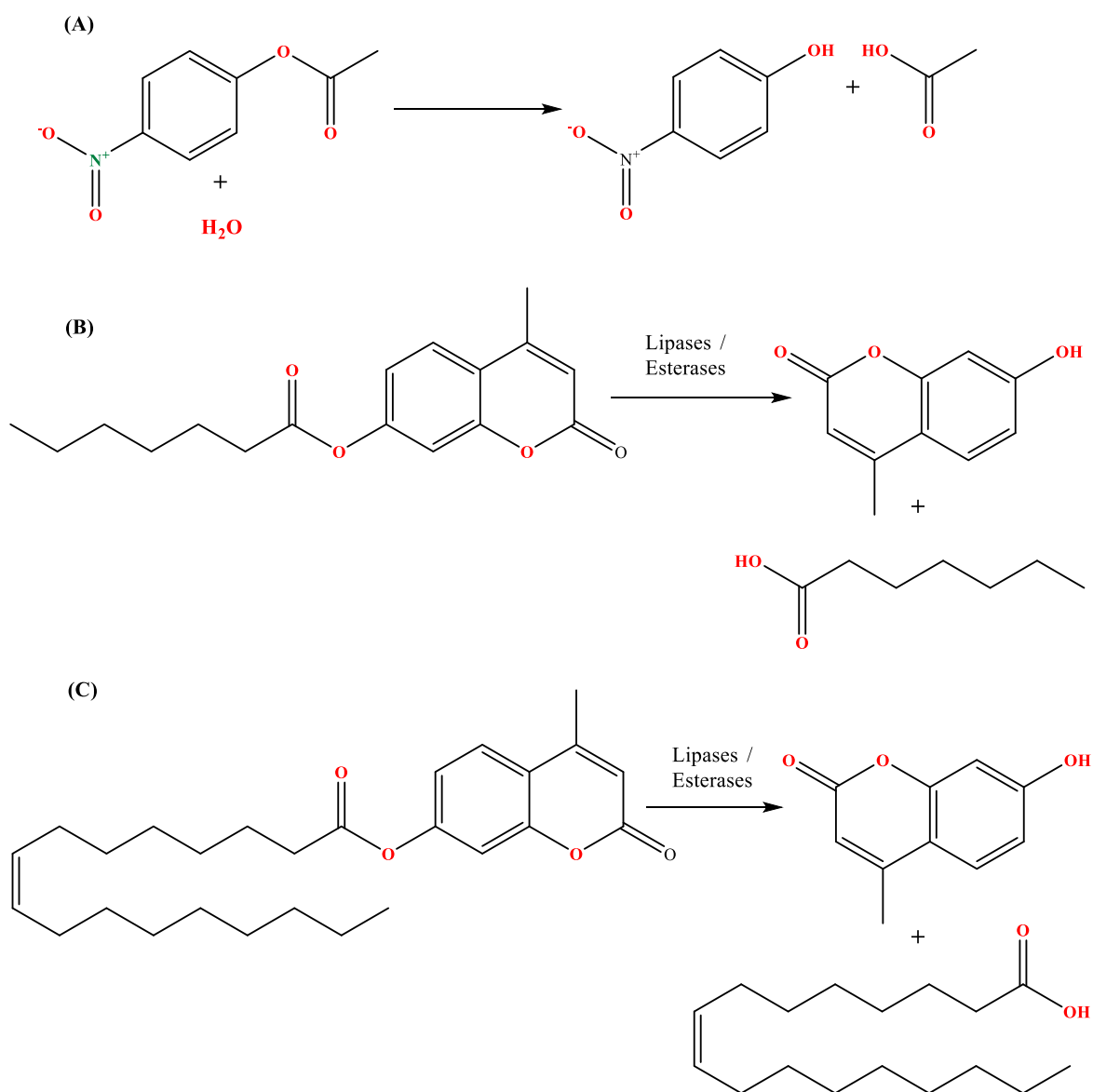


Figure 3.1 (A) 4-Nitrophenyl acetate hydrolysis to acetic acid and 4-nitrophenol, which can be detected by monitoring absorbance at 405 nm.

(B) Cleavage of the 4-MUH ester bond produces the fluorescent compound 4-methylumbelliferone detected at  $\lambda_{ex}$  355nm;  $\lambda_{em}$  460nm and the by-product, heptanoic acid. (C) Hydrolysis of the 4-MUO ester bond produces the same fluorescent product, 4-methylumbelliferone.

The preliminary investigations involving the testing of 4-NPA and 4-MUO were performed collaboratively with Sadia Shabnam and Dr Nada Mahmoud, an MRes and PhD student, respectively. The subsequent investigations involving the detailed characterisation of 4-MUH were performed collaboratively with Dr Nada Mahmoud.

## 3.1 Results

### 3.1.1 4-NPA as a potential HTS substrate

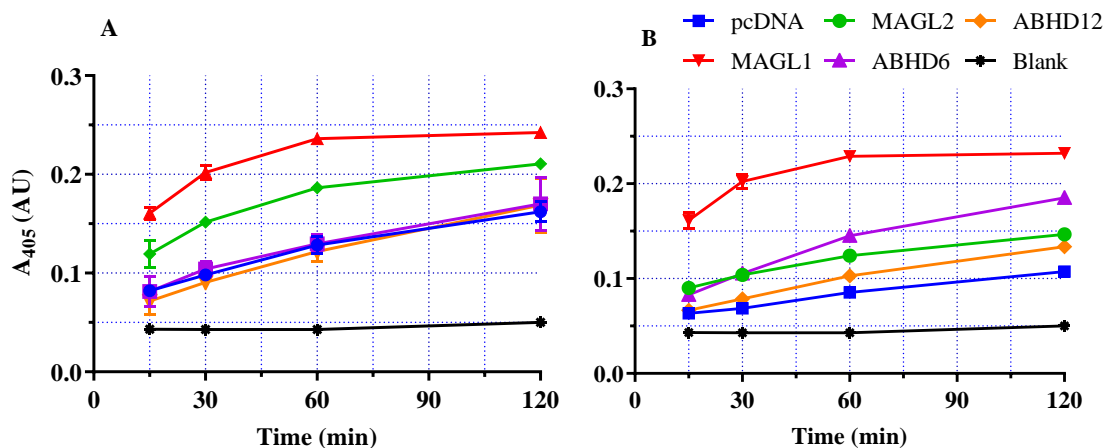


Figure 3.2 Hydrolysis of 2 mM 4-NPA by (A) particulate and (B) soluble fractions of HEK293 cells.

HEK293 cells were transfected with the indicated cDNAs and hydrolysis was measured at  $\lambda=405$  nm. Data represent the mean  $\pm$  standard error of the mean (SEM) of a single experiment performed in quadruplicate and repeated on four further preparations.

The blank, consisting of 4-NPA in the absence of tissue, remained stable over the 120 min of the reading time. The negative control pcDNA demonstrated a linear increase of 4-NPA hydrolysis over time. The particulate fractions of ABHD6 and ABHD12 produced hydrolysis that was not different from the empty vector pcDNA, while MAGL1 evoked the greatest hydrolysis rate followed by MAGL2. Using the soluble fractions, the largest hydrolysis rate was also observed with MAGL1, followed by ABHD6. ABHD12 and MAGL2 produced hydrolysis that was not distinct from the pcDNA control.

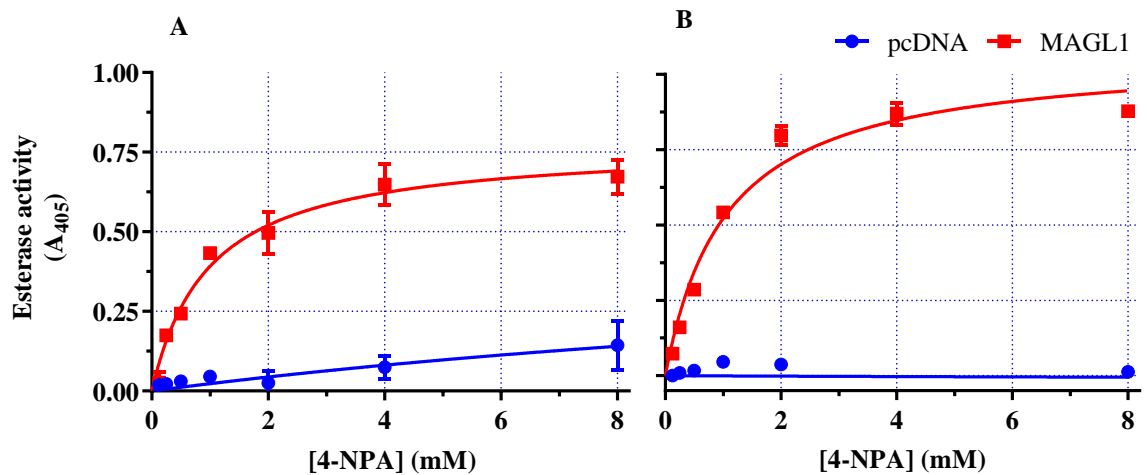


Figure 3.3 Hydrolysis of various 4-NPA concentrations by MAGL1 or pcDNA-transfected HEK293 cell by (A) particulate and (B) soluble preparations.

Data were plotted subsequent to Michaelis-Menten analysis by GraphPad Prism after subtracting background absorbance. Data represent the mean  $\pm$  SEM of one experiment performed in quadruplicate and repeated on four further occasions.

The MAGL1 isoform produced the highest rates of 4-NPA hydrolysis and was investigated at different concentrations to estimate  $K_m$  and  $V_{max}$  over a period of 120 min. Both fractions induced hydrolysis activity at all substrate concentrations and saturation was achieved at  $\sim$ 4 mM. The obtained  $K_m$  values of both the particulate and soluble fractions was 1.0 mM, while  $V_{max}$  was 0.8 and 1.1 AU, respectively.

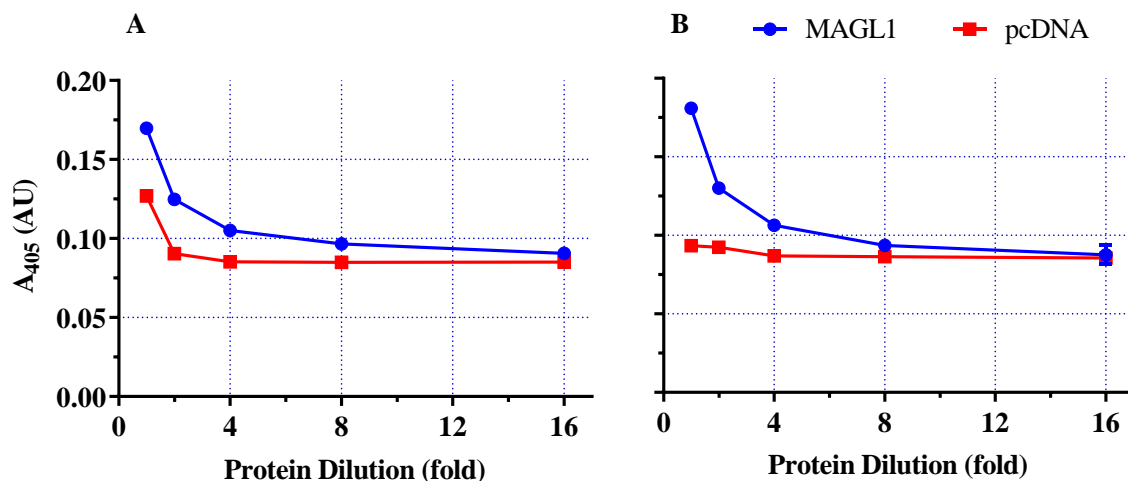


Figure 3.4 Hydrolysis of 2 mM 4-NPA by five protein dilutions. The protein dilutions represent (A) particulate and (B) soluble fractions of HEK293 cells expressing recombinant MAGL1 and pcDNA. Data represent the mean  $\pm$  SEM of a single experiment performed in quadruplicate and repeated in further five independent repeats.

As evident on the figure, diluting the recombinant MAGL1 preparations lead to diminished activity and at high protein dilutions, MAGL1 produced an activity that was not different from the negative control pcDNA. Therefore, further investigations employing this substrate were suspended at this stage due to the poor rate of hydrolysis which would require the use of large quantities of recombinant MAGL1.

### 3.1.2 4-MUO as a potential HTS substrate

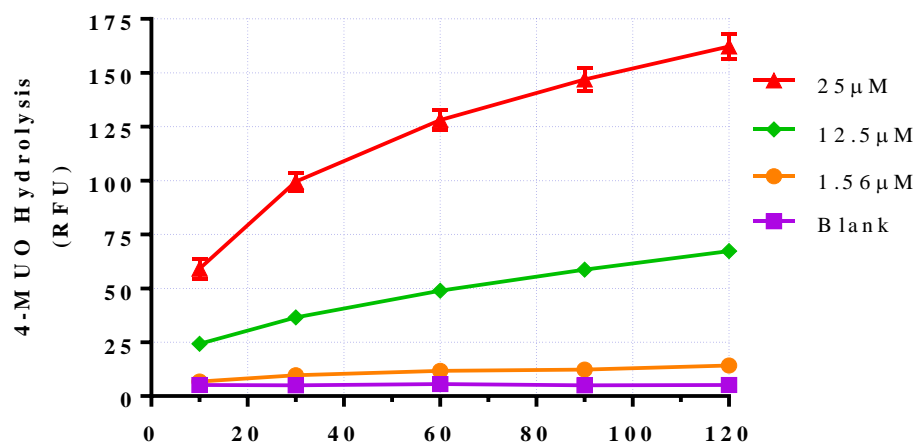


Figure 3.5 Hydrolysis of various concentrations of 4-MUO by the soluble fraction of rat liver.

Data represent the mean  $\pm$  SEM of a single experiment performed in quadruplicate and repeated on two further occasions.

The background hydrolysis of 4-MUO in the absence of tissue was low and relatively constant throughout the period of incubation implying that it was a potentially stable substrate. The hydrolysis of the lowest concentration of 4-MUO (1.56  $\mu$ M) in the presence of rat liver cytosol was not different from the blank. At 12.5  $\mu$ M, the rat liver cytosol generated around 50 times the fluorescence compared to the blank, while at the highest concentration used (25  $\mu$ M) the hydrolysis was 150 times more than the blank. The intermediate concentration at 12.5  $\mu$ M was employed in further investigations as it produced adequate readings combined with economy of use.

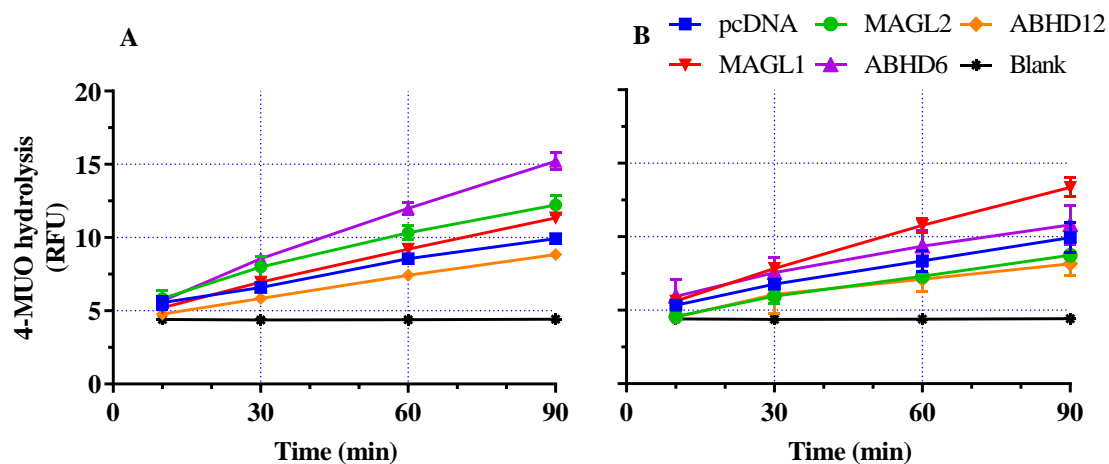


Figure 3.6 Hydrolysis of 12.5  $\mu$ M 4-MUO by (A) particulate and (B) soluble fractions of HEK293 cells expressing the recombinant enzyme transfects. Data represent the mean  $\pm$  SEM of a single experiment performed in quadruplicate and repeated on two further occasions.

Consistent with Figure 3.5, the enzyme blank was stable throughout the reading time. The hydrolysis of 4-MUO in the presence of preparations from the pcDNA negative control showed a linear increase in both fractions over time. Both particulate and soluble fractions of the transfected cell preparations induced 4-MUO hydrolysis that was not distinct from the pcDNA control. The membrane fraction of ABHD6-transfected cells was the only condition that produced rates of hydrolysis that were distinct from the pcDNA. The fluorescence produced following 4-MUO hydrolysis was essentially low, and thus, further investigations using this substrate were discontinued at this stage.

### 3.1.3 4-MUH as a potential HTS substrate

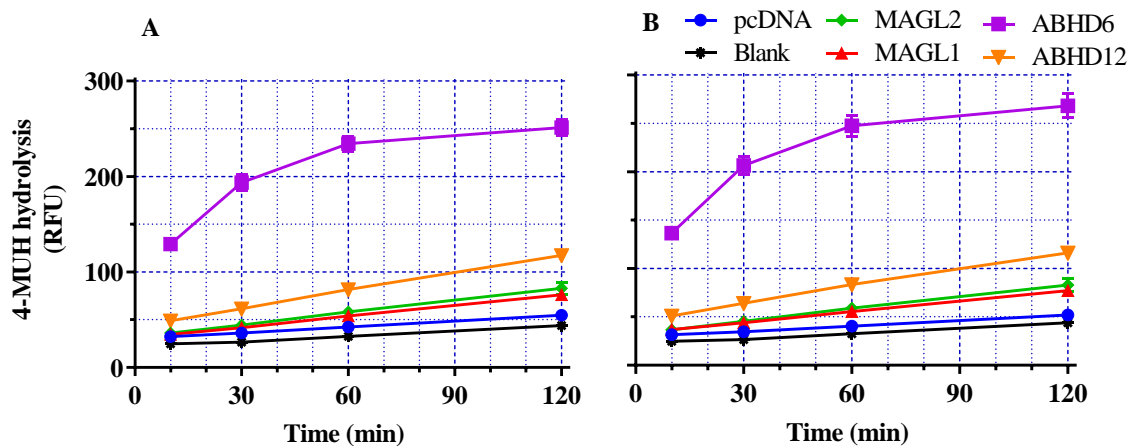


Figure 3.7 Time course of 250  $\mu$ M 4-MUH hydrolysis by (A) particulate and (B) soluble preparations from transiently transfected HEK293 cells. Data represent the mean  $\pm$  SEM of a single experiment conducted in sextuplicate and repeated on four further distinct transfect preparations.

The initial screen indicated that 4-MUH in the absence of tissue produced low background hydrolysis over time. There was a noticeable increase in the rate of hydrolysis in the presence of ABHD6 particulate and soluble fractions, such that 15 min incubation resulted in approximately 5-fold increase in MUH hydrolysis. By contrast, hydrolysis in the presence of preparations of ABHD12, MAGL1 and MAGL2 transfects. Therefore, additional work was performed to characterise 4-MUH further as a potential ABHD6 substrate.

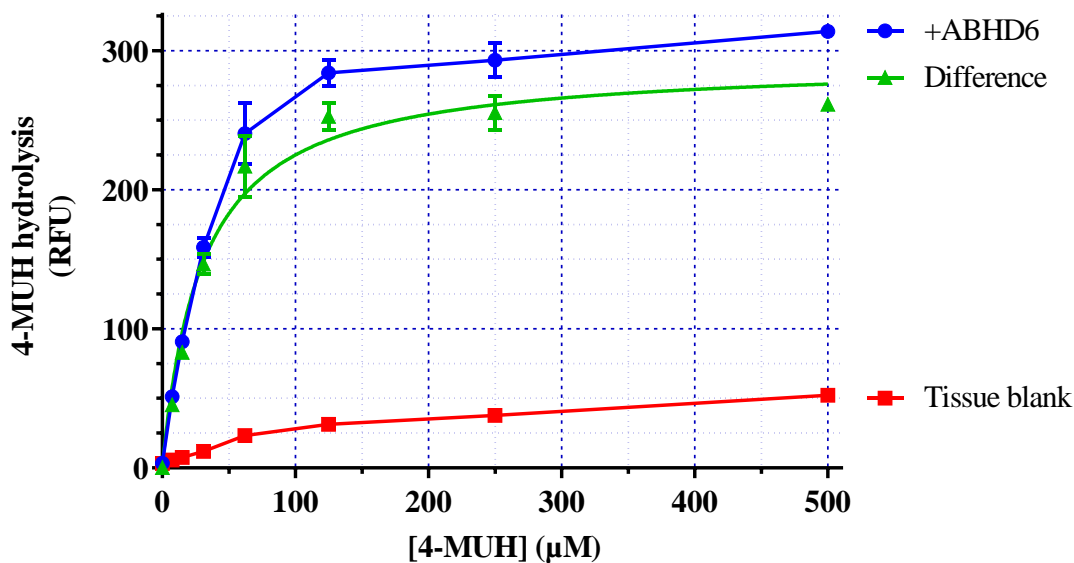


Figure 3.8 Hydrolysis of a range of 4-MUH concentrations by human recombinant ABHD6 particulate preparations.

Data represent the mean  $\pm$  SEM of a single experiment conducted in triplicate and repeated on five further independent transfect preparations. Data from the calculated tissue-dependent hydrolysis (identified as 'Difference') were analysed using Graph-Pad Prism and fit to a Michaelis-Menten plot.

The negative blank in this experiment was 4-MUH incubated in the absence of an enzyme source; there was no increase in fluorescence under these conditions. With increasing concentrations of 4-MUH, there was an increase in 4-MUH hydrolysis in the presence of particulate preparations of the ABHD6-transfected HEK293 cells until saturation was achieved at around 125  $\mu$ M substrate. Calculated  $K_m$  values were  $41 \pm 11 \mu$ M ( $n=5$ ), hence subsequent experiments were performed using 50  $\mu$ M MUH. The ABHD6 transfect preparations used in the assay was diluted at 1:100-fold dilutions to a final protein concentration of 17-29  $\mu$ g protein/assay in TRIS buffer and the prepared plates were measured kinetically at 37  $^{\circ}$ C.

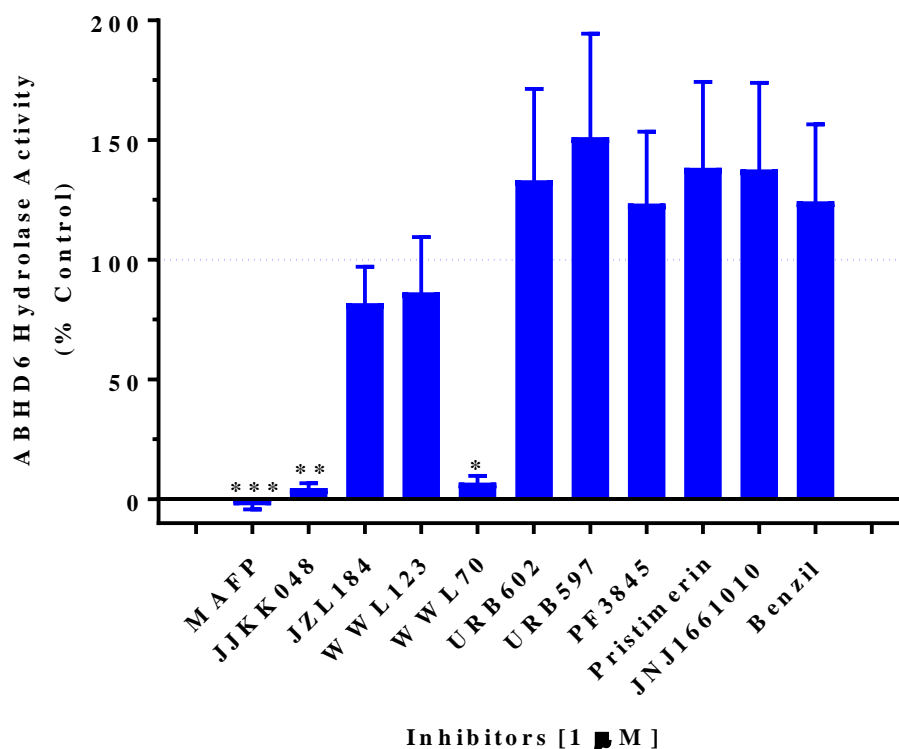


Figure 3.9 Hydrolysis of 50  $\mu\text{M}$  4-MUH by human recombinant ABHD6 in the presence of eleven enzyme inhibitors (1  $\mu\text{M}$ ) of different selectivities. Data represent the mean  $\pm$  SEM of seven independent experiments conducted in duplicate, analysed using Graph-Pad Prism. Data were analysed for statistical significance by a blinded observer (Dr Stephen Alexander) using Friedman analysis with uncorrected Dunn's test (\*  $p \leq 0.05$ , \*\*  $p \leq 0.01$  and \*\*\*  $p \leq 0.001$ ).

The first objective of performing this experiment was to confirm that the enzyme showed an inhibitor profile consistent with the published literature. The second objective was to check the suitability of the assay for screening multiple compounds. The control for normalisation of the data used in this experiment was the combination of ABHD6 preparations and 4-MUH in the absence of any inhibitors. The experiment involved a 15 min pre-incubation at 37 °C of ABHD6 transfects with the potential inhibitors (1  $\mu\text{M}$ ). Subsequently, the plates were incubated at 37°C on a temperature controlled dry block heater for 60 min and the plates were read as an end-point measurement using the Fluoroskan™ Microplate Fluorometer. As evident in Figure 3.9, MAFP, JJK048 and WWL70 induced complete inhibition while JZL184 and WWL123 caused around 20% inhibition. All of the other inhibitors were ineffective at inhibiting the 4-MUH hydrolysis evoked by ABHD6 preparations.

Table 3.1 The properties and potencies of the inhibitors used in the screening assay

<b>Compound</b>	<b>Property</b>
<b>Benzil</b>	Potent and selective inhibitor of carboxylesterases (Hatfield and Potter, 2011; Wadkins et al., 2005) K <sub>i</sub> = 15 nM for human recombinant intestinal CES K <sub>i</sub> = 45 nM for human recombinant CES1 K <sub>i</sub> = 103 nM for rat recombinant CES
<b>JJKK048</b>	Potent and selective MAGL inhibitor (Aaltonen et al., 2013) IC <sub>50</sub> = 43 nM for rat recombinant MAGL IC <sub>50</sub> = 15 nM for mouse recombinant MAGL IC <sub>50</sub> = 6 nM for human MAGL
<b>JNJ1661010</b>	Potent irreversible FAAH-2 inhibitor (Karbarz et al., 2009; Keith et al., 2008) IC <sub>50</sub> = 10 nM for rat recombinant FAAH IC <sub>50</sub> = 12 nM for human FAAH
<b>JZL184</b>	A selective MAGL inhibitor (Aaltonen et al., 2013) IC <sub>50</sub> = 2 nM for mouse and human MAGL IC <sub>50</sub> = 25 nM for rat MAGL
<b>MAFP</b>	Non-selective irreversible inhibitor of ABHD6, ABHD12, FAAH and MAGL (Aaltonen et al., 2013; Ogawa and Kunugi, 2015) IC <sub>50</sub> = 1-3 nM for rat and mouse recombinant FAAH IC <sub>50</sub> = 0.33 nM for human recombinant FAAH IC <sub>50</sub> = 2.2 nM for rat recombinant MAGL IC <sub>50</sub> = 26 nM for human recombinant MAGL
<b>PF3845</b>	A selective inhibitor of FAAH (Booker et al., 2012; Ogawa and Kunugi, 2015) IC <sub>50</sub> = 18 nM for human recombinant FAAH
<b>Pristimerin</b>	Potent and selective MAGL inhibitor (King et al., 2009) IC <sub>50</sub> = 93 nM for recombinant MAGL
<b>URB597</b>	An irreversible inhibitor of FAAH (Kwilasz et al., 2014; Piomelli et al., 2006) IC <sub>50</sub> = 5 nM for rat brain membranes IC <sub>50</sub> = 3 nM for human liver microsomes
<b>URB602</b>	A MAGL inhibitor (Hohmann et al., 2005; King et al., 2009) IC <sub>50</sub> = 28 μM for rat brain MAGL
<b>WWL70</b>	Potent and selective ABHD6 inhibitor (Li et al., 2007; Marrs et al., 2010) IC <sub>50</sub> = 70 nM for mouse brain ABHD6
<b>WWL123</b>	An ABHD6 inhibitor (Naydenov et al., 2014) IC <sub>50</sub> = 0.43 μM in <i>in vivo</i> mice

Since the four inhibitors JJKK048, MAFP, WWL70 and WWL123 were effective at inhibiting 4-MUH hydrolysis induced by the recombinant ABHD6, concentration-response curves of these inhibitors were conducted, and the curves were fitted using the four-parameter logistic equation (Figure 3.10). The non-selective inhibitor MAFP caused 100% inhibition at  $10^{-7}$  M. The MAGL-selective inhibitor JJKK048 also evoked complete inhibition at  $10^{-6}$  M. The selective ABHD6 inhibitor, WWL70 produced almost 90% inhibition at  $10^{-5}$  M, while WWL123 demonstrated only 50% inhibition at that concentration.

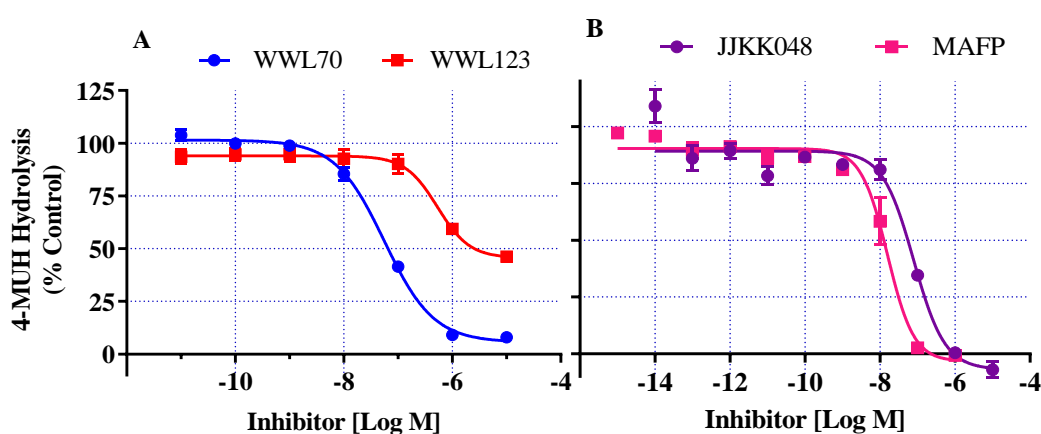


Figure 3.10 The potency of four different inhibitors on the hydrolysis of 50  $\mu$ M 4-MUH by human recombinant ABHD6.

Data were normalized as a percentage of control 4-MUH hydrolysis and represent the mean  $\pm$  SEM of (A) five (WWL70 and WWL123) and (B) four (JJKK048 and MAFP) independent transfects assessed in duplicate.

Table 3.2 Potencies of the four inhibitors at human recombinant ABHD6 investigated at n=5 for WWL70 and WWL123 and n=4 for JJKK048 and MAFP

Inhibitor	pIC <sub>50</sub>	R <sub>max</sub> (% inhibition)	Slope
<b>JJKK048</b>	7.1 $\pm$ 0.1	96 $\pm$ 7	-1.34 $\pm$ 0.29
<b>MAFP</b>	8.0 $\pm$ 0.2	125 $\pm$ 12	-0.46 $\pm$ 0.15
<b>WWL70</b>	7.3 $\pm$ 0.1	96 $\pm$ 0	-0.99 $\pm$ 0.07
<b>WWWL123</b>	6.3 $\pm$ 0.1	50 $\pm$ 3	-1.13 $\pm$ 0.11

To define the usefulness of the assay for screening, the  $Z'$  score was computed using 1  $\mu$ M WWL70 as the positive control in order to estimate the efficiency and validity of this established high-throughput (HTS) screening assay. This score or 'screening window coefficient' (Zhang et al., 1999) is a statistical parameter that is recommended to assess the efficiency of HTS assay in a simplified way. If the obtained parameter were 1, the assay would be considered ideal, if the  $Z'$  score ranged between 0.5-1, the established HTS assay would be considered excellent, between 0-0.5 would be a borderline assay compelling individual verification of any hits and a  $Z'$  value less than 0 indicated an assay impractical for screening.

$$Z' = 1 - \frac{(3 * SD \text{ of sample}) + (3 * SD \text{ of control})}{(\text{Mean of sample}) - (\text{Mean of control})}$$

Based on the above equation, the calculated  $Z'$  score for ABHD6 HTS assay was found to be 0.42, suggesting a borderline assay and therefore, further compounds were screened.

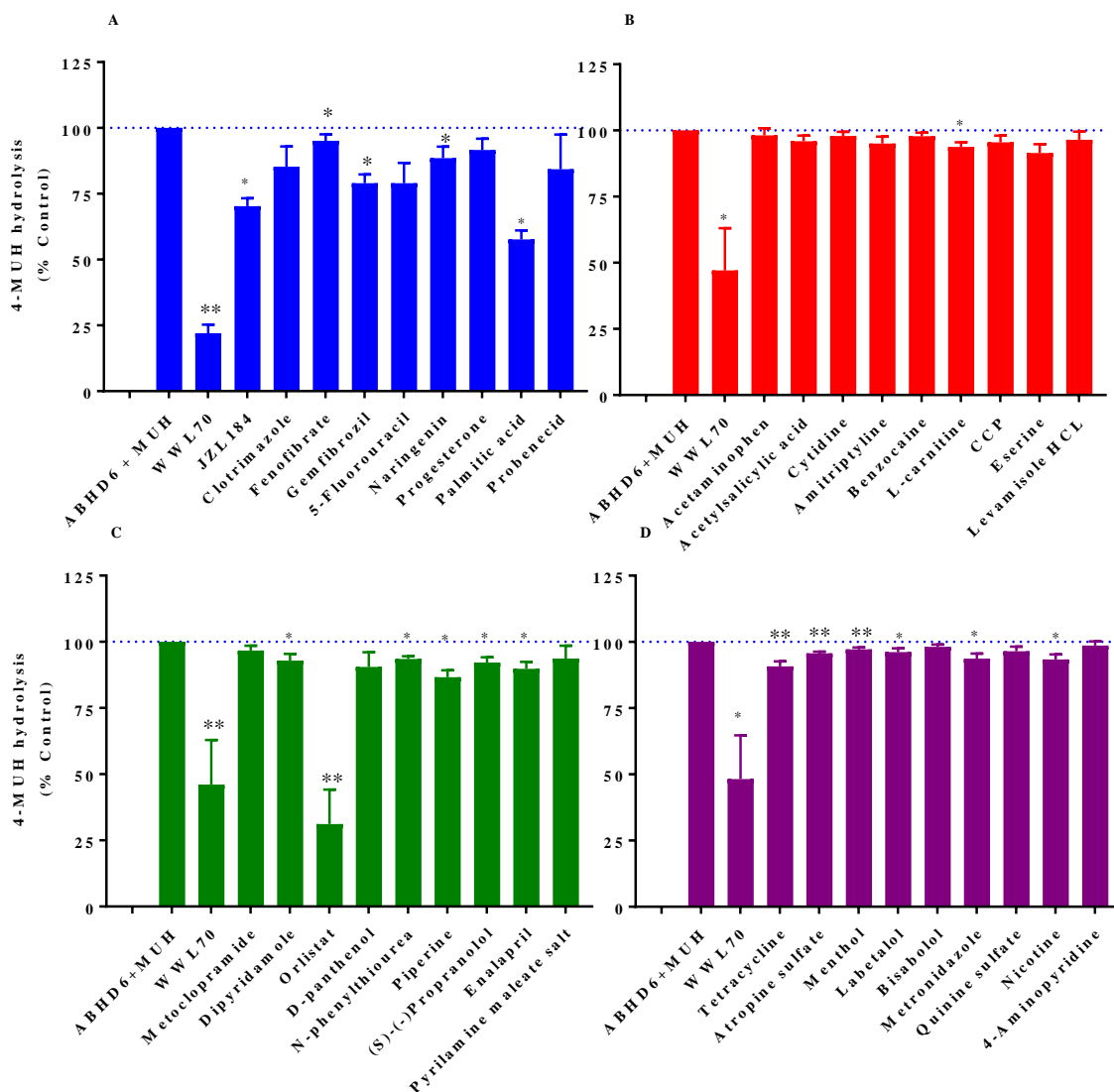


Figure 3.11 Hydrolysis of 50  $\mu\text{M}$  4-MUH by human recombinant ABHD6 in the presence of 36 potential inhibitors at 10  $\mu\text{M}$ ; WWL70 as the positive control was assessed at 1  $\mu\text{M}$ .

Data represent the mean  $\pm$  SEM of four independent experiments conducted in duplicate. Data were analysed blind (by Dr Stephen Alexander) using one-way ANOVA with Dunnett's multiple comparison analysis compared to the control (ABHD6+MUH) (\*  $p \leq 0.05$ , \*\*  $p \leq 0.01$  and \*\*\*  $p \leq 0.001$ ). CCP in (B) represents N-cyclohexanecarbonylpentadecylamine, a selective inhibitor of NAAA (Tsuboi et al., 2004).

The ABHD6 transfects were simultaneously incubated with the potential inhibitors to be screened in addition to 50  $\mu\text{M}$  4-MUH. Plates were incubated at 37°C on a temperature controlled dry block heater for 60 min and

then read as an endpoint using a Fluoroskan™ Microplate Fluorometer. The 36 screened compounds were chosen for their diverse structures and range of biological activities. Most of the compounds were ineffective at inhibiting 4-MUH hydrolysis. Fenofibrate, gemfibrozil, naringenin, benzocaine, dipyridamole, N-phenylthiourea, piperine, propranolol, enalapril, tetracycline, atropine, menthol, labetalol, metronidazole and nicotine evoked statistically significant inhibition that was only approximately 10% and might be considered pharmacologically irrelevant. Therefore, these compounds were not investigated further. Orlistat and palmitic acid induced inhibitions of  $31 \pm 13\%$  of 69% inhibition of the control and  $53 \pm 12\%$  of 25% inhibition of the control, respectively, and hence, orlistat was further investigated over multiple concentrations.

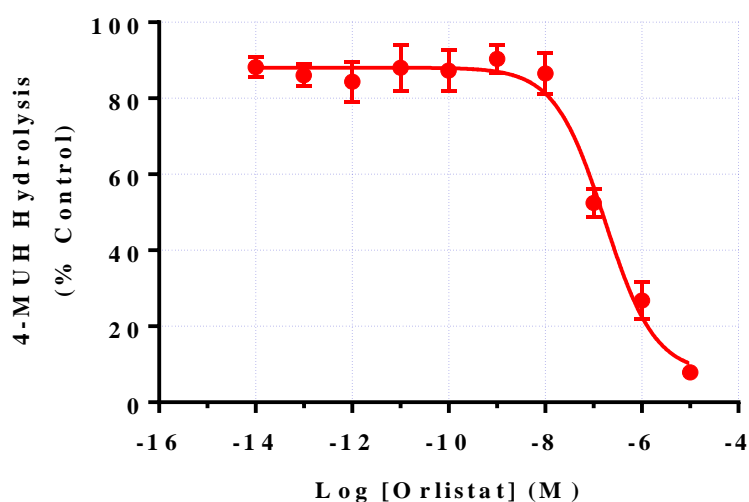


Figure 3.12 The effect of increasing orlistat concentration on the hydrolysis of  $50 \mu\text{M}$  4-MUH by human recombinant ABHD6. Data represent the mean  $\pm$  SEM of five independent experiments conducted in duplicate.

Orlistat demonstrated a concentration-dependent inhibition of 4-MUH hydrolysis, such that  $10^{-5}$  M caused  $\sim 95\%$  inhibition of the 4-MUH hydrolysis, with a calculated  $\text{pIC}_{50}$  value =  $6.73 \pm 0.12$  and  $R_{\text{max}} = 82 \pm 4\%$  performed at  $n = 5$ .

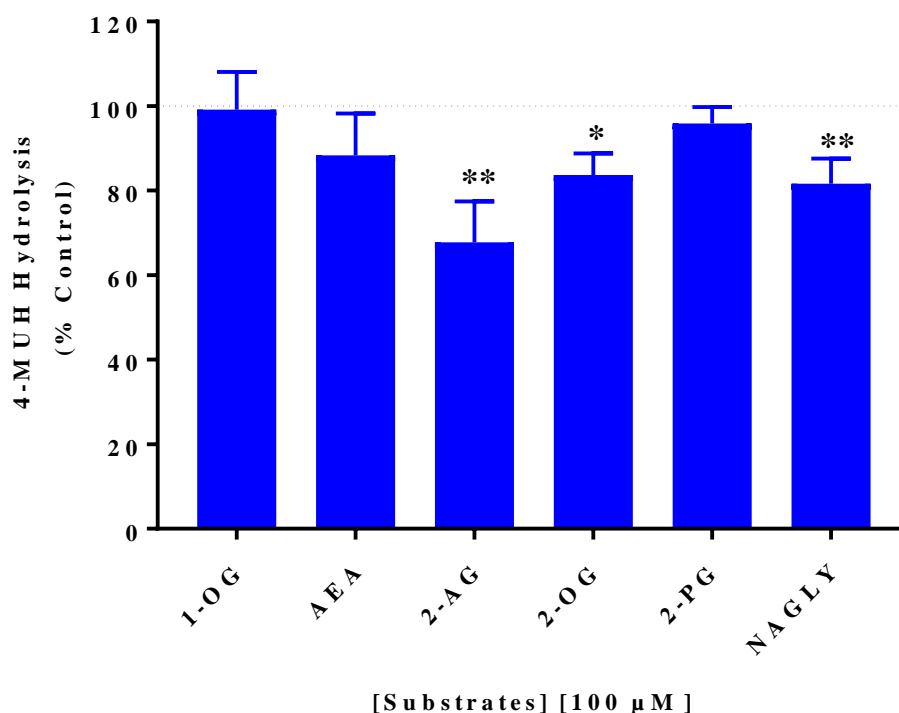


Figure 3.13 Hydrolysis of 50  $\mu\text{M}$  4-MUH by human recombinant ABHD6 in the presence of potential alternative substrates (100  $\mu\text{M}$ ).

Data represent the mean  $\pm$  SEM of seven independent experiments conducted on different transfects of ABHD6 in duplicate. Data were analysed blind (by Dr Stephen Alexander) using one-way ANOVA with Dunnett's multiple comparison analysis (\*  $p \leq 0.05$  and \*\*  $p \leq 0.01$ ) compared to the control (ABHD6+MUH).

To investigate the substrate selectivity of ABHD6, a range of substrates were investigated including 1-oleoyl glycerol (1-OG), 2-AG, 2-palmitoyl-rac-glycerol (2-PG), 2-oleoylglycerol (2-OG) and N-arachidonoyl glycine (NAGLY) co-incubated with 4-MUH for 60 min. 2-AG, 2-OG and NAGLY evoked small, but significant, inhibitions of 2-AG evoked the greatest inhibition of 4-MUH hydrolysis. Since the inhibition evoked by 2-AG was less than 50% ( $68 \pm 4\%$  control), its potency was not explored further.

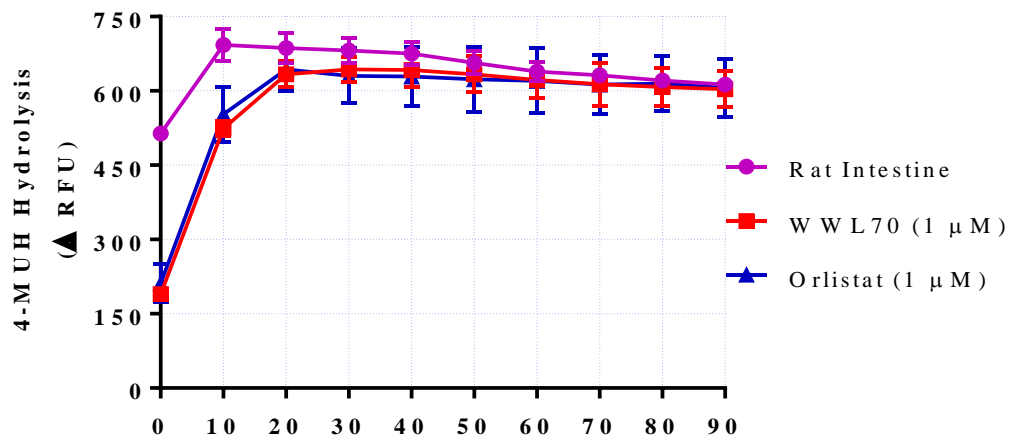


Figure 3.14 Hydrolysis of 50  $\mu\text{M}$  4-MUH by Wistar rat small intestine preparations diluted 125-fold ( $\sim 50 \mu\text{g/mL}$  protein). Data represent the mean  $\pm$  SEM of one representative experiment performed in triplicate repeated using four different tissue preparations. Background hydrolysis of 4-MUH in the absence of added tissue was subtracted prior to analysis.

After investigating the assay using the recombinant expression of human ABHD6, the subsequent step was to apply the assay to ‘real’ tissue. Wistar rat small intestine had been previously identified to express ABHD6 mRNA with lower levels of MAGL mRNA than in other rat tissues (Nada S Mahmood PhD thesis). Samples were prepared and investigated under identical assay settings to the recombinant enzyme. Different dilutions of the tissue were used from 2-fold (ca. 3 mg protein/mL) to 625-fold (ca. 10  $\mu\text{g}$  protein/mL) dilutions (125-fold dilution is presented in Figure 3.8). As demonstrated in figure 3.14, the rat small intestine preparation alone at  $\sim 50 \mu\text{g/mL}$  protein (125-fold diluted) demonstrated an elevated baseline activated at  $t = 0$  min which peaked at 10 min, following which it declined over the course of the 1-h reading. Both inhibitors appeared to reduce 4-MUH hydrolysis initially, although from 20 min onward, there was no difference between the hydrolysis of the control and in the presence of the inhibitors.

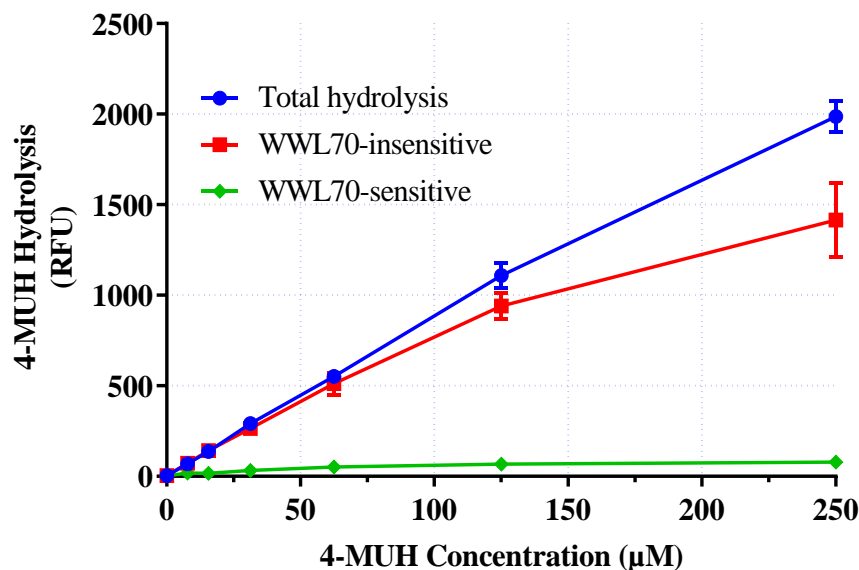


Figure 3.15 Hydrolysis of a range of 4-MUH concentrations by Wistar rat small intestine preparations diluted 125-fold in the presence and absence of 1 µM WWL70.

Data represent the mean  $\pm$  SEM of a single representative experiment conducted in triplicate and repeated in five further independent rat intestinal tissue preparations. Curves were fitted to a Michaelis-Menten plot following subtraction of the baseline.

Since WWL70 was identified as a reasonably potent ABHD6 inhibitor ( $pIC_{50} = 7.3 \pm 0.05$ ) in the previous experiments and is reported to be selective relative to other esterases (Li et al., 2007), it was applied to rat small intestine preparations to identify the contribution of ABHD6 to 4-MUH hydrolysis in this tissue. However, calculating  $K_m$  and  $V_{max}$  values proved complicated either in the presence or absence of WWL70. As evident from figure 3.15, WWL70 was ineffective at inhibiting hydrolysis of lower 4-MUH concentration ( $<125 \mu M$ ). All of the approaches aimed at optimization of the assay to measure ABHD6 activity in rat intestine were unsuccessful, hence no further assessment of the rat intestine was performed.

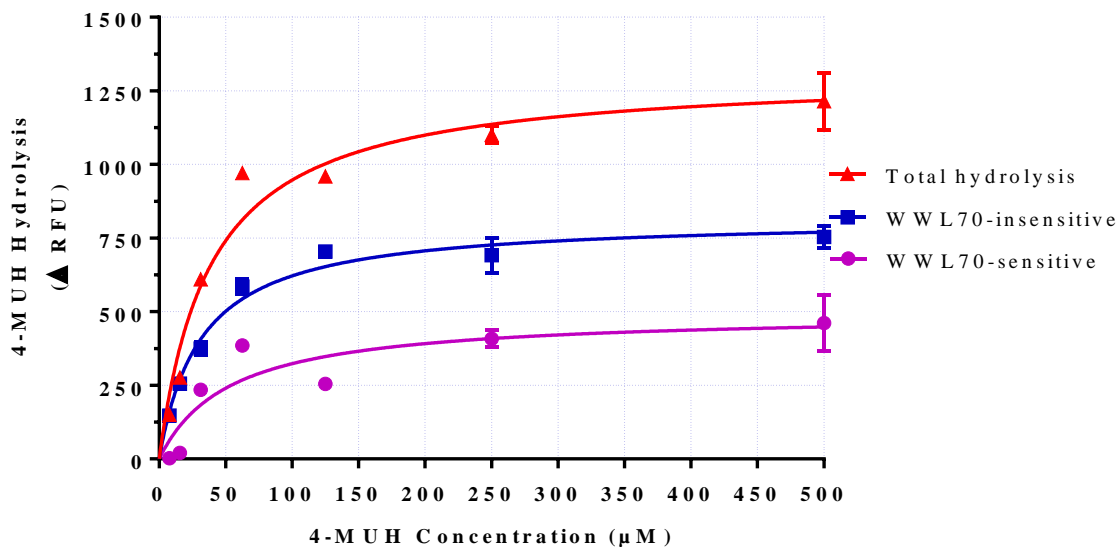


Figure 3.16 Hydrolysis of a range of 4-MUH concentrations by Wistar rat hippocampal preparations in the presence and absence of 1  $\mu\text{M}$  WWL70. Data represent the mean  $\pm$  SEM of a single representative experiment conducted in triplicate and repeated on five further independent rat hippocampal preparations. Data were fitted to a Michaelis-Menten one-site rectangular hyperbola plot following subtraction of the baseline.

Since ABHD6 mRNA is also expressed in the brain (Wei et al., 2016) (Nada S Mahmood, PhD thesis), the rat hippocampus tissue was assessed using 4-MUH as substrate. With increasing concentrations of 4-MUH, there was an increase in 4-MUH hydrolysis until saturation was achieved above 200  $\mu\text{M}$ . The calculated  $K_m$  of the WWL70 sensitive portion was  $45 \pm 7 \mu\text{M}$  (Table 3.3); hence the following experiments were conducted at 50  $\mu\text{M}$  4-MUH with rat hippocampus.

Table 3.3 Calculated  $K_m$  values for 4-MUH hydrolysis by rat hippocampal preparations investigated at  $n=5$ .

	$K_m$ ( $\mu\text{M}$ )
<b>Total MUH hydrolysis</b>	$31 \pm 5$
<b>WWL70 sensitive</b>	$45 \pm 7$
<b>WWL70 insensitive</b>	$25 \pm 4$

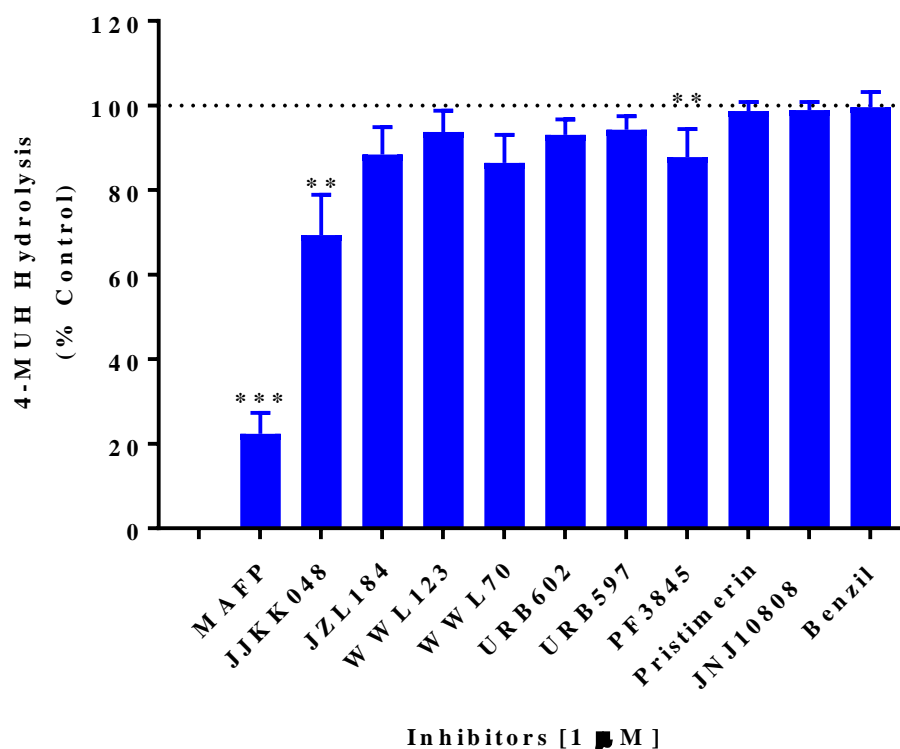


Figure 3.17 Hydrolysis of 50 μM 4-MUH by the rat hippocampus in the presence of eleven inhibitors screened at 1 μM.

Data represent the mean ± SEM of five independent biological repeats conducted in duplicate. Data were analysed blind (Dr Stephen Alexander) using Friedman analysis with uncorrected Dunn's test (\*\*  $p \leq 0.01$  and \*\*\*  $p \leq 0.001$ ) compared to the control (ABHD6+MUH) in the absence of any inhibitor.

The same inhibitors used in the screening of the recombinant system previously were applied in the rat hippocampal tissue. As demonstrated, only MAFP caused a substantial inhibition of 4-MUH hydrolysis (22 ± 10% control). JKKK048 and PF3845 evoked significant inhibitions to 69 ± 10 and 88 ± 7 % control, respectively.

Since WWL70 appeared to produce a small reduction in 4-MUH hydrolysis, it was investigated over a broader range of concentrations (Figure 3.18). The obtained  $pIC_{50}$  value was  $7.9 \pm 0.56$  and  $R_{max}$  was 30 % ± 7 for  $n = 5$ .

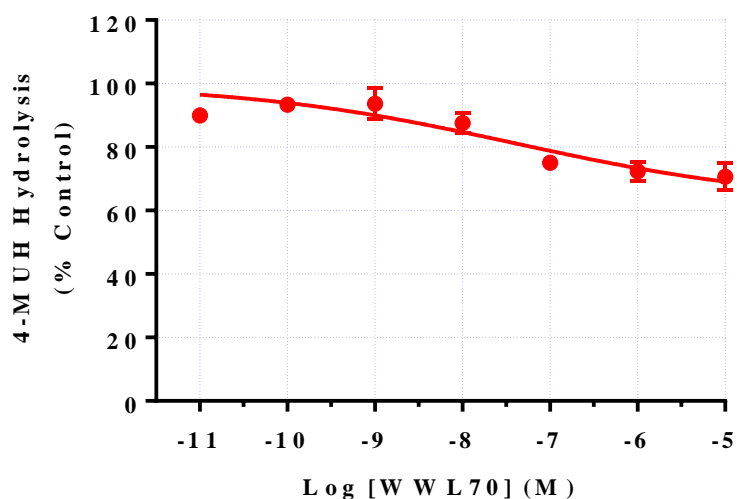


Figure 3.18 The effect of increasing WWL70 concentration on the hydrolysis of 50  $\mu$ M 4-MUH in rat hippocampus. Data represent the mean  $\pm$  SEM of five independent experiments conducted in duplicates.

Given the incomplete inhibition by WWL70 and the implication that there would be other enzymes in the rat hippocampus hydrolysing 4-MUH alongside ABHD6, the inhibitors were further assessed in the presence and absence of 1  $\mu$ M WWL70.

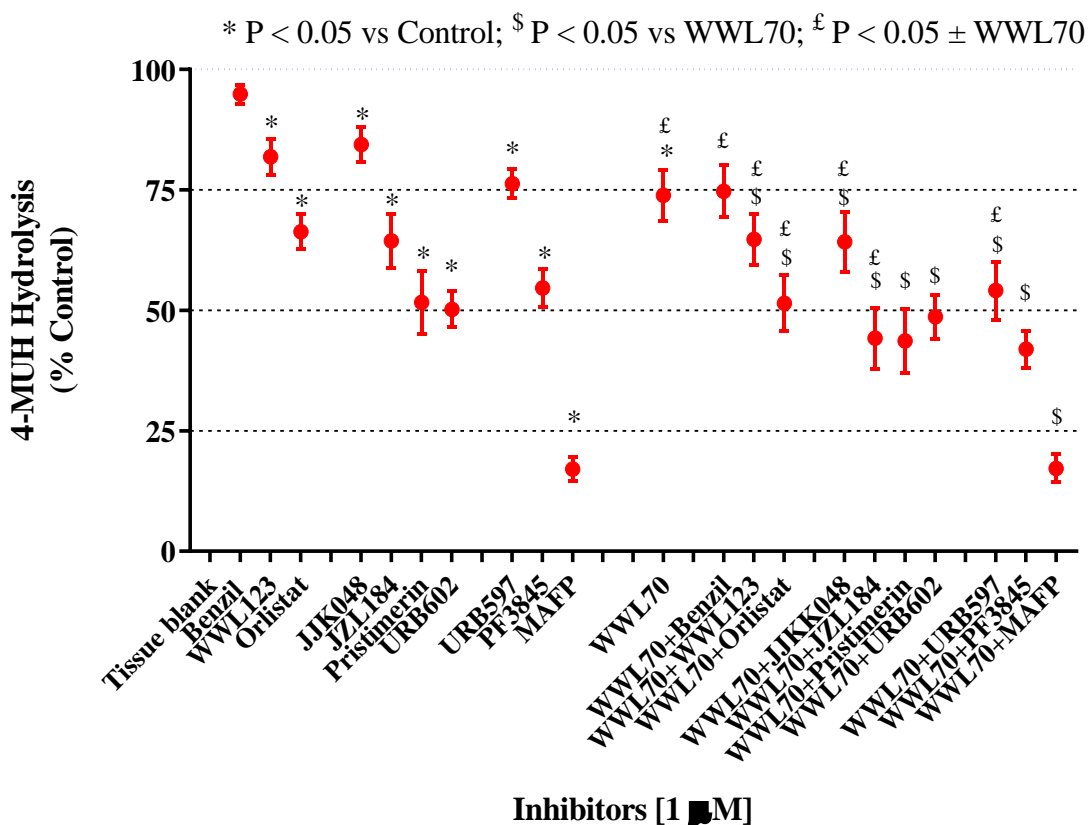


Figure 3.19 The hydrolysis of 50 μM 4-MUH by rat hippocampus preparations, where eleven inhibitors (1 μM) were screened in the presence and absence of 1 μM WWL70.

Data represent the mean ± SEM of five independent biological repeats conducted in duplicate. Data were analysed blind (by Dr Stephen Alexander) using one-way ANOVA followed by Dunnett's multiple comparison test. \* $p < 0.05$  compared to the control; \$ $p < 0.05$  compared to WWL70 alone; £ $p < 0.05$  comparing the presence to the absence of WWL70.

With respect to the total activity, all of the screened inhibitors caused a significant reduction in the hydrolysis of 4-MUH except for benzil. WWL70 on its own caused a substantial, but incomplete (~25% inhibition) inhibition of 4-MUH hydrolysis. MAFP evoked the greatest effect of the inhibitors ( $17 \pm 2\%$  control). PF3845, pristimerin and URB602 also prompted ~50% inhibition ( $55 \pm 4$ ,  $52 \pm 7$  and  $50 \pm 4\%$  control, respectively). This extent of inhibition was quite distinct from that presented in Figure 3.17. When the inhibitors were co-incubated with 1 μM WWL70 and the rat hippocampal tissue, the purpose was to attempt to define the enzymes other than ABHD6 capable of hydrolysing 4-MUH. If WWL70 were capable of selectively blocking ABHD6, further inhibition by another agent could allow the definition of the further

enzymatic activity/activities. In the presence of WWL70, all of the inhibitors induced a further significant decrease in 4-MUH hydrolysis except for benzil. Co-incubation of MAFP and WWL70 did not induce inhibition beyond MAFP alone. The MAGL inhibitors pristimerin, JZL184, JJKK048 and URB602 produced a significant decrease in 4-MUH hydrolysis in the presence of WWL70. The pancreatic lipase and DAGL inhibitor orlistat induced a further inhibition in the presence of WWL70. The FAAH inhibitors URB597 and PF3845 caused a further inhibition of 4-MUH hydrolysis in the presence of WWL70. Finally, the ABHD6 inhibitor WWL123 induced an additional inhibition of 4-MUH hydrolysis in combination with WWL70.

## 3.2 Discussion

### 3.2.1 4-MUH as an ABHD6 Substrate

The development of novel therapeutic compounds targeting the endocannabinoid system requires thorough understanding of the entire endocannabinoid signalling pathway. Assays to measure ABHD6 activity have very recently been reviewed (Deng and Li, 2020). Currently, the ‘Gold Standard’ method for ester endocannabinoid hydrolases utilizes radioactive versions of 2OG and 2AG, namely 2-oleoyl-[<sup>3</sup>H]-glycerol and 2-arachidonoyl-[<sup>3</sup>H]-glycerol respectively, and quantifies the produced <sup>3</sup>H-glycerol following metabolism by the endocannabinoid hydrolysing enzymes (Ghafouri et al., 2004). Alternative techniques for measuring the hydrolytic activity of endocannabinoid hydrolysing enzymes involve gas or liquid chromatography system for quantifying the metabolic product, for example, arachidonic acid released upon the hydrolysis of 2AG (Muccioli and Stella, 2008). Both procedures are time-consuming, difficult to adapt for inhibitor screening and the radiolabelled technique is limited by its high cost and the need for specialised disposal of reagents. There is thus a need for developing an assay that is high-throughput, rapid, cost-effective, reproducible and feasible given the complexity posed by the instability and lipophilic nature of the endocannabinoids, such as 2AG.

Initial pilot investigations investigated multiple substrates including 4-NPA, 4-MUO and 4-MUH as substrates for the endocannabinoid esterases MAGL, ABHD6 and ABHD12. 4-MUH emerged as a promising substrate particularly for ABHD6 compared to the other esterases. 4-MUH is poorly hydrolysed by non-lipolytic esterase enzymes (Gilham and Lehner, 2005), thus further investigations were performed to characterise the recombinant ABHD6 enzyme and to assess whether this assay could be utilized in native tissues. As a fluorescent assay, it is considered sensitive, could be continuously monitored; and has the potential of being applied using robotics.

In order to determine the appropriate 4-MUH concentration to be used in subsequent experiments, the  $K_m$  for recombinant ABHD6 was determined to be  $41 \pm 11 \mu\text{M}$ ; successive experiments were conducted using 50

$\mu\text{M}$  final concentration of the substrate. The fluorescence generated with recombinant ABHD6 and 50  $\mu\text{M}$  4-MUH was greater than 10-fold the background levels indicating a useful dynamic range.

Eleven inhibitors of endocannabinoid hydrolases were screened at 1  $\mu\text{M}$ , benzil, JKKK048, JNJ1661010, JZL184, MAFP, PF3845, pristimerin, URB597, URB602, WWL70 and WWL123. The lack of effect of the FAAH inhibitors URB597, JNJ1661010 and PF3845, the MAGL inhibitors URB602, JZL184 and pristimerin and the carboxylesterase inhibitor, benzil as inhibitors of ABHD6, confirms or identifies their value as selective inhibitors of those enzymes, without altering ABHD6 activity. MAFP, JKKK048, WWL70 and WWL123 caused an inhibition and hence were further investigated over a range of concentrations (Figure 3.10). The irreversible inhibitor of multiple endocannabinoid hydrolysing enzymes MAFP, produced a complete inhibition of ABHD6 activity with a potency ( $\text{pIC}_{50}$  value) of  $8.0 \pm 0.2$ . MAFP has previously been reported to inhibit ABHD6 in the ABPP assay with a  $\text{pIC}_{50}$  value of 9 (Marrs et al., 2010). JKKK048 is described as a selective MAGL inhibitor with high potency ( $\text{pIC}_{50}$  values of 9.4 - 9.7) (Aaltonen et al., 2013). In these experiments, JKKK048 caused a complete inhibition of ABHD6 activity albeit with a lower potency than described as a MAGL inhibitor ( $\text{pIC}_{50}$  of  $7.1 \pm 0.1$ ). This value is similar to the potency of JKKK048 described for ABHD6 hydrolysis of 2AG using a glycerol detection method ( $\text{pK}_i$  of 6.6) (Aaltonen et al., 2013).

WWL70, described as a potent selective ABHD6 inhibitor, demonstrated a complete inhibition of ABHD6 activity with a  $\text{pIC}_{50}$  value of  $7.3 \pm 0.1$ , consistent with the literature potency ( $\text{pIC}_{50}$  value of 7.2) identified using the ABPP technique (Marrs et al., 2010). WWL123 caused an incomplete inhibition of ABHD6 activity with a  $\text{pIC}_{50}$  value of  $6.3 \pm 0.1$ . It was described to inhibit ABHD6 completely using the ABPP assay with a comparable  $\text{pIC}_{50}$  value of 6.4 (Bachovchin et al., 2010).

Taken together, the inhibitor profiling of ABHD6 using 4-MUH as a substrate shows many similarities to literature descriptions, but some interesting differences, which will require some further investigation to identify whether the effects are substrate-dependent, for example.

### 3.2.2 Definition of a high-throughput screening assay

Although WWL70 is a reasonably potent inhibitor of ABHD6 with some selectivity, it has been reported to have some off-target effects independent of ABHD6 (Tanaka et al., 2017). Other ABHD6 inhibitors, which were not available at the time of conducting these experiments have also been described. Thus, JZP430 has an  $IC_{50}$  value of 44 nM (Patel et al., 2015) and KT182 is reported to have a slightly increased potency  $IC_{50}$  value 1.7-15 nM (Hsu et al., 2013). It would be useful, therefore, to have further options as lead inhibitors to allow for different pharmacological / therapeutic applications, such as brain penetration or peripheral restriction.

4-MUH was then investigated to assess its suitability for high-throughput screening. A  $Z'$  score was computed using 1  $\mu$ M WWL70 as the positive control (Zhang et al., 1999). The calculated  $Z'$  score for ABHD6 HTS assay was found to be 0.42, implying a borderline or a marginal assay, albeit close to the threshold for a 'useful' assay. The screening was therefore extended to incorporate thirty-six compounds (Figure 3.11) belonging to diverse structural and enzyme inhibitor classes. None of the compounds evoked a significant inhibition except for the pancreatic lipase and DAGL inhibitor orlistat, also referred to as tetrahydrolipstatin. A concentration-response curve was conducted to establish a  $pIC_{50}$  value of  $6.7 \pm 0.1$ . Previously, orlistat was described to have a  $pIC_{50}$  value of 7.3 in a glycerol detection assay (Savinainen et al., 2014). To further investigate the substrate specificity of ABHD6, 1-OG, 2AG, 2-PG, 2-OG, and NAGLY were investigated in the 4-MUH assay. 2AG, 2-OG and NAGLY appeared to compete with 4-MUH for ABHD6 hydrolysis. However, their overall level of inhibition was not substantial at this concentration, with the maximum level of inhibition induced by 2AG at  $68 \pm 4$  % of the control followed by NAGLY at  $82 \pm 2.2$  % and finally 2-OG at  $84 \pm 1.9$  % of the control. As opposed to the study of (Navia-Paldanius et al., 2012), 1-OG and 2-PG were incapable of inhibiting 4-MUH hydrolysis via ABHD6 although neither substrate approached the effect of 2AG. The two endogenous amides, AEA and NAGLY (Figure 3.13) evoked significant, if modest, inhibitions of 4-MUH hydrolysis induced by ABHD6. Nevertheless, the implication of these findings

is not yet clear and requires further investigation. It seems unlikely that ABHD6 will significantly contribute to anandamide hydrolysis *in vivo*, given the modest inhibitory effect of 100  $\mu\text{M}$  anandamide, as well as the complete inhibition of anandamide hydrolysis by the FAAH inhibitor URB597. The utilisation of 4-MUH as a screening tool for ABHD6 is likely to be a useful tool for the application in recombinant systems either for characterisation of the enzyme (for instance, to investigate the influence of post-translational modifications) or for high throughput screening for inhibitors.

### 3.2.3 The use of 4-MUH in native tissues

‘Real tissue’ from rat gut was explored to identify whether the assay could be employed in native tissue rather than simply the recombinant systems. Tissue preparations obtained from the small and large intestine, from both male and female Wistar rats, were tested in multiple experiments to determine the affinity of 4-MUH hydrolysis. This tissue was chosen because preliminary investigations based on the RT-qPCR investigations found an elevated ABHD6 expression level compared to MAGL in these tissues (Nada S Mahmood, PhD thesis).

However, several experimental approaches using rat intestinal tissue produced  $K_m$  values that were ambiguous and further investigations using intestinal preparations were thus halted. This ambiguity could be attributed to the presence of multiple enzymes in the intestinal preparations, which could be interfering with the assay. Rat hippocampus was investigated as an alternative, based on the high expression profile of ABHD6 in murine brain specifically in the frontal cortex, the hippocampus, striatum and cerebellum (Cao et al., 2019). WWL70 was utilized in these experiments to define ABHD6 activity. The experimental  $K_m$  of the WWL70-sensitive fraction was found to be  $45 \pm 7 \mu\text{M}$ , in a range similar to the human recombinant ABHD6. Subsequent experiments with rat hippocampal fractions were conducted using 50  $\mu\text{M}$  4-MUH, as for the recombinant enzyme. When a concentration-response investigation was conducted for WWL70 using the rat hippocampus, it was found to cause only 25% inhibition of 4-MUH hydrolysis. The potency of WWL70 in the rat hippocampus ( $\text{pIC}_{50}$  value of 7.9) was consistent with the presence of ABHD6

(Figure 3.12). Hence, another enzyme or enzymes other than ABHD6 present in the rat hippocampal tissue appeared to be responsible for the majority of 4-MUH hydrolysis, at least using the assay in its current configuration.

In order to identify what these alternative esterases might be, the rat hippocampus was screened in the presence of the same eleven inhibitors used with the recombinant enzyme. Only the non-selective irreversible inhibitor MAFP caused a greater level of direct inhibition (by 75%). This could be taken to mean that serine hydrolases were responsible for 75 % of 4-MUH hydrolysis in the rat hippocampus, with other esterases responsible for the remainder. None of the other inhibitors reached 50 % reduction in 4-MUH hydrolysis. These inhibitors were further screened at 1  $\mu$ M in the presence of 1  $\mu$ M WWL70 to confirm whether enzymes other than ABHD6 responsible for 4-MUH hydrolysis could be identified. If WWL70 were capable of selectively and ultimately completely blocking ABHD6, and another inhibitor known to target another esterase induced an inhibitory effect during co-incubation, this would imply the involvement of that esterase. In the presence of WWL70, all of the inhibitors induced a further significant decrease in 4-MUH hydrolysis except for benzil. Effectively, therefore, carboxylesterase (the target for benzil, (Hatfield and Potter, 2011)) can be discounted as a 4-MUH esterase in rat hippocampus. The lack of inhibitory effect of benzil in the absence of WWL70 is also consistent with its ineffectiveness against recombinant ABHD6 activity.

The pancreatic lipase and DAGL inhibitor orlistat induced a further inhibition in the presence of WWL70. Orlistat produced an effect in the presence and absence of WWL70 which could indicate a role for DAGL in 4-MUH hydrolysis, given the potential for 4-MUH to be a broad substrate for esterases (Iglesias et al., 2016). Indeed, a similar substrate, 6,8-difluoro-4-methylumbelliferyloctanoate, has been used to assay recombinant DAGL $\alpha$  (Singh et al., 2016).

The MAGL inhibitors JKKK048, JZL184, pristimerin and URB602 all produced a significant decrease in 4-MUH hydrolysis in the absence of WWL70. This could be taken as evidence for the involvement of MAGL in 4-MUH hydrolysis in the rat hippocampus (Aaltonen et al., 2013; King et al.,

2009). However, the interpretation is complicated since only JJKK048 and JZL184 evoked further inhibitions in the presence of WWL70. Given that pristimerin and URB602 failed to inhibit recombinant ABHD6, the lack of further inhibition when combined with WWL70 is not easy to explain. It is possible that, although 4-MUH is not a good substrate for recombinant MAGL activity, the levels of MAGL activity in the brain are so high, that a small hydrolytic capacity is measurable using this assay. This could be tested using the same preparation from rat hippocampus and measuring <sup>3</sup>H-2-OG hydrolysis in the presence of 4-MUH to identify whether there is a crossover between the two substrates.

The FAAH inhibitors URB597 and PF3845 caused different levels of inhibition of 4-MUH hydrolysis in the absence of WWL70. The level of inhibition was increased in the presence of WWL70, while the rank order was maintained. The inhibitory effect induced by PF3845 and URB597 could be attributed to 4-MUH hydrolysis by FAAH (Booker et al., 2012; Kwilasz et al., 2014; Ogawa and Kunugi, 2015). The capacity for FAAH to hydrolyse esters should, therefore, be further investigated, for instance using rat hippocampal preparations and testing <sup>3</sup>H-anandamide hydrolysis in the presence of 4-MUH.

Finally, the ABHD6 inhibitor WWL123 evoked a lower inhibition than WWL70, and this inhibition of 4-MUH hydrolysis was maintained in combination with WWL70.

The level of inhibition induced by MAFP was the largest of all the inhibitors and was not altered in the presence of WWL70, suggesting a prominent effect of serine hydrolases. Unfortunately, due to the non-selective nature of MAFP (acting on ABHD6, ABHD12, FAAH and MAGL (Aaltonen et al., 2013)), it is not possible to get further clarity as to which enzymes are involved.

One further complication to the interpretation of the analysis of 4-MUH hydrolysis in the rat hippocampus is the possibility of species differences between the rat tissue and the human recombinant enzymes which have typically been used to investigate the inhibitors.

### **3.3 Conclusion**

The 4-MUH HTS assay using the recombinant ABHD6 system appears to be very encouraging for screening potentially novel inhibitors for this enzyme. However, the assay in its current configuration applied to 'real' tissues, including rat intestine and hippocampus, generated data that was complex and difficult to interpret. It is possible that further adapting this assay may resolve these issues, but it does appear to be a challenge.

## Chapter 4 : Functional Activity of the Fenofibrate Derivatives at the Cannabinoid CB<sub>2</sub> Receptor

There continues to be reluctance towards the use of *Cannabis*-derived medicinal preparations in many countries because of the unwanted psychotropic effects due to CB<sub>1</sub> receptor activation. By contrast, CB<sub>2</sub> receptor stimulation evokes desirable therapeutic effects in multiple preclinical models. The low expression of CB<sub>2</sub> receptors in the CNS renders CB<sub>2</sub> receptor selective drugs appealing as potential therapeutic agents as they would evoke negligible psychoactive effects (Buckley et al., 2000). CB<sub>2</sub> receptor agonists and ligands that alter endocannabinoid degradation to enhance endocannabinoid system signalling have potential use as antiemetics, immunomodulatory drugs, analgesics, anti-asthmatics, antiepileptics, hypnotics, neuroprotective and anti-inflammatory agents (Cabral and Griffin-Thomas, 2009; Grant and Cahn, 2005). CB<sub>2</sub> receptor agonists have also been proposed to have therapeutic benefits in hepatic fibrosis, atherosclerosis and bone formation (Svizenska et al., 2008).

A number of studies have demonstrated the involvement of the endocannabinoid system, its receptors and associated ligands in coordinating physiological functions (Di Marzo and Petrosino, 2007) as elaborated upon in Chapter 1.5.4. There appears to be a predominant involvement of the endocannabinoid system and its receptors in neurodegenerative diseases with anti-inflammatory effects. Because of these anti-inflammatory and neuroprotective effects, the application and use of CB<sub>2</sub> receptor agonists is proposed to have an interesting and promising therapeutic potential for the management of an array of diseases (Cassano et al., 2017), Chapter 1.5.4. The recognition of CB<sub>2</sub> receptor as a therapeutic potential has gained significant interest over the past years. Nonetheless, further studies and investigations are required to gain an enhanced understanding of the regulation of CB<sub>2</sub> receptors, the physiological functions they mediate and its potential clinical applications (Dhopeshwarkar and Mackie, 2014). Despite possessing initial promising effects in multiple clinical trials, CB<sub>2</sub> receptor agonists have not yet proceeded to the clinical level till date (Dhopeshwarkar and Mackie, 2014; Onaivi et al., 2015).

We sought to expand upon the current understanding of the function and signalling transduction of the cannabinoid CB<sub>2</sub> receptor given its growing interest as a therapeutic target. The upcoming chapters are predominantly focused on investigations performed aiming to characterize the human cannabinoid CB<sub>2</sub> receptors *in vitro*, in particular making use of novel chemical entities to gain an enhanced understanding of the different signalling pathways associated with CB<sub>2</sub> receptors. These chapters aim to characterize the cannabinoid CB<sub>2</sub> receptors, in particular, to understand the residues of the CB<sub>2</sub> receptor that influence its signalling profile.

Recent investigations have revealed that a series of fenofibrate derivatives with increasing hydrophobicity of an attached substituent, altered the ligand profile from acting as a full agonist, to partial agonist, to antagonist and inverse agonist at the CB<sub>2</sub> receptor [<sup>35</sup>S]-GTPγS binding assay. This profile suggested the presence of target residues that contribute to this molecular switch. This project aimed to explore this molecular switch while simultaneously investigating the multiple signalling pathways of the recombinant CHO-CB<sub>2</sub> receptor, in addition to the receptor's interactions and site-directed mutagenesis to more closely identify the locus of this molecular switch and its functional outcomes.

#### 4.1 Fenofibrate Derivatives: FD24, FD43, FD44 and FD46 and the commercially available alternatives: SER601 and COR170

A recent doctoral thesis investigated producing novel fenofibrate derivatives by molecular docking procedures generated an interesting series namely, FD24, FD43, FD44 and FD46 (Chapter 2: Table 2.1) aimed at possessing therapeutic advantages of the anti-inflammatory effects of CB<sub>2</sub> receptors and the antihyperlipidemic effects of the PPAR $\alpha$  receptors simultaneously. As the group attached at the amide terminus was altered from piperidin-1-yl, exo-norborn-2-yl, R-(+)-born-2-yl to adamant-1-yl shifted the functional activity of the compounds from acting as a full agonist to partial agonist to antagonists/inverse agonists, respectively. The primary focus of this chapter was to investigate the signalling profiles of these compounds in order to gain an enhanced understanding of CB<sub>2</sub> receptor signalling and the molecular switch induced subsequent to the modification of these hydrophobic substituents.

Furthermore, the selection of the investigated ligands was broadened to include SER601 (also referred to as COR167) and COR170 to the existing fenofibrate derivatives as commercially available alternatives with similar hydrophobic substitutions projected to act at the same molecular switch of the cannabinoid CB<sub>2</sub> receptor. The published literature suggests that adding bulk to the side chain by modifying the *iso*-propyl substituent to a phenyl group altered their activity from acting as a full agonist (SER601) (Contartese et al., 2012) to an inverse agonist (COR170) (Pasquini et al., 2010). The effect of this molecular switch, and the effect of increased bulkiness and hydrophobicity of the compounds was investigated within the different CB<sub>2</sub> receptor signalling pathways.

### 4.1.1 [<sup>3</sup>H]-CP55,940 Competition Binding Assay

The investigation started with optimizing the protein concentration for radioligand binding studies, with the highest signal to noise ratio obtained at 100 µg/mL. This was employed in subsequent experiments.

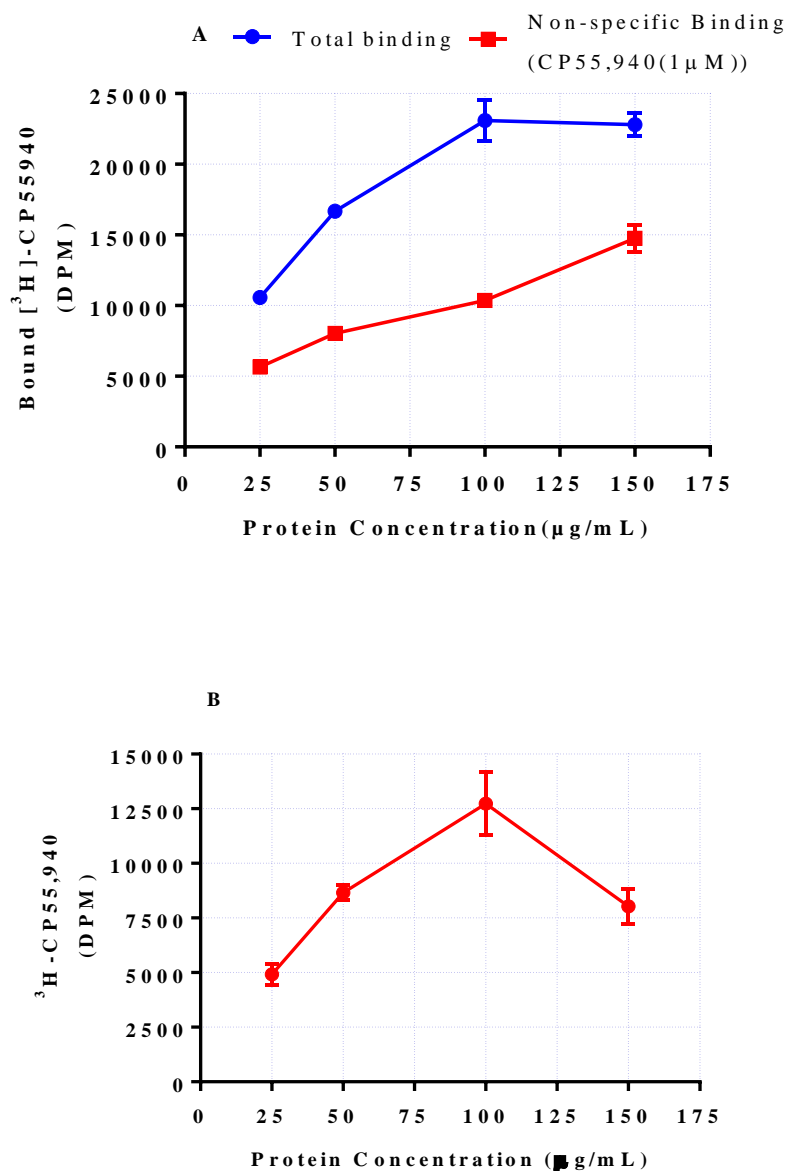


Figure 4.1 (A) Displacement binding of <sup>3</sup>H-CP55,940 to membrane suspensions of CHO-CB<sub>2</sub> cells reported as dpm. (B) Specific binding of <sup>3</sup>H-CP55,940 at different protein concentrations. Data are the mean ± SEM of a single optimization experiment performed in triplicate, subtracting the non-specific binding induced by 1 µM unlabelled CP55,940 from the total binding.

Preliminary studies using autologous competition of [<sup>3</sup>H]-CP555940 binding with CP55940 allowed identification of  $K_d$  and  $B_{max}$  values as  $0.63 \pm 17$  nM and  $382 \pm 68$  fmol/mg, respectively. Using these values, the generated curves were fit using GraphPad Prism using One-Site Fit  $K_i$  and the obtained affinities ( $pK_i$  values) were 7.12 and 6.59 for FD24 and FD43 respectively. FD44 and FD46 on the other hand induced an incomplete inhibition approaching around 50% displacement of [<sup>3</sup>H]-CP555940 at the highest investigated concentration of  $10^{-5}$  M for both compounds.

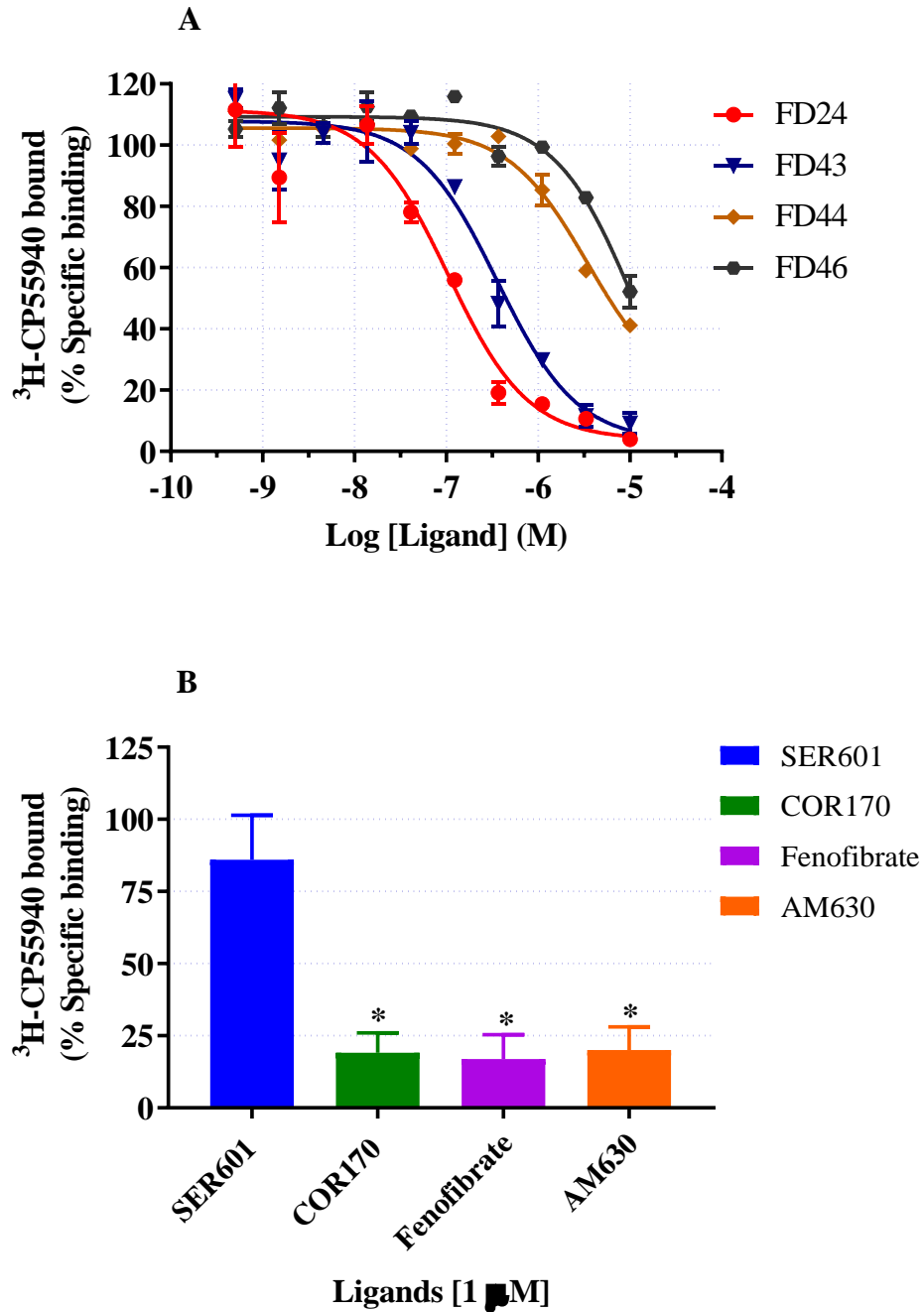


Figure 4.2 Specific binding of [ $^3\text{H}$ ]-CP55,940 from membrane suspensions of CHO-CB<sub>2</sub> cells.

(A) Data are mean  $\pm$  SEM of a single experiment performed in duplicate for each of the novel fenofibrate derivatives. The generated curves were fit using non-linear regression and One-Site Fit  $K_i$  constraining values for the radioligand [ $^3\text{H}$ ]-CP55940 concentration to 0.25 nM and  $K_d$  to 0.63 nM. (B) Data represent the mean  $\pm$  SEM of three individual experiments performed in duplicate screening of SER601, COR170, fenofibrate and AM630 investigated at a single concentration of 1  $\mu\text{M}$ . \* $p \leq 0.05$ , One-way ANOVA test with Dunnett's multiple comparison analysis.

The single point investigation of the other four compounds at 1  $\mu\text{M}$  revealed that COR170, fenofibrate and AM630 exhibited more than 80% displacement, while SER601 displayed no significant occupancy of CB<sub>2</sub> receptor at 1  $\mu\text{M}$ . Since AM630 was expected to demonstrate a higher receptor occupancy given it has a reported  $K_i$  value of 31.2 nM (Ross et al., 1999) and the lack of receptor occupancy demonstrated by SER601, both of these compounds were further investigated over a range of concentrations.

The affinities of SER601 and AM630 were calculated via a One-Site Fit  $K_i$  as  $\text{p}K_i$  values of  $6.35 \pm 0.02$  and  $6.51 \pm 0.15$ , respectively for  $n = 3$  (Figure 4.3). These values were quite distinct from the reported  $\text{p}K_i$  values of SER601 = 8.20 (Pasquini et al., 2008) and AM630 = 7.51 (Ross et al., 1999).

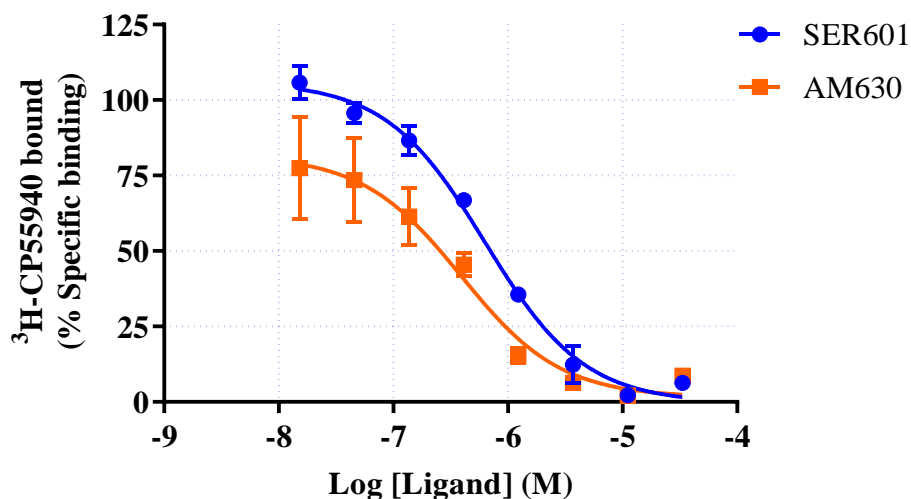


Figure 4.3 Specific binding of [<sup>3</sup>H]-CP55940 to membrane suspensions of CHO-CB<sub>2</sub> cells displaced by AM630 and SER601.

Data are the mean  $\pm$  SEM of three independent experiments performed in duplicate.

### 4.1.2 Fluorescent Binding Assay

Subsequent to the use of the radioactive displacement assay, and since the use of radioactive ligands imposes financial and practical constraints and is limited to being an endpoint assay, the following step involved the use of fluorescent binding assay which offers a more flexible alternative. Moreover, the washing steps involved at the end of the experiment hinder the possibility of any kinetic measurements in a single experiment. Therefore, the utilisation of fluorescent probes provides an alternative that allows investigation of the binding affinities and kinetic parameters of CB<sub>2</sub> receptor ligands without using radioactive material. A novel assay was investigated (in collaboration with David Sykes and Dmitry Veprintsev of COMPARE), which makes use of a Time Resolved fluorescence resonance energy transfer (FRET) assay in which CB<sub>2</sub> receptor is modified to covalently link a terbium atom, which is prompted to fluoresce when a fluorescent ligand (in this assay RO7297590) binds to the CB<sub>2</sub> receptor. Binding assays based on FRET are currently used which occurs between a ‘donor’ fluorophore and an ‘acceptor’ fluorophore (Bosma et al., 2017). HEKS293T cells overexpressing SNAP-tagged CB<sub>2</sub> receptors were labelled with a SNAP-Lumi4-Tb FRET donor as mentioned in [section 2.11](#) and laser excitation at 337 nm wavelength of this donor initiates energy transfer (FRET) to a proximal fluorescent acceptor. Initially, the saturation binding of RO7297590 was investigated using the particular batch of CB<sub>2</sub> receptor membranes employed (Figure 4.4).

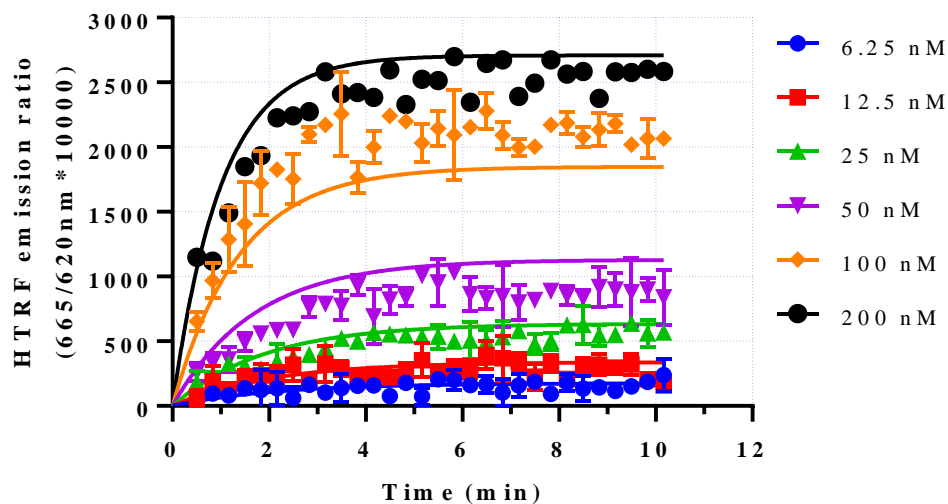


Figure 4.4 Determination of saturation binding of the fluorescent compound R07297590 to human CB<sub>2</sub> receptor membranes. Data are mean  $\pm$  SEM from one representative experiment performed in duplicate repeated using three different membrane preparations.

Data were analysed using GraphPad Prism and the generated curves were fitted via Association Kinetics – two or more concentrations of the tagged ligand in order to obtain estimates of  $K_{on}$  and  $K_{off}$  which would be used subsequently in the analysis of data obtained by the investigated compounds. The obtained  $K_d$  following the use of R07297590 at concentrations ranging from 6.25 – 200 nM was determined to be  $164 \pm 30$  nM and  $B_{max} = 4514 \pm 290$ . Thereafter, a series of CB<sub>2</sub> receptor ligands were co-incubated with CB<sub>2</sub> receptor preparations and the fluorescent ligand R07297590 (Figure 4.5).

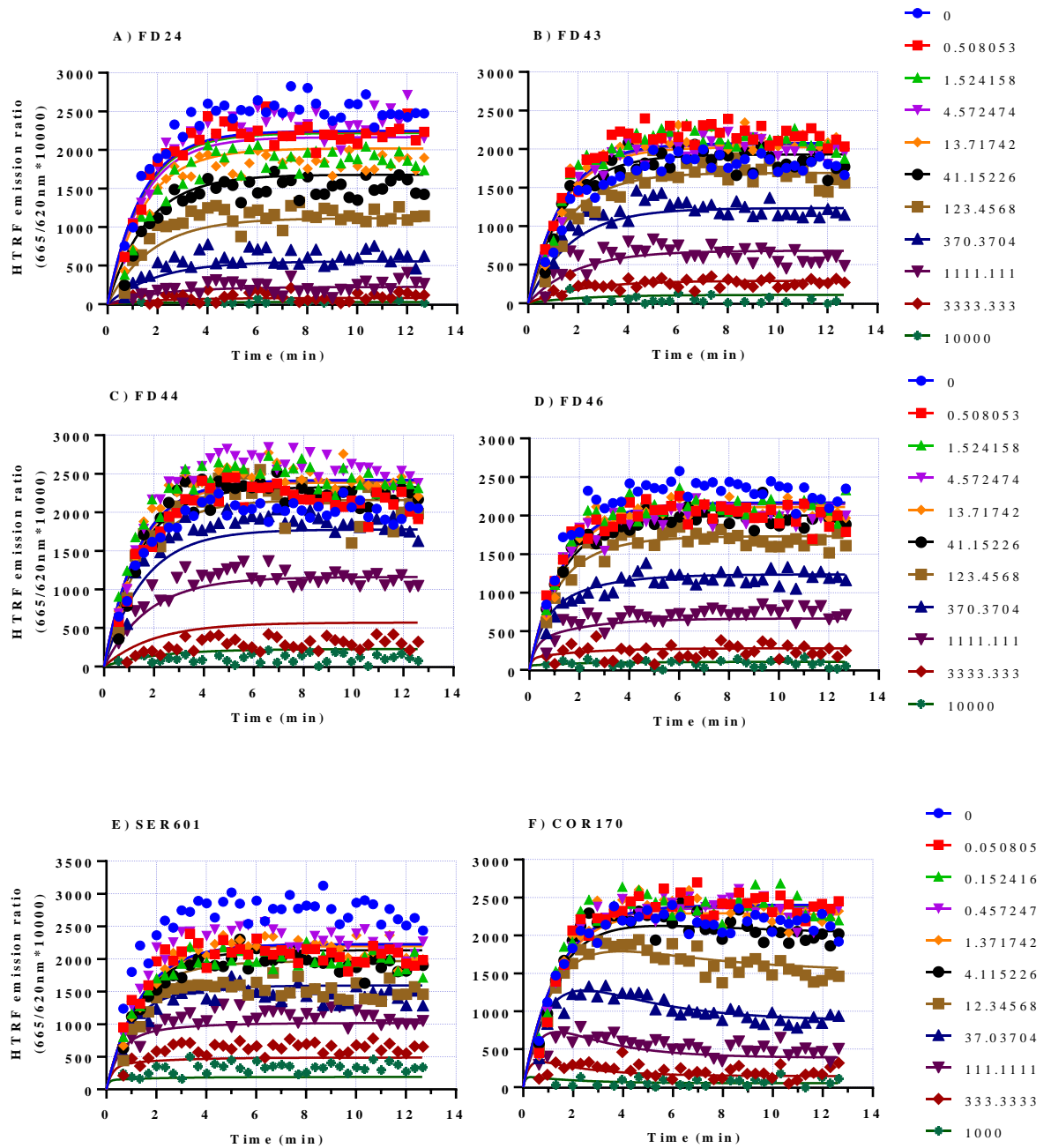


Figure 4.5 Kinetic competition analysis for binding of RO7297590 in the presence of the indicated concentrations of FD24, FD43, FD44, FD46, SER601 and COR170.

Data are the mean  $\pm$  SEM of a representative experiment repeated three times using three different membrane preparations.

Data were analysed using GraphPad Prism via non-linear regression and kinetics of competitive binding and constrained as follows;  $K_1 = K_{on}$  obtained from the  $K_d$  of the fluorescent radiolabelled compound,  $K_2 = K_{off}$  obtained based upon the  $K_d$  analysis,  $[L]$  represents the concentration of RO7297590 = 100 nM used in all of the performed experiments (Section 2.11.1).

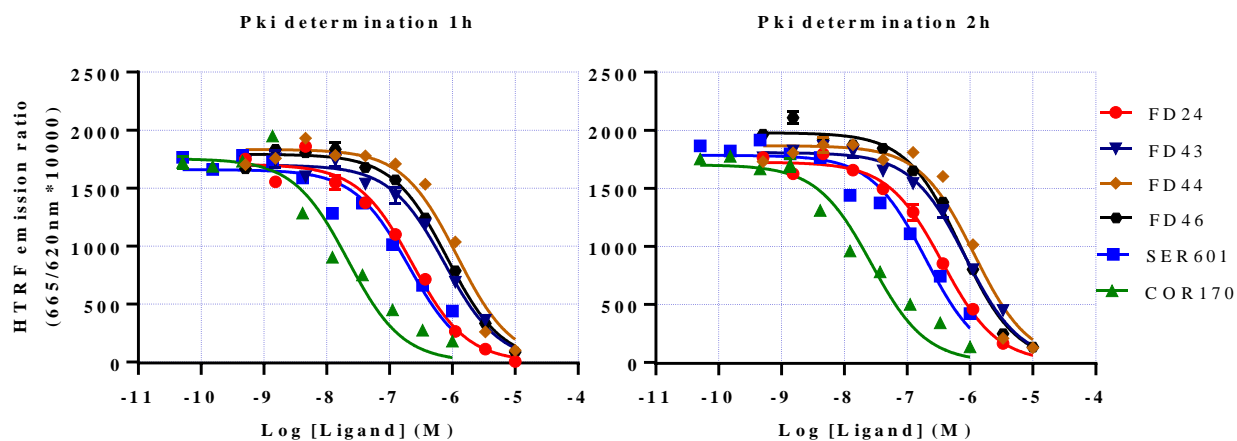


Figure 4.6 Determination of  $pK_i$  values of the six investigated compounds at 1 h and 2 h following the kinetic reading of the plates expressed Log ligand concentration versus the HTRF emission ratio at 665 and 620 nm wavelengths. Data are the mean  $\pm$  SEM of a representative experiment repeated three times using three different membrane preparations.

Data were analysed using GraphPad Prism via non-linear regression and One Site-Fit  $K_i$  and constraining the values of the fluorescent tagged ligand R07297590, to a concentration of 100 nM and  $K_d$  to the value obtained in Figure 4.4. The calculated  $pK_i$  values of the six investigated compounds at 1 and 2 h are described in Table 4.1.

Table 4.1 The  $pK_i$  values of the investigated compounds at 1 and 2 h from three independent experiments.

	<b>FD24</b>	<b>FD43</b>	<b>FD44</b>	<b>FD46</b>	<b>SER601</b>	<b>COR170</b>
$pK_i$ 1h	6.81 $\pm$ 0.11	6.31 $\pm$ 0.09	5.99 $\pm$ 0.11	6.48 $\pm$ 0.13	7.07 $\pm$ 0.10	7.70 $\pm$ 0.13
$pK_i$ 2h	6.62 $\pm$ 0.11	6.32 $\pm$ 0.09	6.19 $\pm$ 0.09	6.46 $\pm$ 0.16	6.84 $\pm$ 0.27	7.64 $\pm$ 0.13

Table 4.2 Binding parameters of the compounds interacting with CB<sub>2</sub> receptors

	<b>FD24</b>	<b>FD43</b>	<b>FD44</b>	<b>FD46</b>	<b>SER601</b>	<b>COR170</b>
K <sub>d</sub> (nM)	89 ± 4	398 ± 17	753 ± 16	454 ± 41	74 ± 4	18 ± 1
B <sub>max</sub> (fmol/mg)	7102 ± 1039	6620 ± 924	7436 ± 1240	6327 ± 376	7105 ± 993	7356 ± 1242

The rank order of the binding affinity of the FD series was COR170 > SER601 ≥ FD24 > FD43 > FD46 > FD44. B<sub>max</sub> is a representative of the total density of receptors and is equivalent to the maximum specific binding. The B<sub>max</sub> values were similar in the six conditions.

### 4.1.3 Calcium Mobilization

A rapid response to CB<sub>2</sub> receptor activation in our CHO-CB<sub>2</sub> cells resulted in an elevation of the release of intracellular calcium levels. Since CHO cells express P2Y receptors, 10 μM ATP was used as a positive control (Magni and Ceruti, 2019) to validate responses on each plate. ATP induced a peak of Ca<sup>2+</sup> release by ~25 s which was progressively reduced over the 120 s time-course. The subsequent figure represents the Ca<sup>2+</sup> release by CB<sub>2</sub> receptor agonists CP55940, FD24, fenofibrate and the antagonist AM630 expressed as relative fluorescent units (RFU). Cells treated with CB<sub>2</sub> receptor agonists induced an elevation in the Ca<sup>2+</sup> release which in the upcoming experiments was normalised to 10 μM ATP. By contrast, the antagonist/inverse agonist AM630 did not induce an effect distinguishable from the basal (Figure 4.7).

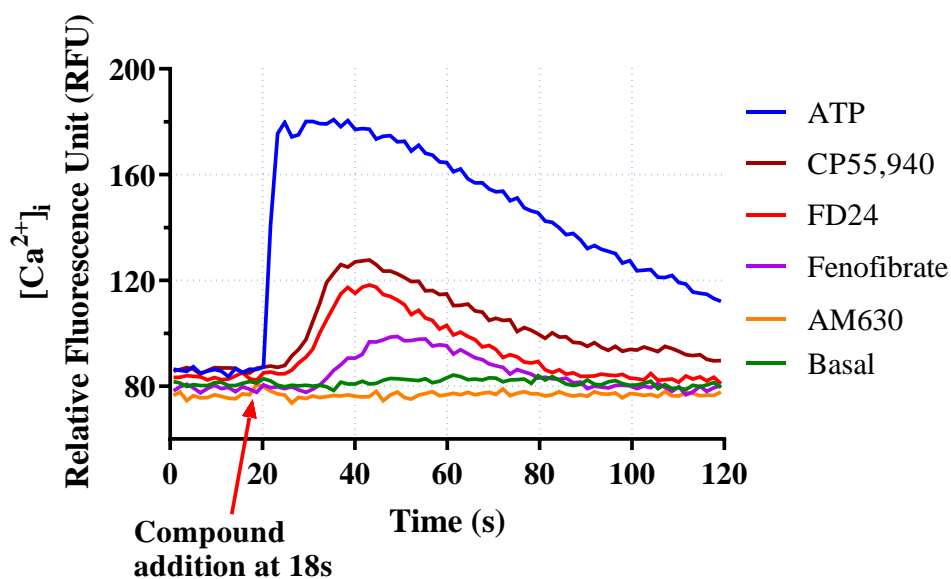


Figure 4.7 The time-course of  $\text{Ca}^{2+}$  ion elevation induced by the compounds indicated, expressed as RFU from a single experiment.

Ligands were initially screened at  $1 \mu\text{M}$  compared to a vehicle control of 0.1% DMSO. As evident from Figure 4.8, only CP55940, fenofibrate and FD24 induced significant  $\text{Ca}^{2+}$  ion elevations. AM630, and the fenofibrate analogues FD43, FD44, and FD46 all failed to alter intracellular calcium levels. The structurally divergent  $\text{CB}_2$  receptor ligands SER601 (Zhang et al., 2016) and COR170 (Contartese et al., 2012) both failed to alter the intracellular  $\text{Ca}^{2+}$  ion levels.

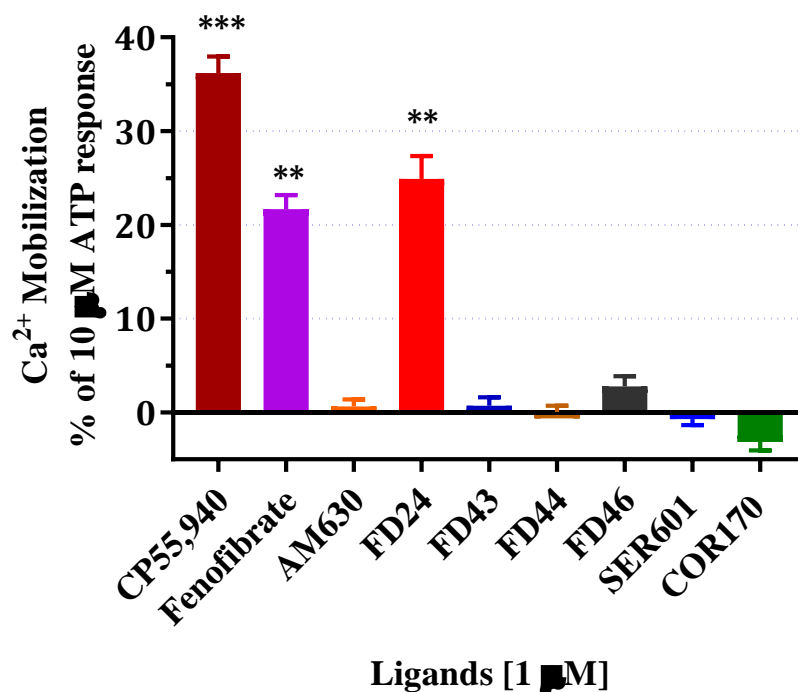


Figure 4.8 Calcium responses evoked by cannabinoid ligands (1 μM) expressed as a percentage of responses to 10 μM ATP (positive control). Total calcium mobilization (calculated as the area under the curve (AUC) over the 120 s incubation period) was normalised to the response to 10 μM ATP. Data are the mean ± SEM of four independent experiments performed in triplicate on different passages of CHO-CB<sub>2</sub> cells. \*\*  $p \leq 0.001$  and \*\*\*  $p \leq 0.0001$ , One-way ANOVA test with Dunnett's multiple comparison analysis compare to 10 μM ATP.

The compounds capable of inducing Ca<sup>2+</sup> ion elevations were further investigated for concentration-dependence. Responses to CP55940, FD24 and fenofibrate were saturable. FD43 was also investigated as it was anticipated to be a partial agonist and its fitting to the four-parameter logistic equation failed to converge, however. Table 4.3 indicates potencies (pEC<sub>50</sub>), maximal responses (E<sub>max</sub> values) and Hill slopes of responses to these compounds.

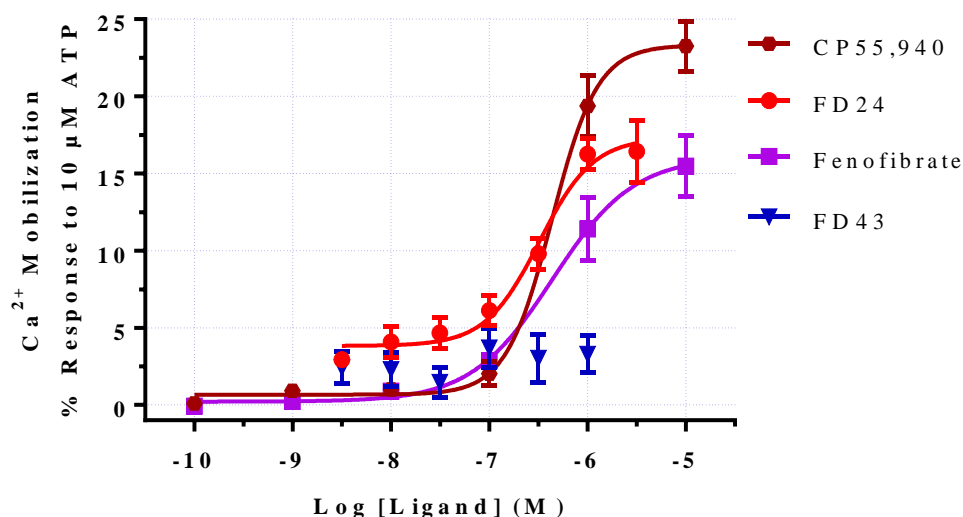


Figure 4.9 Concentration dependence of fenofibrate analogues evoked  $\text{Ca}^{2+}$  responses.

Total  $\text{Ca}^{2+}$  mobilization (calculated as AUC over the 120 s incubation period) was normalised to the response of 10  $\mu\text{M}$  ATP. Data are mean  $\pm$  SEM of three (CP55,940 and fenofibrate) and four (FD24 and FD43) independent experiments performed in triplicate on different passages of CHO-CB<sub>2</sub> cells. The obtained concentration responses were fitted via non-linear regression four parameter logistic equation.

Table 4.3 Concentration-response parameters for fenofibrate analogue-evoked calcium elevations in CHO-CB<sub>2</sub> cells performed at n=3 for CP55,940 and fenofibrate and n=4 for FD24 and FD43.

Compound	Maximal responses $E_{\text{max}}$ (%)	Potencies $\text{pEC}_{50}$	Hill Slope (nH)
CP55,940	$23 \pm 2$	$6.4 \pm 0.04$	$2.07 \pm 0.55$
Fenofibrate	$16 \pm 1$	$6.3 \pm 0.10$	$1.03 \pm 0.22$
FD24	$15 \pm 2$	$6.5 \pm 0.10$	$1.70 \pm 0.33$
FD43	No response	No response	No response

One sample t test analysis of the hill slope indicated that CP55,940, fenofibrate and FD24 had a hill slope that was not statistically different from one. Given that FD44 and FD46 were projected to be antagonists/ inverse agonists, these compounds were investigated in the presence of CB<sub>2</sub> receptor agonists CP55940, fenofibrate and FD24. AM630 was used as a reference antagonist for

comparison. Cells were pre-incubated with AM630, FD44 and FD46 for 30 min prior to addition of the agonists, which were employed at 1  $\mu$ M. CP55940, fenofibrate and FD24 all evoked a significant  $\text{Ca}^{2+}$  release, while the partial agonist FD43 induced no  $\text{Ca}^{2+}$  mobilization. AM630 reduced the  $\text{Ca}^{2+}$  ion elevations evoked by CP55940, fenofibrate and FD24, while neither FD44 nor FD46 significantly altered intracellular  $\text{Ca}^{2+}$  ion responses to any of the investigated  $\text{CB}_2$  receptor agonists.

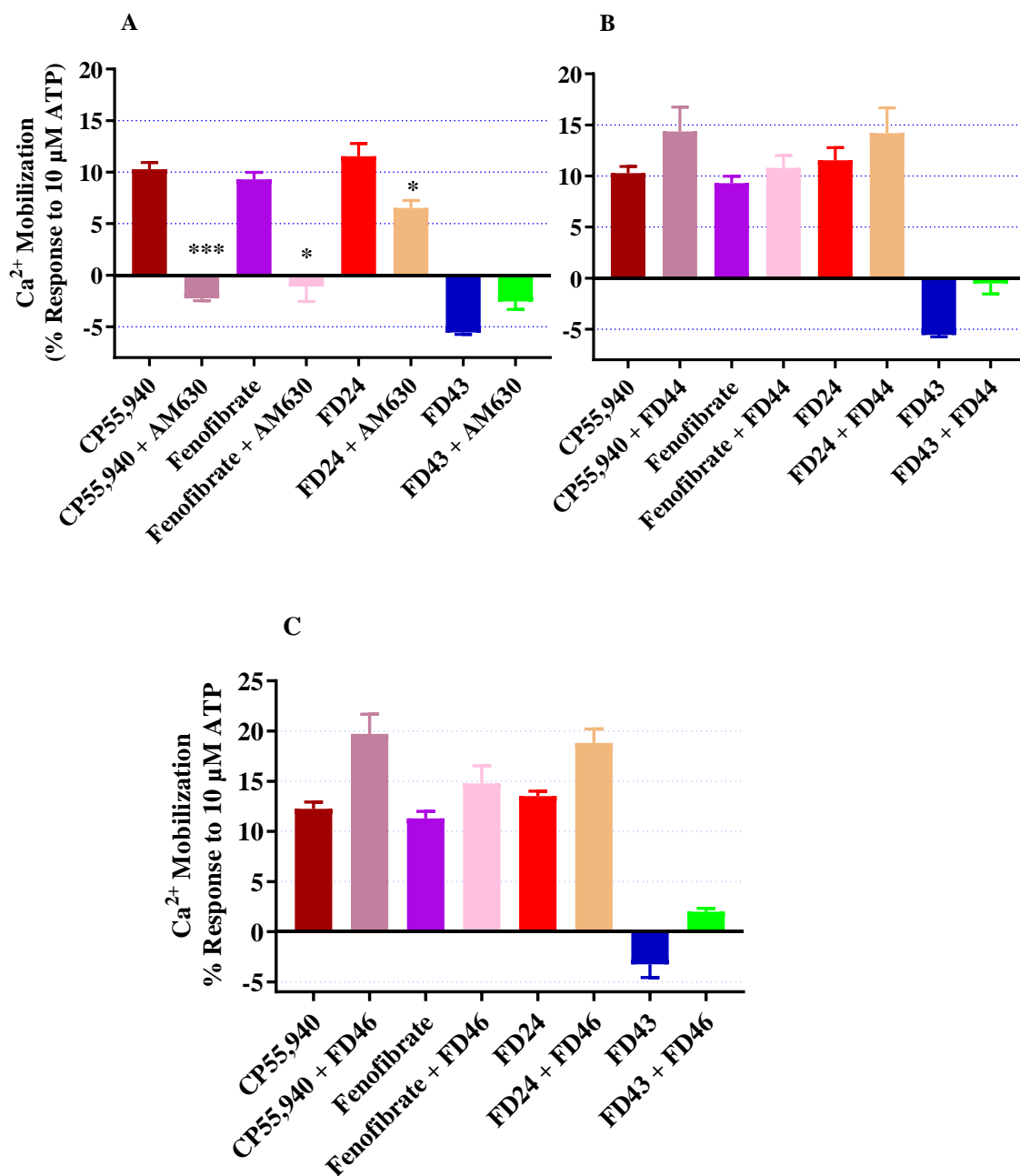


Figure 4.10 Calcium responses to fenofibrate analogues in the absence and presence of putative antagonists.

Responses were induced by the investigated ligands in the presence and absence of (A) the antagonist AM630 or the anticipated (B) inverse agonist and (C) antagonist FD44 and FD46 respectively. Total calcium mobilization (calculated as AUC over the 120 s incubation period) was normalised to the response to 10 μM ATP. Data are the mean ± SEM of four independent experiments performed in triplicate on different passages of CHO-CB<sub>2</sub> cells. \*  $p \leq 0.05$ , \*\*  $p \leq 0.01$  and \*\*\*  $p \leq 0.001$ , One-way ANOVA test with Sidak's multiple comparison analysis comparing the Ca<sup>2+</sup> mobilization in the presence and absence of the antagonists.

#### **4.1.4 In-Cell Western: ERK1/2 Activation**

A second, rapidly responding pathway was selected in order to analyse potential bias in the signalling pathways activated by the fenofibrate analogues. ERK activation is readily monitored using an in-cell western approach, which has previously been applied for CB<sub>1</sub> and CB<sub>2</sub> receptors in the laboratory.

To identify an appropriate time-point for measuring the stimulation of the ERK pathway in CHO-CB<sub>2</sub> cells, a time-course investigation was performed (Figure 4.11A). The peak of ERK stimulation was detected at 5 min; therefore, successive experiments were performed at this time-point. FBS was used as a positive control for normalisation purposes and so a range of concentrations were investigated (Figure 4.11B). Since 1% FBS was capable of inducing significant ERK phosphorylation similar to levels observed with concentrations up to the maximal 10%, the lower 1% FBS was employed as the positive control in subsequent investigations.

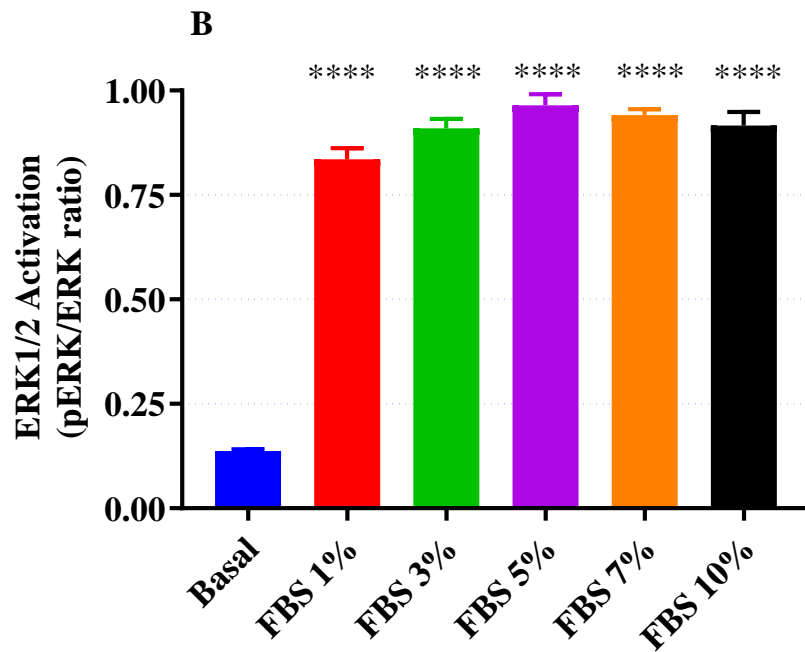
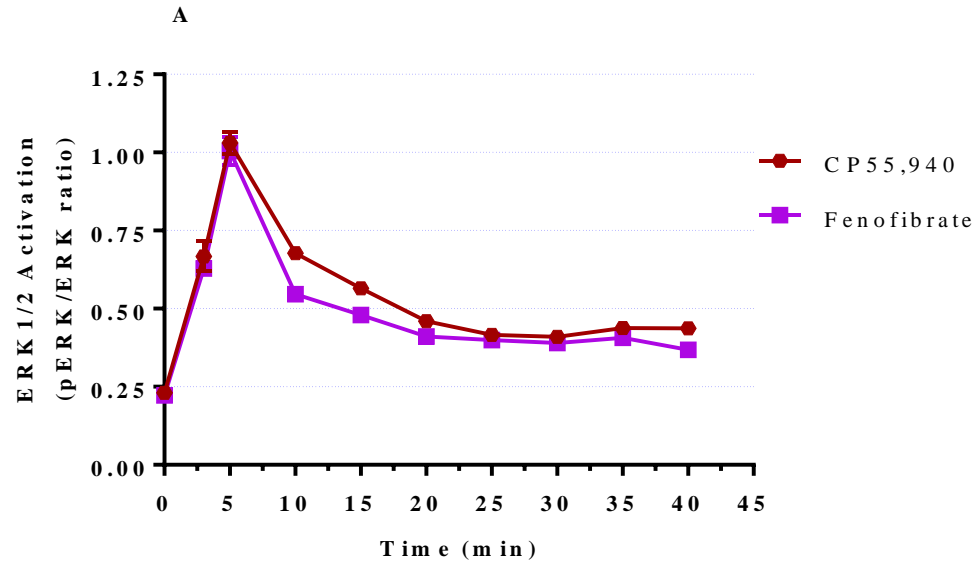


Figure 4.11 (A) Time course of ERK phosphorylation in CHO-CB<sub>2</sub> cells in the presence of the CB<sub>2</sub> receptor agonists CP55940 and fenofibrate at 1  $\mu$ M. Data are the mean  $\pm$  SEM of one experiment performed in triplicate twice for confirmation over a 40 min period and expressed as a ratio of the phosphorylated ERK to Total ERK intensity. (B) The impact of different concentrations of FBS on ERK activation in CHO-CB<sub>2</sub> cells measured at 5 min of ERK activation. Data are the mean  $\pm$  SEM of five independent experiments performed in triplicate on different passages of CHO-CB<sub>2</sub> cells. \*\*\*\*  $p \leq 0.0001$ , Two-way ANOVA test with Dunnett's multiple comparison analysis compared to the basal.

The cannabinoid receptor agonists CP55,940 and fenofibrate induced ERK activation similar to the levels evoked by 1 % FBS (Figure 4.12). FD24 also significantly induced ERK activation at a level roughly 80% of that evoked by the CB<sub>2</sub> receptor agonists CP55,940 and fenofibrate, while FD43 caused a significant ERK activation of 40 %. The antagonists/inverse agonist FD44 and FD46 failed to stimulate ERK phosphorylation. The cannabinoid receptor antagonist AM630 also failed to alter ERK phosphorylation. The quinolone-3-carboxamides also displayed a differential effect on ERK phosphorylation, such that the agonist SER601 evoked a response comparable to FD43, while responses to COR170 failed to reach statistical significance (Figure 4.12).

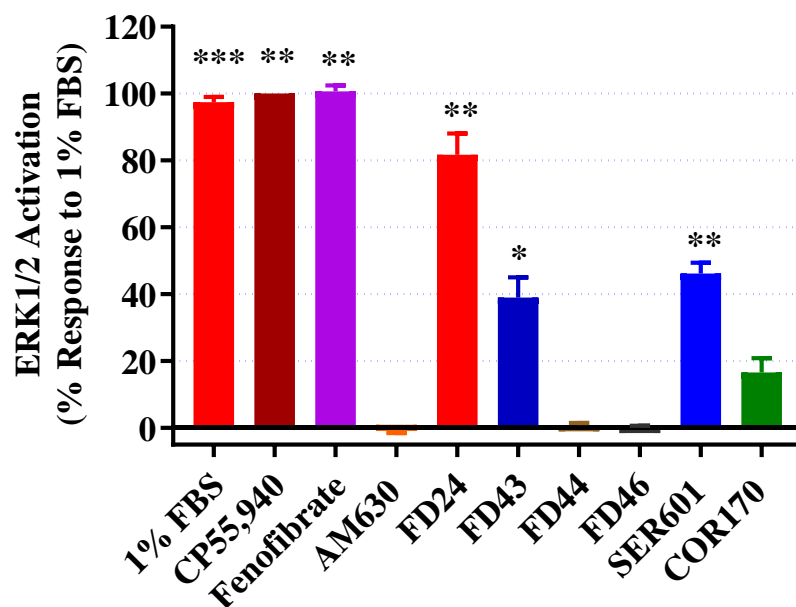


Figure 4.12 Activation of the ERK signalling pathway by CB<sub>2</sub> receptor ligands (1  $\mu$ M) measured at 5 min of ERK activation.

Data are the mean  $\pm$  SEM of five independent experiments performed in triplicate expressed as a percentage of the response to 1% FBS. \*  $p \leq 0.05$ , \*\*  $p \leq 0.01$ , \*\*\*  $p \leq 0.001$  and \*\*\*\*  $p \leq 0.0001$ , One-way ANOVA test with Dunnett's multiple comparison analysis compared to the basal.

A more detailed analysis was prompted and so a range of ligand concentrations were investigated (Figure 4.13, Table 4.4).

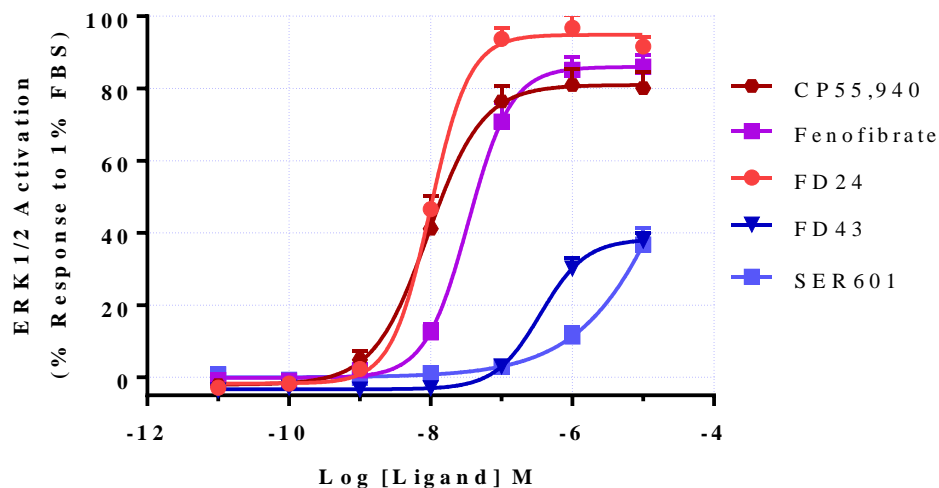


Figure 4.13 Concentration response curves for CB<sub>2</sub> receptor ligand evoked ERK phosphorylation measured at 5 min of ERK activation. Data are the mean  $\pm$  SEM of five independent experiments performed in triplicate expressed as a percentage of the response to 1% FBS. Lines were fitted using the four-parameter logistic equation.

Table 4.4 Parameters for concentration-dependent stimulation of ERK phosphorylation in CHO-CB<sub>2</sub> cells performed at n=5.

Compound	Maximal responses E <sub>max</sub> (%)	Potencies (pEC <sub>50</sub> )	Hill Slope (nH)
CP55,940	83 $\pm$ 4	8.1 $\pm$ 0.1	1.30 $\pm$ 0.14
Fenofibrate	86 $\pm$ 4	7.5 $\pm$ 0.1	1.51 $\pm$ 0.10
FD24	97 $\pm$ 2	8.0 $\pm$ 0.01	1.65 $\pm$ 0.15
FD43	42 $\pm$ 2	6.4 $\pm$ 0.1	1.43 $\pm$ 0.130
SER601	Not converged	<5.0 Not converged	Not converged

The table represents the half maximal effective concentration (pEC<sub>50</sub>), the percentage of maximal response expressed as E<sub>max</sub> and the Hill slope of the compounds investigated in a concentration response manner. One sample t test analysis of the hill slope indicated that only CP55,940 produced a hill slope that was not statistically different from one while fenofibrate, FD24 and FD43 produced a hill slope that was statistically different from one. The rank order of potencies of the investigated compounds was CP55940 > FD24 > fenofibrate > FD43. FD43 achieved half of the maximal response attained using the agonists

CP55940, fenofibrate and FD24 which was consistent with a partial agonist profile. SER601 failed to achieve saturation of ERK phosphorylation responses and hence it was not possible to compute its respective values.

The fenofibrate analogues FD44 and FD46, which failed to stimulate ERK phosphorylation, were investigated as potential antagonists and compared to AM630 (Figure 4.14). These three agents were pre-incubated with the cells for 15 min prior to adding agonists. JWH133, fenofibrate and FD24 all evoked significant activation of the ERK pathway, while FD43 was less effective. The cannabinoid receptor antagonist AM630 caused a complete inhibition of responses to JWH133 and FD24, but only partially blocked the effect of fenofibrate. FD44 and FD46 only partially inhibited responses to JWH133, fenofibrate and FD24.

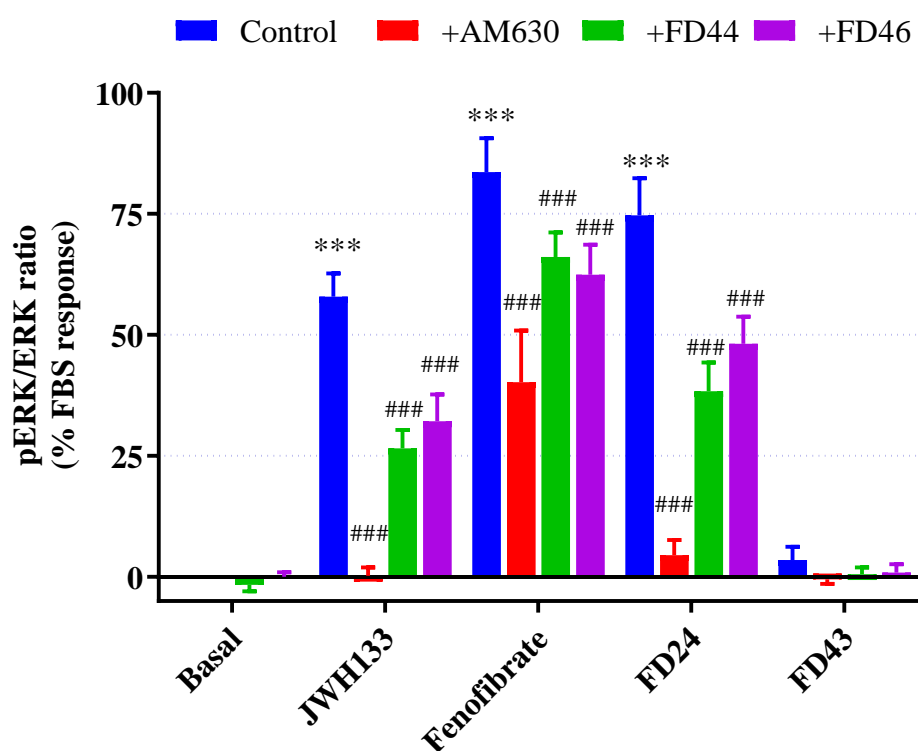


Figure 4.14 An investigation of the antagonist potential of FD44 and FD46. Data are the mean  $\pm$  SEM of five independent experiments performed in triplicate and measured at 5 min of ERK activation \*\*\*  $p \leq 0.001$  for the absence or presence of the agonists, ###  $p < 0.001$  for the absence or presence of the antagonists, Two-way ANOVA followed by Tukey's multiple comparison test.

The quinolone-3-carboxamides were investigated further in this assay. The reduced maximal response evoked by SER601 was completely blocked in the presence of 1  $\mu$ M AM630, a concentration, which also blocked responses to 30 nM CP55940 (Figure 4.15A).

The effect of COR170 was investigated as an inverse agonist/antagonist (Figure 4.15B). In this assay, responses to the submaximal concentration of CP55940 (30 nM) were completely blocked in the presence of either 1  $\mu$ M AM630 or 1  $\mu$ M COR170.

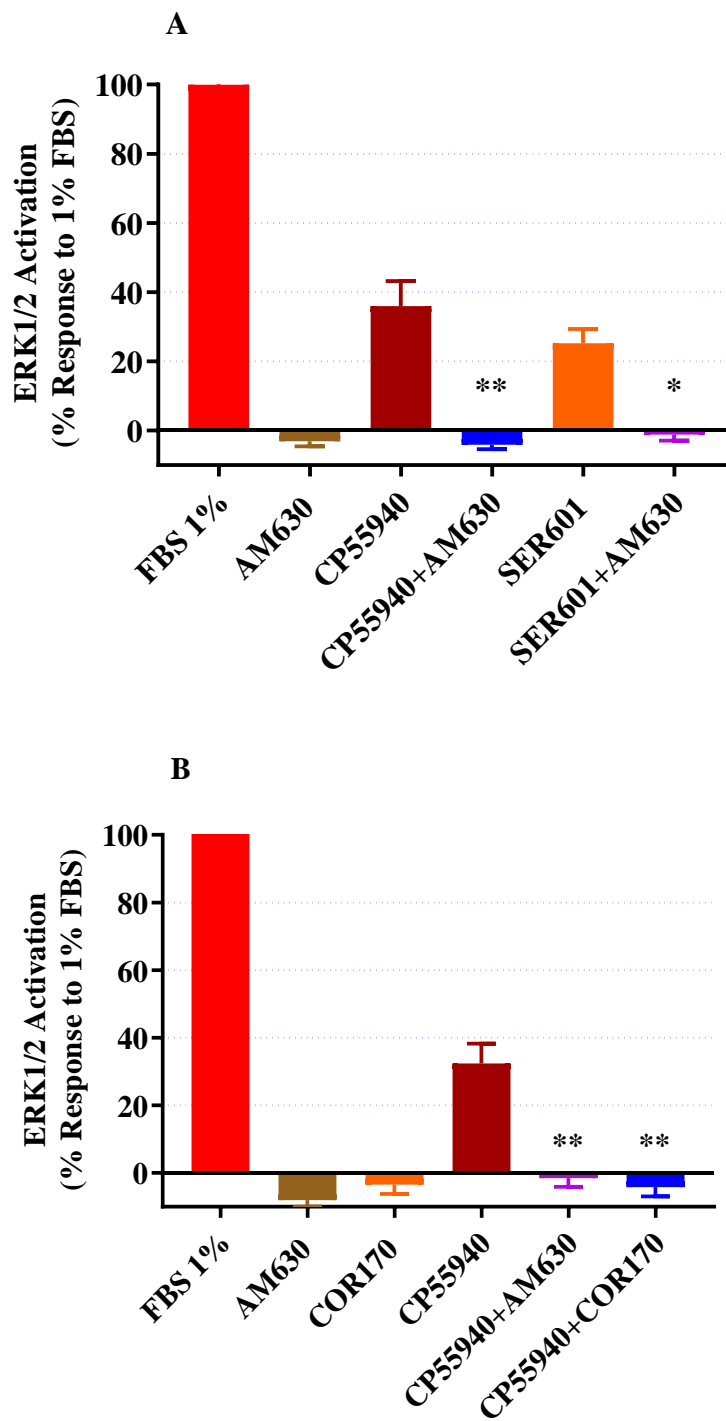


Figure 4.15 Investigating CB<sub>2</sub> receptor-mediated effects of quinolone-3-carboxamide analogues. Data are the mean  $\pm$  SEM of five independent experiments performed in triplicate and measured at 5 min of ERK activation. \*  $p \leq 0.05$  and \*\*  $p \leq 0.01$  for the absence or presence of the antagonists, One-way ANOVA multiple comparison test.

The effects of the quinolone-3-carboxamides were assessed in the presence of the endogenous agonist 2AG (Figure 4.16). The ERK response to 1  $\mu$ M 2AG was smaller than that observed in the presence of either 1  $\mu$ M CP55940 or fenofibrate (Figure 4.12), which were similar to the responses to 1 % FBS. Combining the synthetic agonists CP55940 or fenofibrate with 2-AG evoked responses greater than those to 2-AG alone, to levels similar to the synthetic agonists alone. As anticipated, AM630 blocked the 2-AG response, while neither COR170 nor SER601 had an effect on 2AG-evoked ERK phosphorylation.

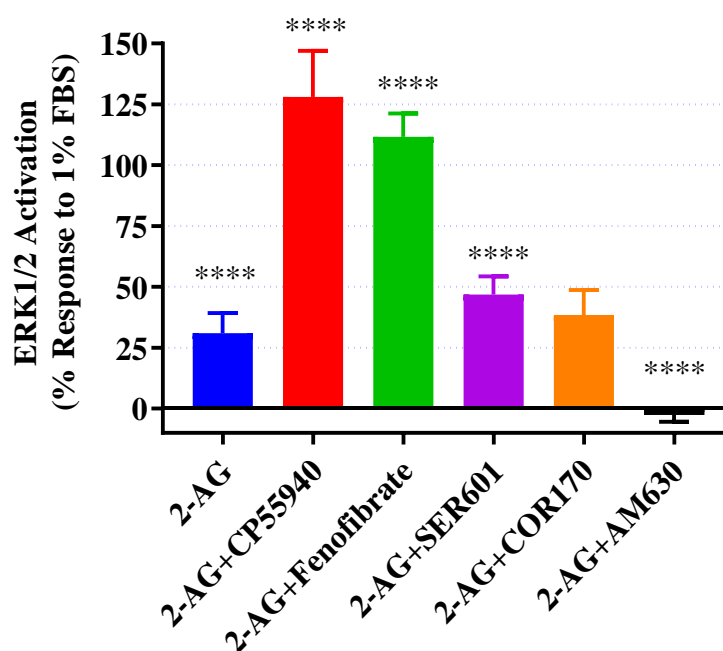


Figure 4.16 2AG-evoked ERK phosphorylation in CHO-CB<sub>2</sub> cells. All the ligands were present at 1  $\mu$ M. Data are the mean  $\pm$  SEM of seven independent experiments performed in triplicate and measured at 5 min of ERK activation. \*\*\*\*  $p \leq 0.0001$  Two-way ANOVA and Dunnett's multiple comparison test.

### 4.1.5 [<sup>35</sup>S]-GTP $\gamma$ S Binding Assay

The quinolone-3-carboxamides SER601 and COR170 were investigated in the [<sup>35</sup>S]-GTP $\gamma$ S binding assay using membranes from CHO-CB<sub>2</sub> cells. The non-selective cannabinoid receptor agonist CP55940 was used as the positive control and evoked a response double the background level. By contrast, SER601 and COR170 both produced an inverse agonist profile (Figure 4.17, Table 4.5).

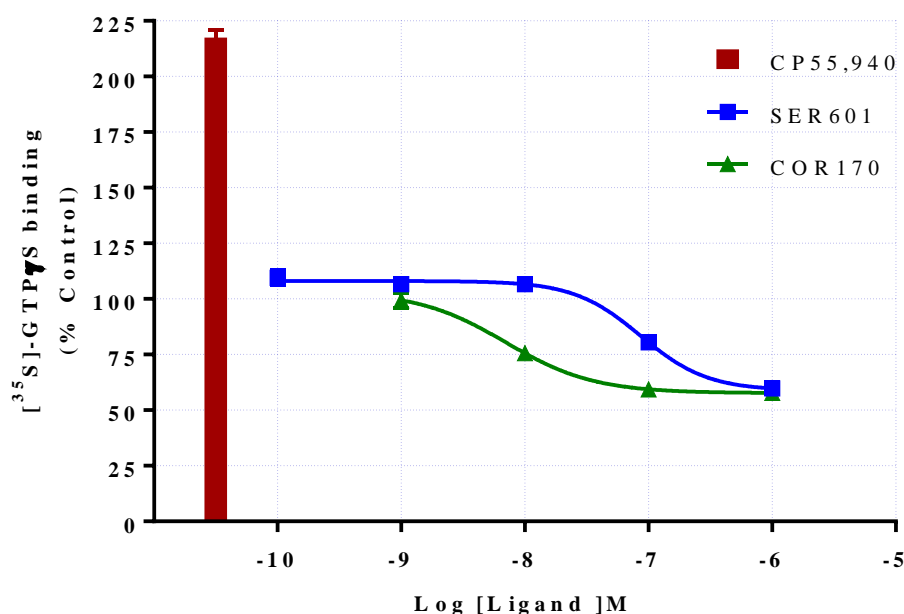


Figure 4.17 The [<sup>35</sup>S]-GTP $\gamma$ S binding in membrane suspension of CHO-CB<sub>2</sub> cells in the presence of cannabinoid ligands.

Data are the mean  $\pm$  SEM from a representative experiment conducted in duplicate and repeated on three further independent experiments.

Table 4.5 Quantitative assessment of SER601 and COR170 influences on the binding of [<sup>35</sup>S]-GTP $\gamma$ S to CHO-CB<sub>2</sub> membranes performed at n=3.

Compound	Maximal responses E <sub>max</sub> (%)	Potencies pEC <sub>50</sub>	Hill Slope (nH)
SER601	-33 $\pm$ 9	7.6 $\pm$ 0.3	-1.43 $\pm$ 0.26
COR170	-32 $\pm$ 7	8.0 $\pm$ 0.1	-1.01 $\pm$ 0.10

One sample t test analysis of the hill slope indicated that both SER601 and COR170 produced a hill slope that was not statistically significant from -1.

#### 4.1.6 [<sup>3</sup>H]-cAMP Accumulation

The classical signalling pathway for cannabinoid receptors is the inhibition of cAMP levels (Pertwee et al., 2010). As anticipated, CB<sub>2</sub> receptor agonists CP55940, fenofibrate and FD24 evoked inhibitions of forskolin-stimulated cAMP accumulation by approximately 80% (Figure 4.18). FD43 induced a lower inhibition of forskolin-stimulated cAMP accumulation compared to the full agonists. Both the antagonist/inverse agonist FD44 and FD46 evoked an increased cAMP accumulation comparable to that of AM630. The quinolone-4-carboxamides SER601 and COR170 were not effective in this assay.

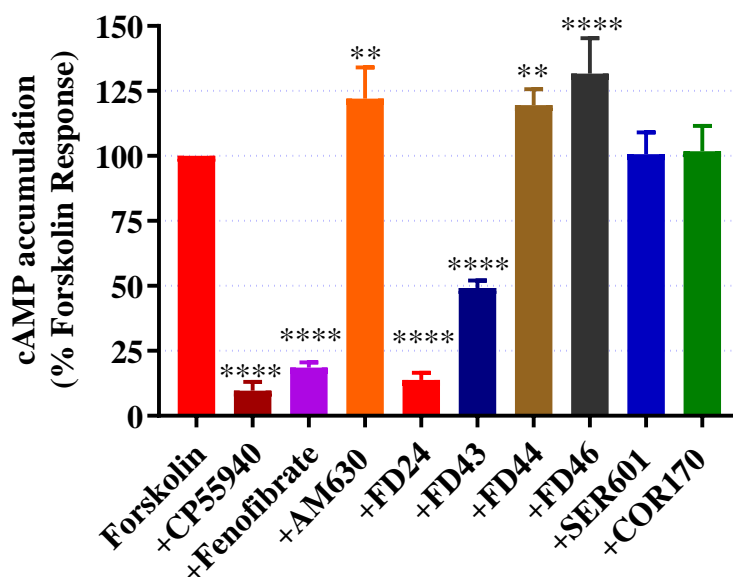


Figure 4.18 Modulation of forskolin-induced cAMP accumulation in CHO-CB<sub>2</sub> cells by cannabinoid ligands.

Data are the mean  $\pm$  SEM of four independent experiments performed in triplicate. \*\*  $p \leq 0.01$ , \*\*\*  $p \leq 0.001$  and \*\*\*\*  $p \leq 0.0001$ , Two-way ANOVA and Dunnett's multiple comparison test.

A number of these ligands were investigated in more detail over several concentrations (Figure 4.19). The positive control CP55940 evoked a concentration-dependent inhibition of cAMP accumulation with a potency (pEC<sub>50</sub> value) of 8.6 and maximal inhibition of 79 % (Figure 4.19, Table 4.5). Fenofibrate and FD24 were less potent but showed a similar level of inhibition of the cAMP elevation evoked by forskolin. FD43 was less potent and slightly

less efficacious. By contrast, AM630 evoked a concentration-dependent increase in cAMP accumulation (Figure 4.19B) with a potency of 7.6 (Table 4.6).

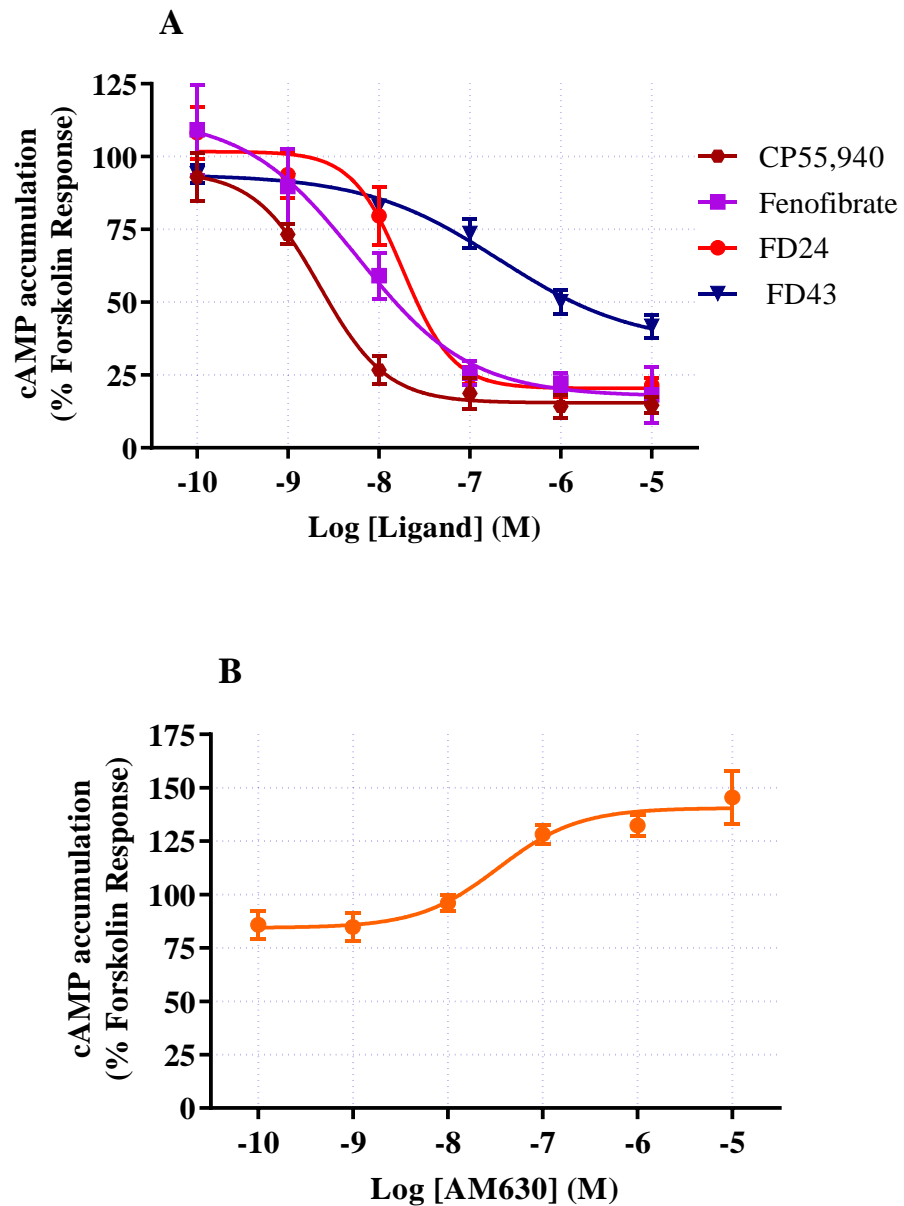


Figure 4.19 Modulation of forskolin stimulated cAMP accumulation in CHO-CB<sub>2</sub> cells.

Data are the mean  $\pm$  SEM of (A) three (CP55,940, fenofibrate, FD24 and AM630) and (B) four (FD43) independent experiments performed in triplicate. Concentration response curves were fitted to the four-parameter logistic equation.

Table 4.6 Concentration-dependence for modulation of cAMP accumulation by cannabinoid ligands in CHO-CB<sub>2</sub> cells performed at n=3 for CP55,940, fenofibrate, FD24, AM630 and n=4 for FD43.

<b>Compound</b>	<b>Maximal responses E<sub>max</sub> (%)</b>	<b>Potencies pEC<sub>50</sub></b>	<b>Hill Slope (nH)</b>
CP55,940	-79 ± 8	8.6 ± 0.2	-1.72 ± 0.50
Fenofibrate	-101 ± 27	8.3 ± 0.1	-0.74 ± 0.18
FD24	-89 ± 13	7.8 ± 0.2	-1.66 ± 0.62
FD43	-57 ± 2	6.7 ± 0.1	-0.65 ± 0.09
AM630	65 ± 11	7.6 ± 0.1	0.96 ± 0.31

One sample t test analysis of the hill slope indicated that CP55,940, fenofibrate and FD24 produced a hill slope that was not statistically significant from -1 while FD43 and AM630 produced a hill slope that was statistically different from -1. A further characterization of the fenofibrate analogues that failed to inhibit the forskolin response in Figure 4.18 was conducted to identify whether they had antagonist capacity. These agents were added to the 24-well plate along with medium containing rolipram and incubated at 37°C for 15 min prior to the addition of agonists. All of the compounds were investigated at 1 μM with the exception of CP55,940 which was employed at 30 nM. As evident in Figure 4.20(A) and (B), neither of the antagonists/inverse agonists FD44 and FD46 altered responses to CB<sub>2</sub> receptor agonists CP55940 or fenofibrate. AM630, on the other hand, (4.20 C) evoked a significant reversal of the cAMP inhibition evoked by CP55940 and fenofibrate.

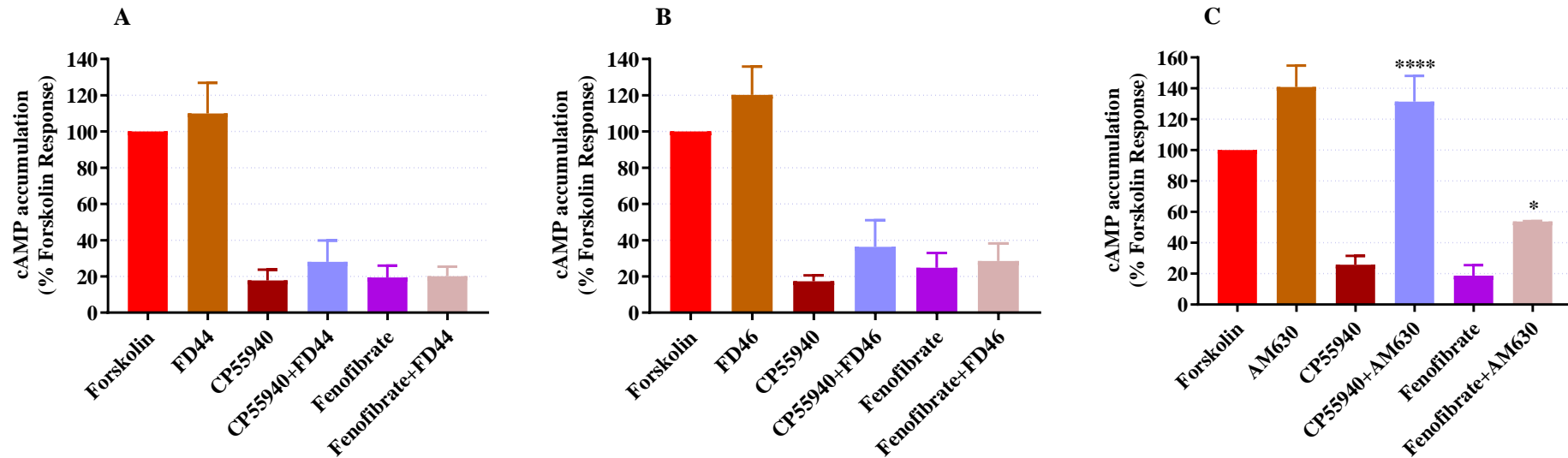


Figure 4.20 Antagonism of CB<sub>2</sub> receptor agonist inhibition of cAMP accumulation in CHO-CB<sub>2</sub> cells.

Data are the mean  $\pm$  SEM of three independent experiments performed in triplicate. \*  $p \leq 0.05$  and \*\*\*\*  $p \leq 0.0001$ , One-way ANOVA multiple comparison test.

Table 4.7 Effects induced by the ligands at the different signalling pathways

	Calcium Mobilization		ERK phosphorylation		cAMP		<sup>[35S]</sup> -GTP $\gamma$ S
	Control	Effect of 1 $\mu$ M antagonist	Control	Effect of 1 $\mu$ M antagonist	Control	Effect of 1 $\mu$ M antagonist	
CP55940	↑ pEC <sub>50</sub> =6.4	Blocked by AM630 No effect by FD44 No effect by FD46	↑ pEC <sub>50</sub> =8.1	NA	↓ pEC <sub>50</sub> =8.6	Blocked by AM630 No effect by FD44 No effect by FD46	↑
Fenofibrate	↑ pEC <sub>50</sub> =6.3	Blocked by AM630 No effect by FD44 No effect by FD46	↑ pEC <sub>50</sub> =7.5	Partially Blocked by AM630, FD44 and FD46	↓ pEC <sub>50</sub> =8.3	Blocked by AM630 No effect by FD44 No effect by FD46	NA
FD24	↑ pEC <sub>50</sub> =6.5	Partially Blocked by AM630 No effect by FD44 No effect by FD46	↑ pEC <sub>50</sub> =8.0	Blocked by AM630 Partially Blocked by FD44 and FD46	↓ pEC <sub>50</sub> =7.8	NA	NA
FD43	No effect		↑ pEC <sub>50</sub> =6.4		↓ pEC <sub>50</sub> =6.7		NA
FD44	No effect		No effect		↑		NA
FD46	No effect		No effect		↑		NA
SER601	No effect		↑		No effect		↓ pEC <sub>50</sub> =7.6
COR170	No effect		No effect		No effect		↓ pEC <sub>50</sub> =8.0
AM630	No effect		No effect		↑ pEC <sub>50</sub> =7.6		NA

NA: the compound was not investigated in that pathway

↑: Calcium mobilization: compound induced Ca<sup>2+</sup> ion elevation

↑: ERK phosphorylation: compound stimulated ERK phosphorylation

↓: cAMP: compound inhibited forskolin-stimulated cAMP accumulation

↑: [<sup>35</sup>S]-GTP $\gamma$ S compound stimulated the [<sup>35</sup>S]-GTP $\gamma$ S pathway

## 4.2 Discussion

### 4.2.1 The fenofibrate analogues: FD24, FD43, FD44 and FD46

The PPAR $\alpha$  agonist fenofibrate (Berger and Moller, 2002) has been recently identified by our laboratories as a potent agonist at human CB<sub>2</sub> receptors and a partial agonist/antagonist at human CB<sub>1</sub> receptors, with pEC<sub>50</sub> values of 6.3 and 7.7, respectively (Priestley et al., 2015). A recent pair of doctoral theses from the University of Nottingham (Loo, 2015; Spencer, 2011) aimed at producing novel fenofibrate derivatives possessing therapeutic advantages of the anti-inflammatory effects of CB<sub>2</sub> receptors and PPAR $\alpha$  receptors combined. Subsequent to molecular docking, a series of fenofibrate derivatives were synthesised namely, FD24, FD43, FD44 and FD46 based on the scaffold structure of fenofibrate. As the group attached at the amide terminus was changed from piperidin-1-yl, exo-norborn-2-yl, R-(+)-born-2-yl to adamant-1-yl ([Chapter 2, Table 2.1](#)), the functional activity of the compounds in the CB<sub>2</sub> receptor [<sup>35</sup>S]-GTP $\gamma$ S binding assay was sequentially modified from acting as a full agonist to partial agonist to antagonists/inverse agonists, respectively.

The CB<sub>2</sub> receptor binding mode of the fenofibrate derivatives demonstrated comparable evidence to mutagenesis research that binding of these ligands occurs through hydrogen bonding, aromatic stacking and hydrophobic interactions (Loo, 2015; Xie et al., 2003). This alteration in the functional activity of CB<sub>2</sub> receptors from a full agonist to a complete antagonist on the basis of an increase in hydrophobicity of the substituent suggests that there are specific residues in the receptor that affect the signalling profile of the different ligands, hence rendering it a “molecular switch”. These investigations were aimed at finding whether these effects could be dependent on the different signalling pathways, namely calcium, cAMP and the ERK phosphorylation signalling pathways. Alternatively, it could provide a mechanism for agonist bias, should the ligands exhibit differential activation of the different signalling routes.

To commence, the ligands FD24, FD43, FD44 and FD46 were tested in the [<sup>3</sup>H]-CP55940 radioligand displacement binding assay to confirm the binding of this novel series of fenofibrate derivatives to CHO-hCB<sub>2</sub> homogenates. Binding assays are keystone pharmacological studies essential for comprehending the targeting of receptors by drugs. Displacement binding assays are non-functional assays that are typically based upon the use of radioactive probes with the main purpose of identifying whether a particular compound is capable of binding to a particular receptor.

The membrane concentration to be used was optimised to 100 µg protein which evoked an appropriate signal to noise ratio. Based on the preliminary investigations performed in the lab, the K<sub>d</sub> for [<sup>3</sup>H]-CP55940 was computed to be 0.63 nM, and following fitting to a one-site model, the experimental affinities (pK<sub>i</sub> values) of the fenofibrate derivatives were 7.12, 6.59, 5.60 and 5.08 for FD24, FD43, FD44 and FD46, respectively. When compared to the initial characterization, which described affinities of the agonist and partial agonist, FD24, FD43 as 6.93 and 6.58, respectively (Loo, 2015), a good convergence was observed. However, the affinities of the antagonists/inverse agonists FD44 and FD46 obtained previously were 6.38 and 7.04 (Loo, 2015), over 1.5 log units higher affinity. This might be attributed to the fact that this was a pilot assay with a single repeat for the purposes of confirmation. Further repeats would clearly be helpful in identifying a more precise estimate of ligand affinity.

The fenofibrate derivatives were further investigated in a novel fluorescent agonist competition binding assay. Since the use of radioactive ligands as tracers in the displacement binding assay possesses both financial and practical limitations (notably limited to endpoint assays), the use of fluorescent binding assay offers a flexible alternative. Traditional displacement binding assay involve several washing steps before reading the bound radioactivity rendering it difficult to perform as an HTS assay. There is also the need for specialist storage and disposal facilities. As a practicality, the washing steps hinder kinetic measurements in a single experimental sample. The use of fluorescent probes offer a harmless approach and allow kinetic analysis (Cottet et al., 2011).

The patent Roche compound R07297590 was used as the fluorescent ligand (Sarott et al., 2019; Sarott et al., 2020) and the high affinity selective CB<sub>2</sub> receptor inverse agonist SR144528 (Bouaboula et al., 1999) was used in the determination of NSB in order to calculate specific binding required for the construction of IC<sub>50</sub> curves (Figure 4.5). Following 2 h kinetic read of the plates, the obtained affinities for FD24, FD43, FD44 and FD46 were  $6.62 \pm 0.11$ ,  $6.32 \pm 0.09$ ,  $6.19 \pm 0.09$  and  $6.46 \pm 0.06$  respectively. Compared to the [<sup>3</sup>H]-CP55940 displacement binding, the binding affinities for FD24, FD43, FD44 were comparable to those obtained via the fluorescent binding, while that obtained for the antagonist FD46 was quite distinct. The binding affinities were comparable to the affinities obtained by the preliminary investigations by Loo, 2015.

The fenofibrate compounds were subsequently assessed in different signalling mechanisms with relatively rapid responses to characterise their function at CB<sub>2</sub> receptors. The first of these was intracellular calcium mobilization monitored using a FlexStation 96-well microtiter plate reader. Initial single-point concentration screening of the fenofibrate derivatives at 1  $\mu$ M were examined alongside the potent non-selective CB<sub>2</sub> receptor agonist CP55940 (Wiley et al., 1995) as the positive control and the selective CB<sub>2</sub> receptor inverse agonist AM630 (Ross et al., 1999) as the negative control. As anticipated, CP55,940 and fenofibrate were capable of evoking intracellular calcium elevations in addition to the proposed CB<sub>2</sub> receptor agonist FD24. FD43, a partial agonist in [<sup>35</sup>S]-GTP $\gamma$ S binding assays, did not induce any effect on calcium mobilization, which was also true for the antagonists/inverse agonists FD44 and FD46.

The lack of calcium mobilization evident with the partial agonist FD43 could be attributed to the fact that stimulation of calcium elevation via the G $\alpha_{i/o}$  coupled CB<sub>2</sub> receptors is a considerably less well-coupled pathway. It has been implied that the G $\alpha_{i/o}$  coupled CB<sub>2</sub> receptors evoke rapid and transient intracellular calcium release following stimulation using the agonists CP55,940 and 2AG (Ibsen et al., 2017) potentially via the involvement of phospholipase C. This was evident in the current experiments since complete concentration-response curves to the partial agonist FD43 could not be obtained Figure 4.9. By

contrast, the full agonists CP55,940, fenofibrate and FD24 had potencies of  $6.35 \pm 0.04$ ,  $6.31 \pm 0.06$  and  $6.45 \pm 0.08$ , respectively. The antagonists/inverse agonists FD44 and FD46 were subsequently investigated to examine their effects and whether they would impact the calcium mobilization evoked by CB<sub>2</sub> receptor agonists CP55940 and fenofibrate. The CB<sub>2</sub> receptor inverse agonist AM630 (Ross et al., 1999) was used as a positive control and, indeed, AM630 abolished the calcium mobilization evoked by CP55940 and fenofibrate, in addition to substantially diminishing the intracellular calcium release via the proposed agonist FD24. Neither FD44 nor FD46 impacted calcium mobilization evoked by CP55940, fenofibrate or FD24.

Although CB<sub>2</sub> receptors can signal through multiple pathways, the majority of investigations concentrate on adenylyl cyclase and extracellular signal regulated kinases 1/2 (ERK 1/2) pathways. Signalling via arrestins, ion channel modulation and Akt and associated downstream processes are much less intensively examined (Dhopeshwarkar and Mackie, 2014). Therefore, subsequent experiments investigated the fenofibrate derivatives in these two pathways: cAMP inhibition and ERK activation. The ERK1/2 kinases belong to the mitogen activated protein kinase (MAPK) super family which have a prominent role in cell proliferation and apoptosis (Mebratu and Tesfaigzi, 2009). CB<sub>2</sub> receptors induce ERK phosphorylation and this phosphorylation was found to be more robust and stable than other pathways such as Akt (Wang et al., 2008), hence, ERK-induced phosphorylation secondary to CB<sub>2</sub> activation was investigated in this study. One of the prevailing techniques used in the quantification of ERK activation is immunoblotting which is labour intensive and offers limited throughput (Chevalier et al., 2000). Hence, an alternative approach was followed which encompasses the use of the quantitative fluorescent in-cell Western assay. The proteins are immunocytochemically labelled *in situ* in fixed cells in 96-well plates followed by quantification of the total and phosphorylated ERK using a fluorescent bed scanner. This technique is considered high-throughput, reproducible and can readily quantify phosphorylated ERK proteins in fixed cells via specific primary antibodies (Chen et al., 2005).

FBS was investigated in the ERK phosphorylation assay to determine an appropriate concentration; 1 % FBS produced a response not different from 10 % and so was employed as the positive control. ERK phosphorylation is rather rapid, and hence a time course of ERK phosphorylation evoked by the CB<sub>2</sub> receptor agonists CP55,940 and fenofibrate was performed over a 40 min period to assess the appropriate time-point. Consequently, the 5 min stimulation evoked the maximum ERK phosphorylation and was hence employed in all investigations involving the ERK assay. This was consistent with other reports investigating CP55940 as an agonist at the CHO-CB<sub>2</sub> cells and similarly, the peak ERK phosphorylation was measured at 5 min (Atwood et al., 2012; Wang et al., 2018). Initial research investigating the coupling of CHO-CB<sub>2</sub> to the ERK pathway following its stimulation via the CP55940 was measurable at 2 mins with the maximum effect attained between 6 - 15 min (Bouaboula et al., 1996).

The fenofibrate derivatives were screened at a single-point concentration initially to assess their impact on ERK phosphorylation alongside the positive controls CP55940, fenofibrate and the negative control AM630. The agonist FD24 prompted significant ERK phosphorylation to 80% response of the 1 % FBS responses and the partial agonist FD43 evoked around 40% of the FBS ERK stimulation. As anticipated, both the antagonists/inverse agonists FD44 and FD46 failed to alter ERK activation. The compounds capable of activating the ERK signalling pathway were further assessed in a concentration-dependent study to gain an enhanced understanding of their potencies. The experimental potencies obtained for the investigated compounds CP55940, fenofibrate, FD24, FD43 were  $8.14 \pm 0.13$ ,  $7.46 \pm 0.07$ ,  $8.00 \pm 0.01$  and  $6.44 \pm 0.07$ , respectively. The potencies of CP55940 and fenofibrate were similar to published observations from the Nottingham laboratories (pEC<sub>50</sub> values of  $8.5 \pm 0.1$  and  $7.7 \pm 0.1$ , respectively (Priestley et al., 2015). The potencies of CP55940, fenofibrate and FD24 for the ERK signalling pathway were marginally higher than those obtained via calcium mobilization, which may reflect a slightly better coupling efficiency. Similar to the calcium pathway, the inverse agonist FD44 and the antagonist FD46 were subsequently investigated in the presence of CB<sub>2</sub> receptor agonists JWH133, fenofibrate and FD24 to examine whether they

would influence agonist stimulated ERK phosphorylation. In contrast to the calcium signalling pathway, the compounds were found to inhibit 25% of the JWH133 response, 10% of the fenofibrate response and 35% of the FD24 response. Despite being of slight influence, there was a modest modulation of the ERK activation influenced by FD44 and FD46.

Since the cannabinoid CB<sub>2</sub> receptors are G $\alpha_{i/o}$  coupled, agonist stimulation leads to an inhibition of adenylyl cyclase activity which sequentially reduces cAMP levels. This reduction in cAMP levels is identified by incubating the cells with forskolin which is responsible for elevating the cAMP baseline level (Basu and Dittel, 2011; Wang et al., 2008). Subsequent to a short-term 15 min incubation, the cannabinoid CB<sub>2</sub> receptor agonists almost abolished forskolin-induced cAMP accumulation (Basu and Dittel, 2011). Therefore, all of the performed experiments encompassed stimulation of the CHO-CB<sub>2</sub> cells with forskolin to allow the quantification of agonist-induced inhibition of cAMP accumulation. Similar to the previous signalling pathways, the compounds were initially screened at a single-point concentration to examine their impact on the inhibition of cAMP accumulation alongside the positive and negative controls of CP55940 and AM630, respectively. As anticipated, CB<sub>2</sub> receptor agonists CP55940, fenofibrate and FD24 induced substantial inhibition of the forskolin-stimulated cAMP accumulation by more than 80%. The partial agonist FD43 evoked 50% inhibition, AM630 produced an inverse agonist profile as implied by an increase in the forskolin-induced cAMP accumulation (Bolognini et al., 2012). Both FD44 and FD46 produced an inverse agonist profile comparable to that of AM630 by augmenting the forskolin-induced cAMP generation.

The compounds capable of modulating the forskolin-induced cAMP accumulation were further assessed in a concentration-dependent study to establish their potencies. The experimental potencies of the investigated compounds CP55940, fenofibrate, FD24, and FD43 were  $8.62 \pm 0.22$ ,  $8.31 \pm 0.07$ ,  $7.89 \pm 0.22$ , and  $6.71 \pm 0.14$ , respectively. The obtained pEC<sub>50</sub> values of the compounds CP55940, fenofibrate and FD24 were comparable to the ERK and calcium mobilization pathway. The partial agonist FD43 potency was also comparable to that obtained by the ERK phosphorylation pathway. The potency obtained for AM630 in enhancing cAMP levels ( $7.55 \pm 0.14$ ) is also comparable

to that previously reported for the cAMP signalling pathway (Bolognini et al., 2012). Similar to the calcium and ERK-phosphorylation signalling pathways, the inverse agonist FD44 and the antagonist FD46 were subsequently investigated in the presence of the agonists CP55940 and fenofibrate to examine whether they would influence the forskolin-induced cAMP accumulation. AM630 was used as a comparison and, as anticipated, significantly reversed the inhibition of forskolin-induced cAMP accumulation induced by the agonists. In these experiments, neither FD44 nor FD46 modulated or altered the forskolin-induced cAMP accumulation by CP55,940 and fenofibrate.

This study introduced FD24 as a novel promising CB<sub>2</sub> receptor agonist with consistent effects in the different signalling pathways investigated. This compound should be investigated further using CB<sub>1</sub> receptor cell lines in order to determine its selectivity between the cannabinoid receptors. Compounds possessing CB<sub>2</sub> receptor selectivity over CB<sub>1</sub> receptors are devoid of psychotropic effects and are subject to increased therapeutic focus. Given that the FD series were derived from fenofibrate, described as a negative allosteric modulator at the CB<sub>1</sub> receptor (Priestley et al., 2015; Ye et al., 2019), it would be worth investigating the allosteric modulation of the FD44 and the FD46 compounds at CB<sub>1</sub> and CB<sub>2</sub> receptors as they demonstrated distinct effects among the different signalling pathways (method discussed in the upcoming section). Although both the inverse agonist/antagonist FD44 and FD46 did not stimulate calcium and ERK signalling pathways, both compounds did, however, evoke an increase in cAMP accumulation comparable to that of AM630, suggestive of inverse agonism. Moreover, these compounds could be worth investigating in the [<sup>35</sup>S]-GTPγS binding assay to confirm this and to gain further insight into the functional consequences of these compounds.

## 4.2.2 The quinolone-4-carboxamide analogues: SER601 and COR170

The selection of investigated ligands was broadened to include SER601 (also referred to as COR167) and COR170 to the existing fenofibrate derivatives. According to the published literature, they produced a similar switch; that is, adding bulk to the side chain by changing the *iso*-propyl substituent to a phenyl altered their activity from acting as a full agonist (SER601) to an inverse agonist (COR170) (Contartese et al., 2012; Pasquini et al., 2008). SER601/COR167 and COR170 were both previously investigated in *in vivo* studies. *In vitro*, SER601 demonstrated selective binding affinity at CB<sub>2</sub> receptors with a K<sub>i</sub> of 6.3 nM (Pasquini et al., 2008). SER601 was investigated in formalin-induced nocifensive mice and it was regarded as a potential analgesic through a mechanism not entirely established. Given its potency at CB<sub>2</sub> receptors, SER601 was suggested as an appropriate lead compound for the management of brain damage induced by ischemic reperfusion injury *in vivo* by decreasing TNF- $\alpha$  and IL-6 release (Contartese et al., 2012).

When investigated *in vitro*, COR170 bound selectively to CB<sub>2</sub> receptors with a K<sub>i</sub> of 3.8 nM (Pasquini et al., 2008). *In vitro* investigation of the COR170 in the [<sup>35</sup>S]-GTP $\gamma$ S binding assay revealed the selective inverse agonist profile of the compound at CB<sub>2</sub> receptors (Cascio et al., 2010). In a subsequent investigation of a mouse pain model using formalin, COR170 was described as an inverse agonist and hypothesized to produce an anti-inflammatory effect by down regulation of inflammatory cytokines (Contartese et al., 2012). Both compounds appeared to have promising therapeutic potential, but further investigations are yet to be conducted and this research aimed to characterise the function of these compounds via investigating their effects within the different signalling pathways.

A [<sup>3</sup>H]-CP55,940 displacement binding assay was initially performed at a single-point screen of SER601 and COR170 alongside the positive controls fenofibrate and AM630 at 1  $\mu$ M. SER601 demonstrated only 20% displacement of CHO-CB<sub>2</sub> receptor binding revealing that the compound had limited binding to CB<sub>2</sub> receptors, while COR170, fenofibrate and AM630

all demonstrated 80% displacement of CHO-CB<sub>2</sub> receptor binding. Since AM630 was expected to demonstrate a higher receptor occupancy given its reported K<sub>i</sub> of 31.2 nM (Ross et al., 1999) and the lack of receptor occupancy demonstrated by SER601, both of these compounds were further investigated in concentration response analysis. SER601 produced a potency that was quite distinct from that reported in the literature. SER601 produced pK<sub>i</sub> = 6.35 ± 0.02 compared to the published data of 8.20 (Contartese et al., 2012) and AM630 produced 6.51 ± 0.15 compared to the published data of AM630 = 7.51 (Ross et al., 1999). When SER601 and COR170 were investigated in the fluorescent binding assay, they displayed pK<sub>i</sub> values of 6.84 ± 0.27 and 7.46 ± 0.13, respectively. The main purpose of investigating these compounds in the binding assays was to use an alternative insight as to whether the compounds were functioning in a predictable manner. The obtained pK<sub>i</sub> in the fluorescent binding assay was not quite the same as the published data for SER601 = 6.3 nM and COR170 = 3.8 nM (Pasquini et al., 2008). Therefore, these compounds were assessed in the [<sup>35</sup>S]-GTPγS binding assay to determine the functional consequences of these compounds if they bind to the CB<sub>2</sub> receptor.

The [<sup>35</sup>S]-GTPγS binding assay is described as an early functional outcome following receptor occupancy prior to signal amplification. Thus, the assay can determine potency at a proximal stage in a feasible and straightforward assay (Harrison and Traynor, 2003). Nevertheless, when SER601 and COR170 were investigated *in vitro* in the [<sup>35</sup>S]-GTPγS binding assay, both compounds produced an inverse agonist profile with pEC<sub>50</sub> values of 7.62 ± 0.28 and 8.00 ± 0.12, respectively (Figure 4.17). If both compounds functioned as genuine inverse agonists, they should have reversed the agonist profile of CP55940. However, when investigated in the [<sup>35</sup>S]-GTPγS binding assay, both compounds failed to reverse the effect of CP55940.

The contradictory data between the published and the experimental results especially for SER601 which produced an inverse agonist profile in the [<sup>35</sup>S]-GTPγS binding assay and lacked measurable binding in the [<sup>3</sup>H]-CP55940 displacement binding assay, highlighted a need for further investigation in functional signalling pathways. In the calcium mobilization assay, SER601 and COR170 failed to alter intracellular calcium levels. Both

compounds also failed to modulate forskolin-induced cAMP accumulation. However, when SER601 and COR170 were investigated in the ERK in-cell western assay, SER601 induced significant ERK phosphorylation approaching 50% of the positive control. Concentration-response investigation of SER601 however, revealed that the compound failed to attain an asymptote and hence, it was not possible to compute its respective potency values. Considering that ERK-phosphorylation was the only signalling pathway in which SER601 produced an agonist profile opposed to all other signalling pathways and given that SER601 did not demonstrate adequate receptor occupancy, it was important to verify whether the ERK-induced agonist profile was generated via binding of SER601 to the conventional CHO-CB<sub>2</sub> orthosteric binding site.

Consequently, the CB<sub>2</sub> receptor inverse agonist AM630 (Bolognini et al., 2012) was used to confirm whether responses produced by SER601 could be blocked. COR170 was also assessed as an inverse agonist to verify its effect on the ERK phosphorylation evoked by the agonist CP55940. ERK phosphorylation stimulated by SER601 was completely abolished by AM630 and COR170 significantly blocked the CP55940 ERK induced stimulation. However, when the endogenous agonist 2-AG was investigated, COR170 failed to modify ERK phosphorylation. COR170 was apparently ineffective in any of the investigated signalling pathways, while SER601 was evidently an ERK-biased agonist, at least when compared to cAMP inhibition or calcium mobilization.

The intent of employing the quinolone-4-carboxamides SER601 and COR170 was to serve as commercially available alternatives to the fenofibrate FD derivatives. It was anticipated that increasing the hydrophobicity of the *iso*-propyl substituent in SER601 to phenyl in COR170 altered their activity from acting as a full agonist to an inverse agonist, respectively. However, the contradicting data obtained in this study indicated that the compounds did not function as parallels for the FD series. In this study, SER601 performed as an ERK-phosphorylation biased agonist, by functioning as an agonist in this signalling pathway only.

The theory of biased agonism or functional selectivity is interesting since it offers the potential for developing medications with decreased adverse effects. This could be specifically interesting for the development of therapeutics that manage inflammatory pain or neuropathic pain through selective targeting of the cannabinoid CB<sub>2</sub> receptors. Nonetheless, biased agonism at CB<sub>2</sub> receptors yet remains to be fully explored. Moreover, the signalling pathways that mediate the required therapeutic benefit have not been completely identified or whether the desired therapeutic effects could be produced via a single pathway or a combination of signal transduction pathways (Ibsen et al., 2017). Multiple CB<sub>2</sub> receptor ligands appeared to have encouraging pre-clinical data but did not proceed to clinical trials. This is primarily attributed to the functional selectivity of CB<sub>2</sub> receptors (Dhopeshwarkar and Mackie, 2016). Thus, investigating this functional selectivity or signal bias could clarify the reasons behind the failed progression of CB<sub>2</sub> receptor ligands to clinical trials.

As previously discussed, ([section 1.5.6](#)) biased agonists could potentially produce an enhanced therapeutic profile, nevertheless, there are several challenges that are yet to be overcome. Among these challenges is the requirement to quantify agonist bias in a profound manner that would aid in understanding and, hence optimizing biased activity (Kenakin and Christopoulos, 2013). Since different intracellular signalling pathways possess varying sensitivities post agonist stimulation, ligand bias could be identified and computed by comparing the ligand's effects within one assay to a certain standard agonist. The relative effect of the ligand in a single assay could in turn be compared to its relative activity within other assays compared to the standard agonist to compute a relative activity ratio which accounts for system bias and observational bias (Kenakin, 2011; Kenakin and Christopoulos, 2013). The computed ratio could subsequently be utilised among different assays in order to identify true agonist bias between different signalling pathways.

Initial attempts to quantify agonist bias were based on computing the relative activity ratio quantified from  $E_{max}$  (maximal responses) and  $EC_{50}$  (potency) of the ligand relative to a standard reference ligand (Ehlert, 2008; Kenakin and Christopoulos, 2013). Nevertheless,  $EC_{50}$  is dependent on the

investigated compound's affinity, efficacy in addition to system dependent factors including receptor expression and system amplification, whereas  $E_{\max}$  is influenced by the compound's efficacy and the system (Kenakin et al., 2012). Hence, this approach is limited since it doesn't account for receptor density, receptor reserve as well as signal amplification. It would be optimum if agonist bias could be characterised and quantified based on a single parameter that would allow statistical tests to evaluate true agonist effects between ligands. Nevertheless, utilising potency ( $pEC_{50}$ ) values solely to quantify bias would be inappropriate for compounds that induce different maximal responses. Likewise, utilising only maximal responses ( $E_{\max}$ ) to quantify bias would not distinguish between full agonists which prompt a stimulus that surpasses the signalling capacities of the system (Kenakin and Christopoulos, 2013). Thus, an approach that incorporates elements of both  $pEC_{50}$  and  $E_{\max}$  is essential.

Alternative approaches have been described which quantify agonist bias by applying the operational model for quantifying drug responses (Black and Leff, 1983). This approach quantifies agonism in a system-independent parameter based on the operational affinity and efficacy of compounds referred to as transduction coefficient method  $\log(\tau/K_A)$ . The transduction coefficient method quantifies bias based on the efficiency of an agonist in stimulating a certain signalling pathway from the efficiency parameter ( $\tau$ ), receptor coupling, receptor density and ( $K_A$ ) which represents the functional affinity of the compound for the receptor conformation which facilitates the desired cellular response (Black and Leff, 1983; Kenakin and Christopoulos, 2013). The  $\log(\tau/K_A)$  values are then normalised to a standard reference ligand to quantify the ability of the ligand to stimulate a signalling pathway, referred to as  $\Delta\log(\tau/K_A)$ . These ratios are subsequently compared among multiple signalling pathways to calculate  $\Delta\Delta\log(\tau/K_A)$ . It is essential to note that the operational model assumes equilibrium binding, therefore, defining the equilibrium time point for the investigated signalling pathway is crucial for fitting of the operational model (Kenakin et al., 2012).

In this study, SER601 performed as an ERK-phosphorylation agonist only without activating any of the other investigated pathways. Since SER601 only activated one of the investigated pathways, it was not possible to quantify bias. To overcome this dilemma, and in order to be able to appropriately quantify bias and assess whether or not SER601 was a genuine biased agonist, future investigations could aim to investigate the effect of SER601 on other signalling pathways beyond those studied here including  $\beta$ -arrestin, p38, G $\beta\gamma$  subunit release and GIRK pathways. These pathways were not investigated in this thesis because they involve prolonged incubation times, alterations in the cellular environment and/or receptor sequence, which would decrease direct comparability of the performed assays. Nevertheless, it is predominant to perform more assays in order to identify whether SER601 acted as a biased agonist in pathways other than the ERK-phosphorylation and to be quantify this bias. Another significant aspect to note is to utilize a standard reference ligand alongside SER601.

To gain an enhanced understanding of the ligands binding mechanics, it is worth investigating the potential for allosteric modulation by SER601 and COR170 at CB<sub>2</sub> receptors. Pharmacological benefits of both positive and negative allosteric modulators at GPCRs were found to include increased specificity and thus, diminished side-effects (Ye et al., 2019). Furthermore, allosteric modulators were found to offer subtype selectivity between the cannabinoid receptors. Allosteric modulators also prompted enhanced tissue selectivity because they induce their therapeutic effects only in endocannabinoid expression sites, in addition to stimulating or blocking signalling bias at the GPCRs (Gado et al., 2019), given that SER601 produced ERK phosphorylation in this study. This could be achieved via binding kinetic assays through the utilisation of a radiolabelled compound e.g. [<sup>3</sup>H]-CP55940. The radiolabelled compound is initially allowed to attain equilibrium with CB<sub>2</sub> receptors followed by the addition of the test compound as the positive or negative allosteric modulator. The specific binding of the radiolabelled compound is subsequently quantified at different time points to generate dissociation curves to allow calculation of dissociation rate constants. Allosteric modulators prompt shifting of the dissociation rates, such that positive allosteric

modulators decrease dissociation rates while negative allosteric modulators increase dissociation rates of the radiolabelled ligand (Sum et al., 2019). This would provide evidence regarding whether or not SER601 and COR170 function as allosteric modulators at CB<sub>2</sub> receptors. A more involved option would be the co-crystallization of CB<sub>2</sub> receptors with each of the ligands independently to attempt cryo-EM/crystal structure analysis and identification of the locus of the ligands binding in comparison with a classical CB<sub>2</sub> receptor ligand, such as CP55940.

### **4.3 Conclusion**

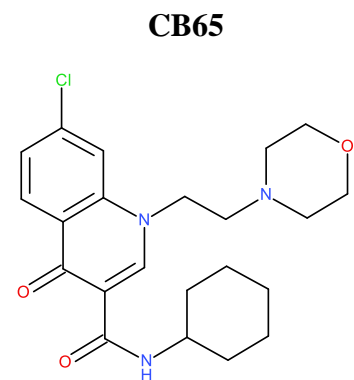
This chapter investigated the FD series of compounds synthesised at the University of Nottingham as well as their commercially available alternatives SER601 and COR170. Subsequent to presenting the SER601 as a potential CB<sub>2</sub> receptor biased agonist, a further range of commercially available cannabinoid CB<sub>2</sub> receptor-selective agonists were investigated to assess this theory of biased agonism by using the same rapid responding assays. This study presented a promising novel CB<sub>2</sub> receptor agonist, FD24 with a consistent potent agonist profile across the investigated signalling pathways. Further research concerning the selectivity of this compound towards CB<sub>2</sub> receptors over CB<sub>1</sub> receptors could identify beneficial therapeutic effects devoid of psychotropic effects. Moreover, SER601/COR167 was introduced as an ERK-phosphorylation biased agonist, functioning as an agonist in this signalling pathway only. Subsequent to further investigations, this compound could be a beneficial target for managing inflammatory pain or neuropathic pain through selective targeting of the cannabinoid CB<sub>2</sub> receptors.

## **Chapter 5 : A broader characterization of commercially available CB<sub>2</sub> receptor-selective agonists**

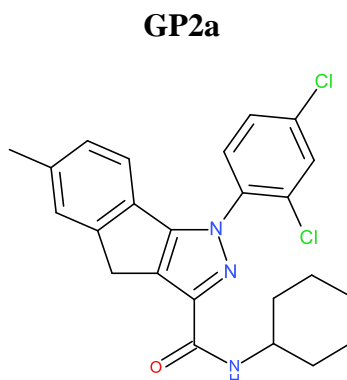
The previous chapter compared the fenofibrate analogues, synthesised within the University of Nottingham, with two commercially available quinolone-4-carboxamide CB<sub>2</sub> receptor selective ligands (SER601 and COR170). These latter compounds were anticipated to recapitulate the pattern observed with the fenofibrate analogues (i.e. substitution of a small aliphatic sidechain with a bulky hydrophobic entity converting an agonist into an antagonist), based on the published profile (Contartese et al., 2012; Pasquini et al., 2008). However, SER601 and COR170 did not function as anticipated as the functional and binding profiles were distinct from the published literature. Intriguingly, though, the quinolone-4-carboxamide described as a selective CB<sub>2</sub> receptor agonist, SER601, appeared to have an exclusive ERK phosphorylation bias. Given that this compound was shown to have an anti-nociceptive profile in a mouse model of acute pain (Pasquini et al., 2008), there is a temptation to align ERK phosphorylation with analgesia. Accordingly, a further range of commercially available cannabinoid CB<sub>2</sub> receptor-selective agonists were investigated to assess this theory of biased agonism by using the same rapid responding assays.

The predominant aim of this Chapter was to gain an enhanced understanding of the function of the cannabinoid CB<sub>2</sub> receptor, its signalling mechanisms, and to provide an insight as to whether reported CB<sub>2</sub> receptor agonists also exhibited the bias observed with SER601 and hence could be therapeutically exploited in the management of pain or other pathological conditions ([Chapter 1.5.4](#)). At the time of initiating this study, there were relatively few CB<sub>2</sub> receptor selective ligands commercially available. Notably, they represent a variety of pharmacophores with a range of physicochemical properties (Table 5.1). These agents were investigated in a series of studies to evaluate their CB<sub>2</sub> receptor signalling properties.

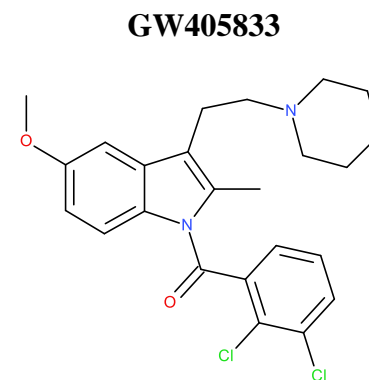
Table 5.1 Chemical structures and physicochemical properties of the CB<sub>2</sub> receptor ligands investigated in this chapter



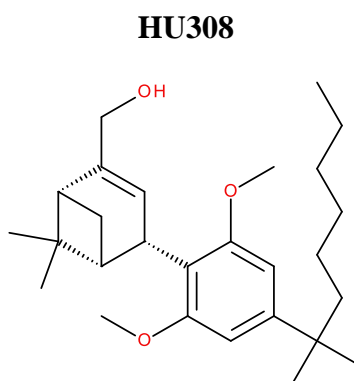
MW: 417.9  
HBA: 5  
HBD: 1  
AlogP: 3.08  
PSA: 61.88



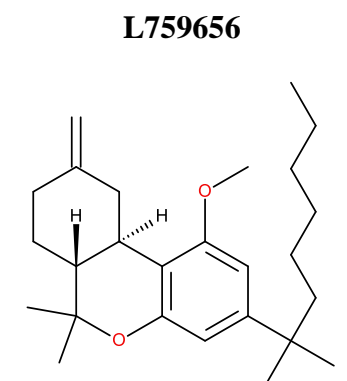
MW: 440.4  
HBA: 2  
HBD: 1  
AlogP: 7.32  
PSA: 46.92



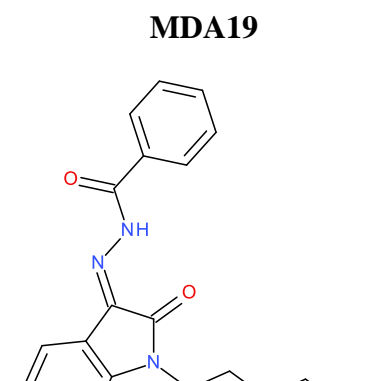
MW: 447.4  
HBA: 4  
HBD: 0  
AlogP: 5.32  
PSA: 43.7



MW: 414.6  
HBA: 3  
HBD: 1  
AlogP: 6.72  
PSA: 38.69



MW: 384.6  
HBA: 2  
HBD: 0  
AlogP: 1.76  
PSA: 18.46



MW: 349.5  
HBA: 3  
HBD: 1  
AlogP: 4.21  
PSA: 61.77

MW, molecular weight; HBA, hydrogen bond acceptors (basic groups); HBD hydrogen bond donors (acidic groups); AlogP, estimated hydrophobicity; PSA, polar surface area. Physicochemical properties were derived by BIOVIA Draw (<https://www.3dsbiovia.com/resource-center/downloads/freeware/index.html>).

Table 5.2 Pharmacological properties of the CB<sub>2</sub> receptor ligands investigated in this chapter

Ligand	hCB <sub>2</sub> affinity (K <sub>i</sub> , nM)	hCB <sub>1</sub> affinity (K <sub>i</sub> , nM)	In vitro effects	In vivo effects
<b>CB65</b>	3.3 <sup>a</sup> 14: human <sup>q</sup> 16: rat <sup>q</sup> 109: dog <sup>q</sup>	>1000 <sup>a</sup>	2-fold increase in human breast cancer cell invasion at 50 nM; blocked by AM630. <sup>g</sup> Suppression of K <sup>+</sup> currents in rat retinal ganglion neurones at 500 nM, which was not blocked by AM630 <sup>h</sup> ; 90 % reduction of HepG2 human hepatoma cell invasion at 0.625 nM but required much higher concentrations of ACEA. <sup>i</sup> CB65 displaced [ <sup>3</sup> H]-CP55940 binding from human, rat and dog CB <sub>2</sub> receptors though with a lower affinity in the dog CB <sub>2</sub> receptors. <sup>q</sup> In the cAMP accumulation assay, CB65 produced no agonist properties in the CHO cells expressing human, dog and rat CB <sub>2</sub> receptors. <sup>q</sup>	1.25 µg ICV injection stimulated food intake in neonatal chicks: sensitive to AM630. <sup>j</sup>
<b>GP2a</b>	7.6 <sup>b</sup>	900 <sup>b</sup>	GP2a significantly increased ERK1/2 expression in HL-60 cells at 5 nM. The ERK1/2 response to CP55940 in these cells was reversed in the presence of 50 nM SR144528. <sup>b</sup>	No reports of an in vivo investigation
<b>GW405833</b>	3.9 <sup>c</sup> 12 <sup>p</sup>	4772 <sup>c</sup> 1917 <sup>p</sup>	Inhibition of cAMP accumulation in CHO-hCB <sub>2</sub> cells with a potency of 0.6 nM with a maximal inhibition of 45 % compared to CP55940 with 84 %. <sup>c</sup>	Up to 30 mg/kg of intraperitoneal doses produced potent analgesic effects in models of chronic inflammatory, neuropathic and incisional pain. The analgesic effect of GW405833 on chronic inflammatory pain was abolished in CB <sub>2</sub> receptor knockout mice. <sup>c</sup>

<b>HU308</b>	22.7 <sup>d</sup> 11.5 <sup>l</sup>	>10000 <sup>d</sup>	LPS-induced nitrite accumulation in BV-2 mouse microglial cells was inhibited with an EC <sub>50</sub> value of 250 nM. <sup>k</sup> [ <sup>35</sup> S]-GTPγS binding to CB <sub>2</sub> -expressing cell membranes was enhanced with an EC <sub>50</sub> value of 6.4 nM and a similar maximal response to CP55940. <sup>l</sup>	50 mg/kg inhibited inflammation-associated increases in mouse ear thickness; sensitive to SR144528 but not rimonabant 1 mg/kg. <sup>d</sup> Chronic daily exposure of 2 mg/ear HU308 for eight days induced ear swelling in mice which was reversed by the antagonist/inverse agonists JTE-907 and SR144528. <sup>m,n</sup> HU308 produced an analgesic effect in formalin-induced peripheral pain model and skin-incision model of postoperative pain in rats which was abolished subsequent to pre-treatment with SR144528. <sup>o</sup>
<b>L759656</b>	11.8 <sup>e</sup>	4888 <sup>e</sup>	Inhibition of cAMP accumulation in CHO-hCB <sub>2</sub> cells with a potency of 3.1 nM with a maximal inhibition of 94 % compared to CP55940 with 78 %. <sup>e</sup>	No reports of an in vivo investigation
<b>MDA19</b>	43.3 <sup>f</sup>	162 <sup>f</sup>	[ <sup>35</sup> S]-GTPγS binding to CB <sub>2</sub> receptor expressing cell membranes was enhanced with an EC <sub>50</sub> value of 83 nM and a maximal inhibition of 65 % compared to 94 % with CP55940. In the cAMP pathway, MDA19 produced no functional activity, while exhibiting an agonist profile in the ERK1/2 in the rat CHO-CB <sub>2</sub> cells which was blocked by AM630. <sup>f</sup>	MDA19 reduced neuropathic pain in spinal nerve ligation neuropathic pain model following intraperitoneal administration to rats which was abolished subsequent to pre-treatment with AM630. <sup>f</sup>

a(Manera et al., 2006); b(Murineddu et al., 2006); c(Valenzano et al., 2005); d(Hanus et al., 1999); e(Ross et al., 1999); f(Xu et al., 2010); g(Farsandaj et al., 2012); h(Zhang et al., 2013); i(Pourkhalili et al., 2013); j(Emadi et al., 2011); k(Martin-Moreno et al., 2011); l(Smoum et al., 2015); m(Ueda et al., 2005); n(Oka et al., 2006); o(Yao et al., 2008); p(Gallant et al., 1996); q(Ndong et al., 2011)

## 5.1 Results

### 5.1.1 Radioligand Binding

The six compounds were investigated in a preliminary radioligand binding study at 1  $\mu$ M (Figure 5.1). At this concentration, four of the ligands (GP2a, GW405833, HU308 and L759656) completely inhibited  $^3\text{H}$ -CP55940 binding to membranes from CHO-CB<sub>2</sub> cells. However, at this concentration, CB65 and MDA19 failed to displace radioligand binding completely.

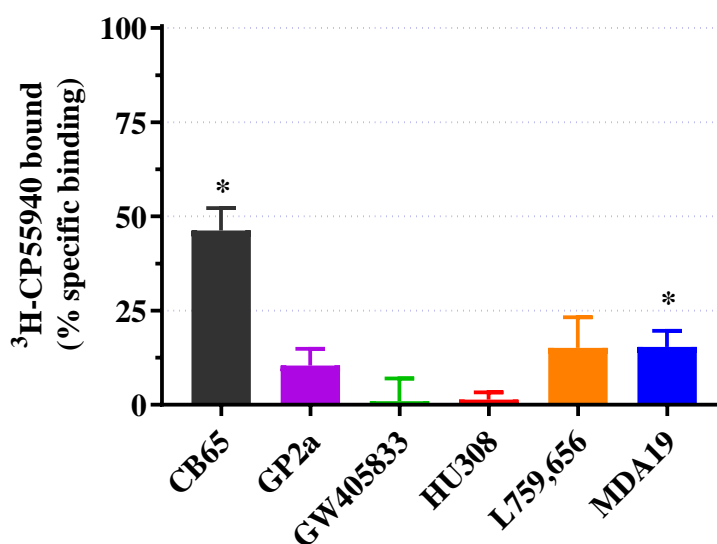


Figure 5.1 Specific binding of [ $^3\text{H}$ ]-CP55940 to membrane suspensions of CHO-CB<sub>2</sub> cells.

Data are the mean  $\pm$  SEM of three individual experiments performed in duplicate. \*  $p \leq 0.05$ , \*\*  $p \leq 0.01$ , One-way ANOVA test and Dunnett's multiple comparison analysis compared to preparations in the presence of an excess of CP55940.

## 5.1.2 Intracellular calcium ion levels

The capacity of these six ligands, in comparison to the positive control CP55940, to increase intracellular calcium levels in CHO-CB<sub>2</sub> cells was evaluated next (Figure 5.2). All of the ligands were screened at 1  $\mu$ M. As evident from Figure 5.2, only CP55,940 and HU308 induced significant elevations in calcium mobilization. MDA19 produced a numerically small effect which was not significant, while CB65, GP2a, GW405833 and L759,656 all failed to alter intracellular calcium levels.

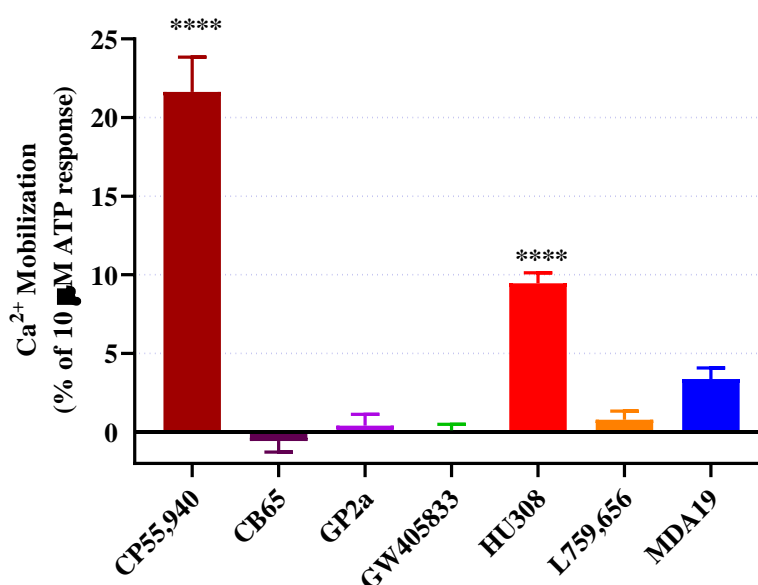


Figure 5.2 Effects of CB<sub>2</sub> receptor ligands on calcium levels in CHO-CB<sub>2</sub> cells. Data are the mean  $\pm$  SEM of five independent experiments performed in triplicate. Data were monitored as AUC and normalised to the response to 10  $\mu$ M ATP. \*\*\*\*  $p \leq 0.0001$ , Two-way ANOVA test with Dunnett's multiple comparison analysis.

Since both HU308 and MDA19 appeared capable of evoking Ca<sup>2+</sup> ion elevations, both compounds were investigated further over a range of concentrations (Figure 5.3). HU308 and MDA19 produced calcium elevations with pEC<sub>50</sub> values of  $5.91 \pm 0.19$  and  $6.60 \pm 0.16$  and E<sub>max</sub> values of  $17.4 \pm 1.4$  and  $7.7 \pm 0.3$  % ATP response, respectively.

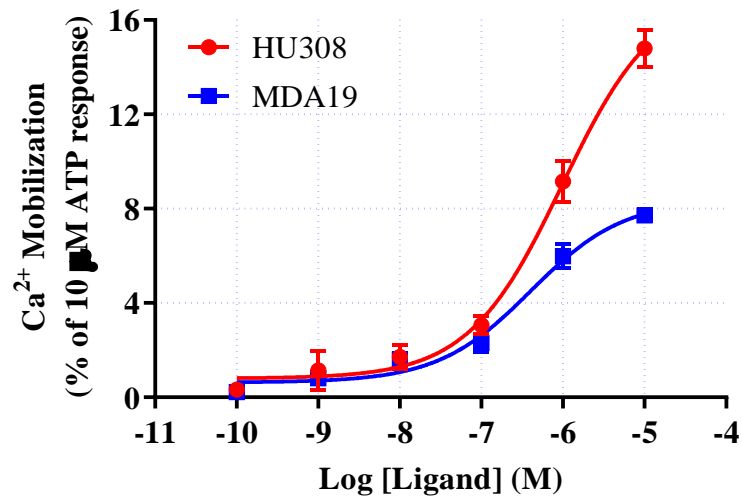


Figure 5.3 Effects of CB<sub>2</sub> receptor ligands on calcium levels in CHO-CB<sub>2</sub> cells. Data are the mean  $\pm$  SEM of three independent experiments performed in triplicate. Data were monitored as AUC and normalised to the response to 10  $\mu$ M ATP. Concentration response curves were fitted using the four-parameter logistic equation.

### 5.1.3 ERK Phosphorylation

The same range of ligands at the same concentration were investigated for stimulation of ERK phosphorylation in an in-cell immunoassay. The non-selective cannabinoid receptor agonist positive control CP55940 evoked a similar level of ERK phosphorylation as 1 % FBS (Figure 5.4). Only HU308 and MDA19 were capable of activating ERK phosphorylation to levels close to those observed with CP55940. L759656 also evoked a statistically significant ERK phosphorylation, but at about 10 % of the response to CP55940.

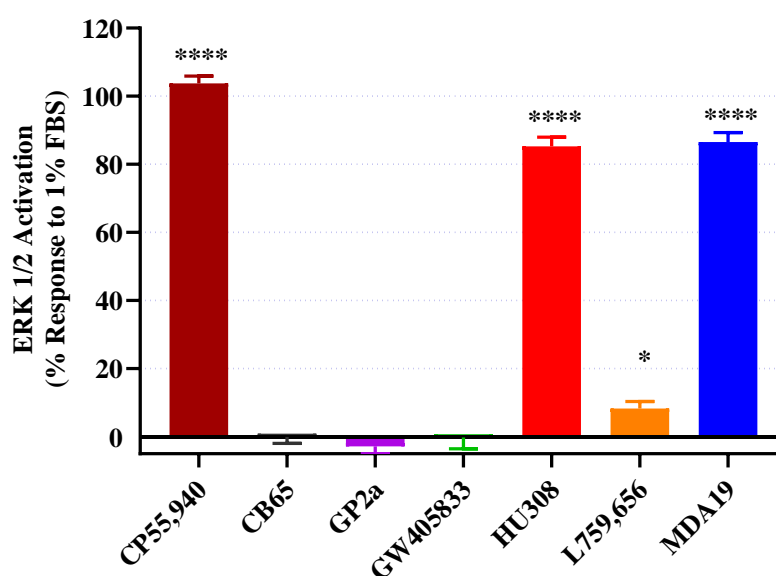


Figure 5.4 Activation of the ERK signalling pathway by CB<sub>2</sub> receptor ligands (1  $\mu$ M).

Data are the mean  $\pm$  SEM of five independent experiments performed in triplicate and measured at 5 min of ERK activation. \*  $p \leq 0.05$  and \*\*\*\*  $p \leq 0.0001$ , Two-way ANOVA test with Dunnett's multiple comparison analysis.

For those agents which stimulated ERK phosphorylation, a range of concentrations was investigated (Figure 5.5). Responses to HU308 and MDA19 saturated at higher concentrations, allowing calculation of pEC<sub>50</sub> values of 7.0 and 6.4, respectively (Table 5.3).

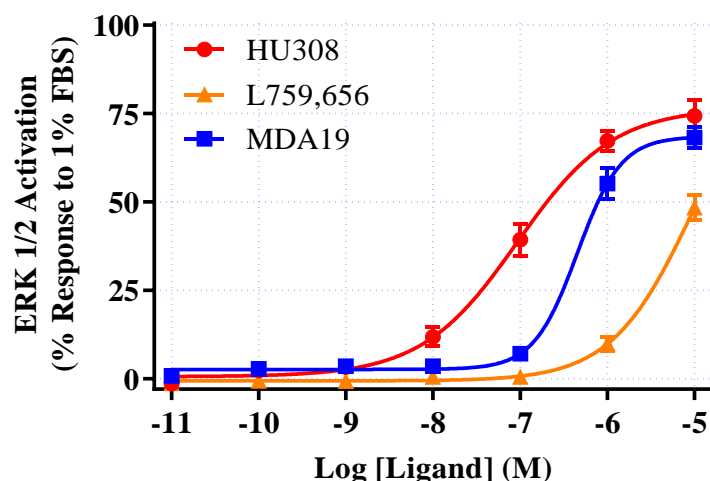


Figure 5.5 The concentration dependence of ERK phosphorylation induced by HU308, L759,656 and MDA19.

Data are the mean  $\pm$  SEM of three (L759,656) or five (HU308 and MDA19) independent experiments performed in triplicate and measured at 5 min of ERK activation. Curves were fitted using the four-parameter logistic equation.

Table 5.3 The quantitative parameters for HU308, L759,656 and MDA19 activation of ERK phosphorylation in CHO-CB<sub>2</sub> cells performed at n = 5 for HU308, MDA19 and n = 3 for L759,656. One sample t test analysis of the hill slope indicated that the slope produced by MDA19 was statistically different from one while that of HU308 was not statistically different from one.

Compound	Maximal responses $E_{max}$ (% FBS)	Potencies (pEC <sub>50</sub> )	Hill Slope (nH)
HU308	76 $\pm$ 5	7.0 $\pm$ 0.10	0.88 $\pm$ 0.14
L759,656	-	-	-
MDA19	66 $\pm$ 3	6.4 $\pm$ 0.10	2.09 $\pm$ 0.25

The effects of these compounds were analysed in the presence of 2AG, in part to predict the outcome for administering the agents *in vivo* under conditions of tonic activation of the CB<sub>2</sub> receptor. All the compounds appeared to induce a statistically significant effect when administered at the same concentration as 2AG (1  $\mu$ M). Two distinct effects were observed in this assay, where the group of agents which failed to stimulate ERK phosphorylation directly (CB65, GP2a and GW405833) evoked an inhibition of the ERK response to 2-AG (Figure 5.6). Combination of 2-AG with the agents which

stimulated ERK phosphorylation (HU308, L759,656 and MDA19) evoked responses greater than those of 2-AG alone.

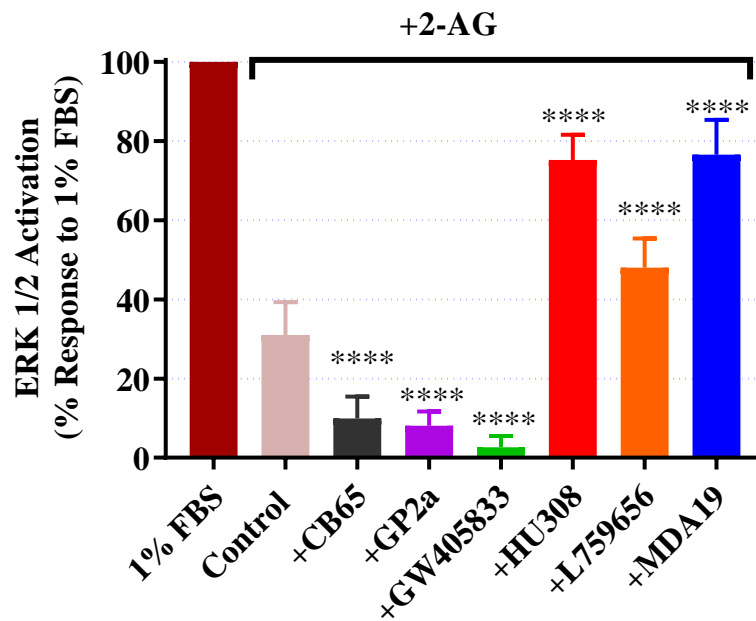


Figure 5.6 Effects of combining CB<sub>2</sub> receptor ligands with the endogenous agonist 2-AG on activation of the ERK pathway in CHO-CB<sub>2</sub> cells. All compounds were tested at 1  $\mu$ M. Data are the mean  $\pm$  SEM of seven independent experiments performed in triplicate and measured at 5 min of ERK activation. \*\*\*\*  $p < 0.0001$ , Two-way ANOVA and Dunnett's multiple comparison test compared to 2-AG alone.

### 5.1.4 Regulation of cAMP accumulation

These same six compounds at 1  $\mu\text{M}$  were investigated for the potential to inhibit forskolin-stimulated cAMP accumulation in CHO-CB<sub>2</sub> cells (Figure 5.7). In this assay, CP55940 evoked a complete inhibition of cAMP accumulation, while CB65 was ineffective. GP2a evoked an increased cAMP accumulation. HU308 and MDA19 inhibited the forskolin cAMP by more than 75%, while L759656 and GW405833 were less effective. Since all compounds, except CB65 produced an effect that was statistically significant, the compounds were subsequently investigated in full concentration-response profiles.

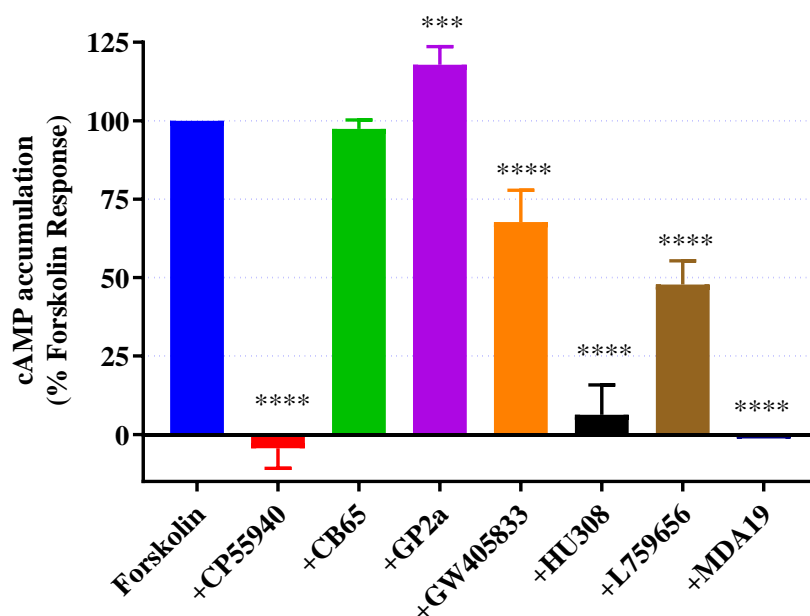


Figure 5.7 Effects of the CB<sub>2</sub> receptor ligands on forskolin-induced cAMP accumulation in CHO-CB<sub>2</sub> cells.

Data are the mean  $\pm$  SEM of four independent experiments performed in triplicate. \*\*\*  $p \leq 0.001$  and \*\*\*\*  $p \leq 0.0001$ , Two-way ANOVA and Dunnett's multiple comparison test.

All five compounds evoked concentration-dependent changes in cAMP accumulation, which could be fitted with sigmoidal curves (Figure 5.8).

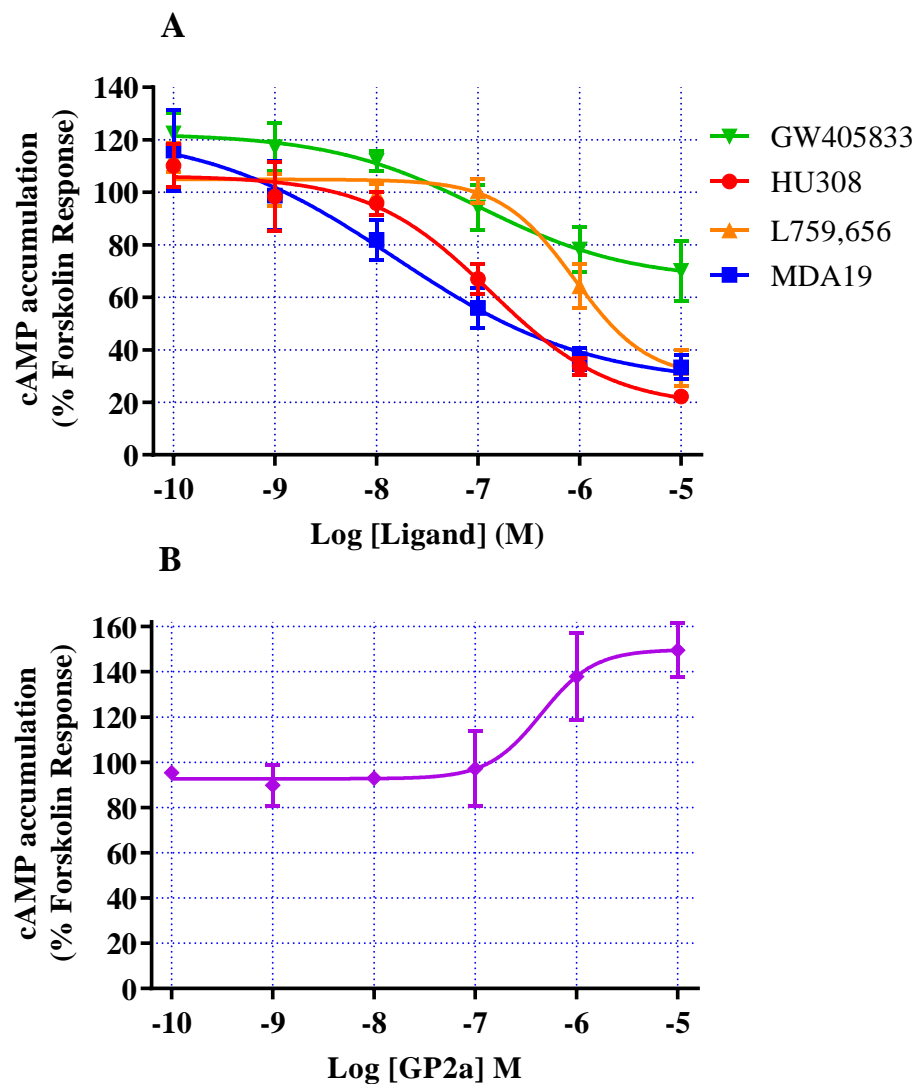


Figure 5.8 Effects of CB<sub>2</sub> receptor ligands on forskolin-induced cAMP accumulation in CHO-CB<sub>2</sub> cells by (A) GW405833, HU308, L759,656, MDA19 and (B) GP2a.

Data are the mean  $\pm$  SEM of three independent experiments performed in triplicate. Concentration response curves were fitted using the four-parameter logistic equation.

Table 5.4 Quantitative parameters for HU308, L759,656 and MDA19 regulation of cAMP accumulation in CHO-CB<sub>2</sub> cells performed at n=3. One sample t test analysis of the hill slope indicated that only GW405833 produced a hill slope that was statistically different from -1 while the hill slope of the other compounds was not statistically different from -1.

<b>Compound</b>	<b>Maximal responses E<sub>max</sub> (%)</b>	<b>Potencies (pEC<sub>50</sub>)</b>	<b>Hill Slope (nH)</b>
GP2a	-61 ± 12	6.3 ± 0.3	5.72 ± 2.20
GW405833	53 ± 17	6.9 ± 0.2	-0.70 ± 0.06
HU308	87 ± 10	6.9 ± 0.2	-0.85 ± 0.08
L759656	76 ± 12	6.0 ± 0.1	-1.42 ± 0.31
MDA19	94 ± 30	7.9 ± 0.3	-0.67 ± 0.16

Table 5.5 Summary of the effects induced by the compounds at the different CB2 receptor signalling pathways

Compound	Radioligand binding displacement	Calcium elevation	ERK phosphorylation		cAMP inhibition	
	Effect at 1 $\mu$ M		Ligand effect	Effect on 2AG responses	Ligand effect	Profile
<b>CB65</b>	50 %	0	0	Inhibited 2AG	0	?
<b>GP2a</b>	88 %	0	0	Inhibited 2AG	6.3 $\pm$ 0.3 -61 $\pm$ 12 %	Inverse agonist
<b>GW405833</b>	100 %	0	0	Inhibited 2AG	6.9 $\pm$ 0.2 53 $\pm$ 17 %	Partial Agonist
<b>HU308</b>	100 %	9.5 $\pm$ 0.7 %	7.0 $\pm$ 0.1 76 $\pm$ 5 %	$\uparrow$ 2AG	6.9 $\pm$ 0.2 87 $\pm$ 10 %	Agonist
<b>L759656</b>	85 %	0	10 %	$\uparrow$ 2AG	6.0 $\pm$ 0.1 76 $\pm$ 12 %	Partial Agonist
<b>MDA19</b>	84 %	3.4 $\pm$ 0.7 %	6.4 $\pm$ 0.1 66 $\pm$ 3 %	$\uparrow$ 2AG	7.9 $\pm$ 0.3 94 $\pm$ 30 %	Agonist
<b>CP55940</b>		21.6 $\pm$ 2.2 %	104 $\pm$ 2	$\uparrow$ 2AG	104 $\pm$ 6 %	Agonist

## 5.2 Discussion

Since the quinolone-4-carboxamide CB<sub>2</sub> receptor-selective ligands SER601 and COR170, did not function as anticipated as the functional and binding profiles were distinct from the published literature, a range of commercially available cannabinoid CB<sub>2</sub> receptor-selective agonists were investigated to assess the theory of biased agonism using the same rapid responding assays. The predominant aim of this was to gain an enhanced understanding of the cannabinoid CB<sub>2</sub> receptor, its signalling mechanisms and whether reported CB<sub>2</sub> receptor agonists demonstrated bias towards one signalling pathway over the others. The investigated cannabinoid CB<sub>2</sub> receptor agonists included CB65 (described as a high affinity selective CB<sub>2</sub> receptor agonist,  $K_i = 3.3$  nM (Manera et al., 2006)), GP2a (described as a selective CB<sub>2</sub> receptor agonist,  $K_i = 7.6$  nM (Murineddu et al., 2006)), GW405833 (described as a selective, high affinity CB<sub>2</sub> receptor partial agonist,  $K_i = 3.92$  nM (Valenzano et al., 2005)), HU308 (described as a potent selective CB<sub>2</sub> receptor agonist,  $K_i = 22.7$  nM (Hanus et al., 1999)), L759,656 (described as a potent selective CB<sub>2</sub> receptor agonist,  $K_i = 11.8$  nM (Ross et al., 1999)), and MDA19 (described as a CB<sub>2</sub> receptor agonist,  $K_i = 43.3$  nM (Xu et al., 2010)). These compounds exhibit distinct pharmacophores (Table 5.1) and were investigated in a series of studies to evaluate their CB<sub>2</sub> receptor signalling properties. The compounds were investigated in the precedingly performed signalling pathways.

### 5.2.1 Comparing the CB<sub>2</sub> receptor agonists with the literature

HU308 completely displaced <sup>3</sup>H-CP55940 binding to the human recombinant CB<sub>2</sub> receptor at a concentration of 1 μM, consistent with the reported affinity of 23 nM (Hanus et al., 1999). HU308 was found to possess the highest efficacy among the six compounds in the calcium and ERK assays and had high efficacy for inhibition of cAMP accumulation. When investigated in the presence of 2AG-evoked ERK phosphorylation, HU308 evoked responses greater than those of 2AG alone. It showed equivalent potency in the ERK and cAMP assays. Although the potency of HU308 in the calcium elevation assay

was not assessed, at 1  $\mu\text{M}$  it produced approximately half the response to 1  $\mu\text{M}$  CP55940. The ligand's functional profile was reasonably consistent with the literature where it was claimed to be the most useful CB<sub>2</sub> receptor agonist for its lack of bias towards any signalling pathway, as well as having useful selectivity, potency and pharmacokinetic profiles (Soethoudt et al., 2017). In this study as well, HU308 did not demonstrate bias in the investigated pathways and produced a profile consistent with a potent CB<sub>2</sub> receptor agonist. Therefore, overall the ligand profile is consistent with the published description.

GP2a was reported to have a higher affinity than HU308 at CB<sub>2</sub> receptors (7.6 nM), although this estimate was obtained using mouse spleen preparations (Murineddu et al., 2006). Using CHO cells expressing human recombinant CB<sub>2</sub> receptors, 1  $\mu\text{M}$  GP2a elicited almost 90 % displacement of <sup>3</sup>H-CP55940 binding. In those cells, it failed to stimulate calcium or ERK pathways, while inhibiting the 2AG ERK response; and producing an inverse agonist profile in cAMP assay. Clearly, therefore, there is a disconnection between the functional profile of GP2a in the literature compared to the present results. This may derive from a species difference in the action of GP2a, although HL60 cells (in which GP2A is reported to stimulate ERK1/2 phosphorylation potently) were human-derived (Murineddu et al., 2006).

GW405833 completely displaced <sup>3</sup>H-CP55940 binding to the human recombinant CB<sub>2</sub> receptor at a concentration of 1  $\mu\text{M}$ , consistent with the reported affinity of 4-12 nM (Gallant et al., 1996; Valenzano et al., 2005). It showed a partial agonist profile in inhibition of cAMP, consistent with the literature (53 % compared to 104 % by CP55940). Valenzano et al. reported a maximal inhibition of 45 % compared to the maximal inhibition evoked by CP55940 (84 %). However, the reported literature potency 9.2, (Valenzano et al., 2005) was much higher than that observed in the present study (potency = 6.9). In a further report using a LANCE assay, GW405883 was reported to be a partial agonist with a potency of 7.5 (McGuinness et al., 2009). It caused no stimulation of the calcium or ERK pathways, while inhibiting the ERK response to 2AG.

L759656 at 1  $\mu$ M produced incomplete displacement of binding which was consistent with the published affinity of 12 nM. The compound had no effect on calcium, induced a small but significant ERK phosphorylation but elicited a saturable inhibition of cAMP accumulation assay. The ligand produced no effect on 2AG-evoked ERK phosphorylation. In a previous report of the cAMP inhibitory potential of L759656, a potency of 3 nM (pEC<sub>50</sub> value of 8.5) with a maximal inhibition not different from CP55940 (Ross et al., 1999). Therefore, the compound displayed reasonable correlation with the available limited literature, though with lower potency.

MDA19 at 1  $\mu$ M demonstrated an incomplete binding displacement which is consistent with the published description of its capacity to displace <sup>3</sup>H-CP55940 from human CB<sub>2</sub> receptors (a pK<sub>i</sub> value of 7.4) (Xu et al., 2010). The ligand produced a marginal (non-significant effect) on calcium responses, and high potency and efficacy consistent with a full agonist in the cAMP assay. In the ERK assay, MDA19 exhibited reduced potency compared to inhibition of cAMP, with a maximal response lower than CP55940. When investigated in the presence of 2AG, MDA19 evoked ERK phosphorylation responses greater than those of 2AG alone. Therefore, the profile of MDA19 was not entirely consistent with the literature, although there is only a limited amount of literature for direct comparison.

### **5.2.2 CB<sub>2</sub> receptor agonists diverging from literature profiling**

The ligand binding of CB65 was not consistent with the reported profile of a K<sub>i</sub> value of 3.3-14 nM (Manera et al., 2006; Ndong et al., 2011), while the present study revealed only 50% displacement of [<sup>3</sup>H]-CP55,940 binding at 1  $\mu$ M. CB65 produced no effect on calcium, ERK or cAMP responses at 1  $\mu$ M, while it partly inhibited the 2AG ERK response at that concentration. There are only very limited descriptions in the literature of CB65 regulation of second messenger signalling in a CB<sub>2</sub> receptor-dependent manner. Thus, Ndong et al., 2011 described an inverse agonist profile in forskolin-stimulated cAMP production with a potency of 1.2 nM. The cell effects and *in vivo* data of CB65 seem to be CB<sub>2</sub> receptor-dependent and consistent with CB<sub>2</sub> receptor activation.

Differences between this study and the literature could possibly be attributed to species differences, as the high potency of the CB65 measured via its ability in displacing [<sup>3</sup>H]-CP55940 was performed in mouse spleen homogenate (Manera et al., 2006), while this research investigated human CHO-CB<sub>2</sub>. CB65 could displace [<sup>3</sup>H]-CP55940 binding in human CHO-CB<sub>2</sub> cells, while it produced an inverse agonists profile in the cAMP accumulation of human CHO-CB<sub>2</sub> clone (Ndong et al., 2011). In order to draw solid conclusions regarding the activity and function of this compound, future investigations in the laboratory could aim to use the mouse CB<sub>2</sub> receptors as well to compare it with the published literature.

### 5.3 Conclusion

The compounds investigated in this study derive from different structural scaffolds. Based on the experiments performed in Chapters 3 and 4 investigating CB<sub>2</sub> receptor function, CP55,940 is an efficacious CB<sub>2</sub> receptor agonist independent of the pathway analysed, while fenofibrate, HU308 and MDA19 evoked a similar pattern, albeit less effective than CP55940. GW405833 appears to be a low efficacy agonist, the visualization of a response presumably depends on the efficiency of coupling of the signalling pathway. GP2a prompted an inverse agonist profile in the cAMP pathway without activation of any of the other investigated pathways, while L759656 evoked inhibition of the cAMP with no significant effects on the other two pathways. As indicated for GW405833, the lack of stimulation in calcium and ERK assays may be a consequence of poorer coupling to those pathways. Both L759656 and GP2a have limited published data investigating their effects at CB<sub>2</sub> receptors. CB65 nevertheless, was quite distinct from the other ligands with an apparent disconnect between *in vitro* and *in vivo* profiles. The compound requires further characterisation before solid conclusions could be drawn towards its activity. Overall, the profile in the current study had some similarities with published literature.

## Chapter 6 : Mutation of Phe117 Phe200 and W258 amino acids of CB<sub>2</sub> receptors

The preceding chapters sought to enhance the understanding of signalling mechanisms associated with CB<sub>2</sub> receptors, through varying the ligand. The aim of this Chapter was to investigate essential residues contributing to CB<sub>2</sub> receptor signalling. Multiple Single Nucleotide Polymorphisms (SNPs) have been identified in the human cannabinoid CB<sub>2</sub> receptor with reasonable frequency; Q36R, Q66R (Hillger et al., 2017) and H316Y (Ishiguro et al., 2013). H316Y was associated with diminished bone density in the population expressing this SNP variant (Hillger et al., 2017) while Q36R was linked with an increased occurrence of idiopathic arthritis, schizophrenia and depression (Ishiguro et al., 2010). Additionally, the presence of the Q36R SNP variant was reported to trigger signalling bias of CB<sub>2</sub> receptors (Hillger et al., 2017).

A study on the cannabinoid CB<sub>1</sub> receptor (building on observations from other GPCR) investigated an aromatic microdomain composed of F190 (3.25), F201 (3.36), W280 (5.43), and W357 (6.48) recognised the significance of F201/W357 in preserving the receptor in the inactive state which needed to be broken for receptor activation to occur. The interaction of these two amino acids described an essential toggle switch required in CB<sub>1</sub> receptor activation. Mutation of F190A was not involved in the TM3-4-5-6 aromatic cluster which characterized the active and inactive state conformation of the CB<sub>1</sub> receptor. Thus, mutation of the aromatic residue of F190 to a non-aromatic residue did not affect agonist-independent receptor activity. Moreover, W280A mutation induced a significant reduction in the ligand binding affinity of WIN55212-2 and rimonabant but not CP55940 (McAllister et al., 2004).

Multiple Trp residues have been reported to be conserved across GPCRs. Another study investigated the effects of mutating W158 (conserved across multiple GPCRs) and W172 (present in both CB<sub>1</sub> and CB<sub>2</sub> receptors) on the binding of compounds to CB<sub>2</sub> receptor. The study concluded that mutation of W172 to F or Y did not affect ligand binding or downstream signalling, while

mutation of W172 to a non-aromatic amino acid, including A or L, completely abolished ligand binding. Likewise, mutation of W158 to Y or A both abolished ligand binding, thus confirming the significance of both W158 and W172 in TM4 and ECL2, respectively, of CB<sub>2</sub> receptors in ligand binding and receptor function (Rhee et al., 2000). Further research investigating mutation of amino acids in CB<sub>2</sub> receptors explored the mutation of S161 and S165 located in TM4 of the receptor. Site-directed mutagenesis of either amino acid to the respective alanine residue abolished both binding and activity of CB<sub>2</sub> receptor inverse agonist SR144528, while not affecting those of the agonist WIN55212-2 (Gouldson et al., 2000).

The CB<sub>1</sub> and CB<sub>2</sub> receptors share around 44% amino acid composition, this study aimed to map selected ligand recognition sites for functioning of the human cannabinoid CB<sub>2</sub> receptor. Previous research demonstrated that site-directed mutagenesis of phenylalanine F200 to alanine in TM3 of the CB<sub>1</sub> receptor produced substantially diminished forskolin-induced cAMP generation and was found to be implicated in receptor stimulation by certain agonists (Shen et al., 2006). The F200 residue is conserved between the cannabinoid CB<sub>1</sub> and CB<sub>2</sub> receptors, therefore; the analogous residue in the cannabinoid CB<sub>2</sub> receptor in TM5 was selected for site-directed mutagenesis to the corresponding alanine residue. Additionally, residues selected for site-directed mutagenesis included phenylalanine F117 and tryptophan W258 which were mutated to the corresponding alanine residues. Both F117 and W258 were found to have a vital role in the hydrophobic  $\pi$ - $\pi$  interactions involved in ligand binding to CB<sub>2</sub> receptors by inducing substantial conformational modifications of the receptors required for ligand binding to occur (Li et al., 2019). This investigation, therefore, aimed to assess the importance of these hydrophobic amino acids towards the receptor ligand binding interactions and site-directed mutagenesis to elucidate individual residue contributions towards functional properties of the cannabinoid CB<sub>2</sub> receptor.

This chapter thus, aimed to assess the importance of the hydrophobic amino acids Phe117, Phe200 and W258 towards the receptor interactions and site-directed mutagenesis to their alanine counterparts would elucidate individual residue contributions towards functional signalling

mechanism/s of the cannabinoid CB<sub>2</sub> receptor. The amino acid residues that were selected for mutation are displayed in Figure 6.1. (F117 in TM3, F200 in TM5 and W258 in TM6) and have not been previously investigated in the literature (Table 6.1).

Table 6.1 Mutagenesis studies of the human cannabinoid CB<sub>2</sub> receptor

<b>Mutation</b>	<b>Location</b>	<b>Impact on binding</b>	<b>Functional impact</b>
C40A <sup>a</sup>	TM1 (1.39)	Loss of <sup>3</sup> H-HU243 binding	
Q63R <sup>b</sup>	ICL1	Competition binding of <sup>3</sup> H-CP with AEA, 2AG, HU, CP and WIN was not altered	Reduced efficacy of WIN and 2AG in cAMP accumulation assays
D80N <sup>c</sup>	TM2 (2.50)	No change in <sup>3</sup> H-CP or WIN affinity	Loss of CP- and WIN-induced inhibition of cAMP accumulation
D80E <sup>c</sup>	TM2 (2.50)	No change in <sup>3</sup> H-CP or WIN affinity	Reduction in CP- and WIN-induced inhibition of cAMP accumulation
C89A <sup>a</sup>	TM2 (2.59)	No effect on <sup>3</sup> H-HU243 binding	
K109A <sup>d</sup>	TM3 (3.28)	No change in <sup>3</sup> H-CP affinity	No change in CP or WIN-induced inhibition of cAMP accumulation
K109R <sup>d</sup>	TM3 (3.28)	No change in <sup>3</sup> H-CP affinity	No change in CP or WIN-induced inhibition of cAMP accumulation
V113E <sup>e</sup>	TM3 (3.32)	Loss of <sup>3</sup> H-CP binding	Loss of CP inhibition of cAMP accumulation
V113L <sup>e</sup>	TM3 (3.32)	No change in CP, SR binding	No change in CP inhibition of cAMP accumulation
D130A <sup>f</sup>	TM3 (3.49)	Loss of <sup>3</sup> H-HU243 binding	Loss of AEA, HU & WIN inhibition of cAMP accumulation Loss of SR enhancement of cAMP accumulation
D130A <sup>g</sup>	TM3 (3.49)	Reduced <sup>3</sup> H-HU243 binding	
R131A <sup>f</sup>	TM3 (3.50)	No effect on <sup>3</sup> H-HU243 binding. Agonist & antagonist competition unchanged	Loss of AEA, HU & WIN inhibition of cAMP accumulation Loss of SR enhancement of cAMP accumulation
R131A <sup>g</sup>	TM3 (3.50)	No effect on <sup>3</sup> H-HU243 binding	Reduced E <sub>max</sub> for HU and WIN inhibition of cAMP accumulation
Y132A <sup>g</sup>	TM3 (3.51)	No effect on <sup>3</sup> H-HU243 binding	Reduced E <sub>max</sub> for HU and WIN inhibition of cAMP accumulation
P139A <sup>h</sup>	ICL2		Minor reduction in potency and efficacy on the inhibition of forskolin-induced cAMP accumulation by WIN
W158 <sup>g</sup>	TM4 (4.50)	W158Y: Loss of <sup>3</sup> H-HU243 binding	Minor inhibition in cAMP accumulation via HU and WIN

		W158A: Loss of <sup>3</sup> H-HU243 binding	Minor inhibition in cAMP accumulation via HU and WIN
		W158F: No effect on <sup>3</sup> H-HU243 binding.	No change in HU and WIN inhibition of cAMP accumulation
S161A <sup>i</sup>	TM4 (4.53)	No change in <sup>3</sup> H-CP competition binding with CP or WIN, while complete loss in <sup>3</sup> H-CP competition binding with SR	No change in CP or WIN-induced inhibition of cAMP accumulation Loss of SR enhancement of cAMP accumulation
V164I <sup>i</sup>	TM4 (4.56)	No change in <sup>3</sup> H-CP competition binding with CP, WIN and SR	
S165A <sup>i</sup>	TM4 (4.57)	No change in <sup>3</sup> H-CP competition binding with CP and WIN affinity, while loss <sup>3</sup> H-CP competition binding to SR	No change in CP or WIN-induced inhibition of cAMP accumulation Loss of SR enhancement of cAMP accumulation
W172 <sup>g</sup>	ECL2	W172L: Loss of <sup>3</sup> H-HU243 binding	Loss of inhibition in cAMP accumulation via HU and WIN
		W172A: Loss of <sup>3</sup> H-HU243 binding	Low inhibition of cAMP accumulation via HU and WIN
		W172F: Retained 80% of <sup>3</sup> H-HU243 WT-binding	No change in HU or WIN-induced inhibition of cAMP accumulation
		W172Y: Retained 60% of <sup>3</sup> H-HU243 WT-binding	No change in HU or WIN-induced inhibition of cAMP accumulation
C174S <sup>i</sup>	ECL2	Complete loss in <sup>3</sup> H-CP competition binding with CP, WIN and SR	
C174A <sup>a</sup>	ECL2	Loss of <sup>3</sup> H-HU243 binding	
C175S <sup>i</sup>	ECL2	No change in <sup>3</sup> H-CP competition binding with CP Moderate decrease in <sup>3</sup> H-CP competition binding with WIN Complete loss in <sup>3</sup> H-CP competition binding with SR	Loss of CP- and WIN-induced inhibition of cAMP accumulation Loss of SR enhancement of cAMP accumulation
C175A <sup>a</sup>	ECL2	Loss of <sup>3</sup> H-HU243 binding	

R177S <sup>i</sup>	ECL2	No change in <sup>3</sup> H-CP competition binding with CP, WIN and SR	
C179S <sup>ij</sup>	ECL2	Complete loss in <sup>3</sup> H-CP competition binding with CP, WIN and SR	
C179A <sup>a</sup>	ECL2	Loss of <sup>3</sup> H-HU243 binding	
L192A <sup>e</sup>	TM5 (5.41)	No change in CP, SR competition for binding	No change in CP inhibition of cAMP accumulation
L192S <sup>e</sup>	TM5 (5.41)	Loss of <sup>3</sup> H-CP binding	Loss of CP inhibition of cAMP accumulation
S193G <sup>i</sup>	TM5 (5.42)	No change in <sup>3</sup> H-CP competition binding with CP, WIN and SR	
W194Y <sup>j</sup>	TM5 (5.43)	No change in CP, binding affinity while reduced binding affinity with WIN and SR in <sup>3</sup> H-CP competition binding assay	Loss of CP and WIN induced inhibition of cAMP accumulation
D240N <sup>k</sup>	TM6 (6.30)	No change in <sup>3</sup> H-CP binding or CP competition	Reduced maximal inhibition without change in potency of CP for cAMP accumulation
A244E <sup>f</sup>	TM6 (6.34)	Loss of <sup>3</sup> H-HU243 binding	Loss of AEA & HU and reduced WIN inhibition of cAMP accumulation Loss of SR enhancement of cAMP accumulation
C257A <sup>a</sup>	TM6 (6.47)	No effect on <sup>3</sup> H-HU243 binding	
C257A <sup>l</sup>	TM6 (6.47)	No change in <sup>3</sup> H-CP or <sup>3</sup> H-WIN binding	No change in AM841 or AM4056 inhibition of cAMP accumulation
C257S <sup>l</sup>	TM6 (6.47)	No change in <sup>3</sup> H-CP or <sup>3</sup> H-WIN binding	No change in AM841 or AM4056 inhibition of cAMP accumulation
V261C <sup>m</sup>	TM6 (6.51)	No change in <sup>3</sup> H-CP competition binding	
L262C <sup>m</sup>	TM6 (6.52)	Increased <sup>3</sup> H-CP binding affinity compared to WT-CB <sub>2</sub>	
L264C <sup>m</sup>	TM6 (6.54)	Increased <sup>3</sup> H-CP binding affinity compared to WT-CB <sub>2</sub>	
M264C <sup>m</sup>	TM6 (6.55)	Increased <sup>3</sup> H-CP binding affinity compared to WT-CB <sub>2</sub>	

L269C <sup>m</sup>	TM6 (6.59)	Increased <sup>3</sup> H-CP binding affinity compared to WT-CB <sub>2</sub>	
T271C <sup>m</sup>	TM6 (6.61)	Increased <sup>3</sup> H-CP binding affinity compared to WT-CB <sub>2</sub>	
C284A <sup>a</sup>	TM7 (7.38)	No effect on <sup>3</sup> H-HU243 binding.	
C284S <sup>l</sup>	TM7 (7.38)	Decrease in <sup>3</sup> H-CP binding	
C284S <sup>n</sup>	TM7 (7.38)	No change in <sup>3</sup> H-CP binding.	Decrease in AM1336 enhancement of cAMP accumulation
S285A <sup>g</sup>	TM7 (7.39)	Reduced affinity of <sup>3</sup> H-HU243 binding	Unchanged profile of HU, CP & WIN inhibition of cAMP accumulation
C288A <sup>a</sup>	TM7 (7.42)	No effect on <sup>3</sup> H-HU243 binding	
C288S <sup>n</sup>	TM7 (7.42)	No change in <sup>3</sup> H-CP binding	Decrease in AM1336 enhancement of cAMP accumulation
S292A <sup>g</sup>	TM7 (7.46)	Unchanged affinity of <sup>3</sup> H-HU243 binding	Unchanged profile of WIN, but reduced potency of HU and CP inhibition of cAMP accumulation
Y299A <sup>o</sup>	TM7 (7.53)	Loss of <sup>3</sup> H-HU243 specific binding	Loss of HU, AEA-and WIN-induced inhibition of cAMP accumulation
C313A <sup>o</sup>	C-term	No effect on <sup>3</sup> H-HU243 specific binding	Loss of HU, AEA an WIN inhibition of cAMP accumulation
H316Y <sup>b</sup>	C-term	Competition binding of <sup>3</sup> H-CP with CP was not altered	No change in CP inhibition of cAMP accumulation

CP, CP55940; HU, HU210; SR, SR144528; WIN, WIN55212-2.

<sup>a</sup>(Zhang et al., 2005); <sup>b</sup>(Carrasquer et al., 2010); <sup>c</sup>(Tao and Abood, 1998); <sup>d</sup>(Tao et al., 1999); <sup>e</sup>(Alqarni et al., 2014); <sup>f</sup>(Feng and Song, 2003); <sup>g</sup>(Rhee et al., 2000); <sup>h</sup>(Zheng et al., 2013); <sup>i</sup>(Gouldson et al., 2000); <sup>j</sup>(Zhang et al., 2011); <sup>k</sup>(Nebane et al., 2006); <sup>l</sup>(Pei et al., 2008); <sup>m</sup>(Nebane et al., 2008); <sup>n</sup>(Mercier et al., 2010); <sup>o</sup>(Feng and Song, 2001)

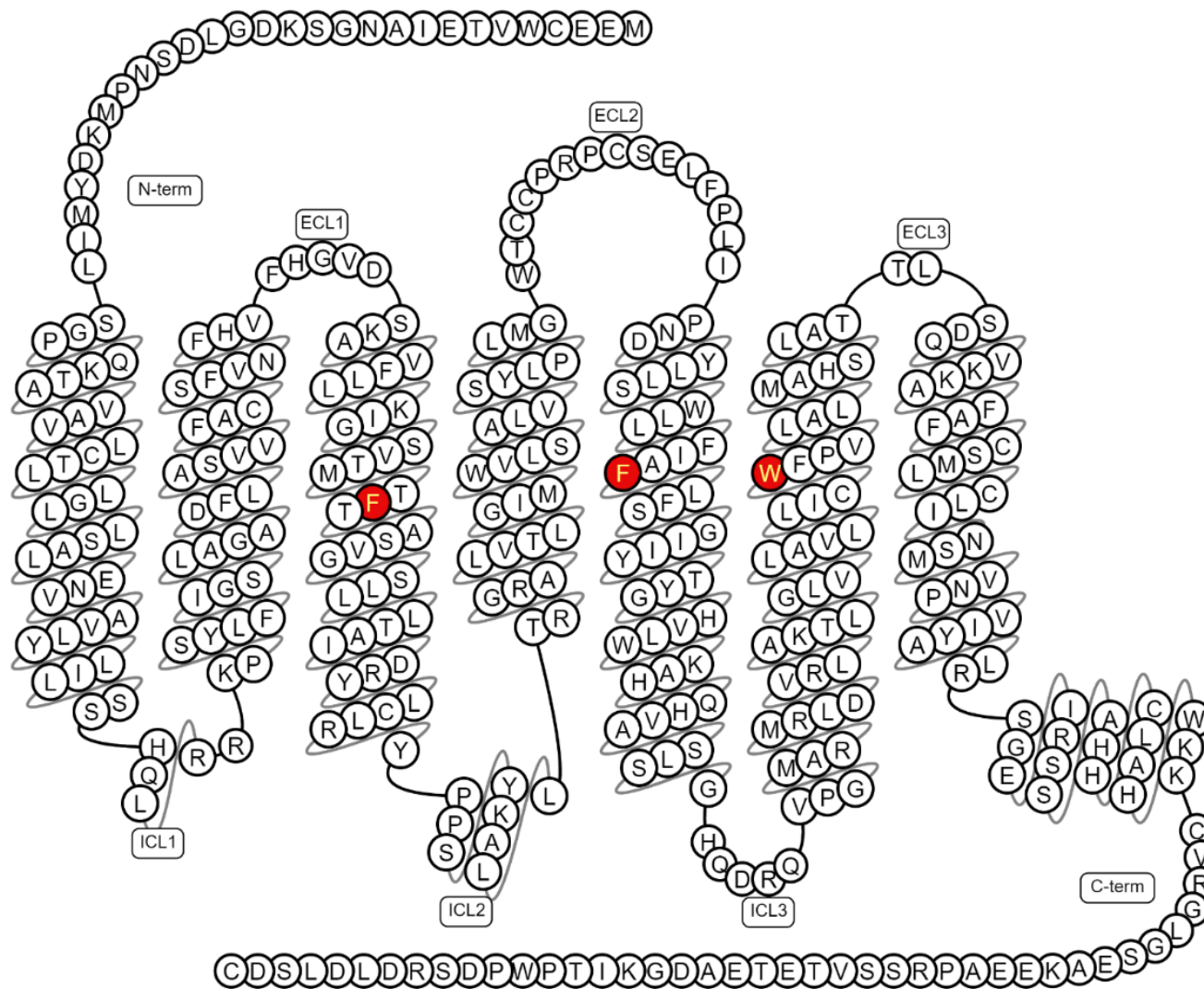
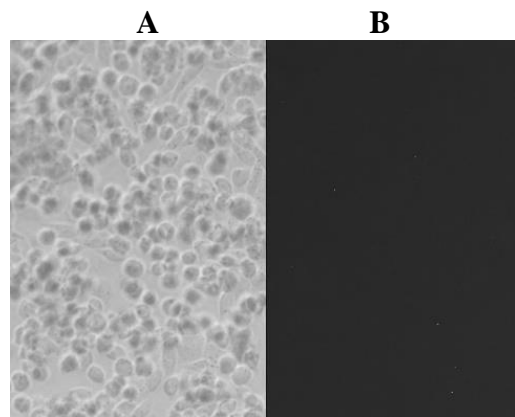


Figure 6.1 Two-dimensional snake plot diagram of the cannabinoid CB<sub>2</sub> receptor demonstrating the mutated amino acids Phe117, Phe200 and W258 respectively highlighted in red which were mutated to the corresponding alanine residues.

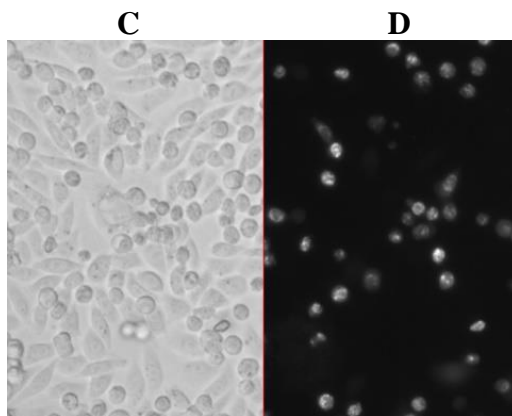
## 6.1 Results

In order to determine appropriate transfection ratios and latency to expression periods of the mutated CB<sub>2</sub> DNA plasmids F117A, F200A and W258A into their host cells, the CHO-K1 cells were first transfected using GFP and at 1:1 and 1:2 transfection ratios and monitored at 24 and 48 h (Figure 6.2).

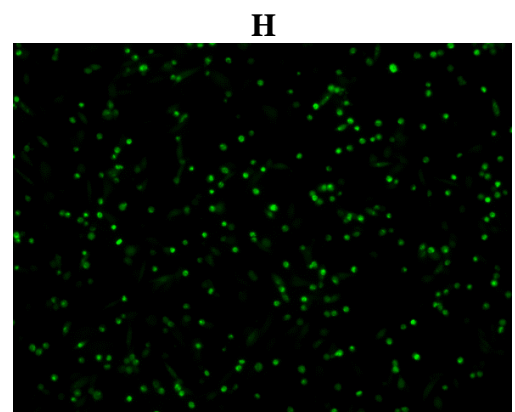
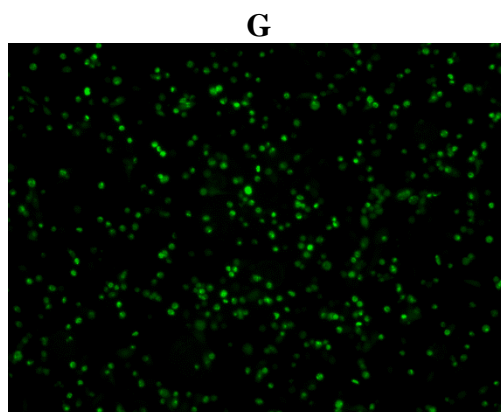
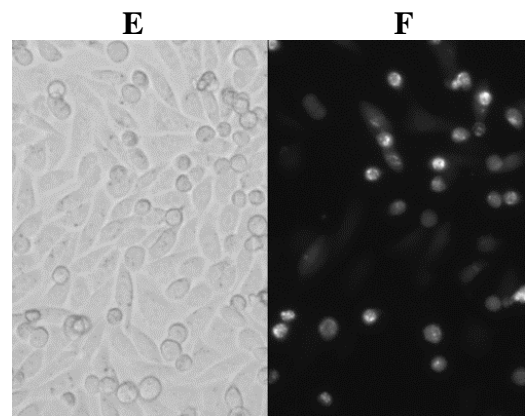
### CHO-K1 Only – No GFP transfection



### 1:1 GFP at 24 h



### 1:2 GFP at 24 h



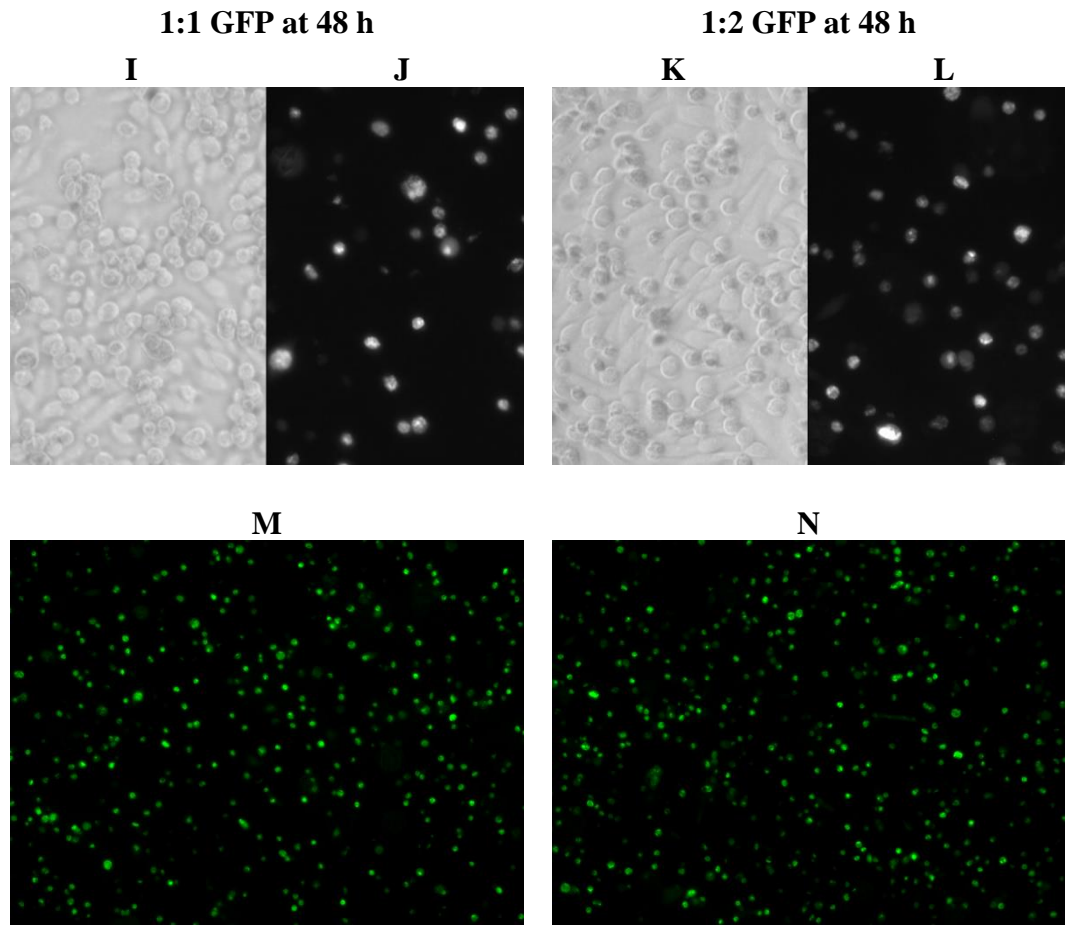


Figure 6.2 The transfection ratios and latency of GFP expression in CHO-K1. CHO-K1 cells were transfected with GFP plasmid using different transfection ratios of XtremeGene for 24 and 48 h. Data represent 24 and 48 h images viewed via the Zeiss Axiovert S100 fluorescent microscope: 20X repeated twice with the wavelength of GFP detected at 475 nm. Panels A, C, E, I, K were captured on light-field, panels B, D, F, J, L were captured on darkfield and panels G, H, M, N represent the fluorescence images.

There was no clear difference between 24 and 48 h timepoints post transfection, nor between 1:1 and 1:2 transfection ratios (Figure 6.2). Both ratios seemed to be quite effective, but no certainty could be concluded based on these images solely. Hence, an On-cell immunoassay was performed using CB<sub>2</sub> receptor polyclonal antibody CNR2 (ThermoFisher Scientific PA1744) at 1:500 final dilution in order to identify whether cell surface expression of the CB<sub>2</sub> receptor was affected by mutation of the three amino acid residues. The results obtained using the stable CHO-CB<sub>2</sub> cell line as the reference for comparison were inconsistent and hence an alternative technique, immunoblotting was employed.

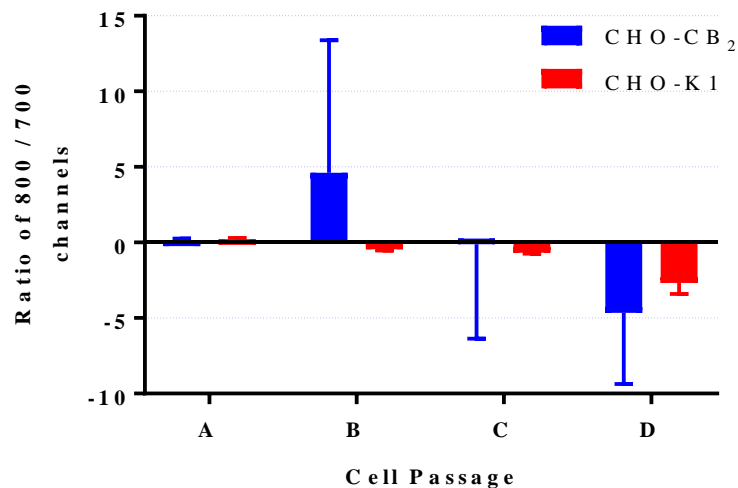


Figure 6.3 On-cell western performed using the CB<sub>2</sub> receptor polyclonal antibody CNR2 to detect cell surface expression of CB<sub>2</sub> receptors. This was repeated on four distinct passages of stable CHO-CB<sub>2</sub> and the negative control CHO-K1.

Cells were seeded in 6 well-plates for 24 h until they approached confluency and were then transfected using X-tremeGENE at different ratios with the DNA empty vector and the WT-CB<sub>2</sub> receptors for 48 h. The blot demonstrated non-specific binding without variation for use of the CB<sub>2</sub> receptor vector.

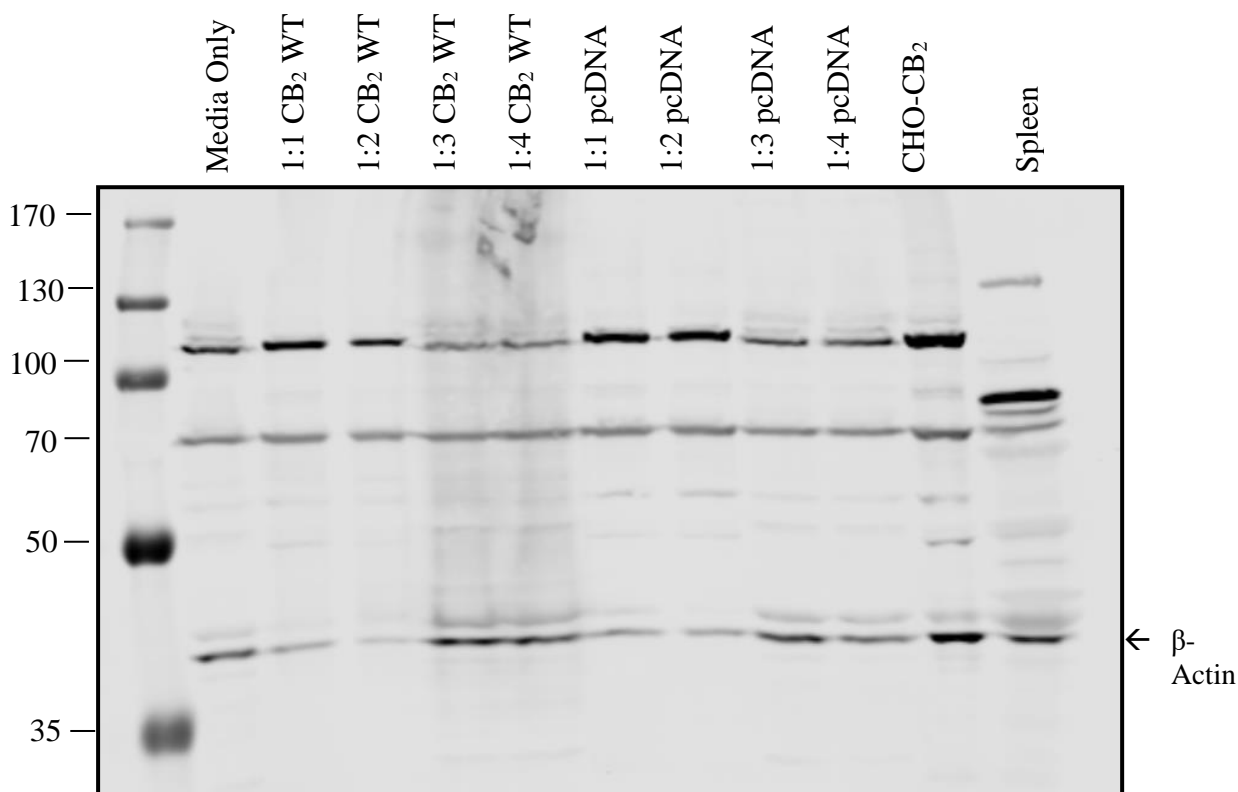


Figure 6.4 CHO-K1 cells were transfected using the transfection reagent X-tremeGENE at 1:1, 1:2, 1:3 and 1:4 ratios.

Rat spleen was used as a positive control and WT CB<sub>2</sub> receptor with the empty plasmid vector was used as the negative control. The primary antibody used in the blot was the polyclonal antibody CNR2.

HeLa cells were substituted for the CHO-K1 cell line as they had previously been optimised with X-tremeGENE at a 1:2 transfection ratio and 48 h in preliminary investigations. Cells were transfected with WT-CB<sub>2</sub>, the mutated CB<sub>2</sub> receptors F117A, F200A and W258A and pcDNA (negative control). The stable CHO-CB<sub>2</sub> and spleen were employed as positive controls. Non-specific binding was detected across all protein preparations, including the wells loaded with medium only, and the negative control of pcDNA. Since the polyclonal antibody CNR2 produced unexpected results in the On-cell western assay as well as in the immunoblotting of CHO-K1 and HeLa samples, a different CB<sub>2</sub> receptor antibody was subsequently investigated.

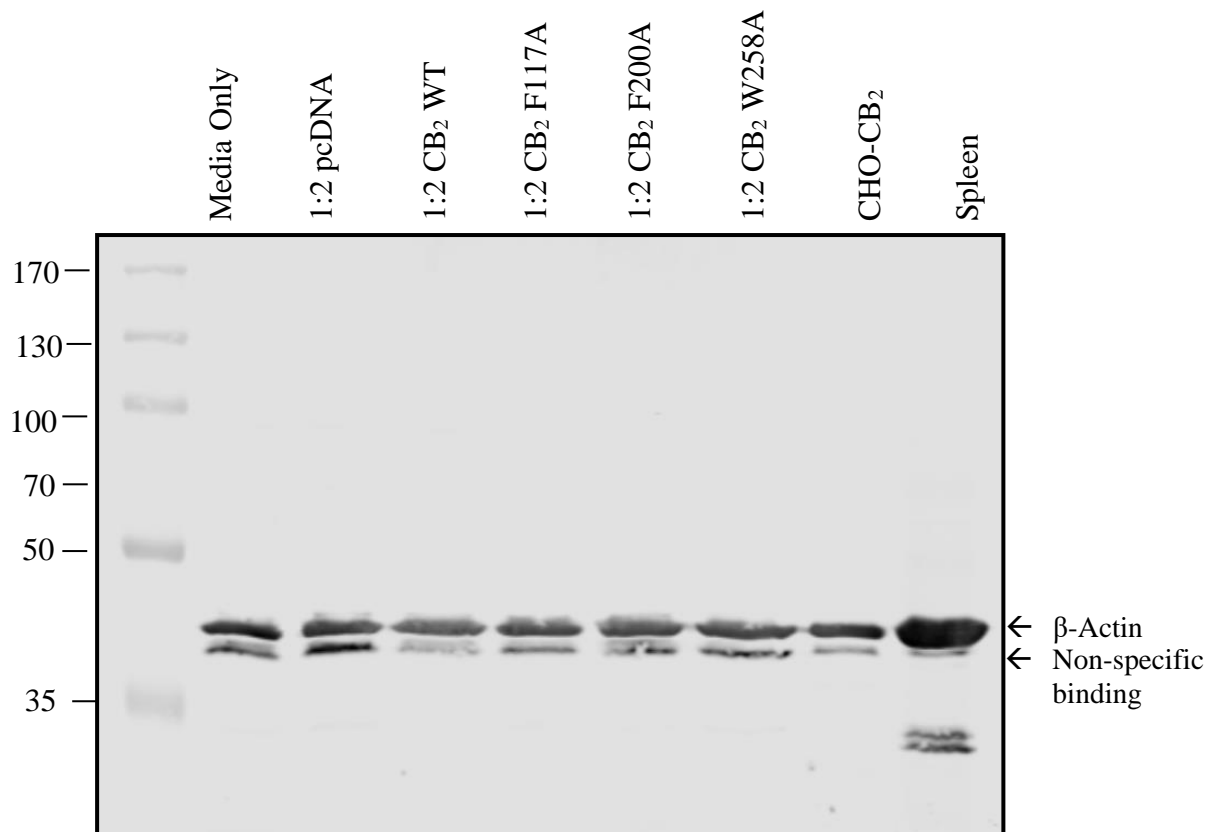


Figure 6.5 HeLa cells were transfected at 1:2 transfection ratio using WT-CB<sub>2</sub> receptor with the DNA vector as the negative control. The primary antibody used in the blot was the polyclonal antibody CNR2.

Cells were transfected with WT-CB<sub>2</sub>, the mutated CB<sub>2</sub> receptors F117A, F200A and W258A and pcDNA as before. The stable CHO-CB<sub>2</sub> and spleen were employed as the positive controls. All samples were processed in RIPA buffer and 50 µg protein samples were loaded into the respective wells with the CB<sub>2</sub> receptor monoclonal antibody (C37) used at 1:1000 final dilution. α-tubulin, the loading control, was detected at 50 kDa as expected; nevertheless, again, there was non-specific binding detected across all protein preparations, including the wells loaded with medium only, and the negative control of pcDNA.

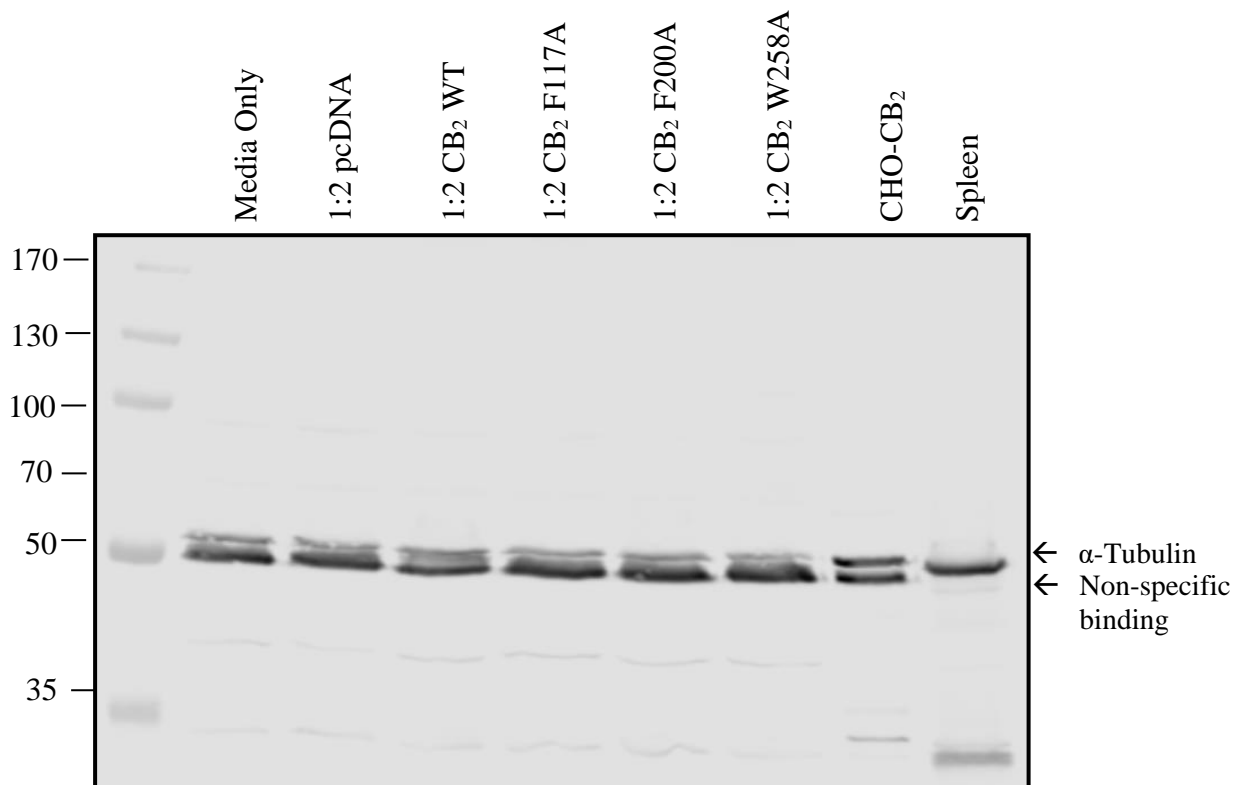


Figure 6.6 HeLa cells were transfected at 1:2 transfection ratio using WT-CB<sub>2</sub> receptor with the DNA vector as the negative control. The primary antibody used in the blot was the CB<sub>2</sub> receptor monoclonal antibody (C37).

Both CB<sub>2</sub> receptor antibodies; polyclonal CNR2 and monoclonal antibody CB<sub>2</sub> receptor antibody (C37) used in both cell lines, CHO-K1 and HeLa, apparently produced non-specific binding. This meant it was impossible to confirm cell surface expression of CB<sub>2</sub> receptors and whether or not this was affected by the mutations. It was therefore determined to attach a FLAG tag to the WT and mutated CB<sub>2</sub> receptors. The tagging of CB<sub>2</sub> receptors was performed by a colleague, Dr Raza Almomani, and in parallel, functionality of the mutated CB<sub>2</sub> receptors was investigated in ERK and cAMP pathways.

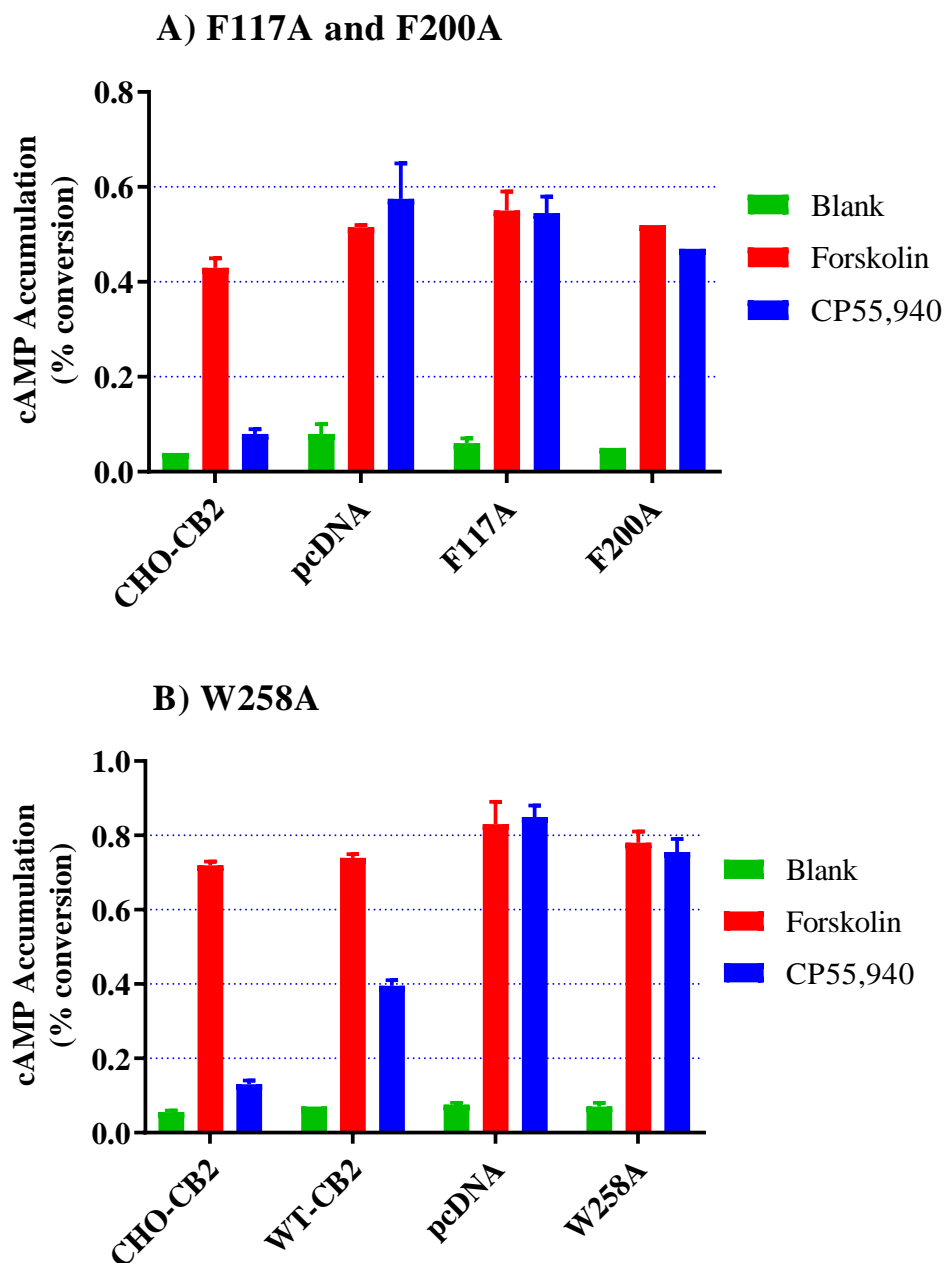


Figure 6.7 Forskolin induced cAMP accumulation in transiently transfected CHO-K1 cells.

Data are the mean  $\pm$  SEM of a single experiment performed in duplicate, expressed as % conversion of  $^3\text{H}$ -adenine nucleotides to  $^3\text{H}$ -cAMP. CHO-CB<sub>2</sub> cells were used as the positive control and CHO-K1 transfected with pcDNA was the negative control. The transiently transfected WT-CB<sub>2</sub> were also used alongside the mutants to confirm whether transient transfection had worked. The cells were seeded in a 24-well plate, transfected at 1:2 ratios using XtremeGENE and the assay was performed 48 h following the transient transfection. Inhibition of forskolin induced cAMP accumulation was investigated using 1  $\mu\text{M}$  CP55940.

The inhibition of cAMP accumulation via CP55940 was evident in the stably expressing CHO-CB<sub>2</sub> cells (Figure 6.7). An inhibitory effect of CP55940, although to a lower extent, was also observed in the transiently transfected CHO-K1 WT-CB<sub>2</sub> cells. All of the cells showed similar responses to forskolin. None of the mutated receptors (A) F117A, F200A or (B) W258A evoked a change in the accumulation of cAMP in the presence of CP55940, and their effects were similar to the negative control pcDNA. However, through this assay alone, it could not be confirmed whether the lack of effect in the cAMP pathway was attributed to the lack of function of the mutated receptors or whether the receptors were not expressed.

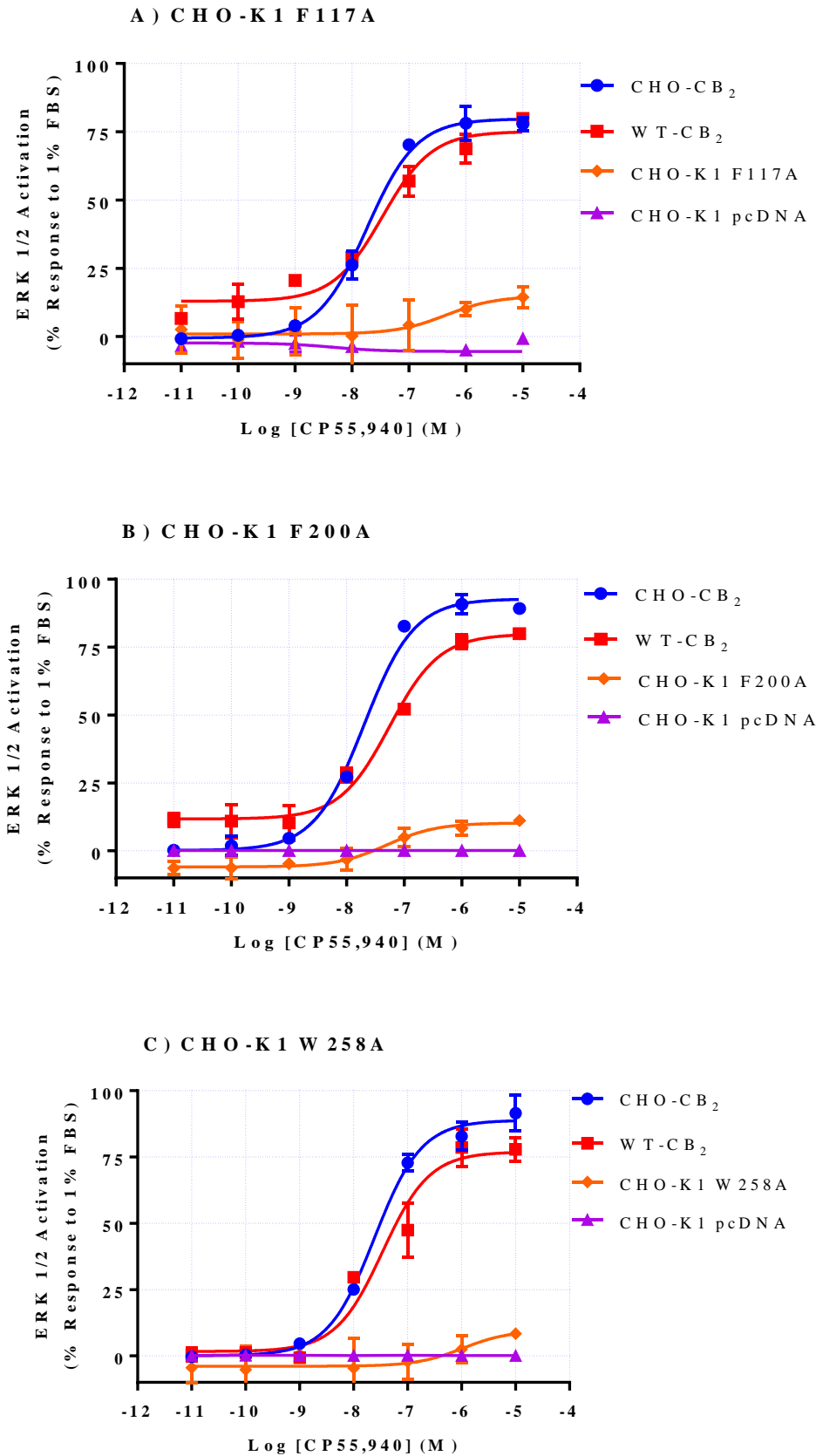


Figure 6.8 Activation of the ERK signalling pathway in transiently transfected CHO-K1 cells.

Data are the mean  $\pm$  SEM of a single experiment investigating the concentration dependence of CP55,940 measured at 5 min of ERK activation. The obtained curves were fitted via four parameter logistic equation. The cells were seeded in a 96-well plate, transfected at 1:2 ratios using X-tremeGENE and the assay was performed 48 h following the transient transfection.

The stable CHO-CB<sub>2</sub> cells were used as a positive control and CHO-K1 cells transfected with pcDNA were the negative control. The transiently transfected WT-CB<sub>2</sub> cells showed a concentration dependent ERK phosphorylation to CP55940 comparable to that of the stable CHO-CB<sub>2</sub> cells, thus, confirming that coupling of the receptor was taking place. The mutated receptors (A) F117A, (B) F200A and W258A failed to show an ERK phosphorylation in response to CP55940, and their effects were comparable to that of the negative control pcDNA.

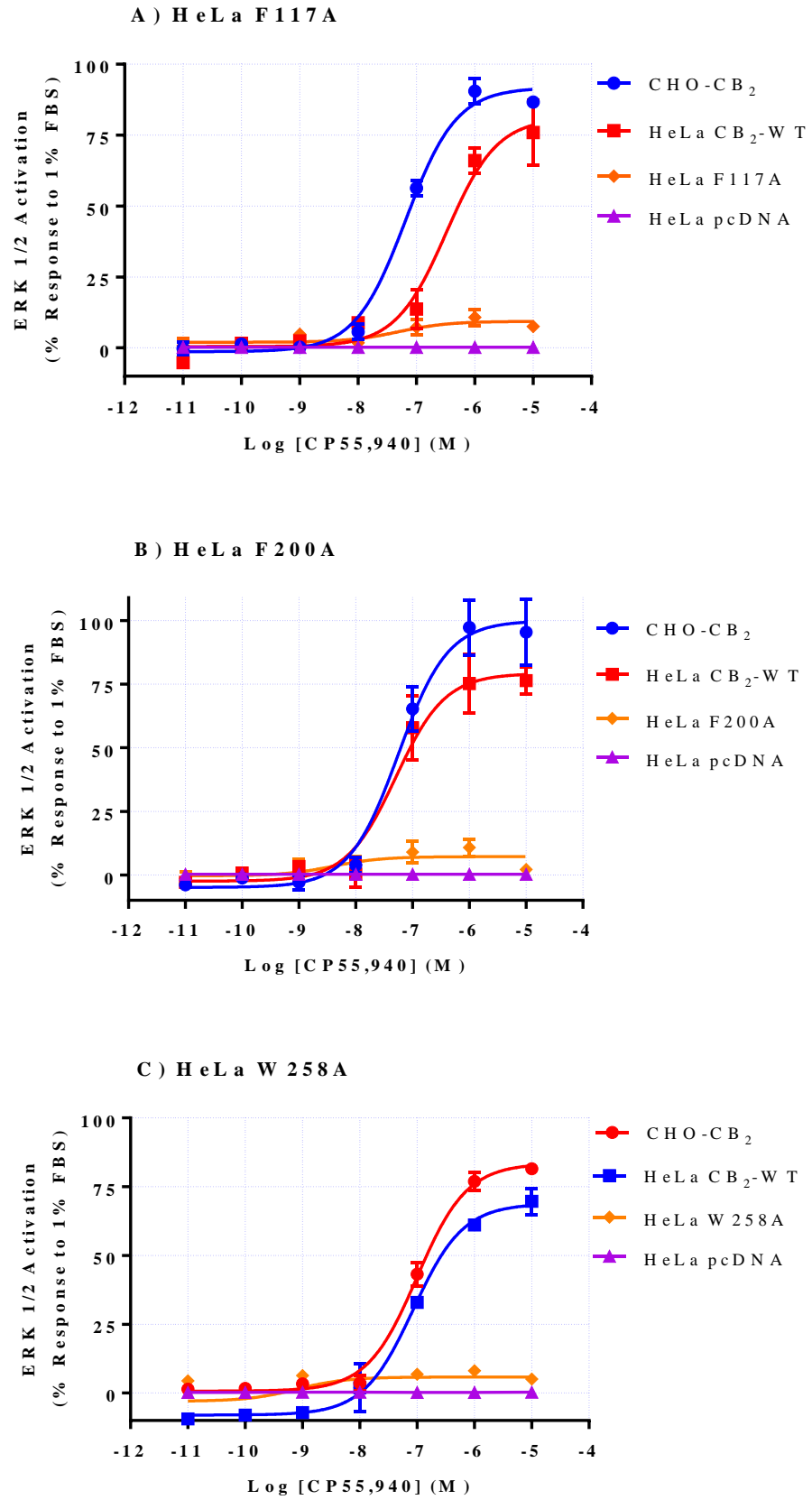


Figure 6.9 Activation of the ERK signalling pathway by CP55940 in transiently transfected HeLa cells, normalised to the response to 1% FBS.

Data are the mean  $\pm$  SEM of a single experiment; curves were fitted via four parameter logistic equation measured at 5 min of ERK activation. Similarly, the cells were seeded in a 96-well plate, transfected at 1:2 ratios using XtremeGENE and the assay was performed 48 h following the transient transfection.

The ERK phosphorylation was further confirmed via the transient transfection of HeLa cells. The stable CHO-CB<sub>2</sub> cells were used as positive controls and HeLa cells transfected with pcDNA as negative controls. The transiently transfected HeLa with WT-CB<sub>2</sub> displayed a concentration dependent ERK phosphorylation to CP55940 comparable to that of the stable CHO-CB<sub>2</sub> cells, also confirming that coupling of the receptor was taking place. Activation of the mutated receptors (A) F117A, (B) F200A and W258A did not evoke ERK phosphorylation; effects were comparable to that of the negative control pcDNA.

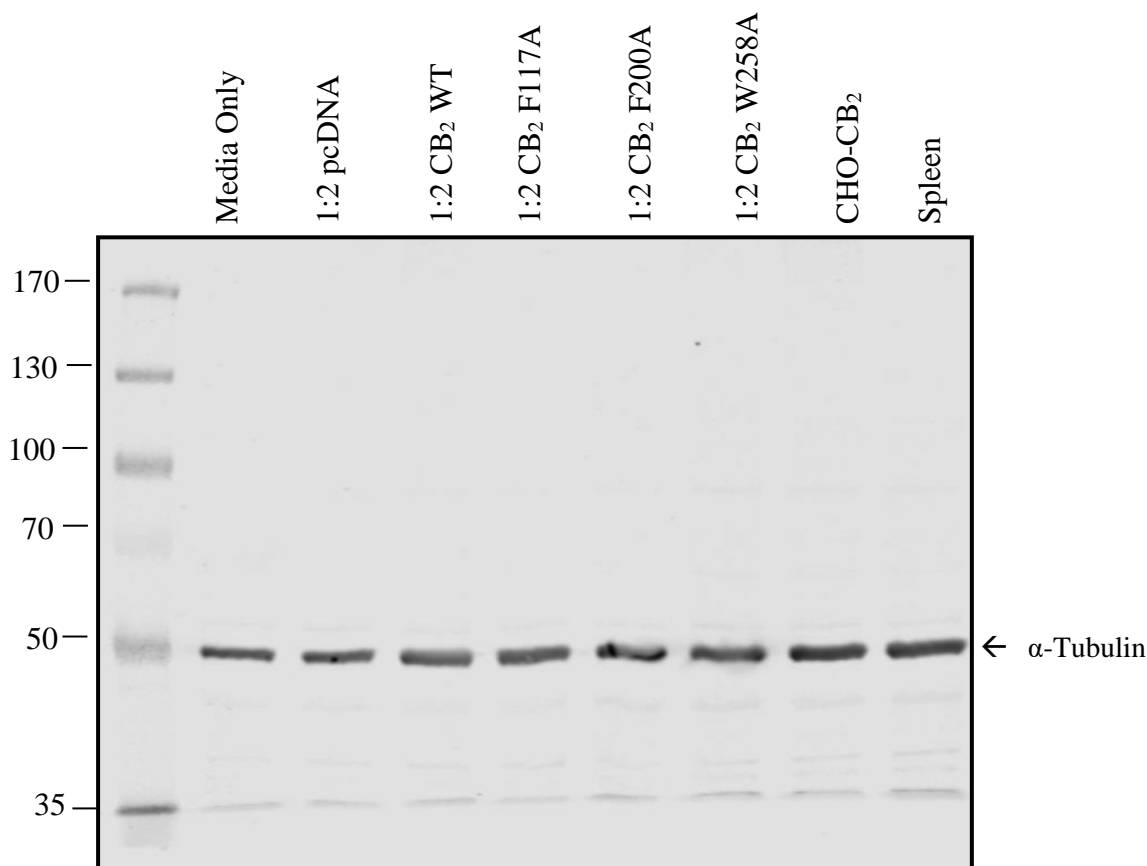


Figure 6.10 FLAG tagged CB<sub>2</sub> receptors were transfected in the HeLa cells at 1:2 ratio with X-tremeGENE.

The tagged WT-CB<sub>2</sub>, the mutated CB<sub>2</sub> receptors F117A, F200A and W258A were all transiently transfected in a 6 well-plate and harvested following 48 h of transfection. The stable CHO-CB<sub>2</sub> cells and rat spleen were employed as negative controls. All samples were processed in RIPA buffer and 50 µg protein samples were loaded onto SDS-PAGE gels for blotting with the monoclonal FLAG antibody (F3165) employed at 1:20,000 final dilution.  $\alpha$ -tubulin as a loading control was detected at 50 kDa; nevertheless, there were no bands for the FLAG-antibody of the CB<sub>2</sub> receptors expected to appear at 38 kDa.

## 6.2 Discussion

This project was further broadened to investigate the impact of potential molecular switches involved in CB<sub>2</sub> receptor responsible for altering the function of compounds from an agonist to antagonist by modification of the attached substituent. The predominant aim of this site-directed mutagenesis study was to elucidate individual residue contributions of the cannabinoid CB<sub>2</sub> receptor towards the receptor's functional outcomes. The prominence of mutagenesis research is to demonstrate essential molecular components of the cannabinoid pharmacophore which could assist in rational drug design of selective cannabinoid CB<sub>2</sub> receptor drugs with enhanced therapeutic potential and diminished side-effects. An enabling objective was to determine the appropriate transfection ratios and time-points to be employed for subsequent investigations. It was also crucial to determine whether the cell surface expression (detected by antibodies) of cannabinoid CB<sub>2</sub> receptors was altered as a result of the mutation. Based on transfection of the native CHO-K1 cells with GFP, there was no real difference between 24 and 48 h, nor 1:1 and 1:2 transfection ratios. Both ratios and both time points were apparently competent, but no certainty could be concluded based solely on microscopic images of GFP. Immunoassays were performed to confirm appropriate transfection ratio/s and time point/s and to ensure that the expression of the cannabinoid CB<sub>2</sub> receptor was not altered as a result of the mutation. Subsequent to the running of blots using both CB<sub>2</sub> receptor antibodies; polyclonal CNR2 (PA1-744) and CB<sub>2</sub> receptor monoclonal antibody (C37) used in both cell lines CHO-K1 and HeLa apparently produced non-specific binding without clear identification of CB<sub>2</sub> receptors. Moreover, the FLAG-tagged mutated and wild type CB<sub>2</sub> receptors did not generate bands at the predicted molecular size.

Concurrent functional assays of ERK-phosphorylation and forskolin-induced cAMP accumulation were performed on the transiently-transfected F117A, F200A and W258A mutated receptors with the transiently-transfected WT-CB<sub>2</sub> receptors and the stable CHO-CB<sub>2</sub> cells as positive controls and CHO-K1 or HeLa cells transfected with pcDNA as the negative control. As evident in (Figure 6.7), CP55940 was capable of inhibiting forskolin-induced

accumulation of cAMP in cells stably expressing CB<sub>2</sub> receptors confirming the validity of the performed experiments. The control cells transiently transfected with WT-CB<sub>2</sub> receptors for 48 h also produced 50% reduction in forskolin-induced accumulation of cAMP via CP55940. Cellular integrity and functionality were confirmed by the presence of a relatively consistent response to forskolin. On the contrary, all of the mutated receptors (F117A, F200A and W258A) when stimulated with CP55940 failed to exhibit an inhibition of forskolin-induced accumulation of cAMP and their effects were similar to the negative control pcDNA.

In the ERK phosphorylation assay, the transiently transfected WT-CB<sub>2</sub> evoked a concentration-dependent response to CP55940 comparable to that of the stable CHO-CB<sub>2</sub> cell line. Thus, confirming the occurrence of coupling of the receptor and the validity of the performed experiments. In the case of the mutated receptors F117A, F200A and W258A, CP55940 failed to evoke ERK phosphorylation at all concentrations. The effects of CP55940 in these cells were comparable to that of the negative control pcDNA. Preliminary experiments suggested that mutating F117, F200 and W258 to the corresponding alanine residues led to complete loss of functional activity of the cannabinoid CB<sub>2</sub> receptor, at least in the investigated signalling pathways.

A major caveat, of course, is that there was an absence of data to confirm whether the transfections of the mutated receptors were effective. This could be confirmed if an optimized CB<sub>2</sub> receptor antibody is found for immunoblotting/immunocytochemistry to confirm that the deficiency of the CB<sub>2</sub> receptor functional activity was a result of the site-directed mutagenesis and not to a loss of the receptor expression as a result of the mutation.

### 6.3 Conclusion

Mutations of F117A, F200A and W258A of the CB<sub>2</sub> receptor lead to a loss of functional activity, which could be attributed to two major factors, either that these amino acids are individually vital for appropriate receptor function or that the receptor is not expressed subsequent to the mutation process. Future investigations could aim to utilise alternative approaches of transfection/infection of the mutated receptor to gain more confidence that the receptor is genuinely expressed. Moreover, mutating an amino acid that is not involved in the receptor signalling or ligand binding could be used (e.g. Trp-6 in the N-terminus) as a positive point of comparison that site-directed mutagenesis was effective, and that the receptor is still functional subsequent to this mutation.

## Chapter 7 : General Discussion and Future Implications

This study aimed to investigate two core aspects in the field of cannabinoid research, metabolism through the endocannabinoid-hydrolysing enzyme ABHD6 and functional signalling through the cannabinoid CB<sub>2</sub> receptor.

Investigations of the endocannabinoid hydrolase enzymes including ABHD6 is anticipated to be a viable therapeutic target through influencing levels of the endocannabinoids. Fine-tuning of the endocannabinoid system has evolved as a novel potential therapeutic for the management of neurodegenerative diseases, including multiple sclerosis, amyotrophic lateral sclerosis, Alzheimer's disease, HIV-associated dementia, Parkinson's disease, and other neuroinflammatory diseases (Centonze et al., 2007). Selective inhibition of ABHD6 in animal models of traumatic brain injury and epileptic seizures was found to induce neuroprotective outcomes (Wen et al., 2015). The initial part of this thesis aimed to optimize a feasible, cost-effective screening methodology for novel ABHD6 inhibitors. The HTS assay optimised in this thesis was apparently promising when used in the recombinant ABHD6 expression, which would be scalable for HTS. As part of the characterization of the enzyme, it was apparent that it was capable of hydrolysing multiple endogenous lipids, albeit with low affinity, suggesting that the 'natural' substrate/s for the enzyme await confirmation. Assessment of this assay in real tissue including rat intestine and hippocampus generated data that was challenging to interpret and imply that further refinement is needed for application to native tissues.

Research over the last decade has established that selective inhibition of ABHD6 guarded against neuroinflammation and neurodegeneration of mouse animal models of multiple sclerosis via stimulation of the cannabinoid CB<sub>2</sub> receptor (Marrs et al., 2010; Wen et al., 2015). Moreover, prompt combination of both neuroprotective effects via ABHD6 inhibition (Wen et al., 2015) and anti-inflammatory approaches via stimulation of the cannabinoid CB<sub>2</sub> receptors (Yang et al., 2015) was apparently beneficial in the

management of the above mentioned disorders. Administration of the reportedly-selective ABHD6 inhibitor WWL70 (Marrs et al., 2010) to animal models of multiple sclerosis augmented 2AG levels in microglia and macrophages subsequent to the inhibition of ABHD6 generated anti-inflammatory outcomes via stimulation of cannabinoid CB<sub>2</sub> receptors (Wen et al., 2015). These findings could therefore be applied in the management of multiple sclerosis in addition to other neurodegenerative diseases. These findings also complement the prominence of the aims of this thesis, where it was aimed to optimize a screening assay for novel ABHD6 inhibitors while simultaneously gaining an enhanced understanding of the function of cannabinoid CB<sub>2</sub> receptors through exploring different signalling pathways.

The endocannabinoid system as an entity has gained therapeutic attention for the management of several disorders, with more focus being shed on the exploitation of the cannabinoid CB<sub>1</sub> and CB<sub>2</sub> receptors as potentially promising therapeutic targets. In particular, selective CB<sub>2</sub> receptor agonists have been suggested to possess favourable effects in diminishing the inflammatory impacts involved in neuroinflammatory diseases including Alzheimer's, Parkinson's and Huntington diseases (Fagan and Campbell, 2014). Clinically, selective blockade of the cannabinoid CB<sub>1</sub> receptor using rimonabant was reported to ameliorate waist circumference, decrease body weight and enhance cardiac function (Van Gaal et al., 2005). Despite being approved in Europe in 2006, for the management of obesity and metabolic syndrome, rimonabant was withdrawn from the market in 2008 following reports of depression and suicidal thoughts (Alexander, 2016). Given the recent identification of fenofibrate as a potent agonist at the CB<sub>2</sub> receptor and a partial agonist/antagonist at CB<sub>1</sub> receptors (Priestley et al., 2015), the fenofibrate structure could potentially serve as a promising building molecule in rational drug design for producing a compound that activates the CB<sub>2</sub> receptor while concurrently blocking the CB<sub>1</sub> receptor. A fenofibrate derivative which could be applied clinically, could allow the management of neuroinflammatory diseases through activation of the CB<sub>2</sub> receptors, managing obesity via blockade of the CB<sub>1</sub> receptor in addition to the management of dyslipidaemia via activation of the PPAR $\alpha$  receptors (Berger and Moller, 2002). The novel investigated fenofibrate derivatives FD24, FD43,

FD44 and FD46 were investigated at the level of CB<sub>2</sub> receptor function. Based on the results presented in this thesis, the fenofibrate derivative FD24 had a consistent function in all of the signalling pathways investigated. FD24 functioned as a potent agonist in the calcium mobilization assay, ERK phosphorylation, forskolin-induced cAMP inhibition and fluorescent binding assay with potencies of 6.5, 8.0, 7.9 and 6.8, respectively.

In future studies, the novel fenofibrate FD24 could be investigated through the different signalling pathways of the cannabinoid CB<sub>1</sub> receptor. This is essential since CB<sub>1</sub> receptor-agonists evoke psychotropic effects associated with the activation of these receptors. Activation of the CB<sub>2</sub> receptor on the contrary, do not appear to produce these psychotropic effects (Deng et al., 2015) and thus could provide a promising compound for treating the proposed medical disorders. Moreover, it would be important to explore the molecular effects of FD24 on the PPAR $\alpha$  receptors. It is also possible that *in vivo* amidase activity would generate fenofibric acid analogue which influences PPAR $\alpha$  activity. If the compound produced the anticipated positive outcomes on both CB<sub>1</sub> receptors and PPAR $\alpha$  receptors, it (or further analogues derived from these structures) could have clinical potential for managing obesity, dyslipidaemia and neuroinflammation.

The commercially available ligands SER601 and COR170, chosen to replicate the fenofibrate series in the transition from agonist to inverse agonist, produced data that was contradictory to the literature. Subsequent to their investigation in the different signalling pathways, SER601 appeared biased towards ERK pathway activation, while producing no other effects in the other pathways. It is established that receptor stimulation is both ligand and tissue specific as the selection and occurrence of intracellular cell signalling differs among the cell types. The theory of “biased cell signalling” also referred to as “stimulus trafficking”, “functional selectivity” or “agonist bias” states that distinct compounds functioning at the same GPCR, in consistent tissue environment could lead to substantially different cellular responses (Ibsen et al., 2017). These compounds are reported to stabilise different CB<sub>2</sub> receptor conformations which subsequently stimulates or inhibits different subsets of signal transduction pathways at distinct efficacies and potencies (Kenakin, 2011)

which would influence the future use of pharmacological procedures in rational and novel drug design and development.

From the therapeutic aspect, it is anticipated that biased cell signalling of GPCRs could potentially target only a desired pathway while circumventing the possibility of side-effects by not inducing an effect on the pathway not involved in the therapeutic target (Ibsen et al., 2017). Hence, functional selectivity is evolving as a novel alternative for enhanced CB<sub>2</sub> receptor specific therapies offering selective, efficacious and safe drugs.

Nonetheless, there is currently limited research and a small number of published data concerning the application and use of CB<sub>2</sub> receptor biased agonists (Morales et al., 2018). The G protein-biased CB<sub>2</sub> receptor agonist LY2828360 manifested promising data *in vivo* in a model of chemotherapy-evoked neuropathic pain, therefore, providing optimism in the exploitation of the functional selectivity of the cannabinoid CB<sub>2</sub> receptor in the development of therapeutically safe and efficacious drugs (Lin et al., 2018). Nevertheless, the compound was ineffective in a Phase II clinical trial of osteoarthritis. Although this is only the initial stages of an investigation, since SER601 markedly stimulated only the ERK-phosphorylation pathway, this compound might become a potential therapeutic compound in an ERK-specific manner. AEA-mediated activation of the CB<sub>2</sub> receptor resulting in ERK1/2 activation lead to the management of neuroinflammatory ailments encompassing multiple sclerosis (Correa et al., 2010). Moreover, selective stimulation of the ERK1/2 pathway via JWH-015 was found to modulate chemotaxis and potentially impose therapeutic potential in chronic inflammatory diseases including atherosclerosis and rheumatoid arthritis (Montecucco et al., 2008). Selective activation of the ERK1/2 pathway via JWH-015 also induced significant reduction in TNF $\alpha$  expression (Romero-Sandoval et al., 2009), reduced reactive oxygen species (Ribeiro et al., 2013) producing anti-inflammatory effects. Therefore, since selective modulation of the ERK1/2 pathway was involved in promising therapeutic potential and following future *in vivo* studies and further characterisation of SER601, this compound could potentially advance into clinical trials.

The investigations comprising site-directed mutagenesis of F117A, F200A and W258A appeared promising in identifying amino acids prominent in the signal transduction of the cannabinoid CB<sub>2</sub> receptor. Functional study of the mutated CB<sub>2</sub> receptor in ERK phosphorylation and forskolin-induced cAMP accumulation, revealed that mutation of any of the three amino acids abolished the functional activity of the CB<sub>2</sub> receptor. The study was limited by the lack of specific bands obtained in immunoblotting using the polyclonal CNR2 (PA1-744) and monoclonal CB<sub>2</sub> (C37) antibodies. HeLa and CHO-K1 cell lines were explored as host cells and the transfection reagent used in preliminary studies were effective in the transfection of different types of receptors. The only variant was the CB<sub>2</sub> receptor antibody, hence more than one type of antibody was employed and both antibodies induced non-specific binding. Antibodies targeting the cannabinoid CB<sub>2</sub> receptor have been consistently disputable, such that antibodies that appeared promising in robust positive controls still failed the specificity tests using negative controls (Marchalant et al., 2014), justifying why the CB<sub>2</sub> receptor had always been referred to as a receptor with an “identity crisis” (Atwood and Mackie, 2010).

This was clearly observed in this study, where non-specific bands were observed in the negative controls. At present, none of the commercially available CB<sub>2</sub> receptor antibodies have been verified versus satisfactory negative controls. When employing any of the CB<sub>2</sub> receptor antibodies in particular the polyclonal antibodies, additional caution must be practiced since it was reported that their specificities fluctuated between the different batches (Baek et al., 2013). In this research, two distinct batches of the polyclonal CNR2 antibody (PA1-744) were used and both demonstrated non-specific bands with the negative controls and a single batch of the monoclonal CB<sub>2</sub> antibody (C37) was used. In future experiments, additional batches of these antibodies might be tested in addition to testing the No. 101550 polyclonal CB<sub>2</sub> receptor antibody from Cayman Chemicals grown in rabbit amino acids 20-33 of the human CB<sub>2</sub> receptor N-terminus (Marchalant et al., 2014) which was reported to be effective.

The FLAG-tagged mutated and wild type CB<sub>2</sub> receptors did not generate bands where anticipated. Future studies aiming to confirm that the CB<sub>2</sub> receptor expression was not altered secondary to the site-directed mutagenesis

could aim to employ a positive control used in preceding research and identified to produce appropriate bands with the FLAG tag or potentially employ alternative tags on the CB<sub>2</sub> receptors. Prospective experiments could also attempt to use a different lysis buffer such as TRIS-EDTA as an alternative to RIPA as RIPA buffer might be too harsh when used in the lysis of the cannabinoid CB<sub>2</sub> receptor membrane homogenates.

## 7.1 Conclusion

This thesis aimed to increase the understanding of the cannabinoid CB<sub>2</sub> receptor and its potential in becoming an important therapeutic target in the management of multiple pathological conditions. Selective modulation of the CB<sub>2</sub> receptor could have therapeutic potential in the management of fibrotic, inflammatory, neuropathic pain and neurodegenerative diseases (Contino et al., 2017) without inducing the psychoactive effects of the CB<sub>1</sub> receptor. Reports of the human CB<sub>2</sub> receptor crystal structure bound to the antagonist AM10257 (Li et al., 2019) and the agonist WIN 55,212-2 (Xing et al., 2020) should increase the success of rational drug design for the CB<sub>2</sub> receptor.

We have identified a novel fenofibrate derivative FD24, which following further characterization, could provide a valuable therapeutic tool in the management of inflammatory diseases, obesity and dyslipidaemia. We have also identified an ERK1/2 phosphorylation-biased agonist, SER601. Despite being in the early stages of investigation, further characterisation of this compound might provide a promising therapeutic target at CB<sub>2</sub> receptors with diminished side-effects. CB<sub>2</sub> receptor therapeutic potential could be enhanced following appreciation of agonist bias and CB<sub>1</sub>/CB<sub>2</sub> receptor selectivity to optimise ligands as anti-inflammatory and/or analgesic compounds while simultaneously decreasing side-effects (Morales et al., 2018). The complexity and the specificity of the CB<sub>2</sub> receptors' signal transduction offer opportunities for the development of novel therapeutic ligands with a certain degree of bias, resulting in enhanced medicinal consequences.

Even though CB<sub>2</sub> receptor agonists demonstrated promising effects in diverse preclinical models, they have not successfully advanced to the clinical level. The rationale behind this disappointing circumstance could be attributed to the lack of correspondence between preclinical and clinical outcomes due to functional selectivity of CB<sub>2</sub> receptors agonists (Dhopeswarkar and Mackie, 2014). Given the advances in genetic, pharmacological and biochemical tools and with the advanced on-going research in understanding the CB<sub>2</sub> receptor agonists' functional selectivity, CB<sub>2</sub> receptors are increasingly promising drug targets. Despite their major therapeutic

potential, further studies and investigations are required to gain an enhanced understanding of the regulation of the CB<sub>2</sub> receptors, the physiological functions they mediate and possible clinical applications. Nonetheless, there is a need for further research to be performed to recognise cell specific CB<sub>2</sub> receptor signalling mechanisms and receptor regulation.

## 7.2 Future Implications

Future investigations could aim to assess the CB<sub>2</sub>/CB<sub>1</sub> receptor selectivity of the novel CB<sub>2</sub> receptor agonist FD24, in addition to its investigation in the PPAR $\alpha$  cell line. If proved effective *in vitro*, the compound could progress to *in vivo* investigations followed by human clinical trials with the aim of managing obesity, dyslipidaemia and neuroinflammatory diseases. Investigations involving biased agonism at the CB<sub>2</sub> receptor are imperative to identify the specific molecular pathways involved in the pharmacological effects and signalling pathways of CB<sub>2</sub> receptor ligands. Thus, biased agonism is evolving as an innovative approach for enhanced CB<sub>2</sub> receptor specific therapies while circumventing undesired side effects. Although this is only at the initial stages of an investigation, since SER601 was an ERK-phosphorylation biased agonist, the compound could be used to assess its impact on inflammatory modulators which could progress to human clinical trials following safety testing. Nevertheless, before further advancement of any investigations of SER601, it would be an essential step to primarily quantify the compound's bias. SER601 only activated one of the investigated pathways and hence, it was not possible to quantify bias. Future investigations could aim to quantify bias, by initially testing the compounds in pathways beyond the ones investigated in this thesis including  $\beta$ -arrestin and GIRK pathways. Moreover, it is also imperative to use a standard reference compound in order to appropriately perform an operational analysis model and quantify agonist bias induced by SER601.

Mutations of F117A, F200A and W258A of the CB<sub>2</sub> receptor led to complete loss of functional activity through ERK phosphorylation and cAMP accumulation. It was not possible to confirm expression of the mutant receptors through immuno- and/or molecular tagging techniques. Thus, future

investigations could aim to utilise alternative approaches of transfection of the mutated receptor to gain more confidence that the receptor was genuinely expressed in addition to employing an alternative tag of the cannabinoid CB<sub>2</sub> receptor. Furthermore, mutating an amino acid that is not implicated in the receptor signalling or ligand binding (e.g. Trp-6 in the N-terminus) could be used as a positive point of comparison that site-directed mutagenesis was effective, and that the receptor is still functional subsequent to this mutation.

## Chapter 8 : References

- Aaltonen N, Savinainen JR, Ribas CR, Ronkko J, Kuusisto A, Korhonen J, Navia-Paldanius D, Hayrinen J, Takabe P, Kasnanen H, Pantsar T, Laitinen T, Lehtonen M, Pasonen-Seppanen S, Poso A, Nevalainen T and Laitinen JT (2013) Piperazine and piperidine triazole ureas as ultrapotent and highly selective inhibitors of monoacylglycerol lipase. *Chem Biol* **20**:379-390.
- Agudo J, Martin M, Roca C, Molas M, Bura AS, Zimmer A, Bosch F and Maldonado R (2010) Deficiency of CB2 Cannabinoid Receptor in Mice Improves Insulin Sensitivity but Increases Food Intake and Obesity With Age. *Diabetologia* **53**:2629-2640.
- Ahn K, Johnson DS and Cravatt BF (2009) Fatty acid amide hydrolase as a potential therapeutic target for the treatment of pain and CNS disorders. *Expert Opin Drug Discov* **4**:763-784.
- Alexander SPH (2012) So what do we call GPR18 now? *Br J Pharmacol* **165**:2411-2413.
- Alexander SPH (2016) Therapeutic potential of cannabis-related drugs. *Prog Neuropsychopharmacol Biol Psychiatry* **64**:157-166.
- Alharthi N, Christensen P, Hourani W, Ortori C, Barrett DA, Bennett AJ, Chapman V and Alexander SPH (2018) n-3 polyunsaturated N-acylethanolamines are CB2 cannabinoid receptor-preferring endocannabinoids. *Biochim Biophys Acta Mol Cell Biol Lipids* **1863**:1433-1440.
- Alqarni M, Myint KZ, Tong Q, Yang P, Bartlow P, Wang L, Feng R and Xie XQ (2014) Examining the critical roles of human CB2 receptor residues Valine 3.32 (113) and Leucine 5.41 (192) in ligand recognition and downstream signaling activities. *Biochem Biophys Res Commun* **452**:334-339.
- Andre CM, Hausman JF and Guerriero G (2016) Cannabis sativa: The Plant of the Thousand and One Molecules. *Front Plant Sci* **7**:19.
- Andresen B (2011) A Pharmacological Primer of Biased Agonism. *Endocr Metab Immune Disord Drug Targets* **11**:92-98.
- Arevalo-Martin A, Vela JM, Molina-Holgado E, Borrell J and Guaza C (2003) Therapeutic Action of Cannabinoids in a Murine Model of Multiple Sclerosis. *J Neurosci* **23**:2511-2516.

- Ashton HC (2001) Pharmacology and effects of cannabis: a brief review. *British Journal of Psychiatry* **178**:101-106.
- Ashton JC, Rahman RM, Nair SM, Sutherland BA, Glass M and Appleton I (2007) Cerebral hypoxia-ischemia and middle cerebral artery occlusion induce expression of the cannabinoid CB2 receptor in the brain. *Neurosci Lett* **412**:114-117.
- Aso E and Ferrer I (2016) CB2 Cannabinoid Receptor As Potential Target against Alzheimer's Disease. *Front Neurosci* **10**:243.
- Atwood BK and Mackie K (2010) CB2: a cannabinoid receptor with an identity crisis. *Br J Pharmacol* **160**:467-479.
- Atwood BK, Wager-Miller J, Haskins C, Straiker A and Mackie K (2012) Functional selectivity in CB(2) cannabinoid receptor signaling and regulation: implications for the therapeutic potential of CB(2) ligands. *Mol Pharmacol* **81**:250-263.
- Bachovchin DA, Ji T, Li W, Simon GM, Blankman JL, Adibekian A, Hoover H, Niessen S and Cravatt BF (2010) Superfamily-wide portrait of serine hydrolase inhibition achieved by library-versus-library screening. *Proc Natl Acad Sci U S A* **107**:20941-20946.
- Backes J, Gibson C, Ruisinger J and Moriarty P (2007) Fibrates: what have we learned in the past 40 years? *Pharmacotherapy* **27**:412-424.
- Baek JH, Darlington CL, Smith PF and Ashton JC (2013) Antibody testing for brain immunohistochemistry: brain immunolabeling for the cannabinoid CB(2) receptor. *J Neurosci Methods* **216**:87-95.
- Baggelaar MP, Maccarrone M and van der Stelt M (2018) 2-Arachidonoylglycerol: A signaling lipid with manifold actions in the brain. *Prog Lipid Res* **71**:1-17.
- Basu S and Dittel BN (2011) Unraveling the complexities of cannabinoid receptor 2 (CB2) immune regulation in health and disease. *Immunol Res* **51**:26-38.
- Battista N, Di Tommaso M, Bari M and Maccarrone M (2012a) The endocannabinoid system: an overview. *Front Behav Neurosci* **6**:9.
- Battista N, Meccariello R, Cobellis G, Fasano S, Di Tommaso M, Pirazzi V, Konje JC, Pierantoni R and Maccarrone M (2012b) The role of

endocannabinoids in gonadal function and fertility along the evolutionary axis. *Mol Cell Endocrinol* **355**:1-14.

- Baur R, Gertsch J and Sigel E (2012) The cannabinoid CB1 receptor antagonists rimonabant (SR141716) and AM251 directly potentiate GABA(A) receptors. *Br J Pharmacol* **165**:2479-2484.
- Belcheva M and Coscia C (2002) Diversity of G Protein-Coupled Receptor Signaling Pathways to ERK/MAP Kinase. *Neurosignals* **11**:34-44.
- Berger J and Moller D (2002) The mechanisms of action of PPARs. *Annu Rev Med* **53**:409-435.
- Bisogno T, Howell F, Williams G, Minassi A, Cascio MG, Ligresti A, Matias I, Schiano-Moriello A, Paul P, Williams EJ, Gangadharan U, Hobbs C, Di Marzo V and Doherty P (2003) Cloning of the first sn1-DAG lipases points to the spatial and temporal regulation of endocannabinoid signaling in the brain. *J Cell Biol* **163**:463-468.
- Black JW and Leff P (1983) Operational Models of Pharmacological Agonism. *Proc R Soc Lond* **220**:141-162.
- Blankman JL, Simon GM and Cravatt BF (2007) A comprehensive profile of brain enzymes that hydrolyze the endocannabinoid 2-arachidonoylglycerol. *Chem Biol* **14**:1347-1356.
- Bolognini D, Cascio M, Parolaro D and Pertwee R (2012) AM630 behaves as a protean ligand at the human cannabinoid CB2 receptor. *Br J Pharmacol* **165**:2561-2574.
- Booker L, Kinsey GK, Abdullah RA, Blankman JL, Long JZ, Ezzili C, Boger DL, Cravatt BF and Lichtman AH (2012) The fatty acid amide hydrolase (FAAH) inhibitor PF-3845 acts in the nervous system to reverse LPS-induced tactile allodynia in mice. *British Journal of Pharmacology* **165**:2485-2496.
- Bosier B, Muccioli GG, Hermans E and Lambert DM (2010) Functionally selective cannabinoid receptor signalling: therapeutic implications and opportunities. *Biochem Pharmacol* **80**:1-12.
- Bosma R, Mocking TAM, Leurs R and Vischer HF (2017) Ligand-Binding Kinetics on Histamine Receptors.115-155.
- Bouaboula M, Desnoyer N, Carayon P, Combes T and Casellas P (1999) Gi protein modulation induced by a selective inverse agonist for the peripheral cannabinoid receptor CB2: implication for

intracellular signalization cross-regulation. *Mol Pharmacol* **55**:473-480.

- Bouaboula M, Poinot-Chazel C, Marchand J, Canat X, Bourrié B, Rinaldi-Carmona M, Calandra B, Le Fur G and Casellas P (1996) Signaling pathway associated with stimulation of CB2 peripheral cannabinoid receptor. Involvement of both mitogen-activated protein kinase and induction of Krox-24 expression. *Eur J Biochem* **237**:704-711.
- Bridges D, Ahmad K and Rice A (2001) The synthetic cannabinoid WIN55,212-2 attenuates hyperalgesia and allodynia in a rat model of neuropathic pain. *Br J Pharmacol* **133**:586-594.
- Brown I, Cascio MG, Rotondo D, Pertwee RG, Heys SD and Wahle KW (2013) Cannabinoids and omega-3/6 endocannabinoids as cell death and anticancer modulators. *Prog Lipid Res* **52**:80-109.
- Buckley NE, McCoy KL, Mezey E, Bonner T, Zimmer A, Felder CC, Glass M and Zimmer A (2000) Immunomodulation by Cannabinoids Is Absent in Mice Deficient for the Cannabinoid CB2 Receptor. *Eur J Pharmacol* **396**:141-149.
- Cabral GA and Griffin-Thomas L (2009) Emerging role of the cannabinoid receptor CB2 in immune regulation: therapeutic prospects for neuroinflammation. *Expert Rev Mol Med* **11**:e3.
- Cabrera-Vera TM, Vanhauwe J, Thomas TO, Medkova M, Preininger A, Mazzoni MR and Hamm HE (2003) Insights into G protein structure, function, and regulation. *Endocr Rev* **24**:765-781.
- Cao JK, Kaplan J and Stella N (2019) ABHD6: Its Place in Endocannabinoid Signaling and Beyond. *Trends Pharmacol Sci* **40**:267-277.
- Carayon P, Marchand J, Dussossoy D, Derocq J, Jbilo O, Bord A, Bouaboula M, Galiègue S, Mondière P, Pénarier G, Fur G, Defrance T and Casellas P (1998) Modulation and functional involvement of CB2 peripheral cannabinoid receptors during B-cell differentiation. *Blood* **92**:3605-3615.
- Carrasquer A, Nebane NM, Williams WM and Song ZH (2010) Functional consequences of nonsynonymous single nucleotide polymorphisms in the CB2 cannabinoid receptor. *Pharmacogenet Genomics* **20**:157-166.

- Cascio MG, Bolognini D, Pertwee RG, Palazzo E, Corelli F, Pasquini S, Di Marzo V and Maione S (2010) In vitro and in vivo pharmacological characterization of two novel selective cannabinoid CB(2) receptor inverse agonists. *Pharmacol Res* **61**:349-354.
- Cascio MG and Marini P (2015) Biosynthesis and Fate of Endocannabinoids, in *Endocannabinoids: Handbook of Experimental Pharmacology* (Pertwee R ed) pp 39-51, Springer International Publishing, Switzerland.
- Cassano T, Calcagnini S, Pace L, De Marco F, Romano A and Gaetani S (2017) Cannabinoid Receptor 2 Signaling in Neurodegenerative Disorders: From Pathogenesis to a Promising Therapeutic Target. *Front Neurosci* **11**:30.
- Centonze D, Finazzi-Agro A, Bernardi G and Maccarrone M (2007) The endocannabinoid system in targeting inflammatory neurodegenerative diseases. *Trends Pharmacol Sci* **28**:180-187.
- Chakravarti B, Ravi J and Ganju R (2014) Cannabinoids as therapeutic agents in cancer: current status and future implications. *Oncotarget* **5**:5852-5872.
- Chen H, Kovar J, Sissons S, Cox K, Matter W, Chadwell F, Luan P, Vlahos CJ, Schutz-Geschwender A and Olive DM (2005) A cell-based immunocytochemical assay for monitoring kinase signaling pathways and drug efficacy. *Anal Biochem* **338**:136-142.
- Chen J, DeVivo M, Dingus J, Harry A, Li J, Sui J, Carty D, Blank J, Exton J, Stoffel R, Inglese J, Lefkowitz R, Logothetis D, Hildebrandt J and lyengar R (1995) A region of adenylyl cyclase 2 critical for regulation by G protein beta gamma subunits. *Science* **268**:1166-1169.
- Cheng Y-C and Prusoff WH (1973) Relationship between the inhibition constant (KI) and the concentration of inhibitor which causes 50 percent inhibition (I50) of an enzymatic reaction. *Biochemical Pharmacology* **22**:3099-3108.
- Chevalier D, Thorin E and Allena B (2000) Simultaneous measurement of ERK, p38, and JNK MAP kinase cascades in vascular smooth muscle cells. *J Pharmacol Toxicol Methods* **44**:429-439.
- Chu ZL, Carroll C, Chen R, Alfonso J, Gutierrez V, He H, Lucman A, Xing C, Sebring K, Zhou J, Wagner B, Unett D, Jones RM, Behan DP and Leonard J (2010) N-oleoyldopamine enhances glucose

homeostasis through the activation of GPR119. *Mol Endocrinol* **24**:161-170.

Contartese A, Valoti M, Corelli F, Pasquini S, Mugnaini C, Pessina F, Aldinucci C, Sgaragli G and Frosini M (2012) A novel CB2 agonist, COR167, potently protects rat brain cortical slices against OGD and reperfusion injury. *Pharmacol Res* **66**:555-563.

Contino M, Capparelli E, Colabufo NA and Bush AI (2017) Editorial: The CB2 Cannabinoid System: A New Strategy in Neurodegenerative Disorder and Neuroinflammation. *Front Neurosci* **11**:196.

Correa F, Hernangomez M, Mestre L, Loria F, Spagnolo A, Docagne F, Di Marzo V and Guaza C (2010) Anandamide enhances IL-10 production in activated microglia by targeting CB(2) receptors: roles of ERK1/2, JNK, and NF-kappaB. *Glia* **58**:135-147.

Coso O, Teramoto H, Simonds W and Gutkind J (1996) Signaling from G Protein-coupled Receptors to c-Jun Kinase Involves  $\beta\gamma$  Subunits of Heterotrimeric G Proteins Acting on a Ras and Rac1-dependent Pathway. *The Journal of Biological Chemistry* **271**:3963-3966.

Cottet M, Faklaris O, Zwier JM, Trinquet E, Pin J-P and Durroux T (2011) Original Fluorescent Ligand-Based Assays Open New Perspectives in G-Protein Coupled Receptor Drug Screening. *Pharmaceuticals* **4**:202-214.

Dalton G, Bass C, Van Horn C and Howlett AC (2009) Signal Transduction via Cannabinoid Receptors. *CNS Neurol Disord Drug Targets* **8**:422-431.

Day T, Rakhshan F, Deutsch D and Barker E (2001) Role of fatty acid amide hydrolase in the transport of the endogenous cannabinoid anandamide. *Mol Pharmacol* **59**:1369-1375.

Deng H and Li W (2020) Therapeutic potential of targeting alpha/beta-Hydrolase domain-containing 6 (ABHD6). *Eur J Med Chem* **198**:112353.

Deng L, Guindon J, Cornett BL, Makriyannis A, Mackie K and Hohmann AG (2015) Chronic cannabinoid receptor 2 activation reverses paclitaxel neuropathy without tolerance or cannabinoid receptor 1-dependent withdrawal. *Biol Psychiatry* **77**:475-487.

- Despres J, Golay A and Sjoström L (2005) Effects of Rimonabant on Metabolic Risk Factors in Overweight Patients With Dyslipidemia. *N Engl J Med* **353**:2121-2134.
- Devane W, Hanus L, Breuer A, Pertwee R, Stevenson L, Griffin G, Gibson D, Mandelbaum A, Etinger A and Mechoulam R (1992) Isolation and structure of a brain constituent that binds to the cannabinoid receptor. *Science* **258**:1946-1949.
- Dhopeswarkar A and Mackie K (2014) CB2 Cannabinoid receptors as a therapeutic target-what does the future hold? *Mol Pharmacol* **86**:430-437.
- Dhopeswarkar A and Mackie K (2016) Functional Selectivity of CB2 Cannabinoid Receptor Ligands at a Canonical and Noncanonical Pathway. *J Pharmacol Exp Ther* **358**:342-351.
- Di Marzo V, Bifulco M and De Petrocellis L (2004) The endocannabinoid system and its therapeutic exploitation. *Nat Rev Drug Discov* **3**:771-784.
- Di Marzo V and De Petrocellis L (2010) Endocannabinoids as regulators of transient receptor potential (TRP) channels: A further opportunity to develop new endocannabinoid-based therapeutic drugs. *Curr Med Chem* **17**:1430-1449.
- Di Marzo V, De Petrocellis L and Bisogno T (2005) The Biosynthesis, Fate and Pharmacological Properties of Endocannabinoids, in *Cannabinoids Handbook of Experimental Pharmacology* (Pertwee RG ed) pp 147-185, Springer, Berlin, Heidelberg.
- Di Marzo V and Petrosino S (2007) Endocannabinoids and the Regulation of Their Levels in Health and Disease. *Curr Opin Lipidol* **18**:129-140.
- Dinh TP, Kathuria S and Piomelli D (2004) RNA interference suggests a primary role for monoacylglycerol lipase in the degradation of the endocannabinoid 2-arachidonoylglycerol. *Mol Pharmacol* **66**:1260-1264.
- Docagne F, Mestre L, Loría F, Hernangómez M, Correa F and Guaza C (2008) Therapeutic Potential of CB2 Targeting in Multiple Sclerosis. *Expert Opin Ther Targets* **12**:185-195.

- Ehlert FJ (2008) On the analysis of ligand-directed signaling at G protein-coupled receptors. *Naunyn Schmiedebergs Arch Pharmacol* **377**:549-577.
- Ehrhart J, Obregon D, Mori T, Hou H, Sun N, Bai Y, Klein T, Fernandez F, Tan J and Shytle RD (2005) Stimulation of cannabinoid receptor 2 (CB2) suppresses microglial activation. *J Neuroinflammation* **2**:29.
- Emadi L, Jonaidi H and Hosseini Amir Abad E (2011) The role of central CB2 cannabinoid receptors on food intake in neonatal chicks. *J Comp Physiol A Neuroethol Sens Neural Behav Physiol* **197**:1143-1147.
- Endsley MP, Aggarwal N, Isbell MA, Wheelock CE, Hammock BD, Falck JR, Campbell WB and Nithipatikom K (2007) Diverse roles of 2-arachidonoylglycerol in invasion of prostate carcinoma cells: Location, hydrolysis and 12-lipoxygenase metabolism. *Int J Cancer* **121**:984-991.
- Fagan S and Campbell V (2014) The influence of cannabinoids on generic traits of neurodegeneration. *Br J Pharmacol* **171**:1347-1360.
- Farsandaj N, Ghahremani MH and Ostad SN (2012) Role of Cannabinoid and Vanilloid Receptors in Invasion of Human Breast Carcinoma Cells. *J Environ Pathol Toxicol Oncol* **31**:377-387.
- Felder C, Joyce K, Briley E, Mansouri J, Mackie K, Blond O, Lai Y, Ma A and Mitchell R (1995) Comparison of the pharmacology and signal transduction of the human cannabinoid CB1 and CB2 receptors. *Mol Pharmacol* **48**:443-450.
- Feng W and Song ZH (2001) Functional Roles of the Tyrosine Within the NP(X)(n)Y Motif and the Cysteines in the C-terminal Juxtamembrane Region of the CB2 Cannabinoid Receptor. *FEBS Lett* **501**:166-170.
- Feng W and Song ZH (2003) Effects of D3.49A, R3.50A, and A6.34E mutations on ligand binding and activation of the cannabinoid-2 (CB2) receptor. *Biochemical Pharmacology* **65**:1077-1085.
- Fernandez-Ruiz J, Romero J and Ramos J (2015) Endocannabinoids and Neurodegenerative Disorders: Parkinson's Disease, Huntington's Chorea, Alzheimer's Disease, and Others, in *Endocannabinoids: Handbook of Experimental Pharmacology* (Pertwee R ed) pp 233-283, Springer International Publishing, Switzerland.

- Fonseca BM, Costa MA, Almada M, Correia-da-Silva G and Teixeira NA (2013) Endogenous cannabinoids revisited: a biochemistry perspective. *Prostaglandins Other Lipid Mediat* **102-103**:13-30.
- Fowler CJ, Doherty P and Alexander SPH (2017) Endocannabinoid Turnover. *Adv Pharmacol* **80**:31-66.
- Fraguas-Sanchez AI and Torres-Suarez AI (2018) Medical Use of Cannabinoids. *Drugs* **78**:1665-1703.
- Fukuda S, Kohsaka H, Takayasu A, Yokoyama W, Miyabe C, Miyabe Y, Harigai M, Miyasaka N and Nanki T (2014) Cannabinoid Receptor 2 as a Potential Therapeutic Target in Rheumatoid Arthritis. *BMC Musculoskeletal Disorders* **15**.
- Gado F, Di Cesare Mannelli L, Lucarini E, Bertini S, Cappelli E, Digiacoimo M, Stevenson LA, Macchia M, Tuccinardi T, Ghelardini C, Pertwee RG and Manera C (2019) Identification of the First Synthetic Allosteric Modulator of the CB2 Receptors and Evidence of Its Efficacy for Neuropathic Pain Relief. *J Med Chem* **62**:276-287.
- Galiègue S, Mary S, Marchand J, Dussossoy D, Carrière D, Carayon P, Bouaboula M, Shire D, Le Fur G and Casellas P (1995) Expression of central and peripheral cannabinoid receptors in human immune tissues and leukocyte subpopulations. *Eur J Biochem* **232**:54-61.
- Gallant M, Dufresne C, Gareau Y, Guay D, Leblanc Y, Prasit P, Rochette C, Sawyer N, Slipetz DM, Tremblay N, Metters KM and Labelle M (1996) New class of potent ligands for the human peripheral cannabinoid receptor. *Bioorganic & Medicinal Chemistry Letters* **6**:2263-2268.
- Gamage TF, Farquhar CE, Lefever TW, Marusich JA, Kevin RC, McGregor IS, Wiley JL and Thomas BF (2018) Molecular and Behavioral Pharmacological Characterization of Abused Synthetic Cannabinoids MMB- and MDMB-FUBINACA, MN-18, NNEI, CUMYL-PICA, and 5-Fluoro-CUMYL-PICA. *J Pharmacol Exp Ther* **365**:437-446.
- Gan TJ and Wase L (2020) Oliceridine, a G protein-selective ligand at the  $\mu$ -opioid receptor, for the management of moderate to severe acute pain. *Drugs Today (Barc)* **56**:269-286.
- Gaoni Y and Mechoulam R (1964) Isolation, Structure, and Partial Synthesis of an Active Constituent of Hashish. *J Am Chem Soc* **86**:1646-1647.

- Garcia C, Palomo-Garo C, García-Arencibia M, Ramos J, Pertwee R and Fernández-Ruiz J (2011) Symptom-relieving and neuroprotective effects of the phytocannabinoid  $\Delta^9$ -THCV in animal models of Parkinson's disease. *Br J Pharmacol* **163**:1495-1506.
- Ghafouri N, Tiger G, Razdan RK, Mahadevan A, Pertwee RG, Martin BR and Fowler CJ (2004) Inhibition of monoacylglycerol lipase and fatty acid amide hydrolase by analogues of 2-arachidonoylglycerol. *Br J Pharmacol* **143**:774-784.
- Gilham D and Lehner R (2005) Techniques to measure lipase and esterase activity in vitro. *Methods* **36**:139-147.
- Gomez-Galvez Y, Palomo-Garo C, Fernandez-Ruiz J and Garcia C (2016) Potential of the cannabinoid CB(2) receptor as a pharmacological target against inflammation in Parkinson's disease. *Prog Neuropsychopharmacol Biol Psychiatry* **64**:200-208.
- Gong JP, Onaivi ES, Ishiguro H, Liu QR, Tagliaferro PA, Brusco A and Uhl GR (2006) Cannabinoid CB2 receptors: immunohistochemical localization in rat brain. *Brain Res* **1071**:10-23.
- Gouldson P, Calandra B, Legoux P, Kernéis A, Rinaldi-Carmona M, Barth F, Le Fur G, Ferrara P and Shire D (2000) Mutational Analysis and Molecular Modelling of the Antagonist SR 144528 Binding Site on the Human Cannabinoid CB(2) Receptor *Eur J Pharmacol* **401**:17-25.
- Grant I and Cahn BR (2005) Cannabis and endocannabinoid modulators: Therapeutic promises and challenges. *Clin Neurosci Res* **5**:185-199.
- Grimaldi P, Orlando P, Di Siena S, Lolicato F, Petrosino S, Bisogno T, Geremia R, De Petrocellis L and Di Marzo V (2009) The endocannabinoid system and pivotal role of the CB2 receptor in mouse spermatogenesis. *PNAS* **106**:11131-11136.
- Groer CE, Tidgewell K, Moyer RA, Harding WW, Rothman RB, Prisinzano TE and Bohn LM (2007) An opioid agonist that does not induce mu-opioid receptor--arrestin interactions or receptor internalization. *Mol Pharmacol* **71**:549-557.
- Gruner BM, Schulze CJ, Yang D, Ogasawara D, Dix MM, Rogers ZN, Chuang CH, McFarland CD, Chiou SH, Brown JM, Cravatt BF, Bogoy M and

- Winslow MM (2016) An in vivo multiplexed small-molecule screening platform. *Nat Methods* **13**:883-889.
- Gui H, Liu X, Liu LR, Su DF and Dai SM (2015) Activation of cannabinoid receptor 2 attenuates synovitis and joint destruction in collagen-induced arthritis. *Immunobiology* **220**:817-822.
- Hanus L, Breuer A, Tchilibon S, Shiloah S, Goldenberg D, Horowitz M, Pertwee R, Ross R, Mechoulam R and Fride E (1999) HU-308: a specific agonist for CB(2), a peripheral cannabinoid receptor. *Proc Natl Acad Sci* **96**:14228-14233.
- Harlow E and Lane D (1988) Immunoblotting protocols, in *Antibodies* pp 494-495, Cold Spring, Harbor, New York.
- Harrison C and Traynor JR (2003) The [35S]GTPgammaS binding assay: approaches and applications in pharmacology. *Life Sci* **74**:489-508.
- Hatfield MJ and Potter PM (2011) Carboxylesterase inhibitors. *Expert Opin Ther Pat* **21**:1159-1171.
- Hauser AS, Attwood MM, Rask-Andersen M, Schioth HB and Gloriam DE (2017) Trends in GPCR drug discovery: new agents, targets and indications. *Nat Rev Drug Discov* **16**:829-842.
- Hejazi N, Zhou C, Oz M, Sun H, Ye JH and Zhang L (2006) Delta9-tetrahydrocannabinol and endogenous cannabinoid anandamide directly potentiate the function of glycine receptors. *Mol Pharmacol* **69**:991-997.
- Hill SJ (2006) G-protein-coupled receptors: past, present and future. *British Journal of Pharmacology* **147**:S27-37.
- Hill SJ, Williams C and May LT (2010) Insights into GPCR pharmacology from the measurement of changes in intracellular cyclic AMP; advantages and pitfalls of differing methodologies. *Br J Pharmacol* **161**:1266-1275.
- Hillard CJ and Jarrahian A (2003) Cellular accumulation of anandamide: consensus and controversy. *Br J Pharmacol* **140**:802-808.
- Hillger JM, Le Roy B, Wang Z, Mulder-Krieger T, Boomsma DI, Slagboom PE, Danen EHJ, AP IJ and Heitman LH (2017) Phenotypic screening of cannabinoid receptor 2 ligands shows different sensitivity to genotype. *Biochem Pharmacol* **130**:60-70.

- Hohmann AG, Suplita RL, Bolton NM, Neely MH, Fegley D, Mangieri R, Krey JF, Walker JM, Holmes PV, Crystal JD, Duranti A, Tontini A, Mor M, Tarzia G and Piomelli D (2005) An endocannabinoid mechanism for stress-induced analgesia. *Nature* **435**:1108-1112.
- Howlett A, Barth F, Bonner T, Cabral G, Casellas P, Devane W, Felder C, Herkenham M, Mackie K, Martin B, Mechoulam R and Pertwee R (2002) International Union of Pharmacology. XXVII. Classification of cannabinoid receptors. *Pharmacol Rev* **54**:161-202.
- Hsu KL, Tsuboi K, Chang JW, Whitby LR, Speers AE, Pugh H and Cravatt BF (2013) Discovery and optimization of piperidyl-1,2,3-triazole ureas as potent, selective, and in vivo-active inhibitors of alpha/beta-hydrolase domain containing 6 (ABHD6). *J Med Chem* **56**:8270-8279.
- Hua T, Vemuri K, Pu M, Qu L, Han GW, Wu Y, Zhao S, Shui W, Li S, Korde A, Laprairie RB, Stahl EL, Ho JH, Zvonok N, Zhou H, Kufareva I, Wu B, Zhao Q, Hanson MA, Bohn LM, Makriyannis A, Stevens RC and Liu ZJ (2016) Crystal Structure of the Human Cannabinoid Receptor CB1. *Cell* **167**:750-762 e714.
- Hurowitz E, Melnyk J, Chen Y, Kouros-Mehr H, Simon M and Shizuya H (2000) Genomic Characterization of the Human Heterotrimeric G Protein  $\alpha$ ,  $\beta$  and  $\gamma$  Subunit Genes. *DNA Research* **7**:111-120.
- Ibsen MS, Connor M and Glass M (2017) Cannabinoid CB1 and CB2 Receptor Signaling and Bias. *Cannabis Cannabinoid Res* **2**:48-60.
- Iglesias J, Lamontagne J, Erb H, Gezzar S, Zhao S, Joly E, Truong VL, Skorey K, Crane S, Madiraju SR and Prentki M (2016) Simplified assays of lipolysis enzymes for drug discovery and specificity assessment of known inhibitors. *J Lipid Res* **57**:131-141.
- Ishiguro H, Horiuchi Y, Ishikawa M, Koga M, Imai K, Suzuki Y, Morikawa M, Inada T, Watanabe Y, Takahashi M, Someya T, Ujike H, Iwata N, Ozaki N, Onaivi ES, Kunugi H, Sasaki T, Itokawa M, Arai M, Niizato K, Iritani S, Naka I, Ohashi J, Kakita A, Takahashi H, Nawa H and Arinami T (2010) Brain cannabinoid CB2 receptor in schizophrenia. *Biol Psychiatry* **67**:974-982.
- Ishiguro H, Leonard CM, Sgro S and Onaivi ES (2013) Cannabinoid receptor gene variations in neuropsychiatric disorders, in *Endocannabinoids: Molecular, Pharmacological, Behavioral and*

*Clinical Features* (Murillo-Rodríguez E ed) pp 3-24, Bentham Science Publishers, 2013, pp. 3–24.

- Izzo AA and Sharkey KA (2010) Cannabinoids and the gut: new developments and emerging concepts. *Pharmacol Ther* **126**:21-38.
- Janero D and Makriyannis A (2009) Cannabinoid receptor antagonists: pharmacological opportunities, clinical experience, and translational prognosis. *Expert Opin Drug Discov* **14**:43-65.
- Kano M, Ohno-Shosaku T, Hashimotodani Y, Uchigashima M and Watanabe M (2009) Endocannabinoid-mediated control of synaptic transmission. *Physiol Rev* **89**:309-380.
- Karbarz MJ, Luo L, Chang L, Tham CS, Palmer JA, Wilson SJ, Wennerholm ML, Brown SM, Scott BP, Apodaca RL, Keith JM, Wu J, Breitenbucher JG, Chaplan SR and Webb M (2009) Biochemical and biological properties of 4-(3-phenyl-[1,2,4] thiadiazol-5-yl)-piperazine-1-carboxylic acid phenylamide, a mechanism-based inhibitor of fatty acid amide hydrolase. *Anesth Analg* **108**:316-329.
- Karlsson M, Contreras J, Hellman U, Tornqvist H and Holm C (1997) cDNA cloning, tissue distribution, and identification of the catalytic triad of monoglyceride lipase. Evolutionary relationship to esterases, lysophospholipases, and haloperoxidases. *J Biol Chem* **272**:27218-27223.
- Keith JM, Apodaca R, Xiao W, Seierstad M, Pattabiraman K, Wu J, Webb M, Karbarz MJ, Brown S, Wilson S, Scott B, Tham CS, Luo L, Palmer J, Wennerholm M, Chaplan S and Breitenbucher JG (2008) Thiadiazolopiperazinyl ureas as inhibitors of fatty acid amide hydrolase. *Bioorg Med Chem Lett* **18**:4838-4843.
- Kenakin T (2011) Functional selectivity and biased receptor signaling. *J Pharmacol Exp Ther* **336**:296-302.
- Kenakin T and Christopoulos A (2013) Signalling bias in new drug discovery: detection, quantification and therapeutic impact. *Nat Rev Drug Discov* **12**:205-216.
- Kenakin T, Watson C, Muniz-Medina V, Christopoulos A and Novick S (2012) A simple method for quantifying functional selectivity and agonist bias. *ACS Chem Neurosci* **3**:193-203.

- Kendall DA and Yudowski GA (2016) Cannabinoid Receptors in the Central Nervous System: Their Signaling and Roles in Disease. *Front Cell Neurosci* **10**:294.
- Kim J, Grotegut CA, Wisler JW, Mao L, Rosenberg PB, Rockman HA and Lefkowitz RJ (2020) The beta-arrestin-biased beta-adrenergic receptor blocker carvedilol enhances skeletal muscle contractility. *Proc Natl Acad Sci U S A* **117**:12435-12443.
- Kind L and Kursula P (2019) Structural properties and role of the endocannabinoid lipases ABHD6 and ABHD12 in lipid signalling and disease. *Amino Acids* **51**:151-174.
- King AR, Dotsey EY, Lodola A, Jung KM, Ghomian A, Qiu Y, Fu J, Mor M and Piomelli D (2009) Discovery of potent and reversible monoacylglycerol lipase inhibitors. *Chem Biol* **16**:1045-1052.
- Kobilka B (2007) G Protein Coupled Receptor Structure and Activation. *Biochim Biophys Acta* **1768**:794-807.
- Kozak KR, Gupta RA, Moody JS, Ji C, Boeglin WE, DuBois RN, Brash AR and Marnett LJ (2002) 15-Lipoxygenase metabolism of 2-arachidonylglycerol. Generation of a peroxisome proliferator-activated receptor alpha agonist. *J Biol Chem* **277**:23278-23286.
- Kozak KR, Rowlinson SW and Marnett LJ (2000) Oxygenation of the endocannabinoid, 2-arachidonylglycerol, to glyceryl prostaglandins by cyclooxygenase-2. *J Biol Chem* **275**:33744-33749.
- Krishna Kumar K, Shalev-Benami M, Robertson MJ, Hu H, Banister SD, Hollingsworth SA, Latorraca NR, Kato HE, Hilger D, Maeda S, Weis WI, Farrens DL, Dror RO, Malhotra SV, Kobilka BK and Skiniotis G (2019) Structure of a Signaling Cannabinoid Receptor 1-G Protein Complex. *Cell* **176**:448-458.
- Kwilasz AJ, Abdullah RA, Poklis JL, Lichtman AH and Negus SS (2014) Effects of the fatty acid amide hydrolase inhibitor URB597 on pain-stimulated and pain-depressed behavior in rats. *Behav Pharmacol* **25**:119-129.
- Lambert D and Fowler C (2005) The endocannabinoid system: drug targets, lead compounds, and potential therapeutic applications. *J Med Chem* **48**:5059-5087.

- Leleu-Chavain N, Baudalet D, Heloïre VM, Rocha DE, Renault N, Barczyk A, Djouina M, Body-Malapel M, Carato P and Millet R (2019) Benzo[d]thiazol-2(3H)-ones as new potent selective CB2 agonists with anti-inflammatory properties. *Eur J Med Chem* **165**:347-362.
- Leung D, Saghatelian A, Simon G and Cravatt B (2006) Inactivation of N-acyl phosphatidylethanolamine phospholipase D reveals multiple mechanisms for the biosynthesis of endocannabinoids. *Biochemistry* **45**:4720-4726.
- Li F, Fei X, Xu J and Ji C (2009) An unannotated alpha/beta hydrolase superfamily member, ABHD6 differentially expressed among cancer cell lines. *Mol Biol Rep* **36**:691-696.
- Li W, Blankman JL and Cravatt BF (2007) A Functional Proteomic Strategy to Discover Inhibitors for Uncharacterized Hydrolases. *J Am Chem Soc* **129**:9594-9595.
- Li X, Hua T, Vemuri K, Ho JH, Wu Y, Wu L, Popov P, Benchama O, Zvonok N, Locke K, Qu L, Han GW, Iyer MR, Cinar R, Coffey NJ, Wang J, Wu M, Katritch V, Zhao S, Kunos G, Bohn LM, Makriyannis A, Stevens RC and Liu ZJ (2019) Crystal Structure of the Human Cannabinoid Receptor CB2. *Cell*.
- Lin X, Dhopeswarkar AS, Huibregtse M, Mackie K and Hohmann AG (2018) Slowly Signaling G Protein-Biased CB2 Cannabinoid Receptor Agonist LY2828360 Suppresses Neuropathic Pain with Sustained Efficacy and Attenuates Morphine Tolerance and Dependence. *Mol Pharmacol* **93**:49-62.
- Liu J, Wang L, Harvey-White J, Osei-Hyiaman D, Razdan R, Gong Q, Chan A, Zhou Z, Huang B, Kim H and Kunos G (2006) A biosynthetic pathway for anandamide. *Proc Natl Acad Sci* **103**:13345-13350.
- Long JZ, Li W, Booker L, Burston JJ, Kinsey SG, Schlosburg JE, Pavon FJ, Serrano AM, Selley DE, Parsons LH, Lichtman AH and Cravatt BF (2009) Selective blockade of 2-arachidonoylglycerol hydrolysis produces cannabinoid behavioral effects. *Nat Chem Biol* **5**:37-44.
- Loo JSE (2015) Molecular modelling of the cannabinoid receptors: structure-based design, synthesis and pharmacological evaluation of novel ligands based on the fenofibrate scaffold, University of Nottingham.

- Magni G and Ceruti S (2019) The role of adenosine and P2Y receptors expressed by multiple cell types in pain transmission. *Brain Res Bull* **151**:132-143.
- Malan T, Ibrahim M, Deng H, Liu Q, Mata H, Vanderah T, Porreca F and Makriyannis A (2001) CB2 cannabinoid receptor-mediated peripheral antinociception. *Pain* **93**:239-245.
- Malan T, Ibrahim M, Lai J, Vanderah T, Makriyannis A and Porreca F (2003) CB cannabinoid receptor agonists: pain relief without psychoactive effects? *Curr Opin Pharmacol* **3**:62-67.
- Mallet C, Dubray C and Duale C (2016) FAAH inhibitors in the limelight, but regrettably. *Int J Clin Pharmacol Ther* **54**:498-501.
- Manera C, Benetti V, Castelli M, Cavallini T, Lazzarotti S, Pibiri F, Saccomanni G, Tuccinardi T, Vannacci A, Martinelli A and Ferrarini P (2006) Design, synthesis, and biological evaluation of new 1,8-naphthyridin-4(1H)-on-3-carboxamide and quinolin-4(1H)-on-3-carboxamide derivatives as CB2 selective agonists. *J Med Chem* **49**:5947-5957.
- Marchalant Y, Brownjohn PW, Bonnet A, Kleffmann T and Ashton JC (2014) Validating Antibodies to the Cannabinoid CB2 Receptor Antibody Sensitivity Is Not Evidence of Antibody Specificity. *J Histochem Cytochem* **62**:395-404.
- Marrs WR, Blankman JL, Horne EA, Thomazeau A, Lin YH, Coy J, Bodor AL, Muccioli GG, Hu SS, Woodruff G, Fung S, Lafourcade M, Alexander JP, Long JZ, Li W, Xu C, Moller T, Mackie K, Manzoni OJ, Cravatt BF and Stella N (2010) The serine hydrolase ABHD6 controls the accumulation and efficacy of 2-AG at cannabinoid receptors. *Nat Neurosci* **13**:951-957.
- Martin-Moreno AM, Reigada D, Ramirez BG, Mechoulam R, Innamorato N, Cuadrado A and de Ceballos ML (2011) Cannabidiol and other cannabinoids reduce microglial activation in vitro and in vivo: relevance to Alzheimer's disease. *Mol Pharmacol* **79**:964-973.
- Matias I, Chen J, De Petrocellis L, Bisogno T, Ligresti A, Fezza F, Krauss AH, Shi L, Protzman CE, Li C, Liang Y, Nieves AL, Kedzie KM, Burk RM, Di Marzo V and Woodward DF (2004) Prostaglandin ethanolamides (prostamides): in vitro pharmacology and metabolism. *J Pharmacol Exp Ther* **309**:745-757.

- Matsuda L, Lolait S, Brownstein M, Young A and Bonner T (1990) Structure of a cannabinoid receptor and functional expression of the cloned cDNA. *Nature* **346**:561-564.
- McAllister SD, Hurst DP, Barnett-Norris J, Lynch D, Reggio PH and Abood ME (2004) Structural mimicry in class A G protein-coupled receptor rotamer toggle switches: the importance of the F3.36(201)/W6.48(357) interaction in cannabinoid CB1 receptor activation. *J Biol Chem* **279**:48024-48037.
- McFarland MJ, Porter AC, Rakhshan FR, Rawat DS, Gibbs RA and Barker EL (2004) A role for caveolae/lipid rafts in the uptake and recycling of the endogenous cannabinoid anandamide. *J Biol Chem* **279**:41991-41997.
- McGuinness D, Malikzay A, Visconti R, Lin K, Bayne M, Monsma F and Lunn CA (2009) Characterizing cannabinoid CB2 receptor ligands using DiscoverX PathHunter beta-arrestin assay. *J Biomol Screen* **14**:49-58.
- McHugh D, Page J, Dunn E and Bradshaw H (2012)  $\Delta(9)$  - Tetrahydrocannabinol and N-arachidonyl glycine are full agonists at GPR18 receptors and induce migration in human endometrial HEC-1B cells. *Br J Pharmacol* **165**:2414-2424.
- Mebratu Y and Tesfaigzi Y (2009) How ERK1/2 Activation Controls Cell Proliferation and Cell Death Is Subcellular Localization the Answer ? *Cell Cycle* **8**:1168-1175.
- Mecha M, Carrillo-Salinas FJ, Feliu A, Mestre L and Guaza C (2020) Perspectives on Cannabis-Based Therapy of Multiple Sclerosis: A Mini-Review. *Front Cell Neurosci* **14**:34.
- Mechoulam R, Ben-Shabat S, Hanus L, Ligumsky M, Kaminski NE, Schatz AR, Gopher A, Almog S, Martin BR, Compton DR, Pertwee RG, Griffin G, Bayewitch M, Barg J and Vogel Z (1995) Identification of an endogenous 2-monoglyceride, present in canine gut, that binds to cannabinoid receptors. *Biochemical Pharmacology* **50**:83-90.
- Mercier RW, Pei Y, Pandarinathan L, Janero DR, Zhang J and Makriyannis A (2010) hCB2 ligand-interaction landscape: cysteine residues critical to biarylpyrazole antagonist binding motif and receptor modulation. *Chem Biol* **17**:1132-1142.
- Michael R, Kendall DA and Alexander SP (2009) G proteins and their downstream signalling cascades in *Fast Track Pharmacology*, Pharmaceutical Press, London, Chicago.

- Milligan G and Kostenis E (2006) Heterotrimeric G-proteins: a short history. *Br J Pharmacol* **147 Suppl 1**:S46-55.
- Minneman KP, Hegstrand LR and Molinoff PB (1979) The Pharmacological Specificity of Beta-1 and Beta-2 Adrenergic Receptors in Rat Heart and Lung in Vitro. *Mol Pharmacol* **16**:21-23.
- Montecucco F, Burger F, Mach F and Steffens S (2008) CB2 cannabinoid receptor agonist JWH-015 modulates human monocyte migration through defined intracellular signaling pathways. *Am J Physiol Heart Circ Physiol* **294**:H1145-1155.
- Montecucco F, Lenglet S, Braunersreuther V, Burger F, Pelli G, Bertolotto M, Mach F and Steffens S (2009) CB2 cannabinoid receptor activation is cardioprotective in a mouse model of ischemia/reperfusion. *J Mol Cell Cardiol* **46**:612-620.
- Morales P, Goya P and Jagerovic N (2018) Emerging strategies targeting CB2 cannabinoid receptor: Biased agonism and allosterism. *Biochem Pharmacol* **157**:8-17.
- Muccioli GG and Stella N (2008) An optimized GC-MS method detects nanomolar amounts of anandamide in mouse brain. *Anal Biochem* **373**:220-228.
- Mugnaini C, Rabbito A, Brizzi A, Palombi N, Petrosino S, Verde R, Di Marzo V, Ligresti A and Corelli F (2019) Synthesis of novel 2-(1-adamantanylcaboxamido)thiophene derivatives. Selective cannabinoid type 2 (CB2) receptor agonists as potential agents for the treatment of skin inflammatory disease. *Eur J Med Chem* **161**:239-251.
- Mukhopadhyay P, Baggelaar M, Erdelyi K, Cao Z, Cinar R, Fezza F, Ignatowska-Janlowska B, Wilkerson J, van Gils N, Hansen T, Ruben M, Soethoudt M, Heitman L, Kunos G, Maccarrone M, Lichtman A, Pacher P and Van der Stelt M (2016) The novel, orally available and peripherally restricted selective cannabinoid CB2 receptor agonist LEI-101 prevents cisplatin-induced nephrotoxicity. *Br J Pharmacol* **173**:446-458.
- Munro S, Thomas K and Abu-Shaar M (1993) Molecular characterization of a peripheral receptor for cannabinoids. *Nature* **365**:61-65.
- Munson A, Harris L, Friedman M, Dewey W and Carchman R (1975) Antineoplastic activity of cannabinoids. *J Natl Cancer Inst* **55**:597-602.

- Murineddu G, Lazzari P, Ruiu S, Sanna A, Loriga G, Manca I, Falzoi M, Dessì C, Curzu M, Chelucci G, Pani L and Pinna G (2006) Tricyclic pyrazoles. 4. Synthesis and biological evaluation of analogues of the robust and selective CB2 cannabinoid ligand 1-(2',4'-dichlorophenyl)-6-methyl-N-piperidin-1-yl-1,4-dihydroindeno[1,2-c]pyrazole-3-carboxamide. *J Med Chem* **49**:7502-7512.
- Nasser MW, Qamri Z, Deol YS, Smith D, Shilo K, Zou X and Ganju RK (2011) Crosstalk between chemokine receptor CXCR4 and cannabinoid receptor CB2 in modulating breast cancer growth and invasion. *PLoS One* **6**:e23901.
- Navia-Paldanius D, Savinainen JR and Laitinen JT (2012) Biochemical and pharmacological characterization of human alpha/beta-hydrolase domain containing 6 (ABHD6) and 12 (ABHD12). *J Lipid Res* **53**:2413-2424.
- Naydenov AV, Horne EA, Cheah CS, Swinney K, Hsu KL, Cao JK, Marrs W, Blankman JL, Tu S, Cherry AE, Fung S, Wen A, Li W, Saporito MS, Selley DE, Cravatt BF, Oakley JC and Stella N (2014) ABHD6 blockade exerts antiepileptic activity in PTZ-induced seizures and in spontaneous seizures in R6/2 mice. *Neuron* **83**:361-371.
- Ndong C, O'Donnell D, Ahmad S and Groblewski T (2011) Cloning and pharmacological characterization of the dog cannabinoid CB(2)receptor. *Eur J Pharmacol* **669**:24-31.
- Nebane NM, Hurst DP, Carrasquer CA, Qiao Z, Reggio PH and Song ZH (2008) Residues accessible in the binding-site crevice of transmembrane helix 6 of the CB2 cannabinoid receptor. *Biochemistry* **47**:13811-13821.
- Nebane NM, Kellie B and Song ZH (2006) The effects of charge-neutralizing mutation D6.30N on the functions of CB1 and CB2 cannabinoid receptors. *FEBS Lett* **580**:5392-5398.
- Nettekoven M, Adam JM, Bendels S, Bissantz C, Fingerle J, Grether U, Gruner S, Guba W, Kimbara A, Ottaviani G, Pullmann B, Rogers-Evans M, Rover S, Rothenhausler B, Schmitt S, Schuler F, Schulz-Gasch T and Ullmer C (2016) Novel Triazolopyrimidine-Derived Cannabinoid Receptor 2 Agonists as Potential Treatment for Inflammatory Kidney Diseases. *ChemMedChem* **11**:179-189.
- Ogawa S and Kunugi H (2015) Inhibitors of Fatty Acid Amide Hydrolase and Monoacylglycerol Lipase: New Targets for Future Antidepressants. *Curr Neuropharmacol* **13**:760-775.

- Oka S, Wakui J, Gokoh M, Kishimoto S and Sugiura T (2006) Suppression by WIN55212-2, a cannabinoid receptor agonist, of inflammatory reactions in mouse ear: Interference with the actions of an endogenous ligand, 2-arachidonoylglycerol. *Eur J Pharmacol* **538**:154-162.
- Oldham WM and Hamm HE (2008) Heterotrimeric G protein activation by G-protein-coupled receptors. *Nat Rev Mol Cell Biol* **9**:60-71.
- Onaivi ES, Carpio O, Ishiguro H, Schanz N, Uhl GR and Benno R (2008) Behavioral effects of CB2 cannabinoid receptor activation and its influence on food and alcohol consumption. *Ann N Y Acad Sci* **1139**:426-433.
- Onaivi ES, Ishiguro H and Liu QR (2015) Future perspectives: Cannabinoid CB2 receptor ligands and their therapeutic potential in mental diseases in *Cannabinoids in Neurological and Mental Diseases* (Fattore L ed) pp 425-444, Elsevier Inc
- Pasquini S, Botta L, Semeraro T, Mugnaini C, Ligresti A, Palazzo E, Maione S, Di Marzo V and Corelli F (2008) Investigations on the 4-Quinolone-3-carboxylic Acid Motif. 2. Synthesis and Structure–Activity Relationship of Potent and Selective Cannabinoid-2 Receptor Agonists Endowed with Analgesic Activity in Vivo. *J Med Chem* **51**:5075-5084.
- Pasquini S, Ligresti A, Mugnaini C, Semeraro T, Cicione L, De Rosa M, Guida F, Luongo L, De Chiaro M, Cascio MG, Bolognini D, Marini P, Pertwee R, Maione S, Di Marzo V and Corelli F (2010) Investigations on the 4-quinolone-3-carboxylic acid motif. 3. Synthesis, structure-affinity relationships, and pharmacological characterization of 6-substituted 4-quinolone-3-carboxamides as highly selective cannabinoid-2 receptor ligands. *J Med Chem* **53**:5915-5928.
- Patel JZ, Nevalainen TJ, Savinainen JR, Adams Y, Laitinen T, Runyon RS, Vaara M, Ahenkorah S, Kaczor AA, Navia-Paldanius D, Gynther M, Aaltonen N, Joharapurkar AA, Jain MR, Haka AS, Maxfield FR, Laitinen JT and Parkkari T (2015) Optimization of 1,2,5-thiadiazole carbamates as potent and selective ABHD6 inhibitors. *ChemMedChem* **10**:253-265.
- Pei Y, Mercier RW, Anday JK, Thakur GA, Zvonok AM, Hurst D, Reggio PH, Janero DR and Makriyannis A (2008) Ligand-binding architecture of human CB2 cannabinoid receptor: evidence for receptor subtype-specific binding motif and modeling GPCR activation. *Chem Biol* **15**:1207-1219.

- Pertwee R (1997) Pharmacology of cannabinoid CB1 and CB2 receptors. *Pharmacol Ther* **74**:129-180.
- Pertwee R (2015) Endocannabinoids and Their Pharmacological Actions., in *Endocannabinoids Handbook of Experimental Pharmacology* (Pertwee R ed), Springer, Cham.
- Pertwee RG, Howlett AC, Abood ME, Alexander SP, Di Marzo V, Elphick MR, Greasley PJ, Hansen HS, Kunos G, Mackie K, Mechoulam R and Ross RA (2010) International Union of Basic and Clinical Pharmacology. LXXIX. Cannabinoid receptors and their ligands: beyond CB(1) and CB(2). *Pharmacol Rev* **62**:588-631.
- Piomelli D, Tarzia G, Duranti A, Tontini A, Mor M, Compton TR, Dasse O, Monaghan EP, Parrott JA and Putman D (2006) Pharmacological Profile of the Selective FAAH Inhibitor KDS-4103 (URB597). *CNS Drug Rev* **12**:21-38.
- Piscitelli F and Di Marzo V (2012) "Redundancy" of endocannabinoid inactivation: new challenges and opportunities for pain control. *ACS Chem Neurosci* **3**:356-363.
- Pourkhalili N, Ghahremani MH, Farsandaj N, Tavajohi S, Majdzadeh M, Parsa M, Lavasani NJ and Ostad SN (2013) Evaluation of anti-invasion effect of cannabinoids on human hepatocarcinoma cells. *Toxicol Mech Methods* **23**:120-126.
- Poursharifi P, Madiraju SRM and Prentki M (2017) Monoacylglycerol signalling and ABHD6 in health and disease. *Diabetes Obes Metab* **19 Suppl 1**:76-89.
- Preet A, Qamri Z, Nasser MW, Prasad A, Shilo K, Zou X, Groopman JE and Ganju RK (2011) Cannabinoid receptors, CB1 and CB2, as novel targets for inhibition of non-small cell lung cancer growth and metastasis. *Cancer Prev Res (Phila)* **4**:65-75.
- Priestley RS, Nickolls SA, Alexander SP and Kendall DA (2015) A potential role for cannabinoid receptors in the therapeutic action of fenofibrate. *FASEB J* **29**:1446-1455.
- Reggio PH (2010) Endocannabinoid Binding to the Cannabinoid Receptors: What Is Known and What Remains Unknown. *Curr Med Chem* **17**:1468-1486.
- Rhee MH, Nevo I, Bayewitch ML, Zagoory O and Vogel Z (2000) Functional Role of Tryptophan Residues in the Fourth Transmembrane

Domain of the CB(2) Cannabinoid Receptor. *J Neurochem* **75**:2485-2491.

Ribeiro R, Yu F, Wen J, Vana A and Zhang Y (2013) Therapeutic potential of a novel cannabinoid agent CB52 in the mouse model of experimental autoimmune encephalomyelitis. *Neuroscience* **254**:427-442.

Ricciotti E and FitzGerald GA (2011) Prostaglandins and inflammation. *Arterioscler Thromb Vasc Biol* **31**:986-1000.

Rog DJ, Nurmikko TJ, Friede T and Young CA (2005) Randomized, controlled trial of cannabis-based medicine in central pain in multiple sclerosis. *Neurology* **65**:812-819.

Romero-Sandoval EA, Horvath R, Landry RP and DeLeo JA (2009) Cannabinoid receptor type 2 activation induces a microglial anti-inflammatory phenotype and reduces migration via MKP induction and ERK dephosphorylation. *Mol Pain* **5**:25.

Ross R, Brockie H, Stevenson L, Murphy V, Templeton F, Makriyannis A and Pertwee R (1999) Agonist-inverse agonist characterization at CB1 and CB2 cannabinoid receptors of L759633, L759656 and AM630. *Br J Pharmacol* **126**:665-672.

Ross R, Craib S, Stevenson L, Pertwee R, Henderson A, Toole J and Ellington H (2002) Pharmacological characterization of the anandamide cyclooxygenase metabolite: prostaglandin E2 ethanolamide. *J Pharmacol Exp Ther* **301**:900-907.

Rossi F, Punzo F, Umamo GR, Argenziano M and Miraglia Del Giudice E (2018) Role of Cannabinoids in Obesity. *Int J Mol Sci* **19**.

Ryberg E, Vu HK, Larsson N, Groblewski T, Hjorth S, Elebring T, Sjogren S and Greasley PJ (2005) Identification and characterisation of a novel splice variant of the human CB1 receptor. *FEBS Lett* **579**:259-264.

Sagredo O, Gonzalez S, Aroyo I, Pazos MR, Benito C, Lastres-Becker I, Romero JP, Tolon RM, Mechoulam R, Brouillet E, Romero J and Fernandez-Ruiz J (2009) Cannabinoid CB2 receptor agonists protect the striatum against malonate toxicity: relevance for Huntington's disease. *Glia* **57**:1154-1167.

Sarott R, Westphal M, Pfaff P, Korn C, Sykes D, Brennecke B, Veprintsev DB and al. e (2019) Highly Specific, Fluorescent Cannabinoid Type 2

Receptor Probes Enable Applications in Microscopy, Flow Cytometry and FRET-based Binding Assays. *ChemRxiv Preprint*.

Sarott R, Westphal M, Pfaff P, Korn C, Sykes D, Veprintsev DB and al. e (2020) Development of High-Specificity Fluorescent Probes to Enable Cannabinoid Type 2 Receptor Studies in Living Cells. *ChemRxiv Preprint*.

Saroz Y, Kho D, Glass M, Graham E and Grimsey N (2019) Cannabinoid Receptor 2 (CB2) Signals via G-alpha-s and Induces IL-6 and IL-10 Cytokine Secretion in Human Primary Leukocytes. *ACS Pharmacol Transl Sci* **2**:414-428.

Savinainen JR, Patel JZ, Parkkari T, Navia-Paldanius D, Marjamaa JJ, Laitinen T, Nevalainen T and Laitinen JT (2014) Biochemical and pharmacological characterization of the human lymphocyte antigen B-associated transcript 5 (BAT5/ABHD16A). *PLoS One* **9**:e109869.

Savinainen JR, Saario SM and Laitinen JT (2012) The serine hydrolases MAGL, ABHD6 and ABHD12 as guardians of 2-arachidonoylglycerol signalling through cannabinoid receptors. *Acta Physiol (Oxf)* **204**:267-276.

Schatz A, Lee M, Condie R, Pulaski J and Kaminski N (1997) Cannabinoid receptors CB1 and CB2: a characterization of expression and adenylyl cyclase modulation within the immune system. *Toxicol Appl Pharmacol* **142**:278-287.

Schmid PC, Reddy PV, Natarajan V and Schmid HH (1983) Metabolism of N-acylethanolamine phospholipids by a mammalian phosphodiesterase of the phospholipase D type. *Journal of Biological Chemistry* **258**:9302-9306.

Scott CE, Tang Y, Alt A, Burford NT, Gerritz SW, Ogawa LM, Zhang L and Kendall DA (2019) Identification and biochemical analyses of selective CB2 agonists. *Eur J Pharmacol* **854**:1-8.

Shen CP, Xiao JC, Armstrong H, Haggmann W and Fong TM (2006) F200A substitution in the third transmembrane helix of human cannabinoid CB1 receptor converts AM2233 from receptor agonist to inverse agonist. *Eur J Pharmacol* **531**:41-46.

Shire D, Carillon C, Kaghad M, Calandra B, Rinaldi-Carmona M, Le Fur G, Caput D and Ferrara P (1995) An amino-terminal variant of the central cannabinoid receptor resulting from alternative splicing. *J Biol Chem* **270**:3726-3731.

- Shoemaker JL, Ruckle MB, Mayeux PR and Prather PL (2005) Agonist-directed trafficking of response by endocannabinoids acting at CB2 receptors. *J Pharmacol Exp Ther* **315**:828-838.
- Shorr R, Lefkowitz R and Caron M (1981) Purification of the  $\beta$ -Adrenergic receptor: Identification of the hormone binding subunit *The Journal of Biological Chemistry* **256**:5820-5826.
- Sigel E, Baur R, Rácz I, Marazzi J, Smart T, Zimmer A and Gertsch J (2011) The major central endocannabinoid directly acts at GABA(A) receptors. *Proc Natl Acad Sci U S A* **108**:18150-18155.
- Simon GM and Cravatt BF (2006) Endocannabinoid biosynthesis proceeding through glycerophospho-N-acyl ethanolamine and a role for alpha/beta-hydrolase 4 in this pathway. *J Biol Chem* **281**:26465-26472.
- Simon GM, Strathmann. M. and Gautam N (1991) Diversity of G proteins in Signal Transduction. *Science* **252**:802-808.
- Singh PK, Markwick R, Howell FV, Williams G and Doherty P (2016) A novel live cell assay to measure diacylglycerol lipase alpha activity. *Biosci Rep* **36**.
- Singla N, Minkowitz HS, Soergel DG, Burt DA, Subach RA, Salamea MY, Fossler MJ and Skobieranda F (2017) A randomized, Phase IIb study investigating oliceridine (TRV130), a novel micro-receptor G-protein pathway selective ( $\mu$ -GPS) modulator, for the management of moderate to severe acute pain following abdominoplasty. *J Pain Res* **10**:2413-2424.
- Smoum R, Baraghithy S, Chourasia M, Breuer A, Mussai N, Attar-Namdar M, Kogan NM, Raphael B, Bolognini D, Cascio MG, Marini P, Pertwee RG, Shurki A, Mechoulam R and Bab I (2015) CB2 Cannabinoid Receptor Agonist Enantiomers HU-433 and HU-308: An Inverse Relationship Between Binding Affinity and Biological Potency. *Proc Natl Acad Sci* **112**:8774-8779.
- Snider NT, Nast JA, Tesmer LA and Hollenberg PF (2009) A cytochrome P450-derived epoxygenated metabolite of anandamide is a potent cannabinoid receptor 2-selective agonist. *Mol Pharmacol* **75**:965-972.
- Soethoudt M, Grether U, Fingerle J, Grim TW, Fezza F, de Petrocellis L, Ullmer C, Rothenhausler B, Perret C, van Gils N, Finlay D, MacDonald C, Chicca A, Gens MD, Stuart J, de Vries H, Mastrangelo N, Xia L, Alachouzos G, Baggelaar MP, Martella A,

- Mock ED, Deng H, Heitman LH, Connor M, Di Marzo V, Gertsch J, Lichtman AH, Maccarrone M, Pacher P, Glass M and van der Stelt M (2017) Cannabinoid CB2 receptor ligand profiling reveals biased signalling and off-target activity. *Nat Commun* **8**:13958.
- Spencer SJ (2011) Novel fenofibrate derivatives as cannabinoid receptor ligands, University of Nottingham.
- Starowicz KM, Cristino L, Matias I, Capasso R, Racioppi A, Izzo AA and Di Marzo V (2008) Endocannabinoid dysregulation in the pancreas and adipose tissue of mice fed with a high-fat diet. *Obesity (Silver Spring)* **16**:553-565.
- Steffens S and Pacher P (2012) Targeting cannabinoid receptor CB(2) in cardiovascular disorders: promises and controversies. *Br J Pharmacol* **167**:313-323.
- Stella N (2004) Cannabinoid signaling in glial cells. *Glia* **48**:267-277.
- Stone NL, Millar SA, Herrod PJJ, Barrett DA, Ortori CA, Mellon VA and O'Sullivan SE (2018) An Analysis of Endocannabinoid Concentrations and Mood Following Singing and Exercise in Healthy Volunteers. *Front Behav Neurosci* **12**:269.
- Sugiura T, Kishimoto S, Oka S and Gokoh M (2006) Biochemistry, pharmacology and physiology of 2-arachidonoylglycerol, an endogenous cannabinoid receptor ligand. *Prog Lipid Res* **45**:405-446.
- Sugiura T, Kobayashi Y, Oka S and Waku K (2002) Biosynthesis and degradation of anandamide and 2-arachidonoylglycerol and their possible physiological significance. *Prostaglandins Leukot Essent Fatty Acids* **66**:173-192.
- Sugiura T, Kondo S, Sukagawa A, Nakane S, Shinoda A, Itoh K, Yamashita A and Waku K (1995) 2-Arachidonoylglycerol: a possible endogenous cannabinoid receptor ligand in brain. *Biochem Biophys Res Commun* **215**:89-97.
- Sum C, Murphy B, Li Z, Wang T, Zhang L and Cvijic ME (2019) Pharmacological Characterization of GPCR Agonists, Antagonists, Allosteric Modulators and Biased Ligands from HTS Hits to Lead Optimization, in *Assay Guidance Manual* (Sittampalam G, Grossman A and Brimacombe Kea eds), Bethesda (MD): Eli Lilly & Company and the National Center for Advancing Translational Sciences.

- Sun Y-X, Tsuboi K, Okamoto Y, Tonai T, Murakami M, Kudo I and Ueda N (2004) Biosynthesis of anandamide and N-palmitoylethanolamine by sequential actions of phospholipase A2 and lysophospholipase D. *Biochem J* **380**:749-756.
- Svizenska I, Dubovy P and Sulcova A (2008) Cannabinoid receptors 1 and 2 (CB1 and CB2), their distribution, ligands and functional involvement in nervous system structures--a short review. *Pharmacol Biochem Behav* **90**:501-511.
- Tanaka M, Moran S, Wen J, Affram K, Chen T, Symes AJ and Zhang Y (2017) WWL70 attenuates PGE2 production derived from 2-arachidonoylglycerol in microglia by ABHD6-independent mechanism. *J Neuroinflammation* **14**:7.
- Tanaka M, Sackett S and Zhang Y (2020) Endocannabinoid Modulation of Microglial Phenotypes in Neuropathology. *Front Neurol* **11**:87.
- Tao Q and Abood ME (1998) Mutation of a Highly Conserved Aspartate Residue in the Second Transmembrane Domain of the Cannabinoid Receptors, CB1 and CB2, Disrupts G-protein Coupling. *J Pharmacol Exp Ther* **285**:651-658.
- Tao Q, McAllister SD, Andreassi J, Nowell KW, Cabral GA, Hurst DP, Bachtel K, Ekman MC, Reggio PH and Abood ME (1999) Role of a Conserved Lysine Residue in the Peripheral Cannabinoid Receptor (CB2): Evidence for Subtype Specificity. *Mol Pharmacol* **55**:605-613.
- Taylor AH, Amoako AA, Bambang K, Karasu T, Gebeh A, Lam PM, Marzcylo TH and Konje JC (2010) Endocannabinoids and pregnancy. *Clin Chim Acta* **411**:921-930.
- Tchantchou F and Zhang Y (2013) Selective inhibition of alpha/beta-hydrolase domain 6 attenuates neurodegeneration, alleviates blood brain barrier breakdown, and improves functional recovery in a mouse model of traumatic brain injury. *J Neurotrauma* **30**:565-579.
- Thapa D, Lee JS, Heo SW, Lee YR, Kang KW, Kwak MK, Choi HG and Kim JA (2011) Novel hexahydrocannabinol analogs as potential anti-cancer agents inhibit cell proliferation and tumor angiogenesis. *Eur J Pharmacol* **650**:64-71.
- Thomas G, Betters JL, Lord CC, Brown AL, Marshall S, Ferguson D, Sawyer J, Davis MA, Melchior JT, Blume LC, Howlett AC, Ivanova PT, Milne SB, Myers DS, Mrak I, Leber V, Heier C, Taschler U, Blankman JL,

- Cravatt BF, Lee RG, Crooke RM, Graham MJ, Zimmermann R, Brown HA and Brown JM (2013) The serine hydrolase ABHD6 Is a critical regulator of the metabolic syndrome. *Cell Rep* **5**:508-520.
- Tsuboi K, Hilligsmann C, Vandevoorde S, Lambert DM and Ueda N (2004) N-Cyclohexanecarbonylpentadecylamine: a selective inhibitor of the acid amidase hydrolysing N-acylethanolamines, as a tool to distinguish acid amidase from fatty acid amide hydrolase. *Biochem J* **379**:99-106.
- Turcotte C, Blanchet MR, Laviolette M and Flamand N (2016) The CB2 receptor and its role as a regulator of inflammation. *Cell Mol Life Sci* **73**:4449-4470.
- Tuteja N (2009) Signaling through G protein coupled receptors. *Plant Signaling & Behavior* **4**:942-947.
- Ueda N, Tsuboi K and Uyama T (2013) Metabolism of endocannabinoids and related N-acylethanolamines: canonical and alternative pathways. *FEBS J* **280**:1874-1894.
- Ueda N, Yamamoto K, Yamamoto S, Tokunaga T, Shirakawa E, Shinkai H, Ogawa M, Sato T, Kudo I, Inoue K, Takizawa H, Nagano T, Hirobe M, Matsuki N and Saito H (1995) Lipoxygenase-catalyzed oxygenation of arachidonylethanolamide, a cannabinoid receptor agonist. *Biochim Biophys Acta* **1254**:127-134.
- Ueda N, Yamanaka K, Terasawa Y and Yamamoto S (1999) An acid amidase hydrolyzing anandamide as an endogenous ligand for cannabinoid receptors. *FEBS Lett* **454**:267-270.
- Ueda Y, Miyagawa N, Matsui T, Kaya T and Iwamura H (2005) Involvement of cannabinoid CB(2) receptor-mediated response and efficacy of cannabinoid CB(2) receptor inverse agonist, JTE-907, in cutaneous inflammation in mice. *Eur J Pharmacol* **520**:164-171.
- Urban JD, Clarke WP, von Zastrow M, Nichols DE, Kobilka B, Weinstein H, Javitch JA, Roth BL, Christopoulos A, Sexton PM, Miller KJ, Spedding M and Mailman RB (2007) Functional selectivity and classical concepts of quantitative pharmacology. *J Pharmacol Exp Ther* **320**:1-13.
- Valenzano KJ, Tafesse L, Lee G, Harrison JE, Boulet JM, Gottshall SL, Mark L, Pearson MS, Miller W, Shan S, Rabadi L, Rotshteyn Y, Chaffer SM, Turchin PI, Elsemore DA, Toth M, Koetzner L and Whiteside GT (2005) Pharmacological and pharmacokinetic characterization

of the cannabinoid receptor 2 agonist, GW405833, utilizing rodent models of acute and chronic pain, anxiety, ataxia and catalepsy. *Neuropharmacology* **48**:658-672.

Van Gaal LF, Rissanen AM, Scheen AJ, Ziegler O and Rössner S (2005) Effects of the cannabinoid-1 receptor blocker rimonabant on weight reduction and cardiovascular risk factors in overweight patients: 1-year experience from the RIO-Europe study. *The Lancet* **365**:1389-1397.

Vara D, Salazar M, Olea-Herrero N, Guzman M, Velasco G and Diaz-Laviada I (2011) Anti-tumoral action of cannabinoids on hepatocellular carcinoma: role of AMPK-dependent activation of autophagy. *Cell Death Differ* **18**:1099-1111.

Vass M, Kooistra AJ, Yang D, Stevens RC, Wang MW and de Graaf C (2018) Chemical Diversity in the G Protein-Coupled Receptor Superfamily. *Trends Pharmacol Sci* **39**:494-512.

Verty AN, Stefanidis A, McAinch AJ, Hryciw DH and Oldfield B (2015) Anti-Obesity Effect of the CB2 Receptor Agonist JWH-015 in Diet-Induced Obese Mice. *PLoS One* **10**:1-19.

Wacker D, Stevens RC and Roth BL (2017) How Ligands Illuminate GPCR Molecular Pharmacology. *Cell* **170**:414-427.

Wadkins R, Hyatt JL, Wei X, Yoon KJP, Wierdl M, Edwards CC, Morton CL, Obenauer JC, Damodaran K, Beroza P, Danks MK and Potter PM (2005) Identification and Characterization of Novel Benzil (Diphenylethane-1,2-dione) Analogues as Inhibitors of Mammalian Carboxylesterases. *J Med Chem* **48**:2906-2915.

Wang J, Xu J, Peng Y, Xiao Y, Zhu H, Ding ZM and Hua H (2018) Phosphorylation of extracellular signal-regulated kinase as a biomarker for cannabinoid receptor 2 activation. *Heliyon* **4**:e00909.

Wang T, Collet JP, Shapiro S and Ware MA (2008) Adverse effects of medical cannabinoids: a systematic review *CMAJ* **178**:1669-1678.

Wei BQ, Mikkelsen TS, McKinney MK, Lander ES and Cravatt BF (2006) A second fatty acid amide hydrolase with variable distribution among placental mammals. *J Biol Chem* **281**:36569-36578.

Wei M, Zhang J, Jia M, Yang C, Pan Y, Li S, Luo Y, Zheng J, Ji J, Chen J, Hu X, Xiong J, Shi Y and Zhang C (2016) alpha/beta-Hydrolase domain-

containing 6 (ABHD6) negatively regulates the surface delivery and synaptic function of AMPA receptors. *Proc Natl Acad Sci U S A* **113**:E2695-2704.

Wen J, Ribeiro R, Tanaka M and Zhang Y (2015) Activation of CB2 receptor is required for the therapeutic effect of ABHD6 inhibition in experimental autoimmune encephalomyelitis. *Neuropharmacology* **99**:196-209.

Wiley J, Barrett R, Lowe J, Balster R and Martin B (1995) Discriminative stimulus effects of CP 55,940 and structurally dissimilar cannabinoids in rats. *Neuropharmacology* **34**:669-676.

Wise A, Jupe SC and Rees S (2004) The identification of ligands at orphan G-protein coupled receptors. *Annu Rev Pharmacol Toxicol* **44**:43-66.

Xie X, Chen J and Billings E (2003) 3D structural model of the G-protein-coupled cannabinoid CB2 receptor. *Proteins* **53**:307-319.

Xing C, Zhuang Y, Xu TH, Feng Z, Zhou XE, Chen M, Wang L, Meng X, Xue Y, Wang J, Liu H, McGuire TF, Zhao G, Melcher K, Zhang C, Xu HE and Xie XQ (2020) Cryo-EM Structure of the Human Cannabinoid Receptor CB2-Gi Signaling Complex. *Cell* **180**:645-654 e613.

Xu JJ, Diaz P, Astruc-Diaz F, Craig S, Munoz E and Naguib M (2010) Pharmacological characterization of a novel cannabinoid ligand, MDA19, for treatment of neuropathic pain. *Anesth Analg* **111**:99-109.

Yamamoto W, Mikami T and Iwamura H (2008) Involvement of central cannabinoid CB2 receptor in reducing mechanical allodynia in a mouse model of neuropathic pain. *Eur J Pharmacol* **583**:56-61.

Yang L, Li FF, Han YC, Jia B and Ding Y (2015) Cannabinoid receptor CB2 is involved in tetrahydrocannabinol-induced anti-inflammation against lipopolysaccharide in MG-63 cells. *Mediators Inflamm* **2015**:362126.

Yao BB, Hsieh GC, Frost JM, Fan Y, Garrison TR, Daza AV, Grayson GK, Zhu CZ, Pai M, Chandran P, Salyers AK, Wensink EJ, Honore P, Sullivan JP, Dart MJ and Meyer MD (2008) In vitro and in vivo characterization of A-796260: a selective cannabinoid CB2 receptor agonist exhibiting analgesic activity in rodent pain models. *Br J Pharmacol* **153**:390-401.

- Ye L, Cao Z, Wang W and Zhou N (2019) New Insights in Cannabinoid Receptor Structure and Signaling. *Curr Mol Pharmacol* **12**:239-248.
- Yiangou Y, Facer P, Durrenberger P, Chessell IP, Naylor A, Bountra C, Banati RR and Anand P (2006) COX-2, CB2 and P2X7-immunoreactivities are increased in activated microglial cells/macrophages of multiple sclerosis and amyotrophic lateral sclerosis spinal cord. *BMC Neurol* **6**:12.
- Yu M, Ives D and Ramesha C (1997) Synthesis of prostaglandin E2 ethanolamide from anandamide by cyclooxygenase-2. *J Biol Chem* **272**:21181-21186.
- Zelasko S, Arnold WR and Das A (2015) Endocannabinoid metabolism by cytochrome P450 monooxygenases. *Prostaglandins Other Lipid Mediat* **116-117**:112-123.
- Zhang CQ, Wu HJ, Wang SY, Yin S, Lu XJ, Miao Y, Wang XH, Yang XL and Wang Z (2013) Suppression of outward K(+) currents by WIN55212-2 in rat retinal ganglion cells is independent of CB1/CB2 receptors. *Neuroscience* **253**:183-193.
- Zhang J, Hoffert C, Vu HK, Groblewski T, Ahmad S and O'Donnell D (2003) Induction of CB2 receptor expression in the rat spinal cord of neuropathic but not inflammatory chronic pain models. *European Journal of Neuroscience* **17**:2750-2754.
- Zhang JH, Chung T and Oldenburg K (1999) A Simple Statistical Parameter for Use in Evaluation and Validation of High Throughput Screening Assays. *Journal of Biochemical Screening* **4**:67-73.
- Zhang R, Hurst DP, Barnett-Norris J, Reggio PH and Song ZH (2005) Cysteine 2.59(89) in the second transmembrane domain of human CB2 receptor is accessible within the ligand binding crevice: evidence for possible CB2 deviation from a rhodopsin template. *Mol Pharmacol* **68**:69-83.
- Zhang X, Gao S, Niu J, Li P, Deng J, Xu S, Wang Z, Wang W, Kong D and Li C (2016) Cannabinoid 2 Receptor Agonist Improves Systemic Sensitivity to Insulin in High-Fat Diet/Streptozotocin-Induced Diabetic Mice. *Cell Physiol Biochem* **40**:1175-1185.
- Zhang Y, Xie Z, Wang L, Schreiter B, Lazo JS, Gertsch J and Xie XQ (2011) Mutagenesis and computer modeling studies of a GPCR conserved residue W5.43(194) in ligand recognition and signal

transduction for CB2 receptor. *Int Immunopharmacol* **11**:1303-1310.

- Zhao S, Mugabo Y, Ballentine G, Attane C, Iglesias J, Poursharifi P, Zhang D, Nguyen TA, Erb H, Prentki R, Peyot ML, Joly E, Tobin S, Fulton S, Brown JM, Madiraju SR and Prentki M (2016) alpha/beta-Hydrolase Domain 6 Deletion Induces Adipose Browning and Prevents Obesity and Type 2 Diabetes. *Cell Rep* **14**:2872-2888.
- Zheng C, Chen L, Chen X, He X, Yang J, Shi Y and Zhou N (2013) The second intracellular loop of the human cannabinoid CB2 receptor governs G protein coupling in coordination with the carboxyl terminal domain. *PLoS One* **8**:e63262.
- Zhou Q, Yang D, Wu M, Guo Y, Guo W, Zhong L, Cai X, Dai A, Jang W, Shakhnovich EI, Liu ZJ, Stevens RC, Lambert NA, Babu MM, Wang MW and Zhao S (2019) Common activation mechanism of class A GPCRs. *Elife* **8**.
- Zou S and Kumar U (2018) Cannabinoid Receptors and the Endocannabinoid System: Signaling and Function in the Central Nervous System. *Int J Mol Sci* **19**.
- Zygmunt P, Petersson J, Andersson D, Chuang H, Sjørgård M, Di Marzo V, Julius D and Högestätt E (1999) Vanilloid receptors on sensory nerves mediate the vasodilator action of anandamide. *Nature* **400**:452-457.